DAAI MARSHALL

Jean N. Jones
EB34

WYLE
LABORATORIES SCIENTIFIC SERVICES & SYSTEMS GROUP

WYLE LABORATORIES - RESEARCH STAFF
TECHNICAL REPORT 66938-01

SIGNAL DETECTION TECHNIQUES FOR DIAGNOSTIC MONITORING OF SPACE SHUTTLE MAIN ENGINE TURBOMACHINERY

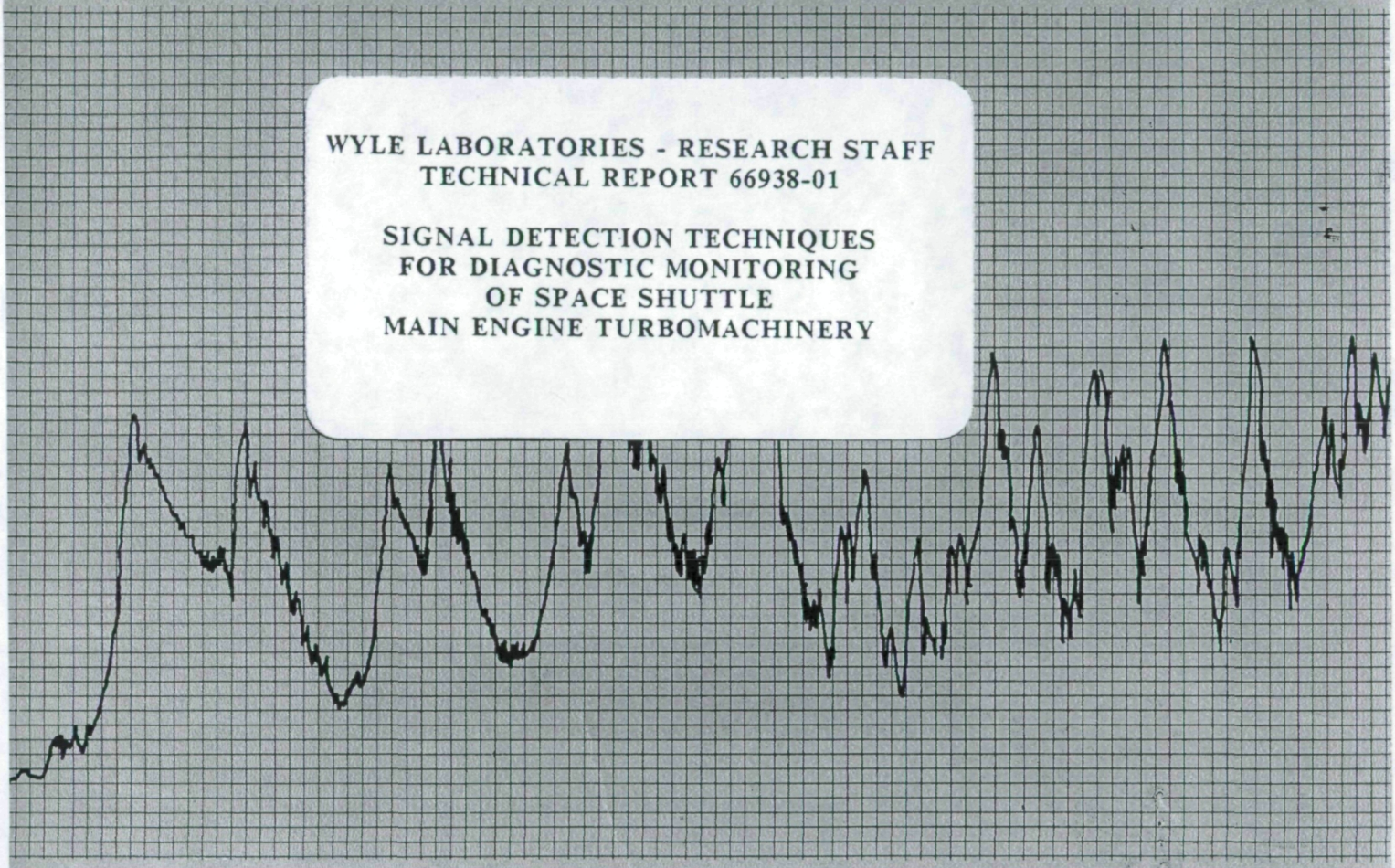

research REPORT

ds W9307657

WYLE LABORATORIES - RESEARCH STAFF
TECHNICAL REPORT 66938-01

SIGNAL DETECTION TECHNIQUES FOR DIAGNOSTIC MONITORING OF SPACE SHUTTLE MAIN ENGINE TURBOMACHINERY

by

Thomas Coffin
Jen-Yi Jong

A final report of
work performed under contract NAS8-34961

for

NATIONAL AERONAUTICS AND SPACE ADMINISTRATION
GEORGE C. MARSHALL SPACE FLIGHT CENTER
MARSHALL SPACE FLIGHT CENTER, ALABAMA 35812

February 1986

FOREWORD

This report was prepared by Wyle Laboratories, Scientific Services & Systems Group, for the George C. Marshall Space Flight Center, National Aeronautics and Space Administration. The work was performed under contract NAS8-34961, entitled "Life Prediction Techniques Using Dynamic Detection Indicators and Analysis."

The authors wish to acknowledge the contribution of Mr. T. Gardner and Mr. G. Anderson, who performed software development and laboratory simulations to demonstrate a number of the techniques discussed in this report. Mr. J. H. Jones, MSFC/ED24 served as Contracting Officer's Technical Representative for the study. In this capacity he provided valuable direction through frequent, informal technical reviews and served as a focal point for defining and obtaining representative SSME test data for technique assessment.

ABSTRACT

This report reviews an investigation to develop, implement, and evaluate signal analysis techniques for the detection and classification of incipient mechanical failures in turbomachinery. A brief description of the Space Shuttle Main Engine (SSME) test/measurement program is presented. Signal analysis techniques available to describe dynamic measurement characteristics are reviewed. Time domain and spectral methods are described, and statistical classification in terms of moments is discussed. Several of these waveform analysis techniques have been implemented on a computer and applied to dynamic signals. A laboratory evaluation of the methods with respect to signal detection capability is described. An unique coherence function (the hyper-coherence) was developed through the course of this investigation, which appears promising as a diagnostic tool. This technique and several other non-linear methods of signal analysis are presented and illustrated by application. Software for application of these techniques has been installed on the signal processing system at the NASA/MSFC Systems Dynamics Laboratory.

TABLE OF CONTENTS

LIST OF FIGURES

LIST OF FIGURES (Concluded)

SECTION I

INTRODUCTION AND SUMMARY

Material and equipment failures of all types -- structural, mechanical, hydraulic, pneumatic, electrical, and electronic -- are the result of two basic causes: structural degradation and chemical contamination. The life cycle of a typical component has been noted to exhibit a highly variable burn-in period, followed by a stable period of growth, and a rapid change in behavior as failure is approached. This behavior pattern is especially well demonstrated by the high cycle fatigue of metals. If failures can be detected incipiently (that is, at an early stage of development) appropriate corrective action can be taken to eliminate the cause or minimize undesired effects before total or catastrophic failure occurs.

Under NASA contract NAS8-34961, Wyle has investigated incipient failure detection techniques applicable to high performance turbomachinery, and the Space Shuttle main engines (SSME) in particular. This report documents the results of the study.

The measurable "output" from a dynamic system includes much subtle information concerning the physical state of the system in terms of unique or characteristic signatures. Methods derived primarily from the statistical communication theory have been successfully applied to problems of crack growth, fatigue, etc. Acoustic emission techniques are now routinely applied to the nondestructive testing of pipelines and pressure vessels. The analysis of machinery life prediction based on dynamic detection indicators has received significant interest in recent years, mainly due to the potential cost savings afforded by scheduled maintenance, to avoid equipment failure and associated plant downtime.

Although little can be done to anticipate mechanical failures which exhibit very short periods of growth, most failures are preceded by growing tolerances, imbalance, bearing element wear, and the like, which may manifest themselves through subtle modifications in the waveform observed by dynamic measurements. Incipient failure detection is based on observing and recognizing measurable phenomena that occur as a result of nominal system operation and those associated with component degradation. The techniques are analytical, but their application is necessarily empirical, based on correlation between derived signature characteristics and observed mechanical condition.

Turbomachinery malfunction may result from a number of distinct failure modes such as turbine blade wear or bearing element fatigue. Each of these mechanisms may be expected to influence the waveform or spectral content measured by a transducer in a somewhat different fashion. Thus, it is clear that a single best signal analysis technique or indicator is not to be expected for system condition monitoring. A series of tests, each designed to detect a given failure mode, is therefore desirable.

The Space Shuttle main engines have undergone and are presently undergoing extensive hot firing tests at which time vibration, dynamic pressure and strain measurements at critical component locations are acquired. Thus, a wealth of dynamic data is available from these components under widely varying operational conditions.

Section II of this report provides a brief overview of SSME operational characteristics, a description of the SSME test program and measurements acquired. A considerable number of methods were evaluated for application to the SSME, and several have been reduced to software and applied to laboratory signals and "real" measurements obtained from the SSME turbopumps during hot firing tests. An interim report, describing these laboratory evaluations is provided in the Appendix. A survey of techniques applied and some representative results are presented in Section III.

The harmonic content in measurements from rotating machinery may indicate equipment operational condition and component degradation (imbalance, rubbing, etc.). Measurements on high-performance rocket engine turbomachinery suffer from severe noise contamination from numerous extraneous sources, which impedes rotating element diagnostic evaluation. It is thus difficult to determine whether an apparent high-level harmonic contribution is indeed related to the fundamental rotational frequency, or possibly due to an independent source. In an effort to relate synchronous speed characteristics with an arbitrary harmonic component, an unique coherence spectrum was devised in the course of this study. The hyper-coherence function defines the nonlinear correlation between waves at a reference frequency and its harmonics. This novel technique, and its application to SSME diagnostic evaluation, is discussed in Section IV. (A new technology report on this topic, recently filed with NASA, is included in the Appendix for reference.)

In addition, several advanced techniques have been recently identified and reduced to software, which appear highly promising as incipient failure detection indicators. These approaches are also described in Section IV, which includes analytical examples and application to SSME measurements. The computer routines for application of these techniques have been adapted to MSFC computers and are presently operational on the MASSCOMP processor in the Systems Dynamics Laboratory.

SECTION II

SSME TESTING AND DYNAMIC MEASUREMENTS

2.1 Background

The Space Shuttle Main Engines (SSME) are required to operate under extreme temperatures with high fluid pressures and rotational pump speeds. Developmental work is presently in progress to uprate SSME performance, including engine certification at FPL (109%). The SSME and components have been subjected to extensive hot firing tests. Acceleration, dynamic pressure and strain data have been acquired during these tests and additionally from Space Shuttle Vehicle (SSV) flights. Data reduction and analysis techniques, to aid in the identification and resolution of sources of malfunction, were developed and applied by Wyle Laboratories under NASA Contract NAS8-34961.

This section presents an overview of the Space Shuttle Vehicle (SSV) system and SSME in particular. The SSME test program is briefly described, and dynamic measurement locations illustrated. Some methods applied by Wyle to the assessment of these dynamic measurements are discussed in subsequent sections.

2.2 The Space Shuttle Vehicle System

The SSV is composed of the Orbiter, an External Tank (ET), which contains the ascent propellant to be used by the Orbiter's three main engines, and two Solid Rocket Boosters (SRB). The Orbiter and SRBs are reusable; the ET is expended on each launch.

A Space Shuttle mission begins with installation of the mission payload into the Orbiter cargo bay. The SRBs and the SSMEs fire together at liftoff. The two SRBs are jettisoned after burnout -- about 45 kilometers (28 miles) high -- and recovered for reuse by means of a parachute recovery system. The SSMEs continue to burn until the Orbiter approaches orbital velocity, at which time the engines are shut down and the ET jettisoned. During its return through the atmosphere, the tank is destroyed.

The orbital maneuvering system is used to attain the desired orbit and to make any subsequent maneuvers that may be needed during a mission. After orbital operations are completed, normally about seven days, deorbiting maneuvers are initiated. The Orbiter reenters the Earth's atmosphere at a high angle of attack. It then

levels into horizontal flight at low altitude for an unpowered aircraft-type approach, landing at a speed of about 335 kilometers per hour (208 miles per hour).

2.3 The Space Shuttle Main Engines

The Orbiter vehicle main propulsion system consists of three SSMEs. The SSMEs are reusable, high-performance, liquid-propellant rocket engines with variable thrust. They are ignited on the ground at launch and operate in parallel, with approximately 500 seconds total firing duration. Each of the rocket engines operates at a mixture ratio (liquid oxygen/liquid hydrogen) of 6:1 and a chamber pressure of approximately 3000 psia to produce a sea-level thrust of 375,000 pounds and a vacuum thrust of 470,000 pounds. The engines are presently throttleable over a thrust range of 60 to 109 percent of the design thrust level. This provides a higher thrust level during liftoff and the initial ascent phase, and allows Orbiter acceleration to be limited to 3 g's during the final ascent phase. The engines are gimbaled ($\pm$10.5 degrees for pitch and $\pm$8.5 degrees yaw) to provide pitch, yaw, and roll control during the Orbiter boost phase.

Significant to meeting performance requirements is the use of a staged combustion power cycle coupled with high combustion chamber pressures. In the SSME-staged combustion cycle, the propellants are partially burned at high pressure and relatively low temperature in the preburners, then completely combusted at high temperature and pressure in the main chamber before expanding through the high-area-ratio nozzle. Hydrogen fuel is used to cool all combustion devices in contact with high-temperature combustion products. An electronic engine controller automatically performs checkout, start, mainstage, and engine shutdown functions. Major components of the SSME are illustrated in Figure 2-1. A more detailed view of the SSME power head is shown in Figure 2-2. This figure provides an indication of the complexity of the SSME turbomachinery.

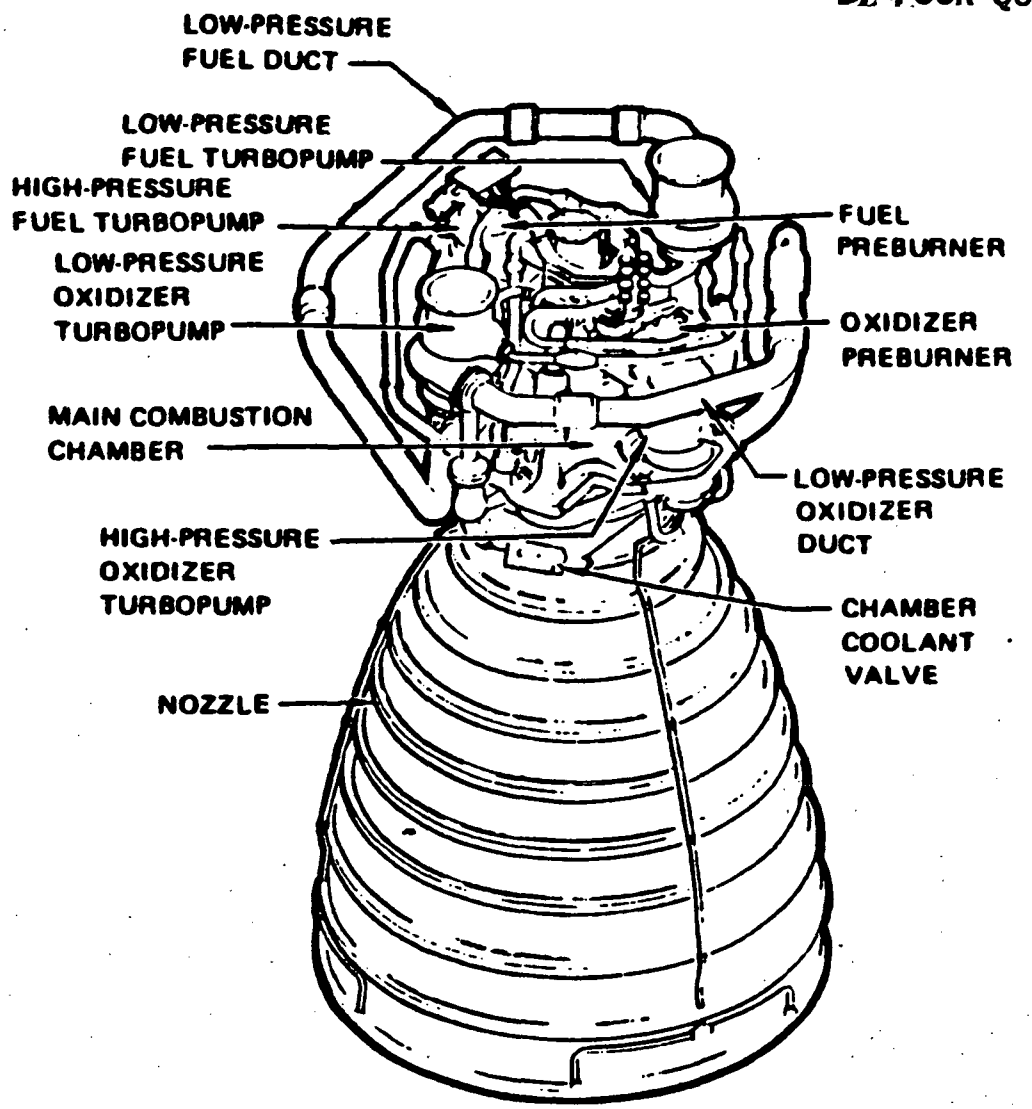

Figure 2-1. Space Shuttle Main Engine

2.4 SSME Development and Acceptance Testing

To validate system performance and ensure equipment reliability, the SSME and components have been and are presently undergoing extensive development and qualification tests. Testing of the engine and components is conducted at several NASA and contractor locations. Full scale engine test firings for development and flight acceptance are performed on two single-engine test stands at the National Space Technology Laboratories (NSTL), Bay St. Louis, Mississippi, and at one stand operated by Rockwell International near Santa Susana, California, with plans to include a development test stand at MSFC. In addition, main propulsion testing (MPT) is performed at NSTL on a stand designed to accommodate the Shuttle main propulsion system elements--the three-engine cluster, the ET, and the Orbiter systems.

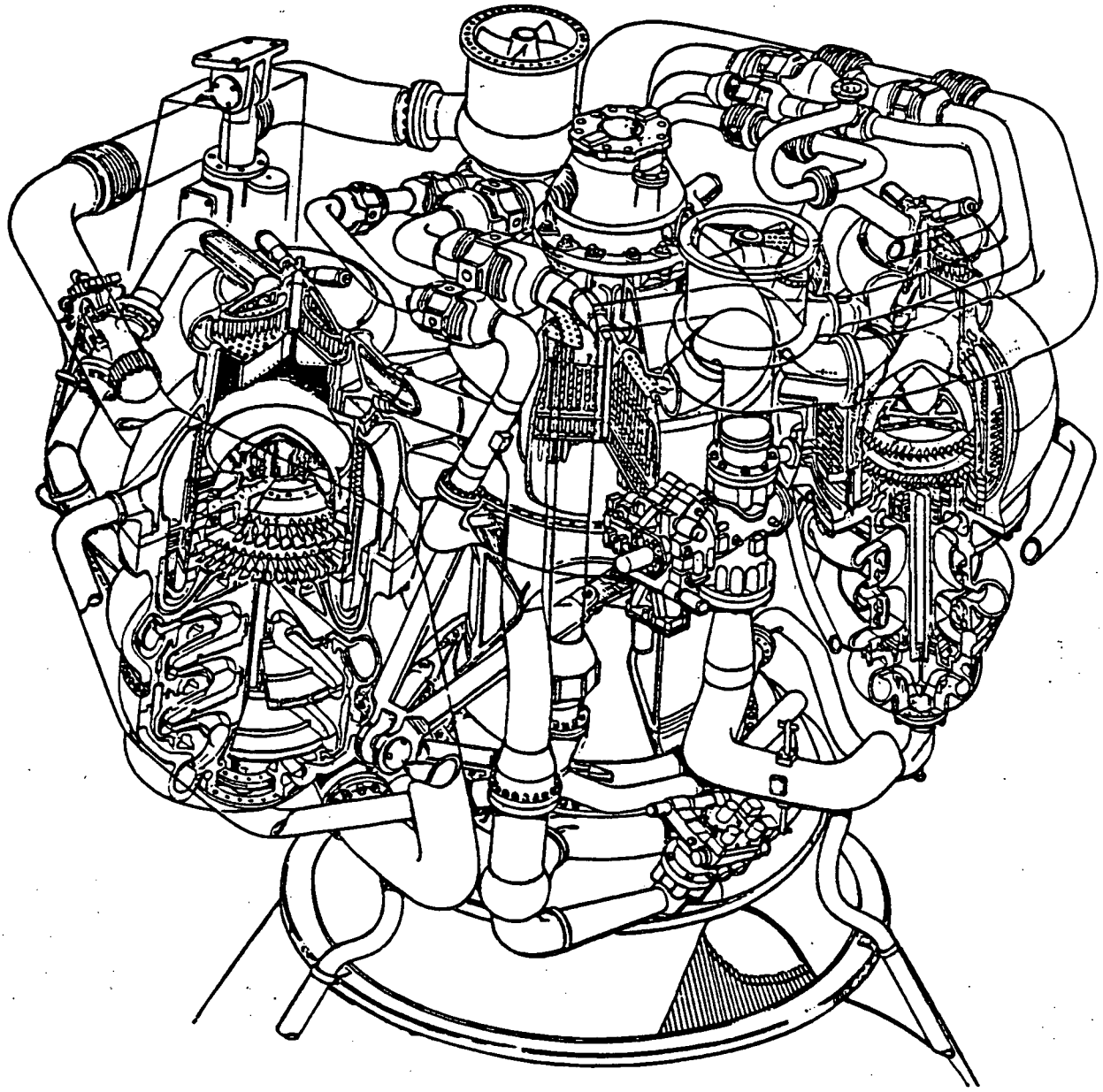

Figure 2-2. Space Shuttle Main Engine Power Head

Testing is being performed on a continuing basis. The length of a given test is dependent on specific test objectives and may run from several seconds to over 800 seconds. Tests are generally designed to satisfy multiple specific objectives, which fall into two broad categories; acceptance/certification firing of flight hardware and development testing directed towards design verification, performance and reliability improvement. Test operations are controlled by a computer called the Command and Data Simulator (CADS) which communicates with the engine, displays vital measurements for on-line observation/control and initiates pre- and post-test procedures.

Approximately 250 measurements are recorded on a given test including wide band vibration, dynamic pressure and strain at critical engine locations. Some of these measurements are utilized on-line as emergency cut-off indicators and all are recorded on magnetic tape for subsequent analysis and evaluation. Limited SSME vibration measurements are recorded on magnetic tape during SSV flights for evaluation with orbiter return. Typical dynamic measurements obtained during SSME operation are illustrated in Figure 2-3.

Acceleration measurements are obtained at fuel and oxidizer turbopump locations during all test firings, providing an extensive vibration data base representing various turbopump builds under widely differing operating conditions. Additional measurements are obtained on a test-specific basis, depending on performance, structural integrity, or rotor dynamic characteristics under evaluation. For example, test series have been performed with some 80 strain measurements to support engine nozzle and injector dynamic stress evaluations. Recent firings have also been conducted with internally instrumented turbopumps to define bearing load and signature characteristics. The above measurements formed a basis for the evaluation of incipient failure detection techniques, discussed in the next section.

ORIGINAL PAGE IS
OF POOR QUALITY

SSME INSTRUMENTATION

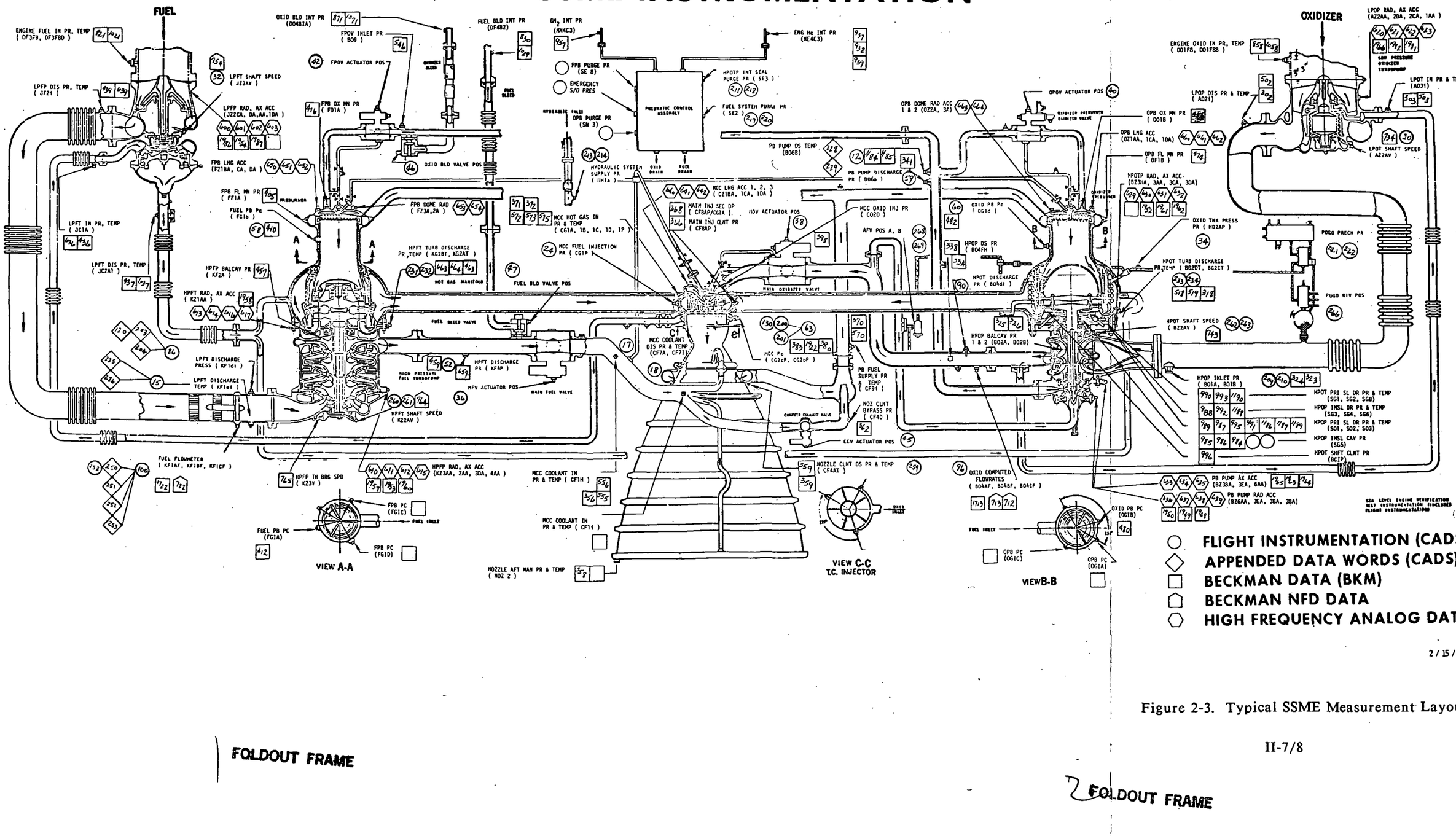

Figure 2-3. Typical SSME Measurement Layout

FOLDOUT FRAME

FOLDOUT FRAME

SECTION III

REVIEW AND EVALUATION OF INCIPIENT FAILURE TECHNIQUES FOR ROTATING MACHINERY

3.1 Introduction

Although little can be done to anticipate mechanical failures which exhibit very short periods of growth, most failures are preceded by growing tolerances, imbalance, bearing element wear, and the like, which may manifest themselves through subtle modifications in the waveform observed by dynamic measurements. Incipient failure detection is based on observing and recognizing measurable phenomena that occur as a result of nominal system operation and those associated with component degradation. The techniques are analytical, but their application is necessarily empirical, based on correlation between derived signature characteristics and observed mechanical condition.

Turbomachinery malfunction may result from a number of distinct failure modes such as turbine blade wear or bearing element fatigue. Each of these mechanisms may be expected to influence the waveform or spectral content measured by a transducer in a somewhat different fashion. Thus, it is clear that a single best signal analysis technique or indicator is not to be expected for system condition monitoring. A series of tests, each designed to detect a given failure mode, is therefore desirable.

The Space Shuttle main engines have undergone and are presently undergoing extensive hot firing tests at which time vibration measurements on the high pressure fuel and oxidizer turbopumps and other critical locations are acquired. Thus, a wealth of vibration data is available from these components under widely varying operational conditions. Under contract with NASA/MSFC, Wyle is investigating techniques of analyzing these data to indicate SSME component condition.

3.2 Techniques and Applications

Review of the literature on machinery condition diagnostic methodologies indicates approaches employing thermal, chemical, metallographic, and vibration analysis techniques (1, 2). This discussion is limited to the assessment of response detected by a transducer fixed to the machine during operation. (Appropriate sensor selection and location is not a trivial consideration with respect to component fault detection.) Historically, the most common diagnostic approach has

been to detect and track the root-mean-square vibration level (displacement, velocity, or acceleration) as an indication of machinery condition. Performing the same analysis in separate frequency bands provides some improvement in fault identification since gross failure modes, such as imbalance, may show up at well-defined frequencies with respect to the synchronous speed. Signature analysis techniques thus fall naturally into two categories, time domain methods and characterization in the frequency domain. Several of the techniques evaluated are next described.

3.2.1 Time Domain Methods

Time Domain Averaging. This method is a well-known technique for extracting periodic signals from noisy or complex waveforms. (3,4) The procedure can be explained by assuming a given signal x(t) is the sum of a periodic component p(t), and additive noise, n(t):

$$x(t) = p(t) + n(t) .$$

By summing one time slice of x(t) with another but delayed one period later than the previous, the periodic component will add coherently, and the noise component, if uncorrelated, will not. After N additions of the signal with itself, the time domain average signature, D(t), may be expressed as

$$D(t) = \frac{1}{N} \sum_{n=0}^{N-1} x(t+nt) .$$

This process is equivalent to a comb filter in the frequency domain as illustrated in Figure 3-1 (4). As the number of replications increases, so does the sharpness of the main lobes and attenuation of nonharmonic frequencies. The TDA method has been effectively applied to large rotating machinery evaluations, and implementation on a small computer is quite direct. It is noted that the process is coherent, requiring that the period of the signal to be extracted be known or assumed. The performance of this method may be improved through order sampling (OSTDA) to synchronize the sample rate with the periodic component to be extracted.

Random Decrement Analysis. The response of a structural dynamic system is a function of both the applied loading and system properties. Changes in system characteristics such as modal frequencies or damping may be indicative of component degradation. The so-called random decrement signature has been applied extensively to the extraction of structural system characteristics in the presence of complex

loading. (5,6) The procedure is similar to the TDA method described above in that the measured signal is repetitively shifted and added to itself:

$$\delta(\tau) = \frac{1}{N} \sum_{n=1}^{N} x(t_n+\tau) .$$

However, in the present case, the time delay between successive segments, t_n, is no longer a fixed period but is determined by the amplitude and/or slope of the signal attaining specified values. The most popular choice in defining a trigger level for acquiring successive samples is to simply specify an amplitude threshold and slope, x_s (such as the rms value of the signal), at which time each segment is initiated, giving, for example

$$t_n = t \text{ when } x(t) = x_s, \dot{x}(t) > 0 .$$

Figure 3-2 illustrates the evolution of a random decrement signature from a complex response measurement (5). An advantage of the randomdec method is that system characteristics need not be known a priori. As structural flaws or cracks develop in a component, the altered structural characteristics will modify the randomdec signature, providing an indication of possible incipient failure.

Characterization by Moments. If our measurement, x(t), be assumed a representative sample function drawn from a stationary process, statistical moments can be estimated in terms of time averages:

$$m_n = (1/T) \int_0^T [\, x(t) - m_1 \,]^n \, dt$$

$$m_1 = (1/T) \int_0^T x(t)dt .$$

The first two moments are the familiar mean and variance, respectively. Note that if the signal is symmetric about the mean, all odd order moments are zero. Of special interest is the normalized fourth moment, or kurtosis coefficient:

$$K = m_4/m^2_2 .$$

Similar to the peak/rms ratio, the kurtosis provides an indication of the spread of

the distribution, i.e. the proportion of extreme values with respect to the rms level. For example,

K = 1, square wave

K = 1.5, sine wave

K = 3, random signal with Gaussian amplitude distribution

Bearing faults or seal rubs often cause intermittent contact over a fraction of a revolution of the machine. The onset of such behavior therefore imparts an impulsive nature to a measurable signal, which may be detected as an increase in the kurtosis coefficient. Since the kurtosis coefficient is normalized by the signal variance, this parameter should be relatively insensitive to machinery loading conditions.

Adaptive Noise Cancellation. Measurements obtained on the SSME turbopump housing during engine operation are corrupted with a high level of undesired noise from a multitude of sources. The concept of adaptive noise cancellation is a means by which signals corrupted by additive noise or interference can be estimated. An adaptive filter is a recursive numerical algorithm which, for stationary stochastic inputs, closely approximates the performance of a fixed Wiener estimation filter. The method uses a "primary" input containing both the desired signal and noise along with a "reference" signal correlated in some unknown way with the primary input noise. The reference input is weighted based on its past values and subtracted from the primary input to yield an estimate of the desired signal. The general concept of adaptive noise cancellation is discussed in detail in Reference (7), and use of the process as applied to machine monitoring is presented in Reference (8). Reference (8) also describes the application of statistical moment and cepstrum analysis techniques to turbine bearing fault detection subsequent to adaptive filtering. Application of the adaptive filtering technique to SSME turbopump measurements is illustrated in the next section.

Envelope Detection. Bearing element and transmission gear mesh frequencies have been observed as an amplitude modulation superimposed on a measured complex vibration time history. Envelope detection has therefore been applied to the identification of related defects. The general approach is to detect the envelope of the measured signal followed by spectrum analysis to extract predominant frequency contributions in the envelope time history. These frequencies have been

associated with flaws, which may not be detectable in the spectrum of the original wideband signal. In 1958, Dugundji introduced the concept of a pre-envelope function defined as

$$z(t) = x(t) + i\,\hat{x}(t)$$

where $x(t)$ is the original time signal, and $\hat{x}(t)$ is the Hilbert transform of $x(t)$.

The pre-envelope is a (mathematically) complex time signal, the modulus of which is the signal envelope.

$$|z(t)| = \{ x^2(t) + \hat{x}^2(t) \}^{1/2} .$$

The availability of microprocessors and the fast Fourier transform (FFT) algorithm has made it possible to implement envelope detection software on Fourier-based analyzers due to the duality between Fourier/Hilbert transforms. Thus, the pre-envelope function may be extracted by Fourier transforming the original vibration signal, discarding all negative frequencies, doubling the positive frequency values, and taking the inverse transform of this one-sided spectrum. The modulus of the resulting complex valued time history yields the desired signal envelope. An obvious computational advantage of the above approach is that the envelope function can be directly extracted using a standard FFT analyzer and calculator. Subsequent spectrum analysis of the envelope time history is then a simple additional step in the computation. It might be noted that the resulting envelope signal may also be analyzed by the above time averaging techniques to investigate signal characteristic/fault correlations.

3.3.2 Frequency Decomposition

Turbomachinery components exhibit distinct characteristic frequencies associated with machine operation such as shaft speed, impeller blade passage, bearing element rotation, etc. Spectral representation of measurements, either by band-pass filtering or frequency transformation, is therefore the most popular approach in practice for machine condition trending and fault identification.

Power Spectral Density (PSD). If a measurement time history is viewed as a representative sample function from a stationary random process, the mean-square density spectrum (or PSD) describes the frequency distribution of the process mean-

square. The PSD may be estimated in several ways but is now most commonly extracted by applying the discrete Fourier transform on a digital spectrum analyzer and estimated by

$$S_x(f) = (1/T) \langle x^*(f)\, x(f) \rangle$$

where $S_x(f)$ is the PSD at frequency f, x(f) is the discrete Fourier transform of a segment of the time history of length T, and the asterisk denotes the conjugate complex; the brackets indicate an ensemble average. Due in part to the availability and efficiency of digital analyzers, the PSD and cross PSD have become the standard format for complex signal description and system parameter identification. Another reason for its popularity is the straightforward interpretation of linear excitation/response relations and system characteristics in the frequency domain.

Bispectrum Analysis. As the PSD is the spectrum of the process second moment, the bispectrum represents the (two-dimensional) spectrum of the third joint moment and can be estimated by

$$B(f_1,f_2) = 1/T \langle x(f_1)\, x(f_2)\, x^*(f_3) \rangle , \; f_1 + f_2 = f_3 .$$

The PSD and bispectrum may be seen to be the first two of a hierarchy if higher order statistical descriptions as the mean and variance are to higher order moments. Higher order spectra have been applied for some time to define joint correlations in statistical data (9) and more recently to dynamic system parameter identification. (10, 11) As a diagnostic tool, the normalized bispectrum may be applied to detect the onset of nonlinear system behavior and possible associated component degradation. The bispectrum analysis technique can be implemented on contemporary FFT analyzers since only one-dimensional transforms are required. Symmetry of the function permits evaluation over only a portion of the two-dimensional frequency plane. This non-linear spectral technique is discussed further in the next section of this report.

Cepstrum Analysis. The power cepstrum (12) was first defined as the power spectrum of the logarithm of the ordinary PSD and may be written as (13)

$$C_x(\tau) = |\mathcal{F}\{ \log S_x(f) \}|^2$$

where $\mathcal{F}$ denotes the Fourier transform and the variable τ in the cepstrum is called the quefrency. Alternative expressions for the power cepstrum include the absolute value of the above, without squaring, and the indicated transform, which is real, as opposed to its squared modulus. In any event, the power cepstrum serves to indicate periodicities in the PSD. Thus, an increase in the harmonic content or uniform sidebands in the signal will be indicated by peaks in the power cepstrum. The quefrency at which a given peak occurs defines the period (or frequency difference) between a series of harmonic components. It may be noted that the power cepstrum is, in truth, a time domain characterization of the measured signal since the quefrency has units of time. The cepstrum technique has been applied successfully to remove echoes (periodic reflections) in acoustic and sonar applications as well as to enhance the harmonic content in bearing element vibration spectra.

3.3 Technique Implementation and Evaluation

Five of the above techniques were implemented early in this study and applied to the extraction of known signals from noise and to SSME turbopump vibration measurements. Software development and results are documented in References (1) and (2). We here illustrate several results indicative of technique performance.

The TDA method was implemented on a Hewlett Packard 5451-C computer system and applied to the extraction of a sinusoid with additive noise. The results of this exercise are illustrated in Figure 3-3. The spectrum of the sinusoid is shown in Figure 3-3(a). The spectrum of the same sine plus noise is shown in Figure 3-3(b). Improvement in the discrimination of the spectral component is illustrated in Figure 3-3(c), representing 50 TDAs and Figure 3-3(d), after 150 TDAs. As noted previously, the TDA method requires a priori knowledge of periodicities sought. However, based on ordered sampling corresponding to tachometer or synchronous speed measurements, improved resolution of significant spectral components by this method has been obtained.

Performance of the randomdec method on a sine wave plus noise process is illustrated in Figure 3-4. The input signal is shown in the top illustration. The associated randomdec signature is shown in the center. Increased periodicity in this signature is evident though the signature is still quite complex. As a matter of interest, a second randomdec was extracted using the first as input and is shown in the lower

time history. The imbedded sine wave is here seen to be well identified. As noted in the above discussion, the randomdec algorithm has the advantage of not requiring prior knowledge of periodicities in the signal. The establishment of optimum threshold conditions for signature extraction requires further investigation.

The adaptive filter concept was implemented using a hard-wired digital filter (DAC 1025I), provided by MSFC. A schematic of the data analysis setup is shown in Figure 3-5. Typical pre- and post-filtered PSDs from a high pressure oxidizer turbopump measurement are shown in Figure 3-6. The first spectrum represents the ordinary PSD of the signal obtained with a 12.5-Hz resolution. The second illustrates the same spectral decomposition obtained after processing of the signal with the adaptive filter. A marked improvement in resolution of turbopump periodic components is clear. Identification of synchronous and blade passage harmonics has been enhanced significantly. The engineering interpretation of spectral amplitudes obtained from adaptive filtered measurements is not simple.

As a final illustration, Figure 3-7 shows some results from a bearing life investigation where the statistical moment technique was applied. (14) This figure illustrates the time history of rms acceleration and kurtosis coefficient measured on the bearing housing of a roller bearing during endurance test on a Timken test machine. Note the distinct increase in kurtosis coefficient at approximately 457 hours, which is not reflected in the acceleration time history. Inspection at this time revealed a small fatigue crack on the inner race though the test continued for 657 hours, at which time extensive bearing damage was observed.

The above results are quite promising. A data base of adaptive filtered spectra for SSME hot firing measurements is documented in Reference (2). A novel method of diagnostic analysis, recently developed under this contract, is described in the following section.

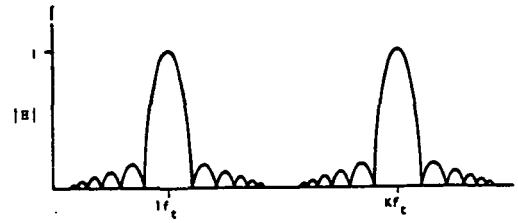

Figure 3-1. Time domain average comb filter

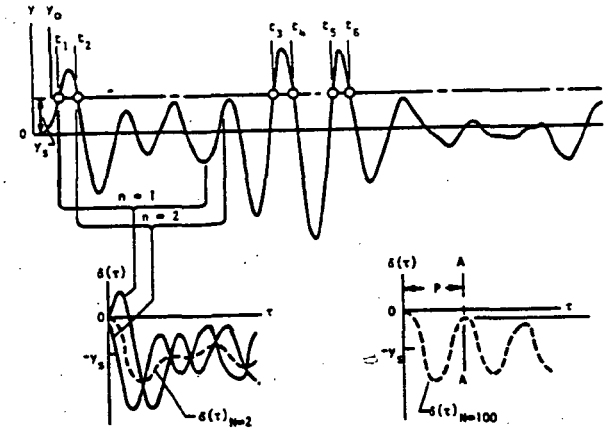

Figure 3-2. Evolution of a random decrement signature (5)

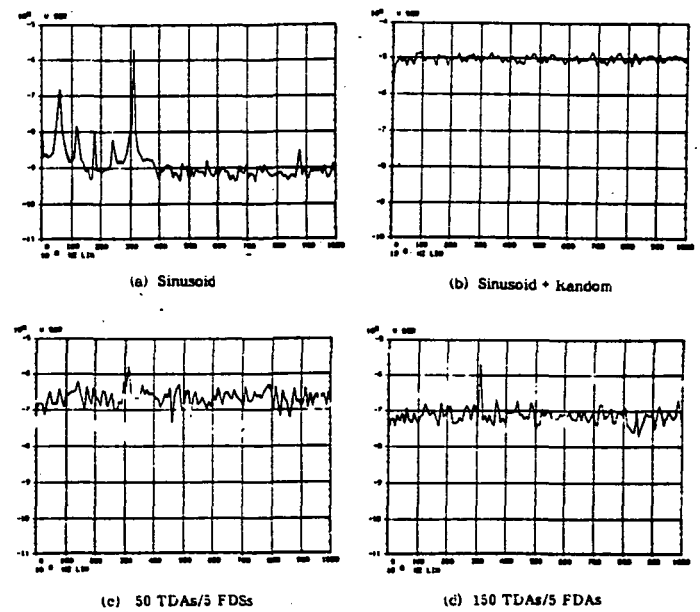

Figure 3-3. Spectrum of time domain averaged signal of sinusoid with additive random noise

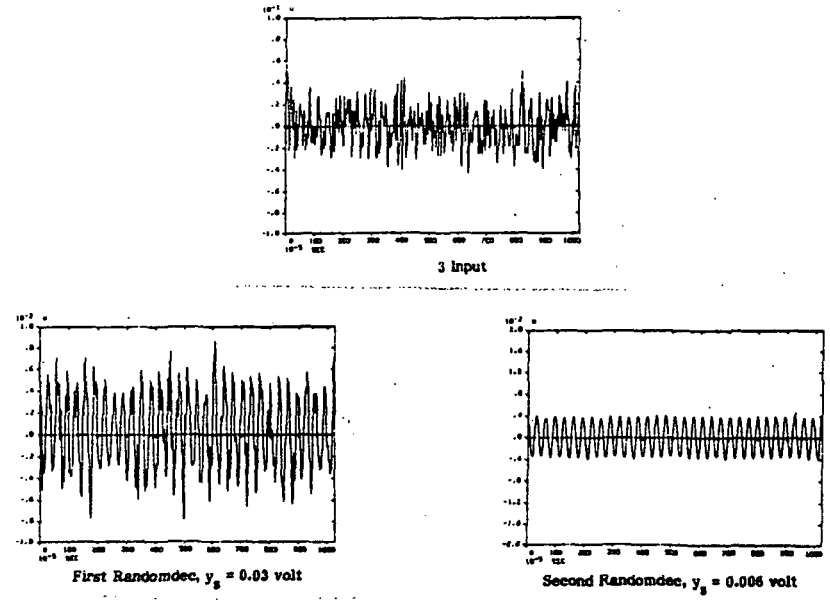

Figure 3-4. Random decrement signature of sinusoid plus noise

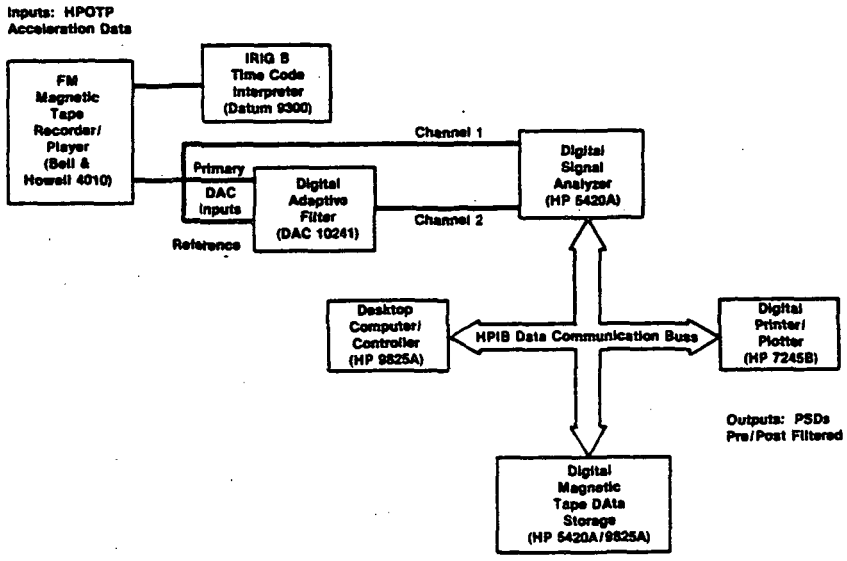

Figure 3-5. Data reduction flowchart for implementing adaptive noise cancellation

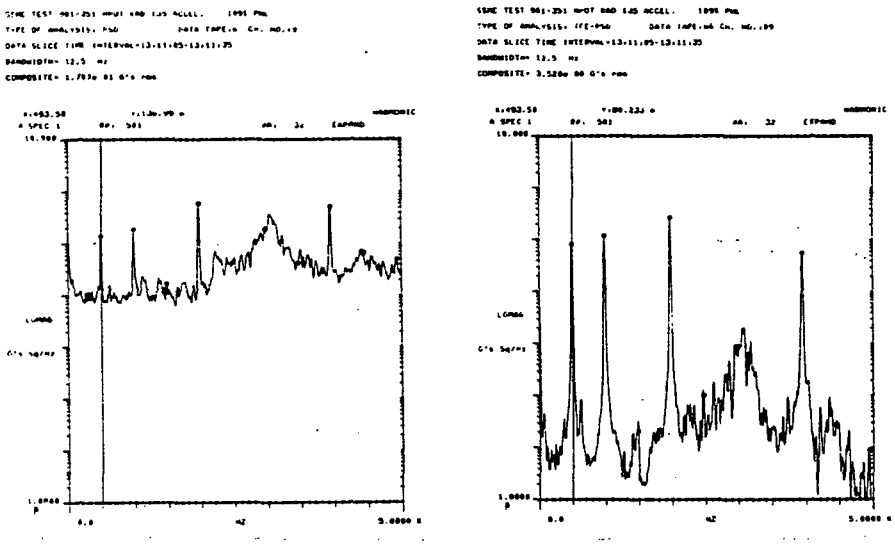

Figure 3-6. Spectrum of SSME turbopump measurement before and after adaptive filtering

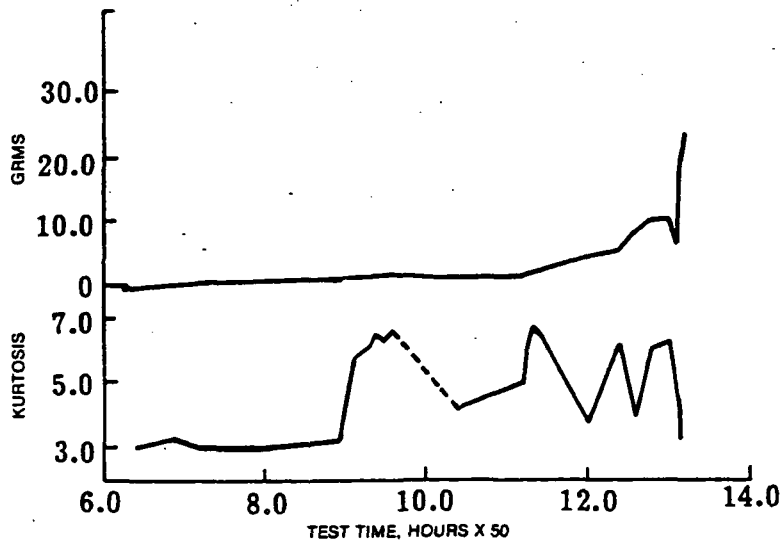

Figure 3-7. Variation of acceleration and kurtosis coefficient with test time (14)

SECTION IV

SOME ADVANCED METHODS RECENTLY APPLIED TO SSME DIAGNOSTIC EVALUATION

4.1 The Maximum Entropy Method

The power spectral density is one of the basic descriptors for signature analysis in the study of dynamic signals, and has been very useful in determining the mechanical characteristics of moving machinery. The importance of spectral analysis is due to the simplicity of the frequency domain description of a stochastic process, and input/output relations for linear systems.

There is a fundamental trade-off between the frequency resolution and statistical uncertainty in the estimation of the power spectrum. The conventional Blackman-Tukey and Direct FFT method for PSD estimation suffer from "leakage" introduced by truncation of the time series (15). The leakage problem becomes particularly acute if the available data is so limited in length, relative to statistical stability requirements, that no fixed window function can be found to resolve the frequency components of interest.

This leakage problem may be overcome by using the Maximum Entropy Method (MEM). The MEM spectral analysis is a nonlinear, data adaptive method which is capable of generating higher resolution spectral estimates from relatively shorter data records than conventional techniques. This ability to use shorter data records can be an important consideration where stationarity or logistics of data collection are a problem. Because MEM is data adaptive it does not suffer from the severe "bias versus variance" trade-off due to finite record length requirements of conventional methods. A trade-off does occur, however, in terms of increased spectral resolution versus computation time, since the procedure is data adaptive.

Entropy is a measure of the average information content contained in a signal. (A Gaussian wave has the maximum entropy of any signal with the same variance.) Maximizing entropy therefore is tantamount to maximizing the information transmitted in a signal. The basic idea of MEM is to estimate the spectrum which corresponds to the most random (i.e. "whitened") time series whose extended autocorrelation function satisfies the constraint that it agree with the limited available known values. This condition is equivalent to an extrapolation of the autocorrelation function of the available time series by maximizing the entropy. Thus, MEM differs

from the conventional linear methods of spectral analysis in that it avoids such severe assumptions as periodic extension of the data or that the data outside the available record length is zero.

It is recalled that the Blackman-Tukey method computes PSD as the Fourier Transform of the autocorrelation function estimated from finite duration time series. The extension of the autocorrelation function which MEM achieves can be viewed as the result of fitting a special model to a finite observation of the autocorrelation function. This model provides the analytic means for extrapolating from "p+1" samples of a known autocorrelation function R(k), k=0, 1, . . . p, to estimate the remaining values, R(k), k=p+1 . . . . It is this extension of the autocorrelation function that provides improved resolution in the final spectral estimate. In a superb development, (16) it has been demonstrated that the maximum entropy extension of the autocorrelation function is given by the following pth order recursion equation:

$$R(k) = -A1\ R(k-1) - A2\ R(k-2) - \ldots - Ap\ R(k-p);\ k>0$$

The parameters {A} are obtained as the solution of the Yule-Walker equation:

$$\begin{bmatrix} R(0) & R(1) & R(2) & \cdot & \cdot & R(p-1) \\ R(1) & R(0) & R(1) & \cdot & \cdot & R(p-2) \\ R(2) & R(1) & R(0) & \cdot & \cdot & R(p-3) \\ \cdot & \cdot & \cdot & \cdot & \cdot & \cdot \\ \cdot & \cdot & \cdot & \cdot & \cdot & \cdot \\ \cdot & \cdot & \cdot & \cdot & \cdot & \cdot \\ R(p-1) & R(p-2) & R(p-3) & \cdot & \cdot & R(0) \end{bmatrix} \begin{bmatrix} A1 \\ A2 \\ A3 \\ \cdot \\ \cdot \\ \cdot \\ Ap \end{bmatrix} = - \begin{bmatrix} R(1) \\ R(2) \\ R(3) \\ \cdot \\ \cdot \\ \cdot \\ R(p) \end{bmatrix}$$

Thus, if given p+1 lags of an autocorrelation function, one can uniquely define the pth order MEM coefficients A1, . . . , Ap and subsequently generate the extended autocorrelation.

The infinite duration autocorrelation function determined as above provides an appealing conceptual framework for MEM. In practice, however, one need never actually compute the extended function in the course of determining the PSD. Instead, it can be shown that the pth order MEM spectrum is uniquely defined as:

$$S(f) = 2\,\sigma_p^2 \Delta \,/\, \left| \{1 - \sum_{k=1}^{p} A_k \exp\left[-j\,2\pi\,k\,f\Delta\right]\} \right|^2$$

where:

A_k are the MEM coefficients, and

$$\sigma_p^2 = R(0) - \sum_{k=1}^{p} A_k R(k)$$

Δ is the sampling increment in seconds.

A computer simulated time series was generated to demonstrate the high resolution capability of MEM. A 1024 point time series was generated which consists of two closely spaced sinusoidal components plus Gaussian white noise. The frequency of the two sinusoids was 1499 and 1501 Hz, sampling frequency was 5000 Hz. Figure 4-1 shows the comparison between the zoom transform PSDs calculated by direct FFT and MEM with 500 poles. The superior capability of the MEM to resolve these two close peaks is clearly illustrated.

To further illustrate practical application of the method, some SSME vibration test data were analyzed. Figure 4-2 shows the comparison between MEM and FFT spectrum estimation of a high pressure oxidizer turbopump measurement from SSME test 901-471 at t=76 seconds. The numbers of data points used were 8, 32 and 128 samples respectively, with a sample rate of 5120 Hz. This figure clearly shows the improved resolution of MEM when the sample length is restricted.

4.2 Higher Order Spectrum Analysis

Spectral peaks at the fundamental rotating frequency and its harmonics in rotational systems may indicate machinery malfunction such as misalignment, imbalance, bent shaft, rubbing and whirl (17). Frequency sum and difference of these spectral components is another important indication of degradation. When one frequency amplitude modulates another frequency, sum and difference frequencies are generated. Examples of this signal include a gear mesh frequency modulated by the speed of one or both gears and a ball pass frequency modulated by the ball spin frequency. A pulse yields a series of spectral lines whose difference frequency is equal to the repetition rate of the pulse. Impacts due to bearing component wear can generate such pulse response. All these signals represent nonlinear phenomena since the spectral components at different frequencies are not independent. The nonlinearities in such signals can thus be identified as symptoms of possible failure modes. However, due to the lack of phase information, conventional linear spectral analyses

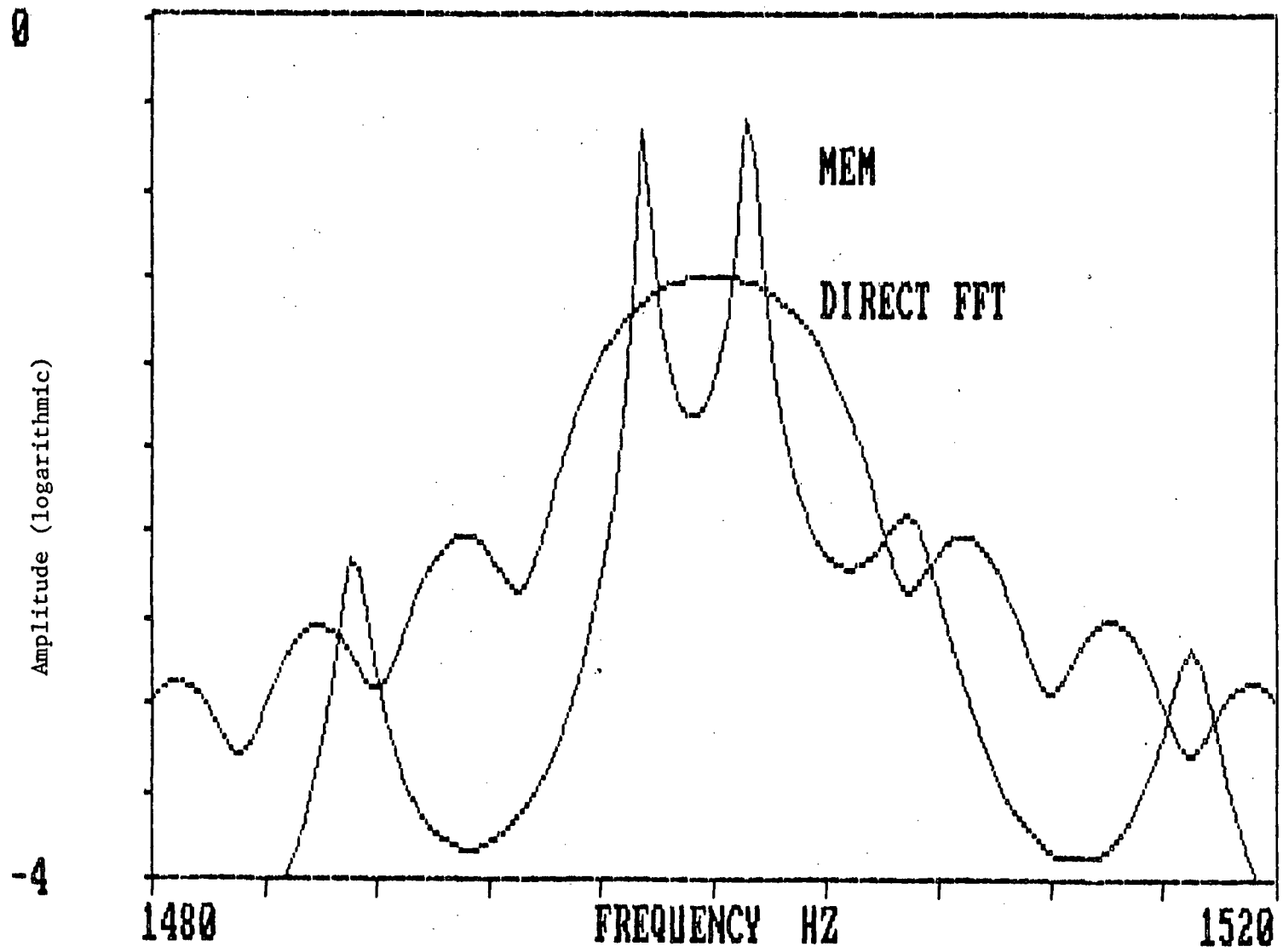

Figure 4-1 Power Spectrum Estimate for One 1024 Point Data Sample by FFT and MEM Techniques

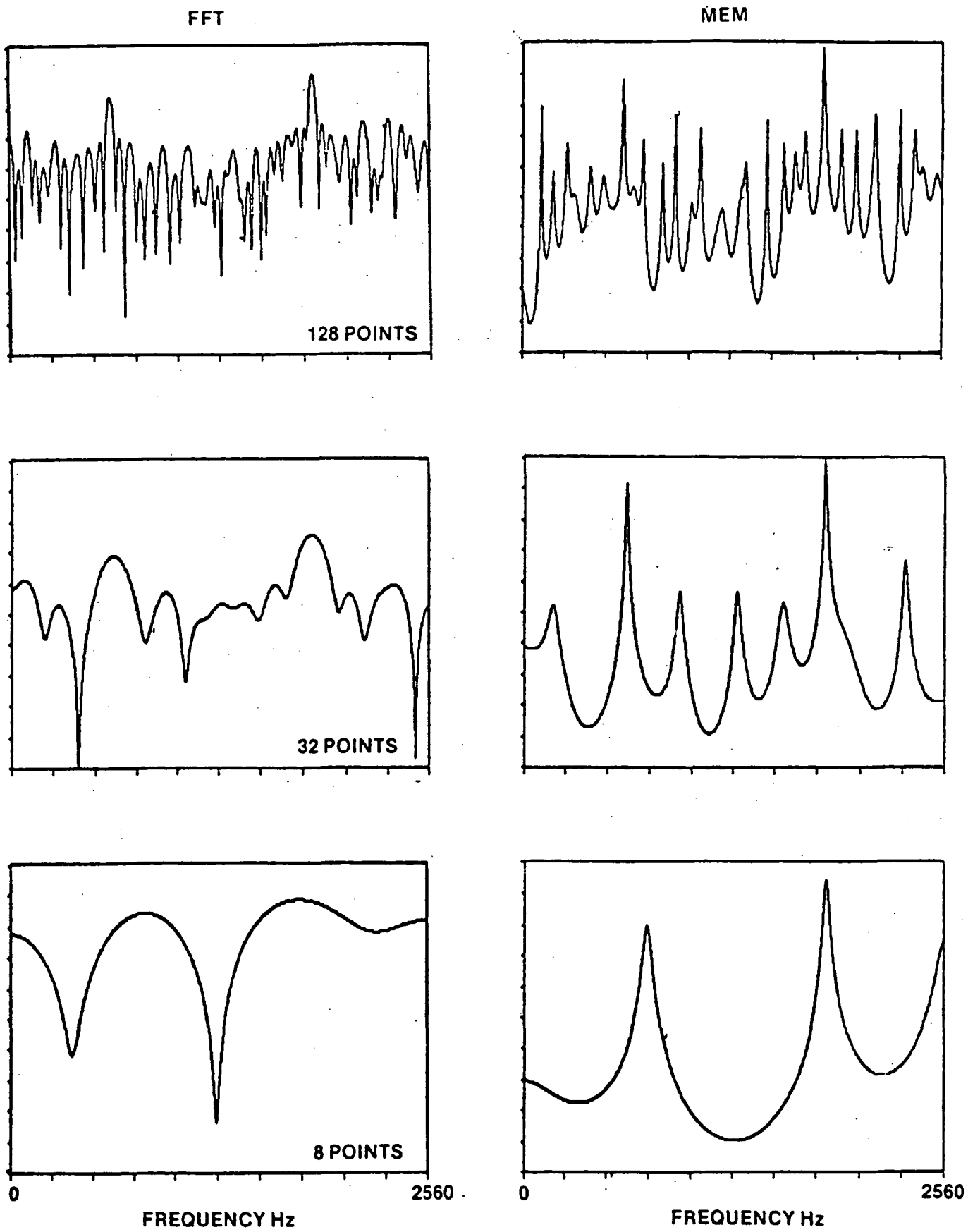

Figure 4-2. Comparison Between FFT and MEM Spectrum for Limited Sample Size

are not able to detect such nonlinear correlation. Therefore, a higher order nonlinear spectral analysis method is required in order to provide insight concerning these nonlinear time series and associated equipment condition.

For a stationary, random time series x(t), the nth order cumulant function is: (18)

$$Cn\ (U1, U2, \ldots, Un\text{-}1) = C\ [x(t)\ x\ (t+U1) \ldots x(t+Un\text{-}1)\ ]$$

where

C [.] represents a cumulant average.

The Fourier representation of Cn (U1, U2, . . . , Un-1) is:

$$F_n(f_1 \ldots f_{n-1}) = \lim_{T\to\infty} \frac{1}{T^{n-1}} \int_{-T/2}^{T/2} \ldots \int_{-T/2}^{T/2} C_n(\tau_1 \ldots \tau_{n-1}) \exp\left[i \sum_{j=1}^{n-1} \omega_j \tau_j \right] d\tau_1 \ldots d\tau_{n-1}$$

Fn is the nth order cumulant spectrum.

It can be shown that (19):

$$C\ [X(f1), X(f2), \ldots, X(fn)\ ] = Fn(f1, f2, \ldots, fn\text{-}1) \qquad \delta\ (\sum_j fj)$$

The above states that cumulant average of the Fourier amplitudes of x(t) will be zero except when their sum frequency vanishes. However, if the waves at frequencies f1, f2, . . . , fn can be divided into statistically independent groups, the cumulant spectrum will be zero even though their sum frequency is zero. Therefore, the cumulant spectrum can be used to identify whether the spectral components at different frequencies are correlated or not.

Let x(t) be a zero mean stationary time series, the auto-bispectrum B(fj, fk) is:

$$
\begin{aligned}
Bxxx(fj, fk) &= C[X(fj)\, X(fk)\, X^*(fj+fk)] \\
&= E[X(fj)\, X(fk)\, X^*(fj+fk)] - E[X(fj)\, X(fk)]\, E[X^*(fj+fk)] \\
&\quad -E[X(fj)\, X^*(fj+fk)]\, E[X(fk)] - E[X(fk)\, X^*(fj+fk)]\, E[X(fj)] \\
&\quad +2\, E[X(fj)]\, E[X(fk)]\, E[X^*(fj+fk)] \\
&= E[X(fj)\, X(fk)\, X^*(fj+fk)]
\end{aligned}
$$

The auto-bicoherence, a normalized auto-bispectrum, b(fj,fk) is defined as:

$$
bxxx(fj,fk) = \frac{| Bxxx(fj,fk) |}{\{ E[\, | X(fj)\, X(fk) |^2]\; E[\, | X(fj+fk) |^2] \}^{1/2}}
$$

By using Schwarz' inequality, it can be shown that the auto-bicoherence b(fj,fk) is bounded by zero and unity. If the wave at fj+fk is correlated to the waves at fj and fk, the auto-bicoherence will equal unity. On the other hand, if these three waves are independent quadratically, the auto-bicoherence will be zero.

Let x(t) and y(t) be two zero mean jointly stationary time series, the cross-bispectrum Bxxy(fj,fk) between x(t) and y(t) is:

$$
Bxxy(fj,fk) = C[\, X(fj)\, X(fk)\, Y^*(fj+fk)\,]
$$

The cross-bicoherence bxxy(fj,fk) between x(t) and y(t) is:

$$
bxxy(fj,fk) = \frac{| Bxxy(fj,fk) |}{\{ E[\, | X(fj)\, X(fk) |^2]\; E[\, | Y(fj+fk) |^2] \}^{1/2}}
$$

In addition to the above discussed capabilities of bi-spectral analysis in identifying nonlinear correlation between different spectral components, another advantage exists in its noise cancellation capability. Notice that an independent noise signal is linear since its waves at different frequencies are all independent. Therefore, in the estimation of the bispectrum, only those spectral components which are quadratically correlated will be detected, while noise components will be rejected. In a real situation, the vibration signals are masked by the high level background noise. Linear spectral analysis is affected directly by additive noise since the noise itself is also linear.

Computer simulation was performed to illustrate the utility of bi-spectral analysis which represents the response of a rotating shaft as a result of whirl and the effect of waveform clipping due to rubbing. Figure 4-3a shows the displacement of a clipped sine wave at frequency 625 Hz. The wave was clipped at 50% amplitude in one direction. This signal was then amplitude modulated by another sine wave at a lower (whirl) frequency W=110 Hz as shown in Figure 4-3b. Figure 4-4 depicts the PSD of the acceleration (second derivative of the displacement) of this modulated, clipped sine wave. The PSD shows strong peaks at N=625 Hz and its harmonics 2N, 3N, 4N . . . due to the waveform truncation. In the vicinity of each harmonic, a pair of sideband components of smaller amplitude due to the modulated wave are also observed. This signal was distorted by addition of independent Gaussian white noise as shown in Figure 4-5, where the sideband peaks have become difficult to identify. It should be emphasized that even though the original sideband amplitudes are low, they have significant implication with respect to rotational stability. Therefore it is desirable to identify whether a small peak near the synchronous speed or its harmonics, is indeed a true sideband or it is from an independent source, such as a case resonance. The waves from independent sources are independent of the waves associated with rotational components, while sideband components are quadratically correlated with them. Therefore the bispectral analysis was applied to identify whether an apparent sideband is statistically correlated with the rotational components.

Figure 4-6 shows the auto-bicoherence function of the modulated clipped sine wave with the first frequency fixed at N+W, i.e. b(N+W, f). The peaks at b(N+W, N-W) and b(N+W, N) indicate that there exists a quadratic correlation among (N+W, N-W, 2N) and (N+W, N, 2N+W) respectively. Other peaks in this bi-coherence function also indicate the quadratic correlation among higher harmonics and their sidebands. (Statistically, these correlations do not establish cause, but contribute evidence.) Notice that the bicoherence also provides desirable signal-to-noise enhancement, as previously discussed. From the above example, we can see that bispectral analysis can be used to identify the existence of quadratic correlation among waves. Next, this method is applied to several SSME vibration test measurements.

Figure 4-7 shows the PSD of acccleration from the high pressure fuel pump on test 901-436 at t=211.8 seconds. Spectral components are observed at frequencies N-W,

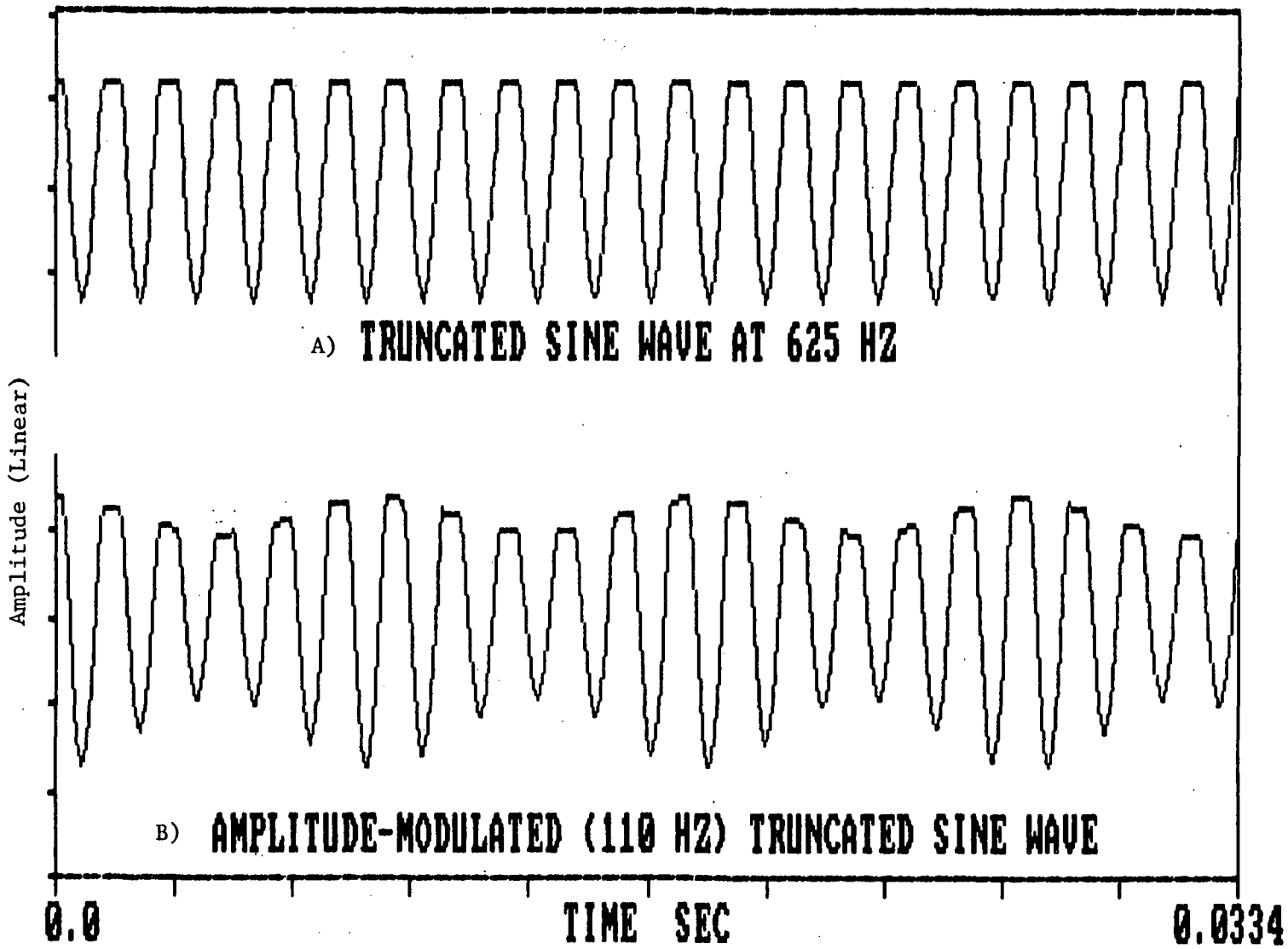

Figure 4-3. Time Slice of Clipped Sine Wave
and Amplitude Modulated Clipped Sine Wave

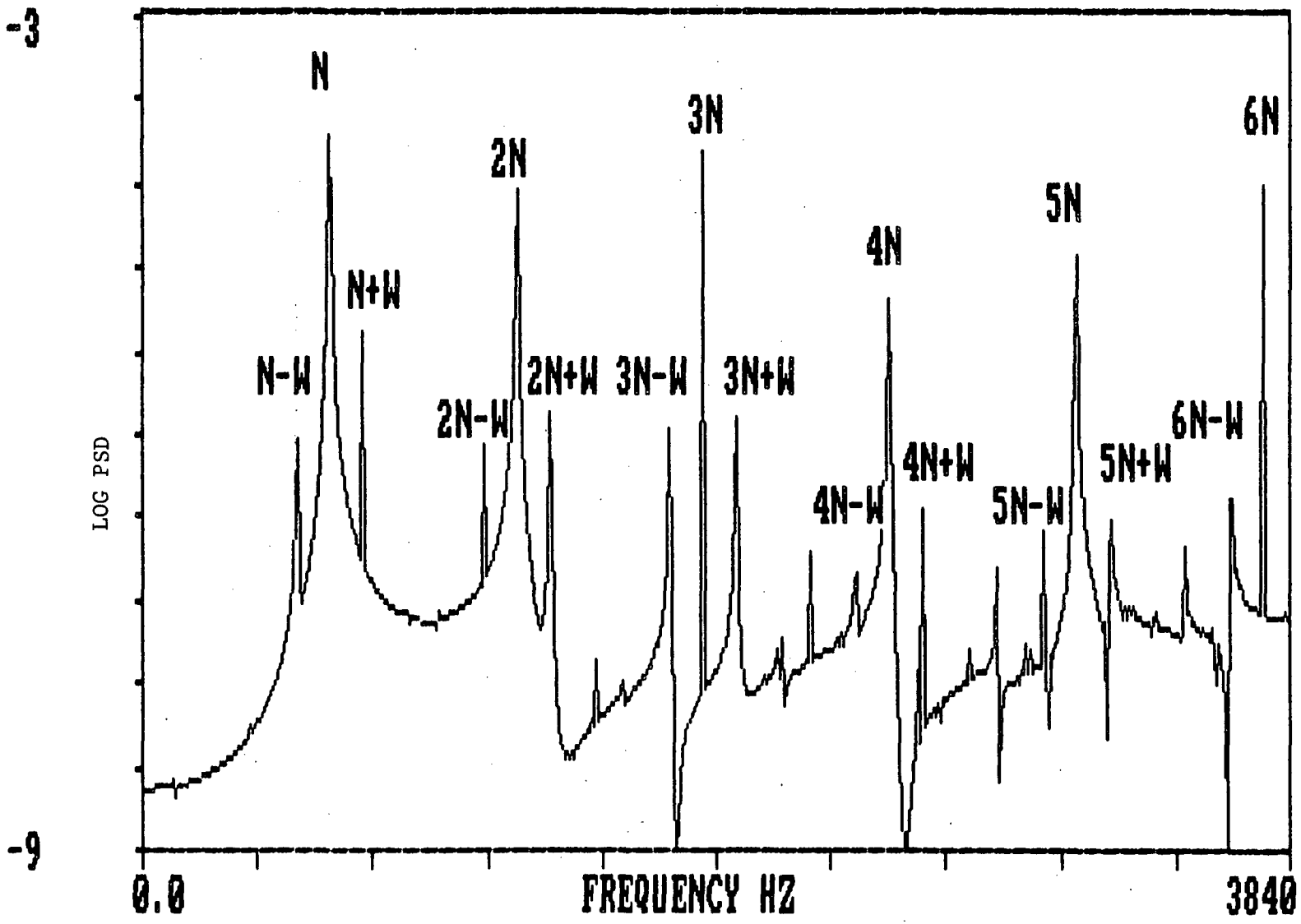

Figure 4-4. PSD of Amplitude-Modulated Truncated Sine Wave (N=625 Hz, W=110 Hz)

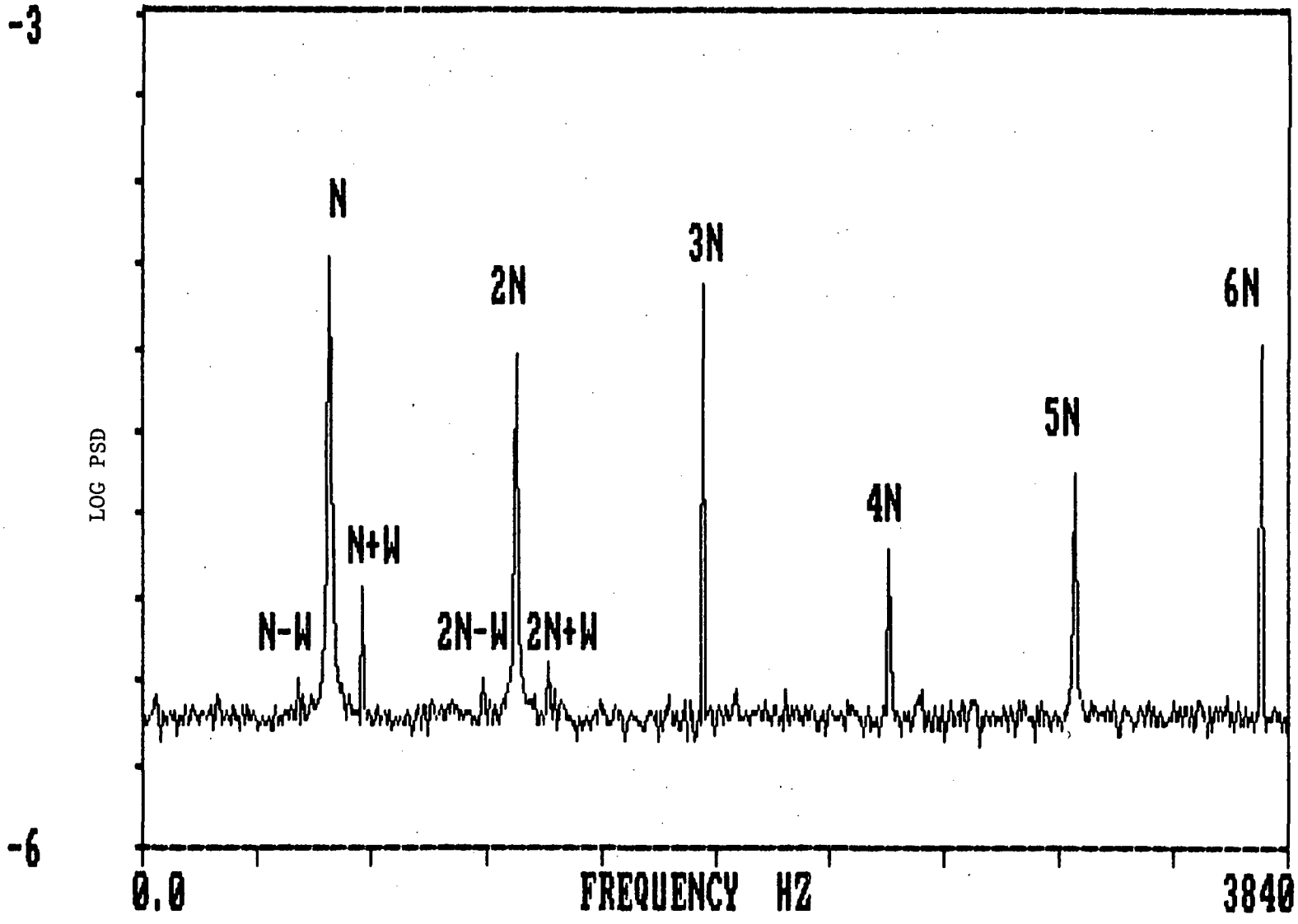

Figure 4-5. PSD of Amplitude-Modulated Truncated Sine Wave + Noise (N=625 Hz, W-110 Hz)

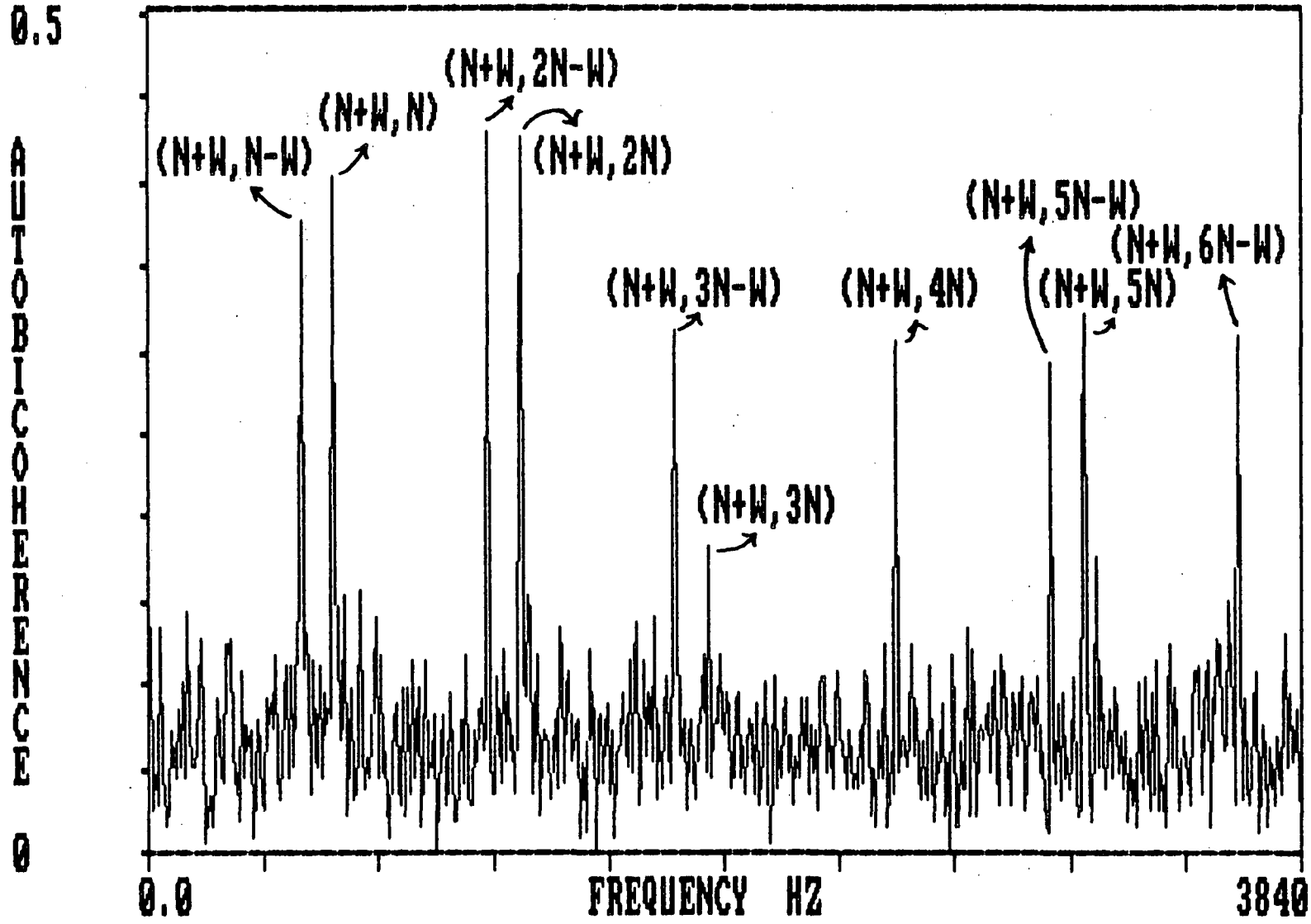

Figure 4-6. Auto-Bicoherence of Amplitude-Modulated Truncated Sine Wave (N=625 Hz, W-110 Hz)

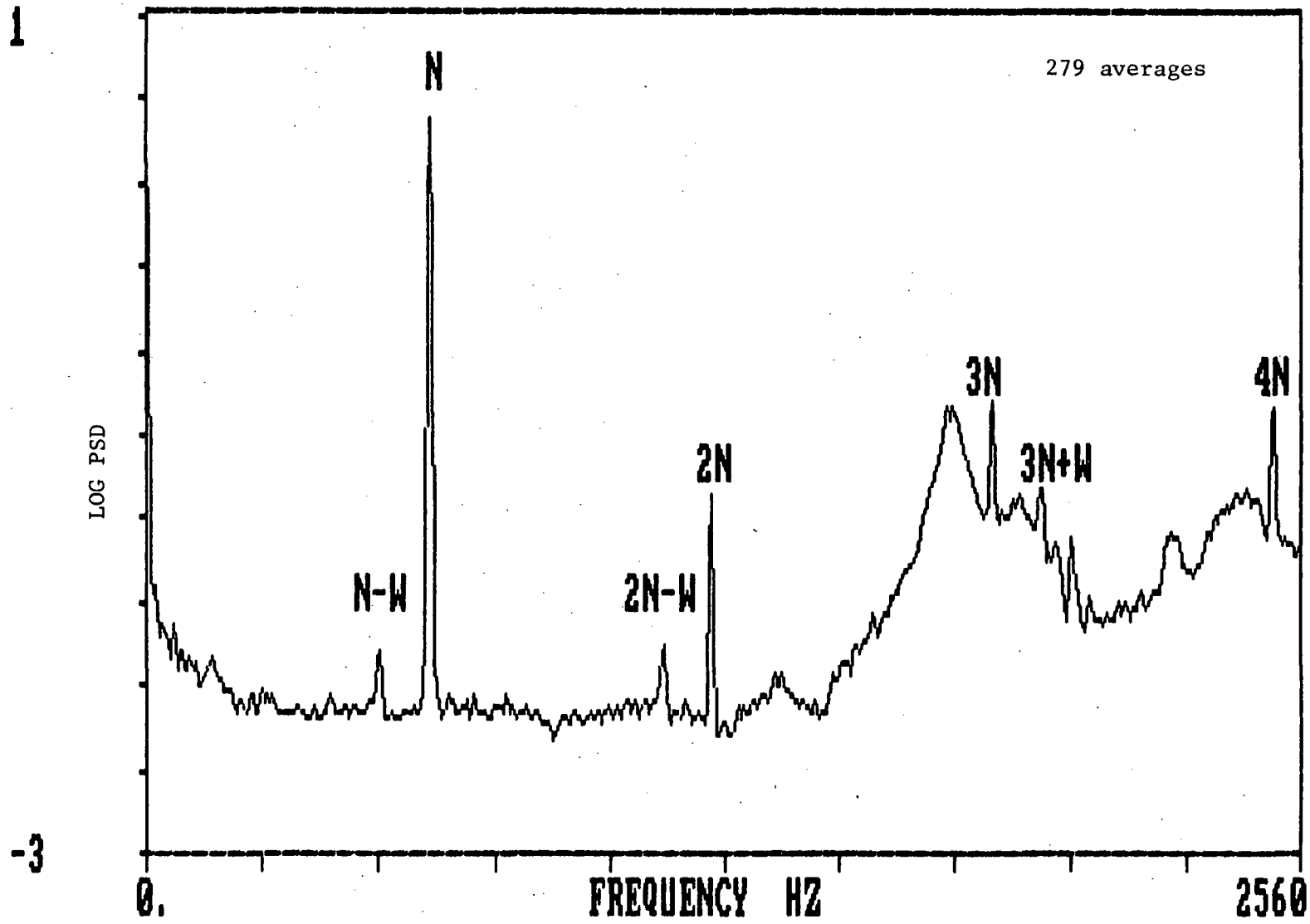

Figure 4-7. PSD of Measurement from SSME Test 901-436 (Start +211.8 Seconds)

2N-W and 3N+W. The question to be answered is: Are these components the related sidebands of the synchronous component and its harmonics or possibly due to independent sources. The auto-bicoherence function shown in Figure 4-8 provides the answer. The peak at b(N-W, N) indicates that the waves at N-W, N and 2N-W are correlated with each other quadratically. The other peak b(N-W, 3N+W) indicates the quadratic correlation among the waves at N-W, 3N+W and 4N. These quadratic correlations suggest that the periodic waveform at the shaft rotational frequency is amplutide modulated (quadratic nonlinearity) by a wave at W=110 Hz. This modulation could indicate whirl or some other abnormality. In fact, engine failure did occur near the end of test 901-436.

4.3 The Hyper-Coherence Spectrum

The harmonic content in measurements from rotating machinery contains much subtle information concerning equipment operational condition and component degradation. For this reason, the power density spectrum (PSD) has long been employed to assess the relative magnitude of contributions. Measurements on high-performance rocket engine turbomachinery suffer from severe noise contamination from numerous extraneous sources, which impedes rotating element diagnostic evaluation. It is thus difficult to determine whether an apparent high-level harmonic contribution is indeed related to the fundamental rotational frequency or possibly due to an independent source. The ordinary PSD is of no assistance to this problem.

As an example, a high level third harmonic in the PSD may represent symptoms such as rubbing, looseness or imbalance. Therefore, such symptoms can be detected by observing the exceeding of a certain level of the PSD 3N amplitude. However, a problem exists with SSME engine test measurements in which some "anomalous" frequency components with high amplitude were observed near or within the observable band of the 3N frequency. This (possibly) anomalous frequency component makes it difficult to determine whether an apparent high-level harmonic contribution is indeed related to the fundamental rotational frequency, or possibly due to an independnet source.

An example of this is shown in Figure 4-9. This figure shows the PSD of a vibration measurement on the high pressure fuel pump from engine test 901-471 calculated from 40 seconds stationary data. A high peak at 3N frequency is observed but was suspected to be from another source from its long term slowly frequency wandering,

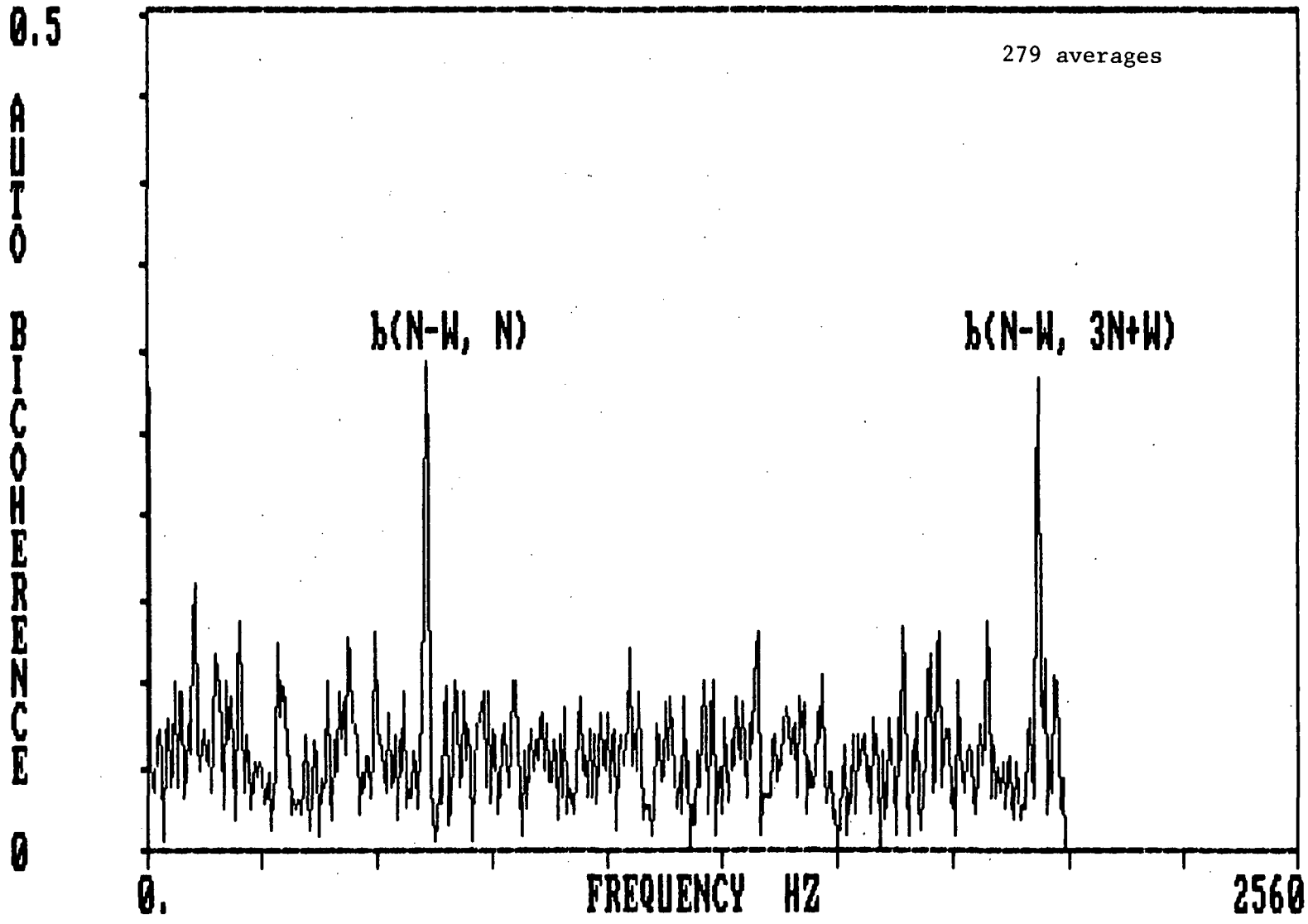

Figure 4-8. Auto-Bicoherence of Measurement from SSME Test 901-436 (Start +211.8 Seconds)

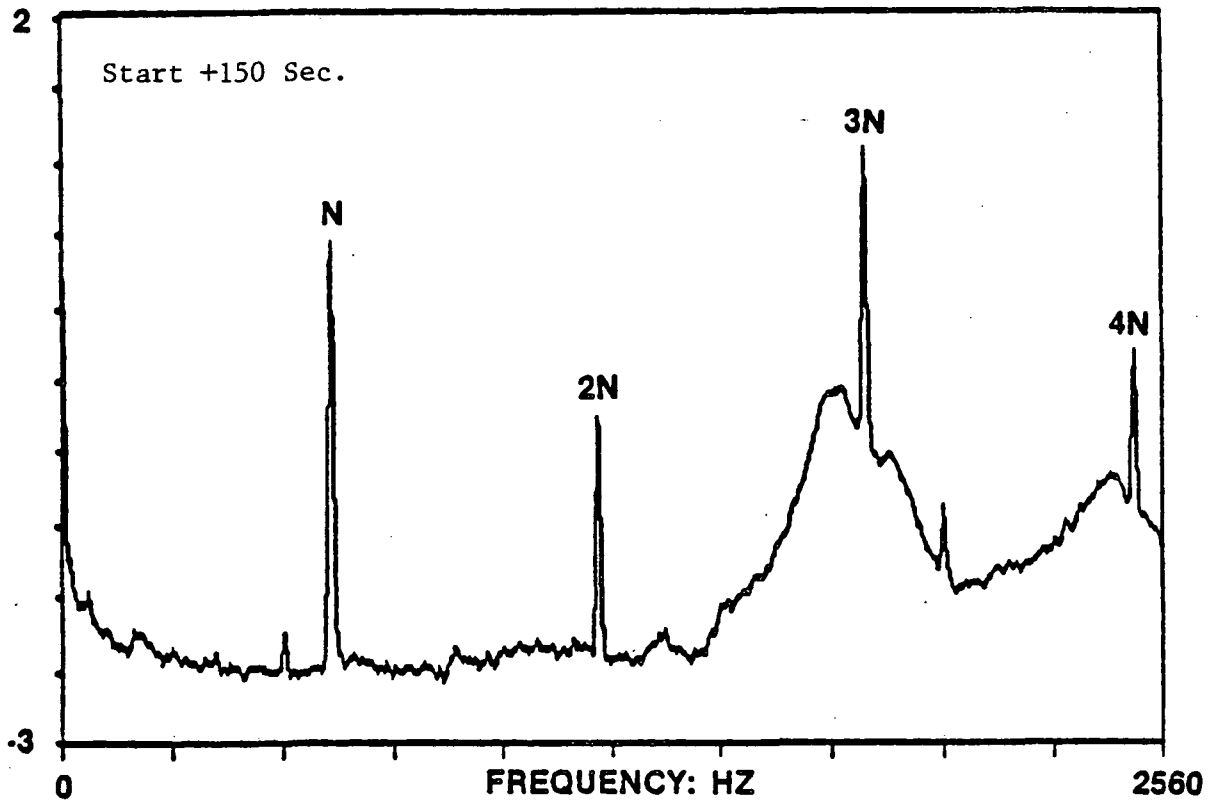

Test 901-436

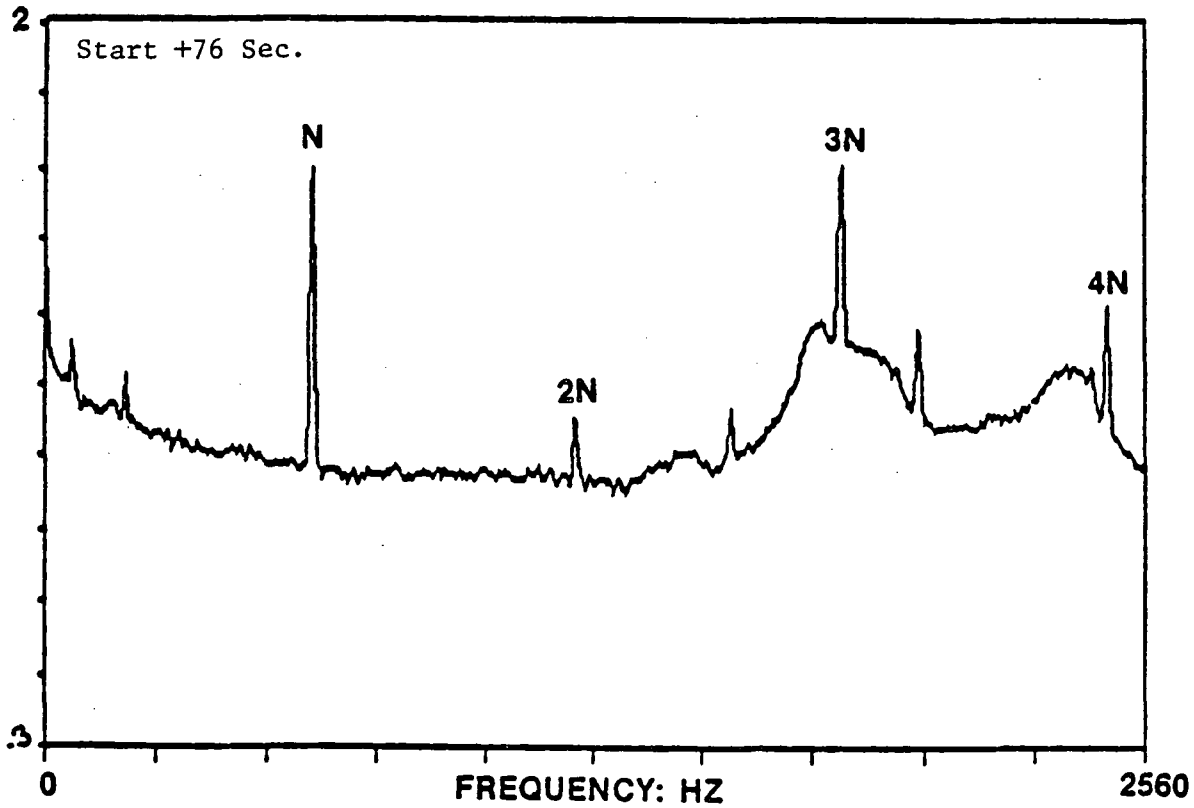

Test 901-471

Figure 4-9. Power Spectra From SSME Turbopump During Two Test Firings

even during constant power operation. Figure 4-9 also shows the PSD of engine test 901-436 calculated from 60 seconds of stationary data which also shows a high amplitude 3N component. The PSD at 3N of these two tests looks almost identical to each other. However, the 3N component observed in test 901-436 is believed to be a true third harmonic instead of an independent frequency component. This problem suggests that a reliable method is required in order to discriminate between independent sources and any true harmonics, since the harmonic components are such an important "defect signature".

The basic approach to this problem is to define the correlation between related sources and those statistically independent of the fundamental rotational frequency (1N) component. The nonlinear correlation between an apparent harmonic and the fundamental frequency component will indicate whether such component is a true harmonic or not (e.g., is correlated with). To achieve this, a unique spectral coherence representation has been recently developed by Wyle, (20) which we call the Hyper-Coherence function, for lack of a better term.

As stated above, the relation between nth order cumulant spectrum Fn(f1, f2, . . . , fn-1) and the Fourier amplitude of x(t) is:

$$Fn\,(f1, f2, \ldots, fn\text{-}1) = C[X(f1)\,X(f2) \ldots X(fn\text{-}1)\,X(-f1\text{-}f2\text{-}\ldots\text{-}fn\text{-}1)]$$

The hyper-coherence function is defined as:

$$J^2(fn;fr) = \frac{|\,Fn(fr,fr,\ldots fr)\,|^2}{\{\,E\,|\,X^n(fr)\,|^2\;E\,|\,X(fn)\,|^2\,\}}$$

$$= \frac{|\,C\,[X^n(fr)\,X(-fn)]\,|^2}{\{\,E\,|\,X^n(fr)\,|^2\;E\,|\,X(fn)\,|^2\,\}}$$

The cumulant average C[ab] = E[ab] - E[a] E[b]. Therefore:

$$J^2(fn;fr) = \frac{|\,E[X^n(fr)\,X(-fn)]\,|^2}{E\,[\,|\,X^n(fr)\,|^2\,]\;E\,[\,|\,X(fn)\,|^2\,]}$$

Let x(t) be a zero-mean stationary time series, and assume the wave at frequency fr be defined as signal (no noise). If the wave at frequency fn is composed of two parts, A and B, if p% of the power at fn is totally correlated with the wave at fr and the rest, 1-p%, is independent of it, then let

$$X(fn) = A(fn) + B(fn)$$

$$Saa(fn)/Sxx(fr) = p\% \text{ and } Sbb(fn)/Sxx(fr) = 1-p\%$$

The hyper-coherence square becomes

$$J^2(fn;fr) = \frac{| E [X^n(fr) A(-fn)] + E [X^n(fr) B(-fn)] |^2}{E [| X^n(fr) |^2] \; E [| X(fn) |^2]}$$

In this equation,

$$E[X^n (fr) B(-fn)] = 0$$

since B(fn) is independent of X(fr). Since A(fn) is totally correlated with X(fr), the relative phase lag between X^n (fr) and A(-fn), is a constant instead of a random variable.

In this case:

$$| E [X^n(fr) A(-fn)] |^2 = E [| X^n(fr) |^2] E [| A(fn) |^2]$$

Then, the above becomes

$$J^2(fn;fr) = \frac{Saa(fn)}{Sxx(fn)} = p\%$$

This equation indicates that hyper-coherence square J^2(fn,fr) represents the percentage of power at fn which is correlated with the wave at fr. Therefore, it provides a valuable tool to discriminate between harmonic interactions, and independent sources.

It should be emphasized that the hyper-coherence concept can be applied to define the degree of correlation between arbitrary harmonics.

To further demonstrate the utility of the hyper-coherence spectrum, two digital time series were generated and analyzed. A first time series, x(t), was generated consisting of a unity amplitude square wave of frequency fr=300 Hz plus independent Gaussian white noise. A second time series, y(t), was formed which was equal to x(t) plus a sine wave at 3fr=1500 Hz with unit amplitude and uniformly distributed random phase. Thus, the 3fr in x(t) is totally correlated with fr, while the 3fr in y(t) is only partially correlated to fr. Figure 4-10a and 4-10b illustrate the PSDs of x(t) and y(t), respectively. Figure 4-11a and 4-11b depict the hyper-coherence spectrum J^2(fn; 300 Hz) for x(t) and y(t) with reference frequency 300 Hz. In Figure 4-11a, J^2(900,300) = 0.99 indicating that all the power at 900 Hz is correlated with the wave at 300 Hz in x(t) except for the small independent noise component. On the other hand, from Figure 4-11b, J^2(900; 300)=0.2 since only about 20% of power at 3*fr is correlated with fr, the remainder, of course, being associated with the independent sine wave and Gaussian noise. The hyper-coherence function is thus shown to be of significant practical value in the diagnostic evaluation of harmonically related frequency component pairs.

This technique was next applied to the above mentioned two engine tests, 901-471 and 901-436, as shown in Figure 4-9. The PSD amplitudes at 3N frequency are very high for both tests and are considered to be a failure symptom. Figures 4-12A and 4-12B depict the hyper-coherence functions of test 901-436 and 901-471 with reference frequencies at the rotational frequencies 625 Hz and 620 Hz, respectively. In Figure 4-13a, J^2(3N; N) = 0.97 indicating that almost all the power at 3N is correlated with the rotational frequency component and is (quite possibly) a true third harmonic. On the other hand, J^2(3N; N) = 0.17 in Figure 4-12b indicates that most of the power at 3N is due to some other uncorrelated event. Therefore, the apparent high level 3N in test 901-471 may be a false symptom of engine failure.

Anomalous frequency components have been observed to appear intermittently. Therefore, it is difficult to identify whether a spectral component observed at some particular time interval is still the same component the next moment, since the anomalous frequency component could possibly appear and coincide with the

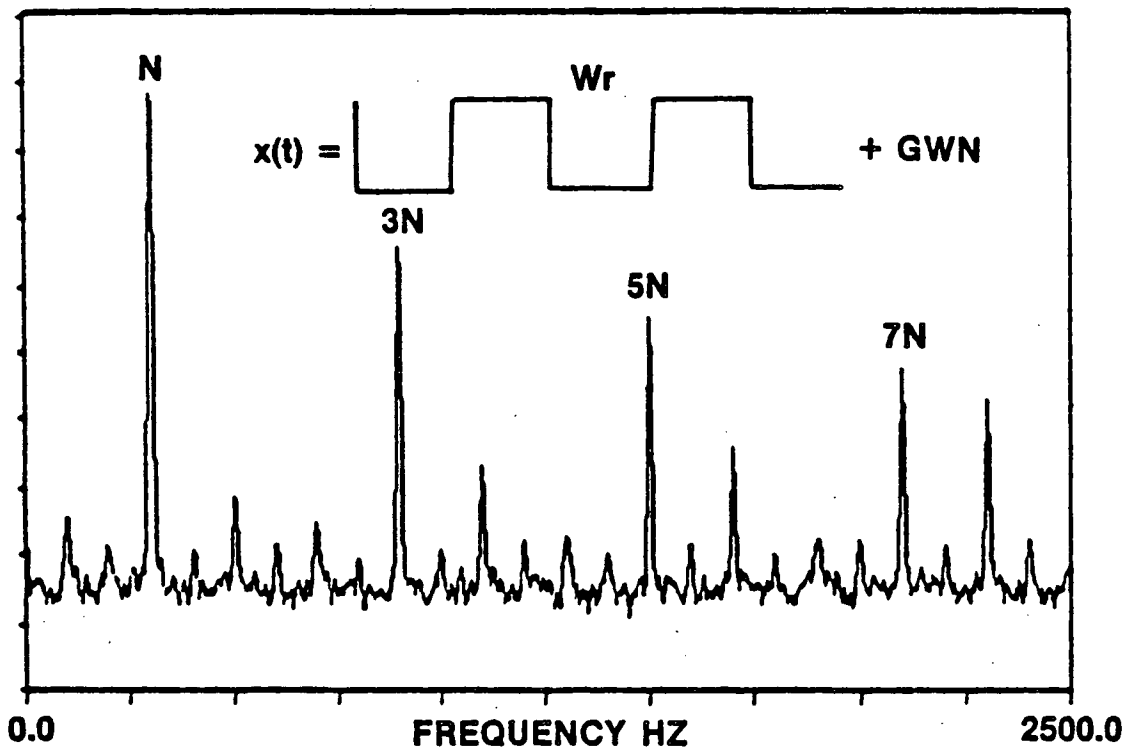

A) Power Spectrum of Square Wave + Noise

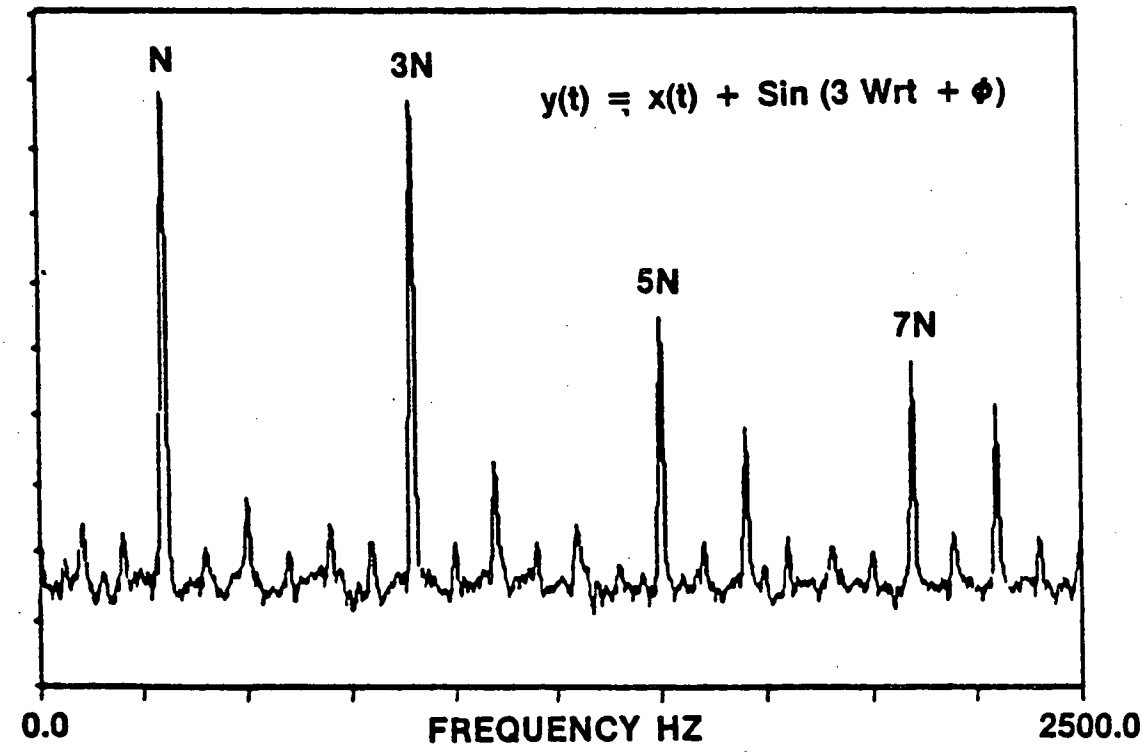

B) Power Spectrum of Square Wave + Uncorrelated Sine Wave + Noise

Figure 4-10. Power Spectra for Two Simulated Time Series

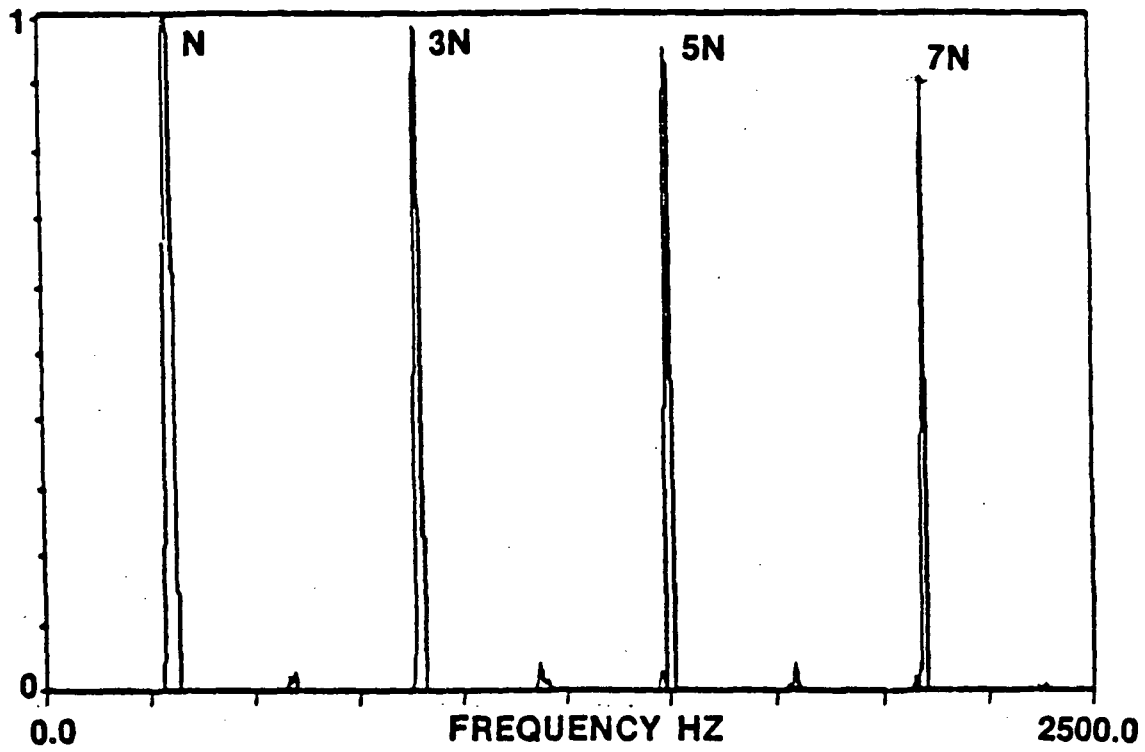

A) Hyper-Coherence Spectrum of Square Wave + Noise

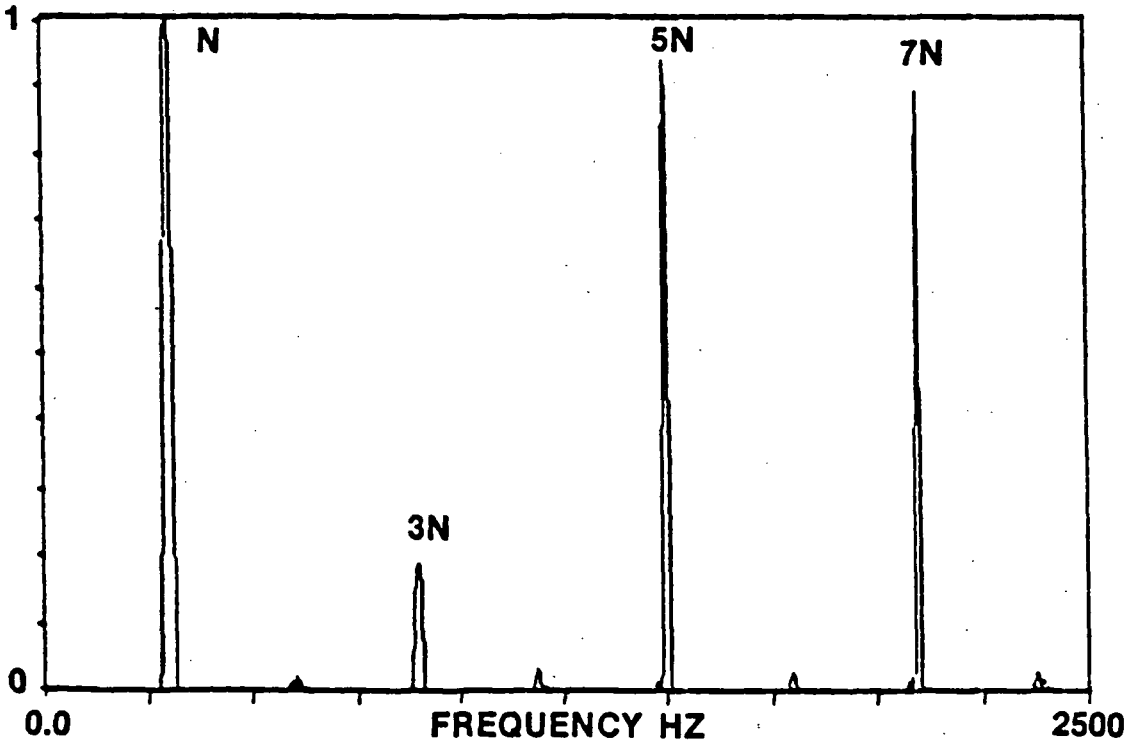

B) Hyper-Coherence Spectrum of Square Wave + Uncorrelated Sine Wave + Noise

Figure 4-11. Hyper-Coherence Spectra of Two Simulated Time Series

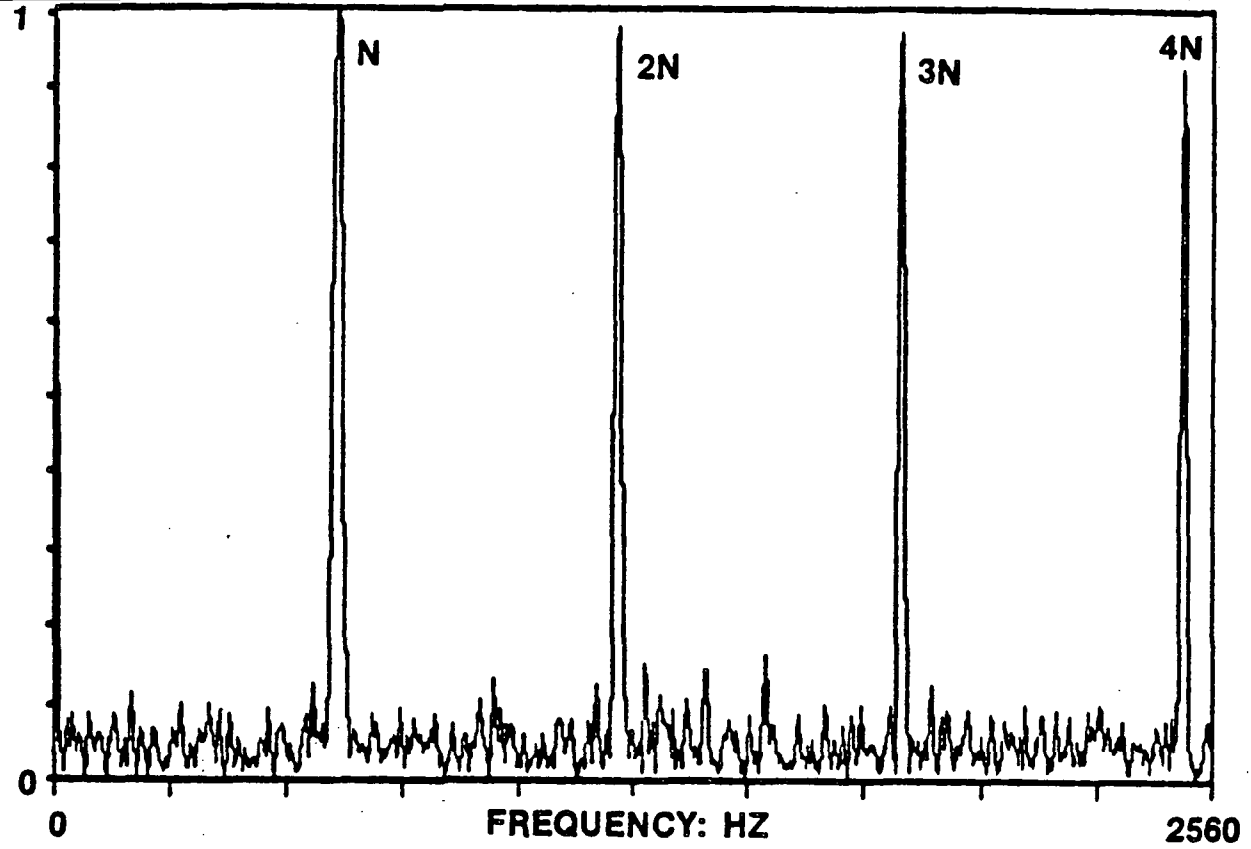

A) T = S + 150 Seconds

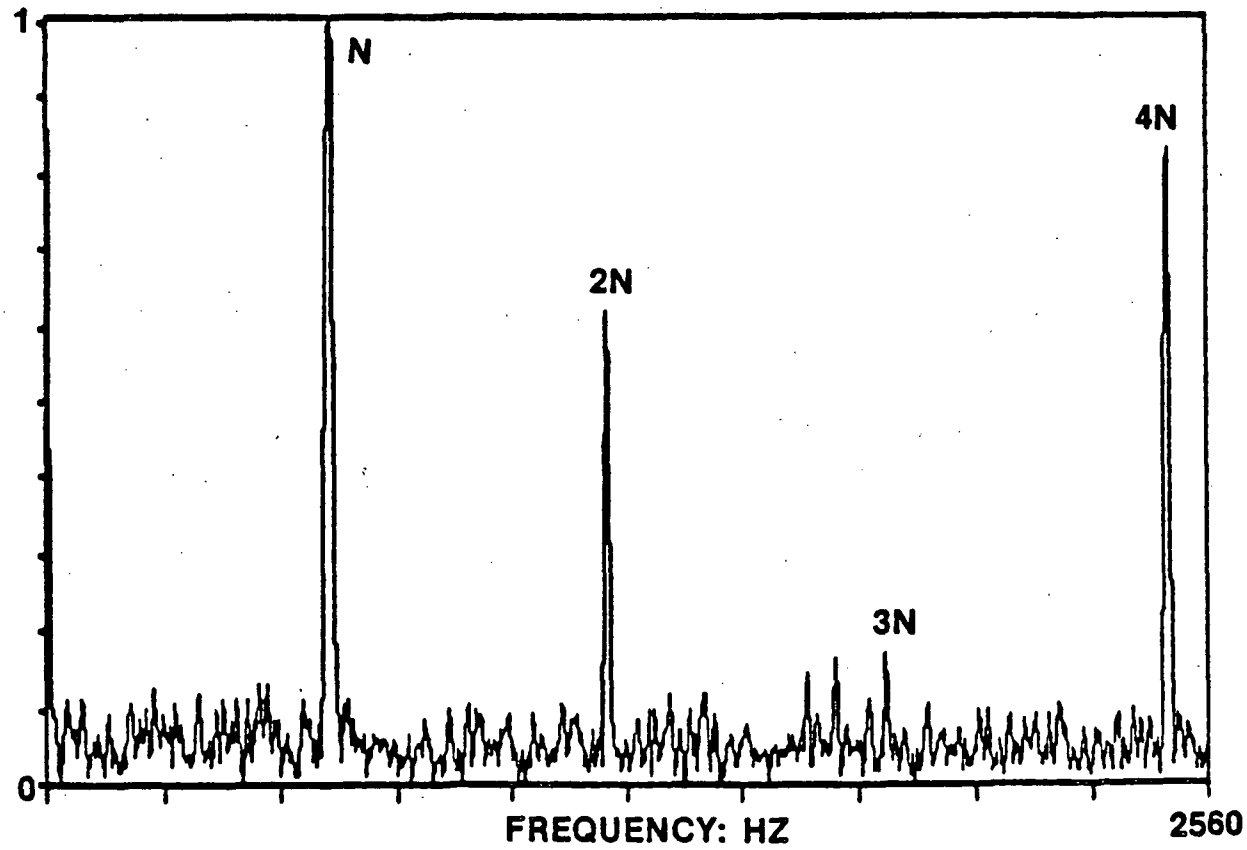

B) T = S + 211.8 Seconds

Figure 4-12. Hyper-Coherence Spectra of Turbopump Measurement from Test 901-436

original observed component. An example of this is shown in Figure 4-13 which is the PSD isoplot for test 901-471 from time t=40.8 seconds to t=120.8 seconds with power level at 100% and 109%. At power 100%, the 3N level is low and is separated from the anomalous frequency component. As the power level was brought up to 109%, at t=75.5 seconds, only one high component is resolved, at 3N frequency. Now the question is whether this high peak is a true third harmonic or is an anomalous frequency component shifted to the 3N frequency and coincident with the third harmonic. If it is a true third harmonic, it would be considered to be a failure symptom because of its high level PSD. Figure 4-14 shows the hyper-coherence function before and after the power level was brought up to 109%, respectively. At power level 100%, even though the 3N level is low, it still exhibits a degree of correlation. But at power level 109% only a small degree of correlation is shown even though the third harmonic level becomes much higher. This indicates that the original "apparent" harmonic frequency component at power level 100% merges into the third harmonic. Therefore, the high level 3N could be a false failure symptom.

Figure 4-15 is the PSD isoplot of the same high pressure turbopump measurement from SSME test 901-436 from time t=150 seconds to 4=273.6 seconds, at constant power level. Originally the 3N level was quite significant. At t=212 seconds, it diminished into a much lower level. This behavior prompted the question whether or not there was an independent frequency component in the neighborhood of the third harmonic, or not. If it is the case, then the high level 3N might just be a false symptom.

Figure 4-16 illustrates the hyper-coherence function before and after the 3N level diminished. Both hyper-coherence functions at 3N frequency remain high before, and after 3N diminishes. This indicates both the high level and low level 3N component are true third harmonic, (or, at least, correlated with engine speed). Therefore, the high level 3N is a true symptom instead of an anomalous frequency component.

As mentioned before, if the wave at 1N is totally correlated with the wave at 3N, then the relative phase difference between them, 3PS(N)-PS(3N), should be a constant instead of an uniformly distributed random variable between $-\pi$ and π. Figure 4-17 is this relative phase lag from t=150 to t=267.6 seconds, which illustrates that this phase lag is by no means an uniformly distributed random phase both before and after the 3N component diminished. An apparent constant mean phase can be

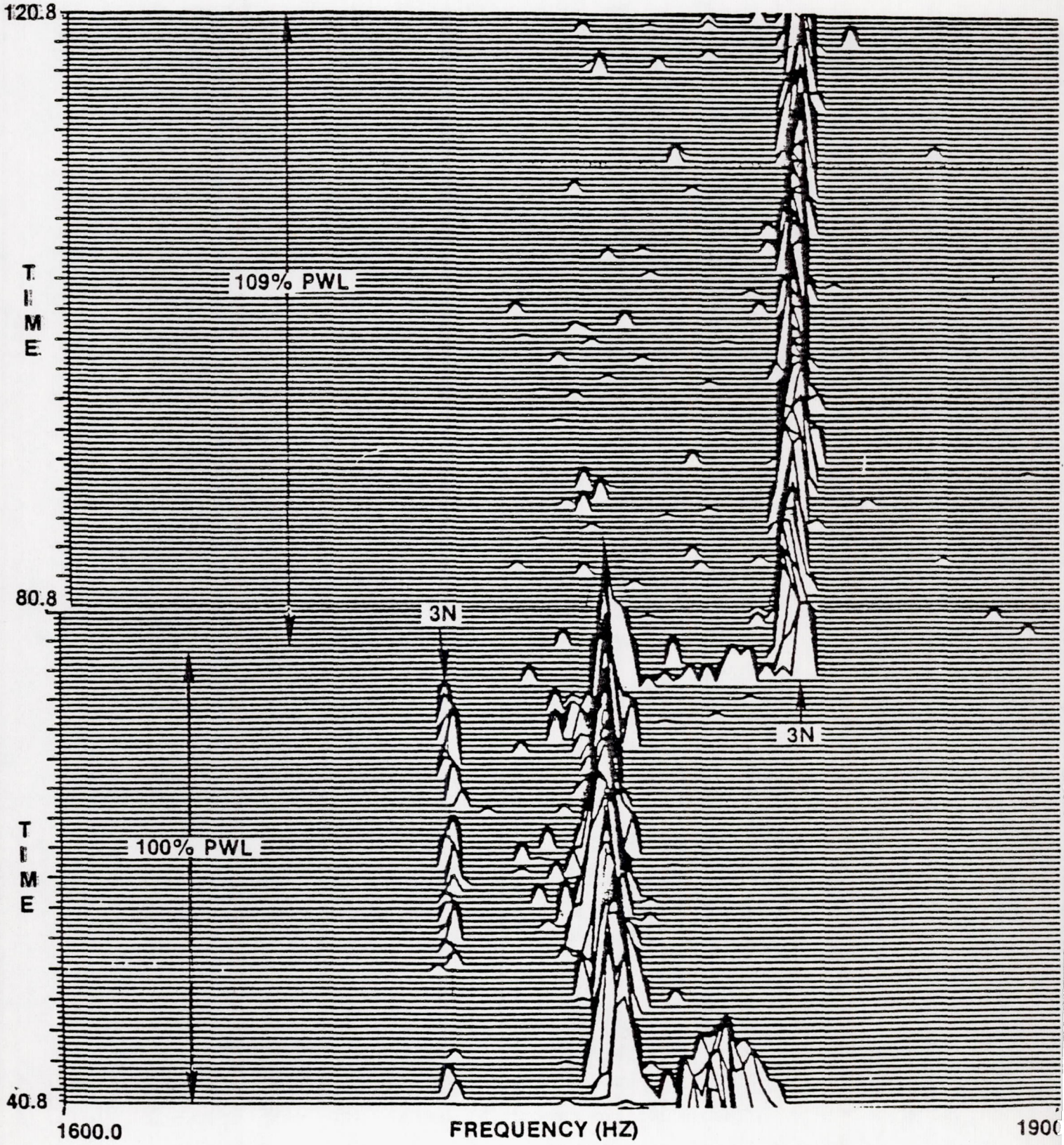

Figure 4-13. Isoplot of Measurement from Test 901-471

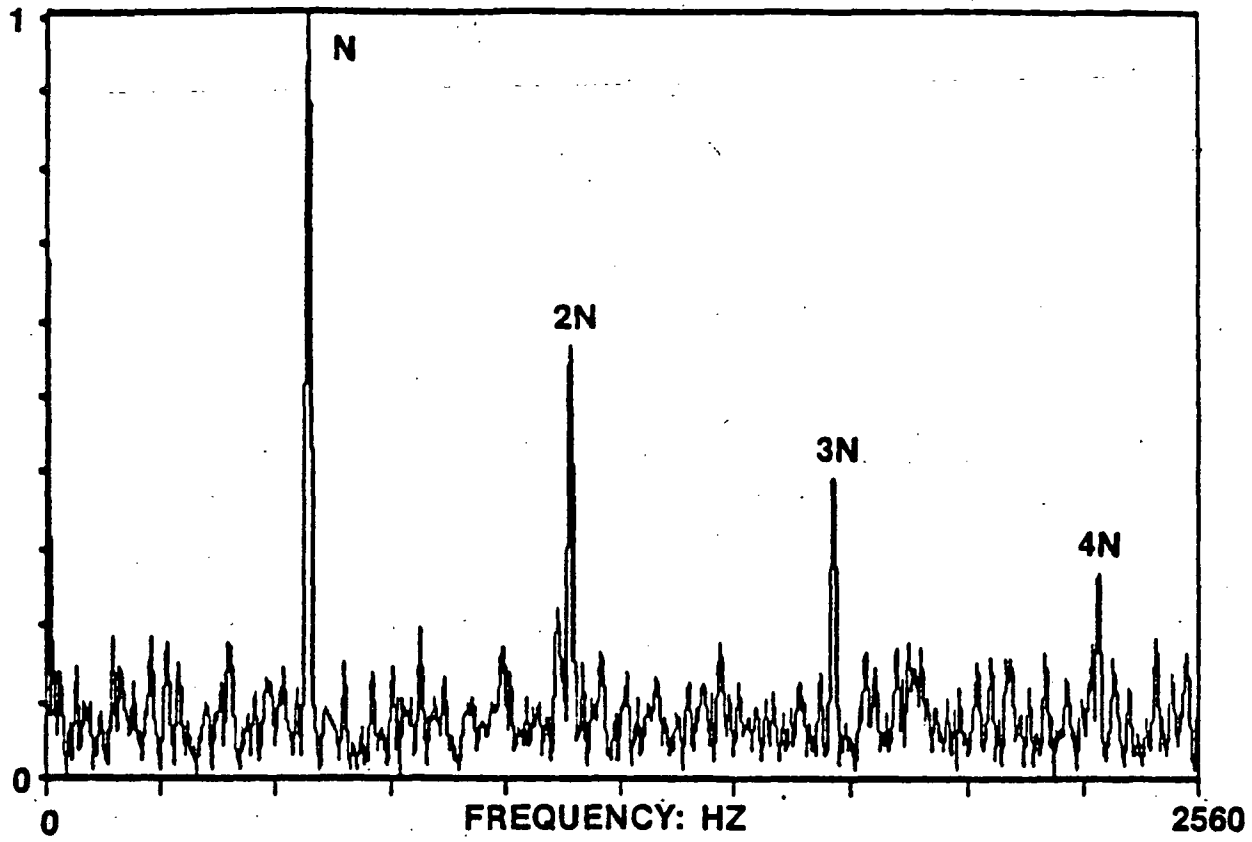

A) 3N and Anomalous Frequency Separated (100% RPL)

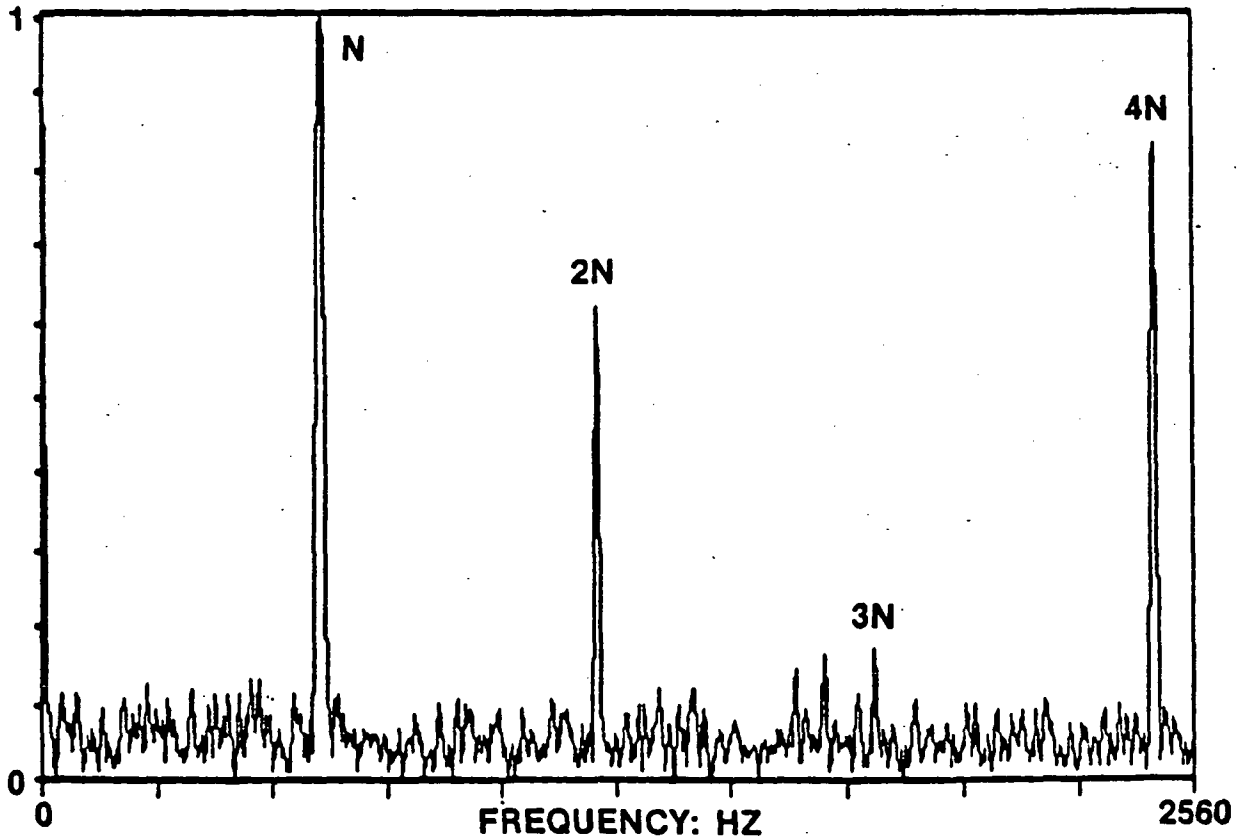

B) 3N and Anomalous Frequency Coincident (109% RPL)

Figure 4-14. Hyper-Coherence Spectra of Turbopump Measurement from Test 901-471 at 100% and 109% Power Level

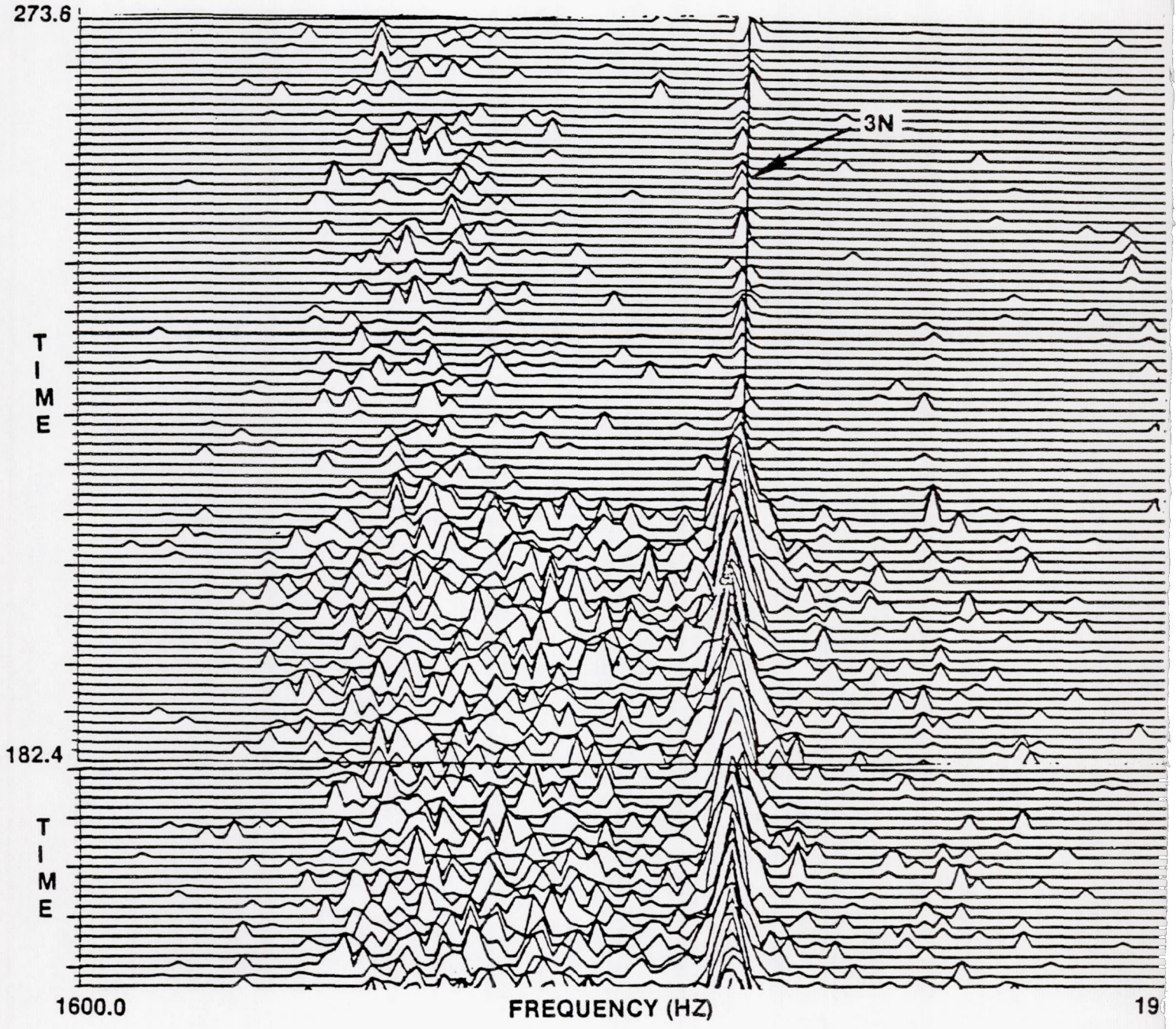

Figure 4-15. Isoplot of Measurement from Test 901-436

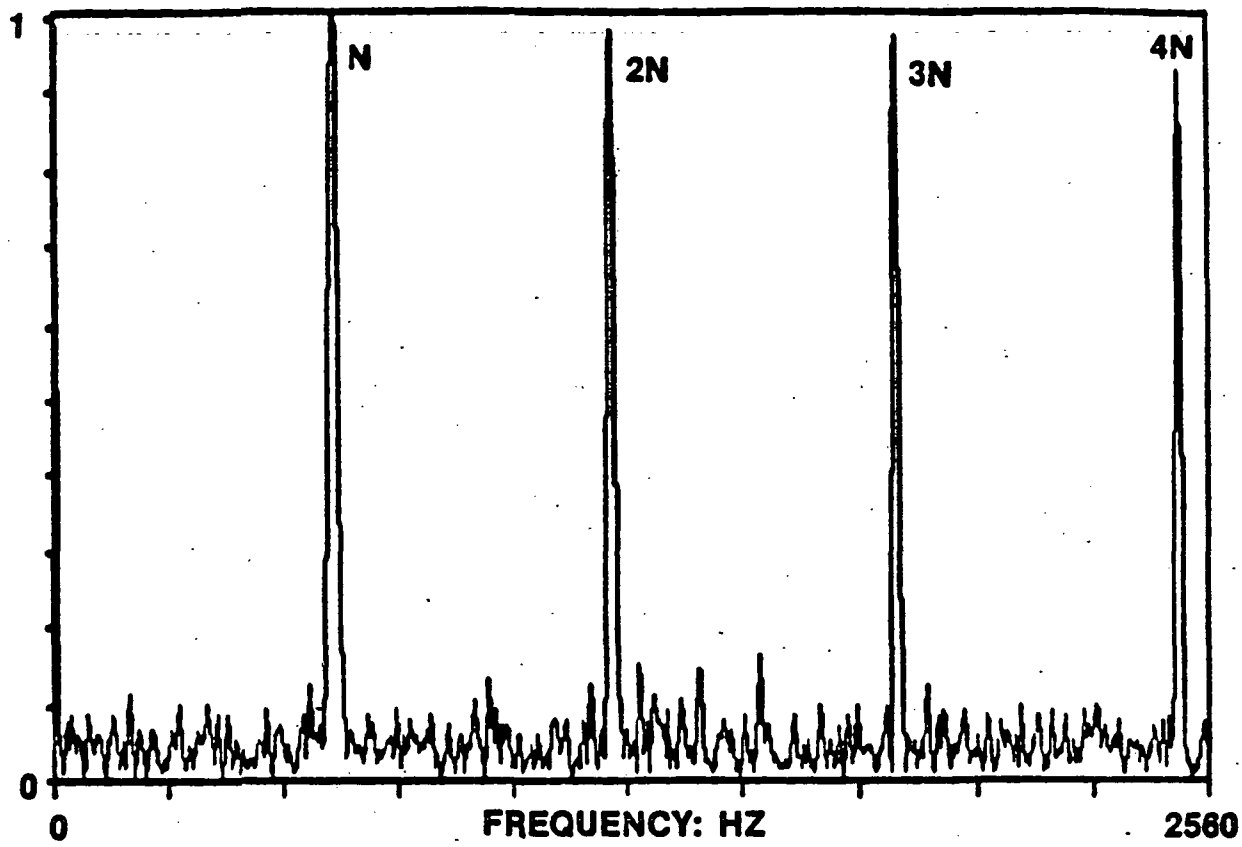

A) High Level 3rd Harmonic

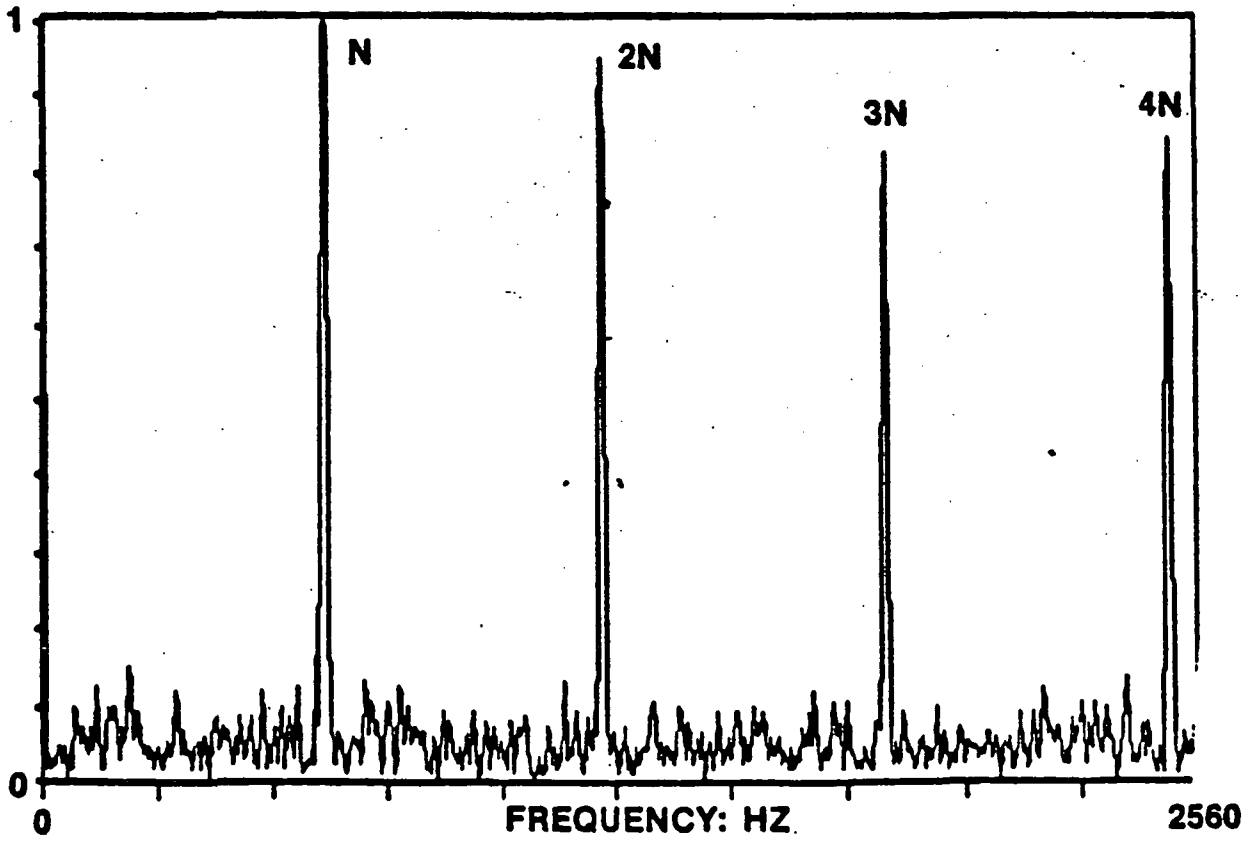

B) Low Level 3rd Harmonic

Figure 4-16. Hyper-Coherence Spectra of Turbopump Measurement from Test 901-436

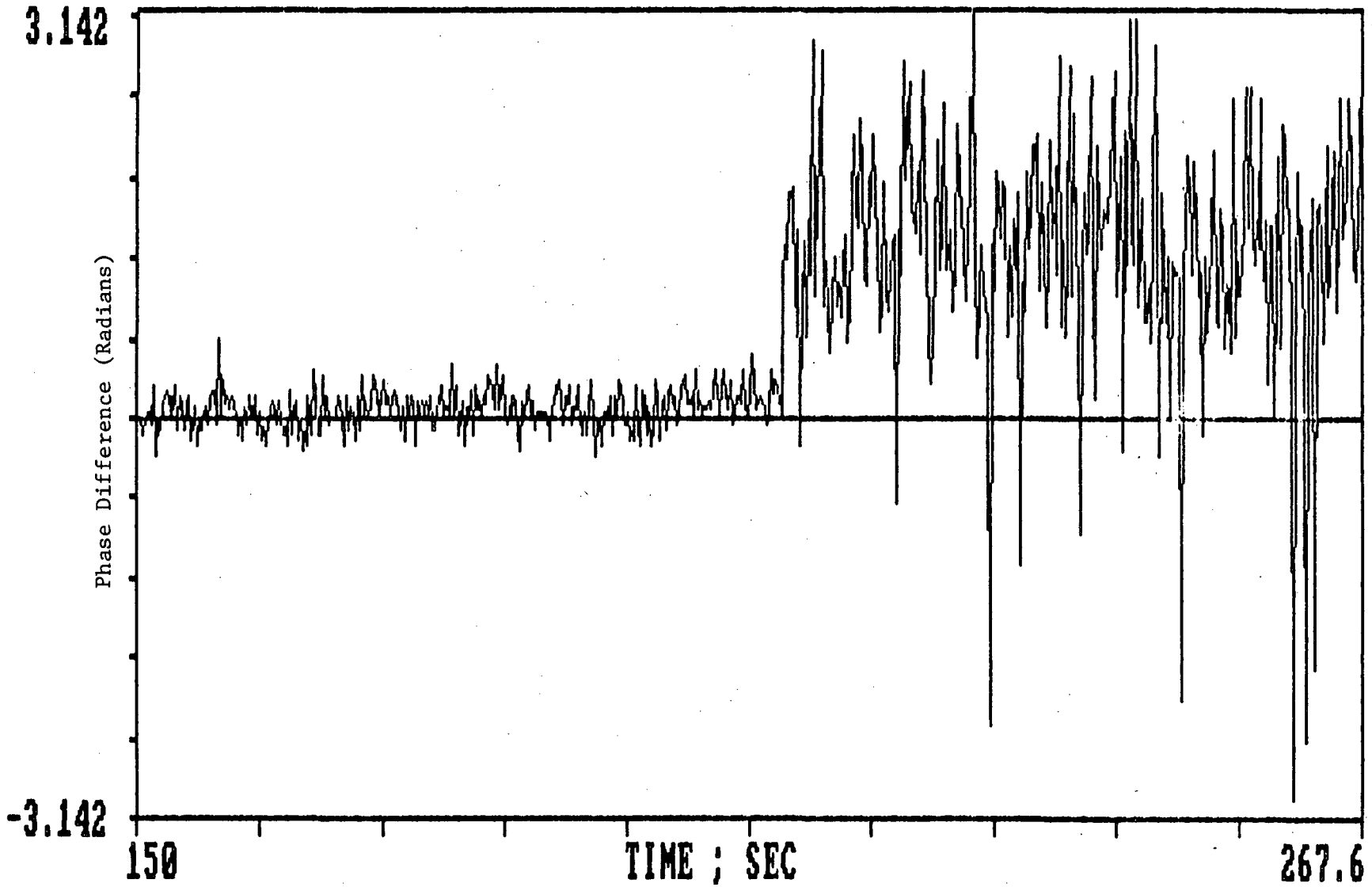

Figure 4-17. Relative Phase Between Synchronous and Third Harmonic (SSME Test 901-436)

identified. The more fluctuating phase lag after 3N diminished is due to the decreased signal to noise ratio with reduced 3N component. Also notice that the mean phase lag has an abrupt change right at the moment 3N diminished. This implies that the waveform has changed at that moment. The phase of the hyper-coherence function should contain additional information about this waveform shifting. Further research work in this direction is presently in progress at Wyle Laboratories.

SECTION V

CONCLUDING REMARKS

This report describes some analytical techniques for the diagnostic evaluation of SSME dynamic measurements. These techniques were applied to analytical signals and SSME hot firing measurements. It might be noted that several common and useful detection methods were not applied. This was primarily due to the instrumentation/ measurements readily available from SSME hot firing tests. For example, acoustic emission measurement is a common non-destructive approach for monitoring structural integrity. However, the method requires specialized instrumentation which was simply not available from the SSME test program. Also, the demodulated resonance technique has proven useful for detecting bearing element degradation, but requires a useable data bandwidth out to approximately 40 KHz, which again was not available.

The techniques evaluated under this study have been implemented on MSFC computers available in the MSFC Systems Dynamics Laboratory. The TDA, OSTDA, Randomdec and Cepstrum methods were developed on a Hewlett Packard 5451C analyzer. The nonlinear techniques recently applied are more computationally intensive. These routines were therefore adapted to the MASSCOMP processor at SDL. A program listing of these routines is included in the appendices. These techniques are presently being applied to the diagnostic evaluation of SSME dynamic measurements.

APPENDIX A

NEW TECHNOLOGY REPORT

"A NON-LINEAR COHERENCE FUNCTION AND ITS APPLICATION TO MACHINERY DIAGNOSTICS"

NATIONAL AERONAUTICS AND SPACE ADMINISTRATION	NT CONTROL NO. *(Official use only)*
NEW TECHNOLOGY REPORT	

INSTRUCTIONS

This report form may be used when reporting inventions, discoveries, improvements or innovations to NASA. Use of this report form is optional; provided, however, that whatever report format is used contain the essential information requested herein.

Please provide information requested in each section as follows:

Section I - A description of the problem that motivated the technology development.

Section II - A technically complete and easily understandable description of the new technology that was developed to solve the problem or meet the objective.

Section III - The unique or novel features of the technology and the results (or benefits) of its application.

Section IV - The inclusion or listing of any pertinent additional documentation or references which aid in the understanding or application of the new technology.

In completing each section, use whatever detail deemed appropriate for a "full and complete disclosure," as required by the New Technology or Property Rights in Inventions Clause. For further guidance as to what constitutes a satisfactory report, please refer to NHB 2170.3, Documentation Guidelines for New Technology Reporting.

Available additional documentation which provides a full, detailed description should be attached, as well as any additional explanatory sheets where necessary.

1. TITLE

A Non-Linear Coherence Function (Hyper-Coherence) and its application to Machinery Diagnostics

2. INNOVATOR (S) *(Name and Social Security No.)*

Thomas Coffin [redacted] Jen Y. Jong [redacted]

3. EMPLOYER *(Organization and division)*	4. ADDRESS *(Place of performance)*
Wyle Laboratories	Huntsville, Alabama
5. NASA PRIME CONTRACT NO.	**6. CONTRACTOR DISCLOSURE NO.**
NAS8-34961	

SECTION I - DESCRIPTION OF THE PROBLEM THAT MOTIVATED THE TECHNOLOGY DEVELOPMENT *(Enter A.-General Description of Problem Objective; B.-Key or Unique Problem Characteristics; C.-Past History/Prior Techniques; D.-Limitations of Prior Techniques)*

The harmonic content in dynamic measurements from rotating machinery contains much subtle information concerning equipment operational condition and component degradation. For this reason, the power density spectrum (PSD) has long been employed to assess the relative magnitude of fault-related spectral contributions. Measurements on high-performance rocket engine turbomachinery suffer from severe noise contamination from numerous extraneous sources, which impedes rotating element diagnostic evaluation. It is thus difficult to determine whether an apparent high-level harmonic contribution is indeed related to the fundamental rotational frequency, f_1, or possibly due to an independent source. The ordinary PSD, being an absolute value, is of no assistance to this problem. In an effort to relate synchronous speed characteristics with an arbitrary harmonic component, an unique coherence spectrum was devised which we call the hyper-coherence function. The hyper-coherence function, $H_n(f_1)$, defines the nonlinear correlation between waves at the fundamental frequency and harmonics at nf_1, $n = 1,2,\ldots$. The computation is straightforward by FFT methods, and results in a line spectrum of correlation coefficients as a function of harmonic number.

SECTION II - TECHNICALLY COMPLETE AND EASILY UNDERSTANDABLE DESCRIPTION OF NEW TECHNOLOGY THAT WAS DEVELOPED TO SOLVE THE PROBLEM OR MEET THE OBJECTIVE *(Enter as appropriate A.-Specific description of item; B.-State of development; C.-Operation as a unit; D.-Functional operation; E.-Supportive theory; F.-Engineering specifications; G.-Peripheral equipment; H.-Drawings, graphs, etc.; I.-Parts or ingredients lists; and J.-Maintenance, reliability, safety factors)*

The bicoherence function allows definition of the phase correlation between two spectral components, and a third component which must have a frequency equal to the sum of the first two. More specifically, the bicoherence function may be representated by

$$b^2(f_1, f_2) = \frac{|E\{x(f_1)\, x(f_2)\, x^*(f_3)\}|^2}{E\{|x(f_1)\, x(f_2)|^2\}\, E\{|x(f_3)|^2\}}, \quad f_1 + f_2 = f_3$$

It should be noted that the above relations represent autobispectrum and autobicoherence functions, since the operations are performed on a single signal. The crossbispectrum and crossbicoherence are defined identically between pairs of time series.

As a diagnostic tool, the normalized bispectrum may be applied to detect the onset of nonlinear system behavior and possible associated component degradation.

The bicoherence function just described allows definition of the phase correlation between two spectral components, and a third component with a frequency equal to the sum of the first two.

Note that, with the bicoherence function, direct (nonlinear) correlation between the fundamental, say f_1, and second harmonic, $2f_1$, is explicitly defined, from the above, by

$$b^2(f_1, f_1) = \frac{|E\{x^2(f_1)\, x^*(2f_1)\}|^2}{E\{|x^2(f_1)|^2\}\, E\{|x(2f_1)|^2\}}$$

which is a function of f_1, $2f_1$, only. To relate the fundamental frequency component with higher order harmonics, product correlations are required by the fundamental requirement that $f_1 + f_2 = f_3$. Thus the bicoherence does not admit an explicit statement concerning the correlation between the fundamental (synchronous) frequency and an arbitrary harmonic only, other than the above demonstrated case. For example, with the bicoherence, the correlation between first and third harmonics is defined implicitly, in combination with the second or fourth harmonic component.

SECTION II - TECHNICALLY COMPLETE AND EASILY UNDERSTANDABLE DESCRIPTION OF NEW TECHNOLOGY THAT WAS DEVELOPED TO SOLVE THE PROBLEM OR MEET THE OBJECTIVE *(Enter as appropriate A.-Specific description of item; B.-State of development; C.-Operation as a unit; D.-Functional operation; E.-Supportive theory; F.-Engineering specifications; G.-Peripheral equipment; H.-Drawings, graphs, etc.; I.-Parts or ingredients lists; and J.-Maintenance, reliability, safety factors)*

In an effort to relate synchronous speed characteristics with any arbitrary harmonic only, a unique spectral coherence representation has been recently developed by Wyle, which we call the hyper-coherence function, for lack of a better term.

We define

$$H^2_n = C^2(f_1, f_2 \ldots f_n) \quad , \quad f_1 = f_2 = \ldots f_n$$

or

$$H^2_n = \frac{\left| E\left\{x^n(f_1)\, x^*(nf_1)\right\}\right|^2}{E\left\{\left|x^n(f_1)\right|^2\right\} E\left\{\left|x(nf_1)\right|^2\right\}}$$

where n is a positive integer, and C is the n^{th} order coherence function.

Observe that an n^{th} order coherence function is represented by an equal order hypersurface in the frequency domain, whereas H^2_n represents only one value from each successive ordered coherence function satisfying the requirement $f_1 = f_2 \ldots = f_n$. Thus H^2_n can be represented as a line spectrum in two dimensions.

To clarify the interpretation of H^2_n, observe that

H^2_1 = 1, (this trivial case represents the linear coherence between the signal and itself, at the same frequency)

H^2_2 = $C^2(f_1, f_1)$, (this represents the ordinary bicoherence between the fundamental and second harmonic, described previously)

H^2_3 = $C^2(f_1, f_1, f_1)$, (third order coherence between f_1 and $3f_1$)

Thus H^2_n is seen to represent the n^{th} order coherence between the fundamental component (f_1) and the n^{th} harmonic component (nf_1). The computation is straightforward.

SECTION II *(Con.)*

SECTION III - UNIQUE OR NOVEL FEATURES OF THE TECHNOLOGY AND THE RESULTS (OR BENEFITS) OF ITS APPLICATION *(Enter as appropriate A.-Novel or unique features; B.-Development or conceptual problems; C.-Operating characteristics, test data; D.-Analysis of capabilities; E.-Source of error; and F.-Advantages/shortcomings)*

The hyper-coherence function defines the non-linear correletion between a reference frequency component in a vibratory signal and its harmonics.

The formulation provides a concise summary of a succession of higher order coherence functions in only two dimensions.

Major benefit is determination of whether an apparent harmonic in a complex vibration signal is indeed correlated with the fundamental or possibly due to an independent source or extraneous noise.

The technique is computationally easy to implement.

The method is limited to assessment of integer multiple frequency components in a signal, and is therefore not applicable to signals involving modulation or more general non-linear dependence.

SECTION III (Con.)

SECTION IV - ADDITIONAL DOCUMENTATION *(Include or list below any pertinent documentation which aids in the understanding or application of the new technology. IF NOT TOO BULKY OR DIFFICULT TO REPRODUCE, INCLUDE COPIES WITH THIS REPORT. For those references or additional documentation available but NOT included in this report (due to their being nonessential to a basic understanding of the new technology and which may be costly to reproduce or handle) complete item A. below)*

A. AVAILABLE DOCUMENTS *(Check and complete)*	XX	1. PAPERS, ARTICLES		4. ASSEMBLY/MFG. DRAWINGS		7. TEST DATA	
		2. CONTRACTOR REPORTS		5. PARTS OR INGRED. LIST		8. ASSEMBLY/MFG. PROCED.	
		3. ENGINEERING SPECS.		6. OPERATING MANUALS	XX	9. COMPUTER TAPES/CARDS	
	10. OTHER *(Specify)* Wyle Monthly Progress Reports NAS8-34961 (May, August, September, 1985)						

B. INDICATE THE DATES OR THE APPROXIMATE TIME PERIOD DURING WHICH THIS TECHNOLOGY WAS DEVELOPED *(i.e., conceived, constructed, tested, etc.)*

5-'85 through 11-'85

C. LIST THE FIRST PUBLICATION OR PUBLIC DISCLOSURE OF THE NEW TECHNOLOGY, AND DATES

Journal of Acoustical Society of America, Supplement 1, Vol. 78, Fall '85, p. 325-326.

D. LIST THE DATES AND ANY PARTICULARLY PERTINENT PAGE NUMBERS OF OTHER PUBLICATIONS WHICH ARE AVAILABLE BUT NOT ATTACHED

See C. above

E. DEGREE OF TECHNOLOGICAL SIGNIFICANCE *(Check in your best judgment the statement which best expresses the degree of technological significance of this technology)*

☐ 1. MODIFICATION TO EXISTING TECHNOLOGY ☒ 2. SUBSTANTIAL ADVANCE IN THE ART ☐ 3. MAJOR BREAKTHROUGH

COMMENTS

The technique represents a minor modification to the non-linear spectral theory. However, application to machinery diagnostics represents a substantial advance in applied technology.

Software has been implemented on MSFC computers and is being applied to SSME data evaluation.

SIGNATURE OF INNOVATOR(S)	DATE
	1-30-86

APPENDIX B

PROGRAM LISTING FOR NON-LINEAR SPECTRUM AND COHERENCE ESTIMATION

D Line# 1 7 Microsoft FORTRAN77 V3.20 02/84

```
      1       PROGRAM MEM
      2 C     LINK MEM+MEMSB
      3       REAL*4 R(2050)
      4       REAL*8 K(2050),A(2050)
      5       CHARACTER*15 F1,F2
      6       CHARACTER IASK
      7 C     DATA PE,R/4100*0.0/K,A/4100*0.0D0/
      8       WRITE(*,'(A)')'  ENTER MAXIMUN LAG IN R(T) ( LE. 2048)'
      9       READ(*,*) MAXLAG
     10       WRITE(*,'(A)')'  ENTER # OF POLES (LE. MAXLAG-1)'
     11       READ(*,*)NPOLE
     12       WRITE(*,'(A)')' ENTER INPUT FILNAM OF AUTOCORRELATION FUNCTION'
     13       READ(*,'(A)') F1
     14       WRITE(*,'(A)')' ENTER OUTPUT FILNAM OF AR COEFFICIENT'
     15       READ(*,'(A)')F2
     16       WRITE(*,'(A)')' ENTER 1 FOR ASCII INPUT'
     17       READ(*,*)IFIP
     18       WRITE(*,'(A)')' ENTER 1 FOR ASCII OUTPUT'
     19       READ(*,*)IFOP
     20       WRITE(*,'(A)')' ENTER # OF BLOCK (ONE BLOCK=ONE R(T) FUNCTION)'
     21       READ(*,*)NB
     22       NPOLE1=NPOLE+1
     23       NPOLE2=NPOLE+2
     24        MI=4*MAXLAG
     25        MO=4*NPOLE2
     26        IF(IFIP.EQ.1)THEN
     27        OPEN(1,FILE=F1,STATUS='OLD')
     28        NB1=1
     29        NB2=NB
     30        ELSE
     31        OPEN(1,FILE=F1,STATUS='OLD',ACCESS='DIRECT',RECL=MI)
     32        WRITE(*,'(A)')' ENTER STARTING AND ENDING BLOCK #'
     33        READ(*,*)NB1,NB2
     34        ENDIF
     35        IF(IFOP.EQ.1)THEN
     36        OPEN(2,FILE=F2,STATUS='NEW')
     37        ELSE
     38        OPEN(2,FILE=F2,STATUS='NEW',ACCESS='DIRECT',RECL=MO)
     39        ENDIF
     40       NOUT=0
     41       DO 9999 II=NB1,NB2
1    42       NOUT=NOUT+1
1    43       WRITE(*,*)II
1    44        IF(IFIP.EQ.1)THEN
1    45        READ(1,*)(R(I),I=1,NPOLE1)
1    46        ELSE
1    47        READ(1,REC=II)(R(I),I=1,NPOLE1)
1    48        ENDIF
1    49       CALL DURBIN(R,NPOLE1,PE,K,A)
1    50       R(NPOLE2)=PE
1    51       DO 66 I=1,NPOLE1
2    52 66    R(I)=A(I)
1    53        IF(IFOP.EQ.1)THEN
1    54        WRITE(2,*)(R(I),I=1,NPOLE2)
1    55        ELSE
1    56        WRITE(2,REC=NOUT)(R(I),I=1,NPOLE2)
1    57        ENDIF
1    58 9999  CONTINUE
     59 420   STOP
```

D Line# 1 7 Microsoft FORTRAN77 V3.20 02/84

```
     60         END

Name     Type          Offset  P Class

A        REAL*8         24602
F1       CHAR*16        41010
F2       CHAR*16        41026
I        INTEGER*4      41090
IASK     CHAR*1         *****
IFIP     INTEGER*4      41042
IFOP     INTEGER*4      41046
II       INTEGER*4      41082
K        REAL*8          8202
MAXLAG   INTEGER*4      41002
MI       INTEGER*4      41062
MO       INTEGER*4      41066
NB       INTEGER*4      41050
NB1      INTEGER*4      41070
NB2      INTEGER*4      41074
NOUT     INTEGER*4      41078
NPOLE    INTEGER*4      41006
NPOLE1   INTEGER*4      41054
NPOLE2   INTEGER*4      41058
PE       REAL           41098
R        REAL               2

      61         SUBROUTINE DZERO(NEL,ARRAY)
      62         REAL*8 ARRAY(1)
      63         IF(NEL.LE.0)RETURN
      64         DO 10 I=1,NEL
1     65 10      ARRAY(I)=0.0D0
      66         RETURN
      67         END

Name     Type          Offset  P Class

ARRAY    REAL*8             4 *
I        INTEGER*4      41106
NEL      INTEGER*4          0 *

      68         SUBROUTINE ZERO(NEL,ARRAY)
      69         REAL*4 ARRAY(1)
      70         IF(NEL .LE. 0) RETURN
      71         DO 10 I=1,NEL
1     72 10      ARRAY(I) = 0.0
      73         RETURN
      74         END

Name     Type          Offset  P Class

ARRAY    REAL               4 *
I        INTEGER*4      41114
NEL      INTEGER*4          0 *

      75 C       ************************************************************
      76         SUBROUTINE DURBIN(R,NPOLE1,PE,K,A)
```

ORIGINAL PAGE IS
OF POOR QUALITY

```
D Line# 1       7
     77 C       OUTPUT A(I),I=1,NPOLE+1 = {1  -A(1)  -A(2) ... -A(L) }t
     78 C         OF BRIGG'S PAPER P.49  EQUATION (3.13)  L=NPOLE
     79         REAL*4 R(1)
     80 C       REAL*4 PE(1),R(1)
     81         REAL*8 K(1),A(1),KDUM,ASTORE(2050)
     82 C       COMMON /WRKSPC/ASTORE
     83 C       CALL ZERO(NPOLE1,PE)
     84         CALL DZERO(NPOLE1,K)
     85         CALL DZERO(NPOLE1,A)
     86         CALL DZERO(NPOLE1,ASTORE)
     87         IPMAX=NPOLE1-1
     88         PE=R(1)
     89 C       PE(1)=R(1)
     90         K(1)=0.0D0
     91         A(1)=1.0D0
     92         ASTORE(1)=1.0D0
     93         DO 50 I=1,IPMAX
1    94         I1=I+1
1    95         KDUM=0.0D0
1    96         DO 10 J=1,I
2    97         KDUM=A(J)*DBLE(R(I1-J+1))+KDUM
2    98 10      CONTINUE
1    99         K(I1)=-1.0*KDUM/DBLE(PE)
1   100 C       K(I1)=-1.0*KDUM/DBLE(PE(I))
1   101         IF(I.EQ.1)GO TO 30
1   102         DO 20 J=2,I
2   103         ASTORE(J)=A(J)+K(I1)*A(I1-J+1)
2   104 20      CONTINUE
1   105 30      ASTORE(I1)=K(I1)
1   106         DO 40 J=1,NPOLE1
2   107 40      A(J)=ASTORE(J)
1   108         PE=(1.0-SNGL(K(I1)**2))*PE
1   109 C       PE(I1)=(1.0-SNGL(K(I1)**2))*PE(I)
1   110 50      CONTINUE
    111         RETURN
    112         END
```

Name	Type	Offset	P	Class
A	REAL*8	16	*	
ASTORE	REAL*8	41122		
DBLE				INTRINSIC
I	INTEGER*4	57526		
I1	INTEGER*4	57534		
IPMAX	INTEGER*4	57522		
J	INTEGER*4	57546		
K	REAL*8	12	*	
KDUM	REAL*8	57538		
NPOLE1	INTEGER*4	4	*	
PE	REAL	8	*	
R	REAL	0	*	
SNGL				INTRINSIC

Name	Type	Size	Class
DURBIN			SUBROUTINE
DZERO			SUBROUTINE

D Line# 1 7 Microsoft FORTRAN77 V3.20 02/84

```
      1 C     PROGRAM MEMPSD
      2 C     LINK MEMPSD+FFTSUB+FFT842+MEMPSDSB
      3       COMMON WTR(2048),WTI(2048),XR(2048),XI(2048),PSD(2050)
      4       CHARACTER*16 F1,F2
      5       WRITE(*,'(A)')' INPUT AR FILE HAS NPOLE+2 DATA POINTS/BLOCK:'
      6       WRITE(*,'(A)')'    NPOLE+1 AR COEFF. [ A(0),A(1),..,A(NPOLE)]'
      7       WRITE(*,'(A)')'     ,PE (PREDICTION ERROR)]'
      8       WRITE(*,'(A)')'                          '
      9       WRITE(*,'(A)')' ENTER # OF BLOCKS ( # OF PSD TO BE ESTIMATED)'
     10       READ(*,*)NB
     11       WRITE(*,'(A)')'  ENTER INPUT FILNAM OF AR COEFFICIENTS'
     12       READ(*,'(A)')F1
     13       WRITE(*,'(A)')'  ENTER OUTPUT PSD FILNAM'
     14       READ(*,'(A)')F2
     15       WRITE(*,'(A)')'  ENTER 1 IF INPUT AR IS ASCII'
     16       READ(*,*)IFIP
     17       WRITE(*,'(A)')'  ENTER 1 IF OUTPUT PSD IS ASCII'
     18       READ(*,*)IFOP
     19       WRITE(*,'(A)')'  ENTER MAXIMUM # OF POLES (MAX ORDER OF MEM)'
     20       READ(*,*)NPOLE
     21       NPOLE1=NPOLE+1
     22       NPOLE2=NPOLE+2
     23       WRITE(*,'(A)')'  ENTER 1 IF EXPAND FROM 0 TO PI(WHOLE RANGE)'
     24       READ(*,*)IFALL
     25       WRITE(*,'(A)')'  NPSD= # OF DATA POINT OF OUTPUT PSD'
     26       IF(IFALL.EQ.1)THEN
     27       WRITE(*,'(A)')' ENTER NPSD eg. 513'
     28       WRITE(*,'(A)')' note: NPSD=NNP2/2 (NPOLE+2 .LE. NNP2)'
     29       ELSE
     30       WRITE(*,'(A)')'  ENTER NPSD (NPSD+NPOLE1 MUST .LE. 1024)'
     31       ENDIF
     32       READ(*,*)NPSD
     33       WRITE(*,'(A)')'  ENTER SAMPLING FREQ IN HZ'
     34       READ(*,*)FS
     35       IF(IFALL.EQ.1)GOTO 123
     36       WRITE(*,'(A)')'  ENTER STARTING FREQ IN HZ'
     37       READ(*,*)FSTART
     38       WRITE(*,'(A)')'  ENTER ENDING FREQ IN HZ'
     39       READ(*,*)FEND
     40       SIGO=FS*ALOG(1.)
     41       DLTSIG=SIGO
     42       OMGO=FSTART
     43       DLTOMG=(FEND-FSTART)/(NPSD-1.)
     44 123   CONTINUE
     45        LI=(NPOLE+2)*4
     46        LO=NPSD*4
     47        IF(IFIP.EQ.1)THEN
     48        OPEN(1,FILE=F1,STATUS='OLD')
     49        ELSE
     50        OPEN(1,FILE=F1,STATUS='OLD',ACCESS='DIRECT',RECL=LI)
     51        ENDIF
     52        IF(IFOP.EQ.1)THEN
     53        OPEN(2,FILE=F2,STATUS='NEW')
     54        ELSE
     55        OPEN(2,FILE=F2,STATUS='NEW',ACCESS='DIRECT',RECL=LO)
     56        ENDIF
     57       DO 9999 KK=1,NB
1    58       WRITE(*,*)KK
1    59        IF(IFIP.EQ.1)THEN
```

```
1     60          READ(1,*)(XR(I),I=1,NPOLE2)
1     61          ELSE
1     62          READ(1,REC=KK)(XR(I),I=1,NPOLE2)
1     63          ENDIF
1     64         PE=ABS(XR(NPOLE2))
1     65         CONS=2*PE/FS
1     66          DO 346 I=NPOLE2,2048
2     67 346      XR(I)=0.
1     68         IF(IFALL.EQ.1)GOTO 125
1     69 C       ************************************************************
1     70          DO 345 I=1,2048
2     71          XI(I)=0.
2     72          WTR(I)=0.
2     73          WTI(I)=0.
2     74 345      CONTINUE
1     75         IF(KK.EQ.1)THEN
1     76         NFFT=NPOLE1+NPSD
1     77         DO 30 I=1,11
2     78         NTEST=2**I
2     79         IF(NTEST.GE.NFFT)GOTO 40
2     80 30      CONTINUE
1     81         WRITE(*,'(A)')'  N TOO BIG FOR FFT'
1     82         STOP
1     83 40      NFFT=NTEST
1     84         ENDIF
1     85         CALL CZT(XR,XI,NPOLE1,NPSD,DLTSIG,DLTOMG,WTR,WTI,SIGO,OMGO,
1     86        1           0,NFFT,FS)
1     87 C       WRITE(*,'(A)')'*****************OUT FROM CZT'
1     88         DO 90 I=1,NPSD
2     89 90      PSD(I)=CONS/(XR(I)*XR(I)+XI(I)*XI(I))
1     90         GOTO 999
1     91 C       ************************************************************
1     92 125     CONTINUE
1     93         NNP2=NPSD*2
1     94         DO 221 I=1,NPOLE1
2     95 221     PSD(I)=XR(I)
1     96         DO 223 I=NPOLE1+1,NNP2
2     97 223     PSD(I)=0.
1     98         CALL FFT(PSD,NNP2,1)
1     99         DO 128 I=1,NNP2
2    100 128     PSD(I)=PSD(I)*(NNP2-2.)
1    101         DO 129 I=2,NNP2,2
2    102         I1=I-1
2    103         J=I/2
2    104         PSD(J)=CONS/(PSD(I1)*PSD(I1)+PSD(I)*PSD(I))
2    105 129     CONTINUE
1    106 999     CONTINUE
1    107          IF(IFOP.EQ.1)THEN
1    108          WRITE(2,*)(PSD(I),I=1,NPSD)
1    109          ELSE
1    110          WRITE(2,REC=KK)(PSD(I),I=1,NPSD)
1    111          ENDIF
1    112 9999    CONTINUE
     113         CLOSE(2)
     114         CLOSE(1)
     115         STOP
     116         END
```

D:Line# 1 7 Microsoft FORTRAN77 V3.20 02/84

```
      1 C     PROGRAM ABC---- CALCULATE AUTO-BICOHERENCE (NOT SQUARE)
      2 C     LINK ABC
      3       DIMENSION U1(1028),U2(1028),D1(1028),D2(1028)
      4       DIMENSION ABC(1028),ABD(1028)
      5       CHARACTER*16 FILNAM
      6       WRITE(*,'(A)')' INPUT BINARY FILE HAS 2*NB BLOCKS'
      7       WRITE(*,'(A)')' ODD BLOCK=AMPLITUDE OF X(W); W=1....NNP22'
      8       WRITE(*,'(A)')' EVEN BLOCK=PHASE OF X(W) ; W=1...NNP22'
      9       WRITE(*,'(A)')' ENTER INPUT FILNAM (OUTPUT FROM FFT)'
     10       READ(*,'(A)')FILNAM
     11       WRITE(*,'(A)')' ENTER # OF DATA/BLOCK IN TIME SERIES'
     12       READ(*,*)NN
     13       WRITE(*,'(A)')' ENTER STARTING AND ENDING BLOCK #'
     14       READ(*,*)NB1,NB2
     15       NNP2=NN+2
     16       NNP22=NNP2/2
     17       NNP221=NNP22-1
     18       OPEN(2,FILE=FILNAM,STATUS='OLD',ACCESS='DIRECT',RECL=4*NNP22)
     19 1     CONTINUE
     20       WRITE(*,'(A)')' ENTER START & ENDING BASE FREQ. #(0--NNP22-1)'
     21       READ(*,*)NBF1,NBF2
     22       WRITE(*,'(A)')' ENTER -1 FOR NEGATIVE REFERNECE FREQ; 1 ELSE'
     23       READ(*,*)NEG
     24       WRITE(*,'(A)')' ENTER OUTPUT AMP OF ABC (COHERENCE) FILNAM'
     25       READ(*,'(A)')FILNAM
     26       OPEN(3,FILE=FILNAM,STATUS='NEW')
     27       WRITE(*,'(A)')' ENTER 1 IF YOU WANT CALCULATE PHASE OF ABC'
     28       READ(*,*)IFABC
     29        IF(IFABC.EQ.1)THEN
     30        WRITE(*,'(A)')' ENTER OUTPUT PHASE OF ABC FILNAM'
     31        READ(*,'(A)')FILNAM
     32        OPEN(4,FILE=FILNAM,STATUS='NEW')
     33        ENDIF
     34       DO 9999 NBF=NBF1,NBF2
1    35       WRITE(*,21)NBF
1    36 21    FORMAT(' BASE FREQ # =',I5)
1    37       DO 22 I=0,NNP221
2    38       U1(I)=0.
2    39       U2(I)=0.
2    40       D1(I)=0.
2    41 22    D2(I)=0.
1    42       DO 999 IJK=NB1,NB2
2    43       WRITE(*,127)IJK
2    44 127   FORMAT(' DATA SEGMENT # =',I5)
2    45       READ(2,REC=IJK*2-1)(ABC(I),I=0,NNP221)
2    46       READ(2,REC=IJK*2)(ABD(I),I=0,NNP221)
2    47 C     ********************************************************
2    48       LIMIT=NNP22-NEG*NBF-1
2    49       IF(LIMIT.GT.NNP221)LIMIT=NNP221
2    50       DO 99 IJ=0,LIMIT
3    51       NFS=NEG*NBF+IJ
3    52       NEG1=1
3    53       IF(NFS.LT.0)NEG1=-1
3    54       NFS=IABS(NFS)
3    55       D1(IJ)=D1(IJ)+(ABC(NBF)*ABC(IJ))**2
3    56       D2(IJ)=D2(IJ)+ABC(NFS)**2
3    57       AA=ABC(NBF)*ABC(IJ)*ABC(NFS)
3    58       AG=NEG*ABD(NBF)+ABD(IJ)-NEG1*ABD(NFS)
3    59       U1(IJ)=U1(IJ)+AA*COS(AG)
```

```
D Line# 1      7                                  Microsoft FORTRAN77 V3.20 02/84
      1 C      SRC.FOR----- SIGNATURE RATIO COHERENCE
      2 C      LINK SRC
      3        REAL*8 TTPP,AAAAAA
      4        DIMENSION NM(513)
      5        REAL*4 ABC(523),ABD(523),HCS(1026)
      6        REAL*8 U1(523),U2(523),D1(523),D2(523),AA,PSRS
      7        CHARACTER*16 FILNAM
      8        WRITE(*,'(A)')' INPUT FILE HAS 2*NB BLOCKS'
      9        WRITE(*,'(A)')' ODD BLOCK=AMPLITUDE OF X(W); W=1....NNP22'
     10        WRITE(*,'(A)')' EVEN BLOCK=PHASE OF X(W) ; W=1...NNP22'
     11        WRITE(*,'(A)')' ENTER INPUT FFT FILNAM (OUTPUT FROM FFT)'
     12        READ(*,'(A)')FILNAM
     13        WRITE(*,'(A)')' ENTER SAMPLING FREQ IN HZ'
     14        READ(*,*)FS
     15        WRITE(*,'(A)')' ENTER # OF DATA/BLOCK IN TIME SERIES'
     16        READ(*,*)NN
     17        WRITE(*,'(A)')' ENTER # OF BLOCK'
     18        READ(*,*)NB
     19        WRITE(*,'(A)')' ENTER STARTING & ENDING BLOCK #'
     20        READ(*,*)NB1,NB2
     21        WRITE(*,'(A)')' ENTER HOW MANY %  WITHIN  HARMONIC  TO BE KEPT'
     22        READ(*,*)PCT
     23        PCT1=1-PCT
     24        NB=NB2-NB1+1
     25        NNP2=NN+2
     26        NNP22=NNP2/2
     27        OPEN(2,FILE=FILNAM,STATUS='OLD',ACCESS='DIRECT',RECL=4*NNP22)
     28 1      CONTINUE
     29        WRITE(*,'(A)')' ENTER STARTING & ENDING BASE FREQ #(0-NNP22-1)'
     30        READ(*,*)NBF1,NBF2
     31        WRITE(*,'(A)')' ENTER OUTPUT AMP & PHASE OF HC FILNAM'
     32        READ(*,'(A)')FILNAM
     33        OPEN(3,FILE=FILNAM,STATUS='NEW')
     34        WRITE(*,'(A)')' ENTER OUTPUT HYPERCOHERENCE SIGNATURE FILNAM'
     35        READ(*,'(A)')FILNAM
     36        WRITE(*,'(A)')' ENTER 1 FOR ACCELERATION TO DISPLACEMENT'
     37        WRITE(*,'(A)')'         INPUT  A(t) IN G (32.174 FT/SEC**2)'
     38        WRITE(*,'(A)')'        OUTPUT D(t) IN INCH'
     39        READ(*,*)NDISP
     40        OPEN(4,FILE=FILNAM,STATUS='NEW')
     41        DO 9999 NBF=NBF1,NBF2
1    42        WRITE(*,21)NBF
1    43 21     FORMAT(' BASE FREQ # =',I5)
1    44        DO 986 I=0,NBF
2    45 986    NM(I)=0.
1    46        DO 987 I=NBF-5,NNP22-1
2    47        NM(I)=1
2    48        PSRS=(I*1.0)/(NBF*1.0)
2    49        NG=PSRS
2    50        RM=PSRS-NG
2    51        IF(RM.GT.PCT.AND.RM.LT.PCT1)THEN
2    52        NM(I)=0
2    53        ENDIF
2    54 987    CONTINUE
1    55        DO 22 I=0,NNP22-1
2    56        U1(I)=0.
2    57        U2(I)=0.
2    58        D1(I)=0.
2    59 22     D2(I)=0.
```

```
D Line# 1      7                                  Microsoft FORTRAN77 V3.20 02/84
1     60 127   FORMAT(' DATA SEGMENT # =',I5)
1     61       DO 999 IJK=NB1,NB2
2     62       WRITE(*,127)IJK
2     63       READ(2,REC=IJK*2-1)(ABC(I),I=0,NNP22-1)
2     64       READ(2,REC=IJK*2)(ABD(I),I=0,NNP22-1)
2     65        DO 99 IJ=0,NNP22-1
3     66        PSRS=(IJ*1.)/(NBF*1.)
3     67        IF(NM(IJ).EQ.0)GOTO 99
3     68         D1(IJ)=D1(IJ)+(ABC(NBF)**PSRS)**2
3     69         D2(IJ)=D2(IJ)+ABC(IJ)**2
3     70         AA=ABC(NBF)**PSRS*ABC(IJ)
3     71         AG=PSRS*ABD(NBF)-ABD(IJ)
3     72         U1(IJ)=U1(IJ)+AA*COS(AG)
3     73         U2(IJ)=U2(IJ)+AA*SIN(AG)
3     74 99      CONTINUE
2     75 999   CONTINUE
1     76       WRITE(*,'(A)')' ********************************'
1     77       DO 61 I=0,NNP22-1
2     78        IF(NM(I).EQ.0)THEN
2     79        ABC(I)=0
2     80        ABD(I)=0
2     81        ELSE
2     82              ABC(I)=SNGL(DSQRT((U1(I)**2+U2(I)**2)/(D1(I)*D2(I))))
2     83        ABD(I)=SNGL(DATAN2(U2(I),U1(I)))
2     84        ENDIF
2     85 61     CONTINUE
1     86 C     ******* OUTPUT HYPER-COHERENCE AMP & PHASE ***********
1     87       WRITE(3,*)(ABC(I),I=0,NNP22-1)
1     88       WRITE(3,*)(ABD(I),I=0,NNP22-1)
1     89       ABC(0)=1.
1     90       FN=FS*2*3.141592653/NN
1     91       FN2=FN*FN
1     92       CCC=SQRT(NB*1.)*NN
1     93       CCCFN=CCC*FN2
1     94       I1=1
1     95       I2=2
1     96       HCS(1)=0.
1     97       HCS(2)=0.
1     98       DO 62 I=1,NNP22-1
2     99        IF(NDISP.EQ.1)THEN
2    100        ABC(I)=DSQRT(D2(I))*ABC(I)/(CCCFN*I*I)
2    101        ELSE
2    102        ABC(I)=DSQRT(D2(I))*ABC(I)/CCC
2    103        ENDIF
2    104       I1=I1+2
2    105       I2=I2+2
2    106       IF(NDISP.EQ.1)ABC(I)=ABC(I)*386.088
2    107       HCS(I1)=ABC(I)*COS(ABD(I))
2    108       HCS(I2)=ABC(I)*SIN(ABD(I))
2    109 62    CONTINUE
1    110       CALL FFT(HCS,NNP2,-1)
1    111 C     WRITE(4,*)(ABC(I),I=0,NNP22-1)
1    112       WRITE(4,*)(HCS(I),I=1,NN)
1    113 9999  CONTINUE
     114 77    FORMAT(5E16.8)
     115       CLOSE(2)
     116       CLOSE(3)
     117       STOP
     118       END
```

```
D Line# 1       7
3     60        U2(IJ)=U2(IJ)+AA*SIN(AG)
3     61 99     CONTINUE
2     62 100    CONTINUE
2     63 999    CONTINUE
1     64        DO 61 I=0,LIMIT
2     65        ABSS=U1(I)*U1(I)+U2(I)*U2(I)
2     66 61     ABC(I)=SQRT(ABSS/(D1(I)*D2(I)))
1     67        IF(NEG.EQ.1)THEN
1     68        DO 62 I=LIMIT,NNP221
2     69 62     ABC(I)=0.
1     70        ENDIF
1     71        WRITE(3,77)(ABC(I),I=1,NNP22)
1     72        IF(IFABC.EQ.1)THEN
1     73        DO 71 I=0,LIMIT
2     74 71     ABD(I)=ATAN2(U2(I),U1(I))
1     75                IF(NBF.GT.1)THEN
1     76                DO 72 I=LIMIT+1,NNP221
2     77 72             ABD(I)=0.
1     78                ENDIF
1     79        WRITE(4,77)(ABD(I),I=0,NNP221)
1     80        ENDIF
1     81 9999   CONTINUE
      82 77     FORMAT(5E16.8)
      83        CLOSE(2)
      84        CLOSE(3)
      85        IF(IFABC.EQ.1) CLOSE(4)
      86        STOP
      87        END
```

Name	Type	Offset	P	Class
AA	REAL	24824		
ABC	REAL	16450		
ABD	REAL	20562		
ABSS	REAL	24836		
AG	REAL	24828		
ATAN2				INTRINSIC
COS				INTRINSIC
D1	REAL	8226		
D2	REAL	12338		
FILNAM	CHAR*16	24674		
I	INTEGER*4	24760		
IABS				INTRINSIC
IFABC	INTEGER*4	24726		
IJ	INTEGER*4	24808		
IJK	INTEGER*4	24768		
LIMIT	INTEGER*4	24804		
NB1	INTEGER*4	24694		
NB2	INTEGER*4	24698		
NBF	INTEGER*4	24730		
NBF1	INTEGER*4	24714		
NBF2	INTEGER*4	24718		
NEG	INTEGER*4	24722		
NEG1	INTEGER*4	24820		
NFS	INTEGER*4	24816		
NN	INTEGER*4	24690		
NNP2	INTEGER*4	24702		
NNP22	INTEGER*4	24706		
NNP221	INTEGER*4	24710		

APPENDIX C

DATA ENHANCEMENT TECHNIQUES FOR INCIPIENT FAILURE DETECTION

WYLE LABORATORIES - RESEARCH STAFF
TECHNICAL MEMORANDUM TM 83-01

DATA ENHANCEMENT TECHNIQUES FOR INCIPIENT FAILURE DETECTION

by

Granville R. Anderson, II

A Phase Report of
Work Performed Under Contract No. NAS8-33379

for

NATIONAL AERONAUTICS AND SPACE ADMINISTRATION
GEORGE C. MARSHALL SPACE FLIGHT CENTER
MARSHALL SPACE FLIGHT CENTER, ALABAMA 35812

February 1983

WYLE LABORATORIES
SCIENTIFIC SERVICES & SYSTEMS GROUP
P. O. Box 1008 • Huntsville, Alabama 35807
TWX(810) 726-2225 • TELEPHONE (205) 837-4411

COPY NO. _____

TABLE OF CONTENTS

LIST OF FIGURES

LIST OF FIGURES (CONCLUDED)

LIST OF TABLES

ABSTRACT

The status of an investigation to develop and evaluate data enhancement techniques and to determine their effectiveness with respect to incipient detection of mechanical failures in turbomachinery is presented. Six waveform analysis techniques have been applied to dynamic data, and their results are reviewed. Software developed for the implementation of the methods is described. A laboratory evaluation of the techniques with respect to failure indicator detection capability as applied to both simulated response signals and measurements from a rocket engine turbopump is summarized. Conclusions are drawn concerning the relative detection capability of the techniques, and recommendations for further investigations are provided.

Section 1

INTRODUCTION

In general, the subject of incipient failure detection is related to the detection of the basic causes of failure. Failures in all types of systems and/or subsystems-- structural, mechanical, hydraulic, pneumatic, electrical, and electronic--are the result of two basic causes: component degradation and/or chemical contamination. Similar to the well-known pattern demonstrated during the fatigue of metals, the failure process is known to exhibit a beginning, growth period, and ending. In most cases, the time frame over which this behavioral pattern is exhibited is long; however, in some cases the failure process may be so short, while not instantaneous, that the symptoms of the onset of failure and the total failure cannot be distinguished. Although little can be done to prevent failures that have extremely short periods of growth, application of incipient failure detection techniques during the early stage of development can provide, in most cases, the time required to initiate appropriate actions to eliminate the cause before the total failure occurs (replacement of worn parts, etc.). Prevention of total failure can often avert damage to nearby components as well as potentially catastrophic events. Incipient detection and monitoring of failures can also allow efficient scheduling of repairs and periodic maintenance, resulting in increased reliability of any system and/or subsystem.

Incipient failure detection is based on observing and recognizing phenomena that occur as a result of system operation, component degradation, and/or chemical contamination. By properly instrumenting an operational system with specific transducers at key locations, the resulting measured waveforms will contain subtle information concerning the physical state of the system and/or subsystem. The extraction of this information and its interpretation are the keys to the successful application of incipient failure detection. The procedures and/or techniques utilized to extract this information include both time and frequency domain signal analysis. Among these signal analysis techniques are acoustic emission, time domain averaging, random decrement averaging, correlation, adaptive filtering, power spectral density, and cepstrum analysis. These techniques may be applied independently and/or in combination. Results from the

application of these techniques are used to establish trends associated with known operational behavior and maintenance conditions for a given system.

Wyle Laboratories is currently involved in research activities to investigate, develop, evaluate, and refine signal analysis techniques for the detection of incipient mechanical failures in space vehicle components and systems. This effort is being conducted under NASA contract NAS8-33379, and this interim report is intended to augment and update the results previously presented [1, 2].

Section 2

BACKGROUND

The space shuttle main engines (SSMEs) are probably the most, if not the most, complicated and sophisticated propulsion systems in operation today. Unfortunately, as with all complicated turbomachinery systems, numerous problems can be encountered during their operation. Some of these problems may be obvious and their solution straightforward; however, when dealing with an extremely complex system operating at extremes in temperature, fluidic pressures, and rotational pump speeds, the seemingly simplest of problems tend to be very difficult to diagnose, isolate, and resolve. For the Space Shuttle, the orbiter main propulsion system consists of three SSMEs. Each is a reusable, high performance, liquid-propellent rocket engine capable of being operated at variable thrust levels. Each engine consists of basically three independent but interrelated systems--one supplying fuel (liquid hydrogen), a second supplying oxidizer (liquid oxygen), and the third providing for their efficient combustion. The turbopump subsystems have experienced the continual problem of bearing failures during the operation of the SSME. In particular, the bearings located in the high pressure oxidizer turbopump (HPOTP) have demonstrated, in several cases, a short lifetime with defects ranging from slight spalling of the balls within the bearing to the disintegration of the entire bearing assembly. In view of this possibility, it is obvious that the need for the capability of incipiently detecting HPOTP bearing failure is acute.

The SSME is a well-instrumented system which is continually undergoing static firing tests to evaluate system modifications and to certify flight hardware. An abundance of data from these tests provides information concerning the operational effectiveness and performance of each system or subsystem within the engine. With this amount and type of data available from numerous tests, it would appear that the basis required to allow incipient detection of bearing failures would be readily available. However, because of the engine's complexity and the large number of parameters to be monitored during a test, the number of transducers that can be installed on the engine is limited. As a result, the ideal transducer in the key location is not necessarily available. In addition, the available transducers are externally mounted to the outer pump casing and/or flange and are exposed to high levels of system noise which tend to mask the bearing

signals necessary to determine bearing condition. Therefore, the incipient detection of bearing failure is compounded into a twofold problem: the extraction of bearing signatures using data enhancement techniques and the identification of indicators within the bearing signature which, when monitored, will correspond to some known bearing maintenance condition.

Section 3

TECHNICAL APPROACH

To solve the problem of incipiently detecting bearing failures, the phenomenon associated with the progressive degradation of bearings must be understood. Once the indicators of bearing degradation have been identified, the process of monitoring and analyzing bearing signatures can be employed, and a qualitative/quantitative assessment of bearing condition can be made. Before the incipient failure detection process can be applied to SSME bearing failure problems, however, a method of extracting uncontaminated bearing signatures from signals heavily masked by noise must be found. For this reason, a limited amount of effort has been expended to identify specific spectral indicators corresponding to specific bearing failure modes. The majority of the work performed under the present contract has been spent identifying, implementing, and evaluating data enhancement techniques to define an optimum method or combination of methods for incipient failure detection.

As pointed out earlier, the problem of incipiently detecting bearing failures is twofold, and the two segments of the problem are not independent. It is not sufficient to reduce extraneous noise from a spectrum/signature at the expense of losing the relatively low-level variations that correspond to bearing degradation; however, these low-level components of the signature cannot be identified and/or monitored when contaminated or masked by high-level noise. Therefore, it is obvious that some compromise between these two extremes must be reached, but no clear cut approach is apparent. The most fundamental question to be answered is where does the signal of interest originate, and how is it being contaminated with noise. Obviously, the signal of interest originates at the bearing, and the noise contamination is provided by all sources other than the bearing.

Insofar as incipient failure detection is concerned, the most useful transducers available on the HPOTP are the radial accelerometers located at the 135^{o}, 90^{o}, and 45^{o} position around the turbine end of the pump housing. These transducers are located relatively close to one of the main bearings in the HPOTP; however, since the transducers are mounted to the exterior of the pump housing (flange), they are subjected to acoustical

as well as vibratory noise. The resulting signals include the bearing response along with noise from both external and internal pump sources. In reality, the bearing response signals are very low level compared to the noise. To minimize this noise contamination, one might consider the relocation of existing transducers or the installation of new transducers inside the pump housing on the bearing supports. With the transducers located closer to the source, it is feasible that the signal-to-noise ratio (SNR) would be improved since the signals from the bearing itself would be stronger. The relocation of the transducers on the exterior of the pump housing to other external locations could possibly provide a better transmission path from the bearing source to the exterior and thereby improve the SNR. Since the noise levels are great, however, it is unlikely that any new exterior locations would be less susceptable to high-level random noise contamination since strong evidence of multipropagation paths is present. In addition, the relocation of transducers, external or internal, would be costly and time consuming; however, it should not be totally ruled out.

A second and somewhat more modest approach to extracting bearing signatures would be to use a data enhancement technique which would reduce the random noise contamination in the signature while having a minimal effect on the remainder of the signature. This approach would allow the use of existing transducers and SSME hot firing test data. In practice, a number of test cases were identified. Each test case centered around a particular high pressure oxidizer pump. The SSME hot firing test data tapes were acquired and the data channels corresponding to the 135^{o}, 90^{o}, and 45^{o} radial accelerometers were reduced using a variety of data analysis/enhancement techniques. The application of a number of techniques to the same test case was performed in an effort to indicate the relative effectiveness of each technique, while the application of the same technique to a group of test cases was used to give an indication of how the signatures varied as a function of run time on a specific pump. Utilization of a semiautomatic data reduction scheme centered around a minicomputer allowed the formation of data bases from which specific indicators and/or trends associated with bearing degradation could be identified.

Section 4

DATA ENHANCEMENT TECHNIQUES

Since actual test data containing both the bearing signature and heavy noise contamination was readily available, the majority of the work performed under the present contract has been spent identifying, implementing, and evaluating a variety of data enhancement/analysis techniques. The data enhancement/analysis techniques that have been applied to SSME hot firing tests data or laboratory-prepared test signals are

- Power Spectral Density (PSD)
- Time Domain Averaging (TDA)
- Order-Sampled Time Domain Averaging (OSTDA)
- Random Decrement Averaging (Randomdec)
- Cepstrum Analysis
- Adaptive Noise Cancellation (ANC-Adaptive Filtered PSD)

Each of these techniques will be discussed from a theoretical standpoint in the following sections.

4.1 Power Spectral Density Analysis

Through the use of the Fourier transform, a time domain signal can be transformed into the frequency domain. The transformation is a decomposition of the time domain waveform into frequency components that comprise the waveform. The power spectral density (PSD) and the autocorrelation function are Fourier transform pairs. The autocorrelation is a time domain quantity given by

$$R(\tau) = \lim_{T\to\infty} 1/T \int_0^T y(t)y(t+\tau)dt.$$

The PSD is the frequency domain equivalent of the autocorrelation and can be expressed as

$$S(f) = \mathcal{F}\{R(\tau)\} = \int_{-\infty}^{\infty} R(\tau)e^{-j2\pi f\tau}\, d\tau.$$

This integral definition of the power spectral density provides a continuous spectral function and is best suited for well-defined continuous waveforms. In general today, power spectral densities are computed from discrete sampled data by using the discrete Fourier transform (DFT). The DFT is calculated on some type of digital computer using the fast Fourier transform (FFT) algorithm. The DFT decomposes the time domain signal into frequency components with a specific bandwidth or resolution (f), and the corresponding amplitudes are normalized by this bandwidth to preserve a true density relationship so that PSDs of varying bandwidths can be compared.

The PSD is a valuable basic tool for quick-look frequency analysis. Spectral or frequency content can be readily determined from the PSD. If low level signals are contaminated by broadband random noise, however, the specific spectral content associated with the low-level signal may not be discernable due to the random components. Nevertheless, the PSD is the best understood and most popular frequency analysis technique for random data analysis.

4.2 Time Domain Averaging

Time domain averaging is a well-known and powerful technique for extracting periodic signals from noisy or complex waveforms. This process is coherent, requiring that the period of the signal to be extracted be known or assumed. It is based on averaging of points one period apart, where the period is the period of the signal to be extracted. The process can be explained by assuming that a signal, x(t), is the sum of a periodic signal, f(t), and additive noise, n(t) [3, 4]:

$$x(t) = f(t) + n(t).$$

By summing one time slice of x(t) with another starting one period later than the previous, the periodic signal, f(t), will add coherently, and the noise signal, n(t), if uncorrelated, will add incoherently. After M summations, we arrive at, in a mean-square sense,

$$\sum_{M} x(t_i) \propto Mf(t_i) + \sqrt{M}\, n(t_i),$$

and the signal-to-noise ratio is therefore enhanced by a factor of $\sqrt{M}$.

To describe the transfer function for the averaging technique, we first consider the function to be averaged, x(t), which is sampled at an interval nT, resulting in samples x(nT). If we denote the averaged period by mT, we can write

$$y(nT) = 1/N \sum_{r=0}^{N-1} x(nT-rmT).$$

Applying the z-transform, we have

$$Y(z) = \frac{X(z)}{N} \sum_{r=0}^{N-1} Z^{-mr} = \frac{X(z)}{N}$$

The transfer function of the averaging process is then

$$H(z) = \frac{Y(z)}{X(z)} = \frac{1}{N} \frac{1 - z^{-mN}}{1 - z^{-m}}.$$

Substituting $z = e^{j\omega t}$, and $mT = T_t = 2\pi/\omega_t = 1/f_t$ (where T_t is the triggering period), the frequency response of H(z) can be written as

$$|H(j\omega)| = \frac{1}{N} \frac{\sin \pi N \omega/\omega_t}{\sin \pi \omega/\omega_t}$$

For values of ω, where $\omega/\omega_t = K$ (an integer),

$$|H| = \frac{1}{N} \frac{\sin \pi NK}{\sin \pi K}$$

Applying L'Hopital's rule, we get

$$|H|_\omega = K\omega_t = 1; K = 0, 1, 2, \ldots .$$

This averaging process is then equivalent to a comb filter with center frequencies of Kf_t ($f_t = \omega_t/2\pi$). Figure 1 shows a typical shape of $|H|$. The filter is composed of the side lobes in addition to the main lobes centered around Kf_t. As the number of averaged ensembles, N, increases, so do the number of side lobes, resulting in increased sharpness of the main lobes and attenuation of frequency components not corresponding to Kf_t.

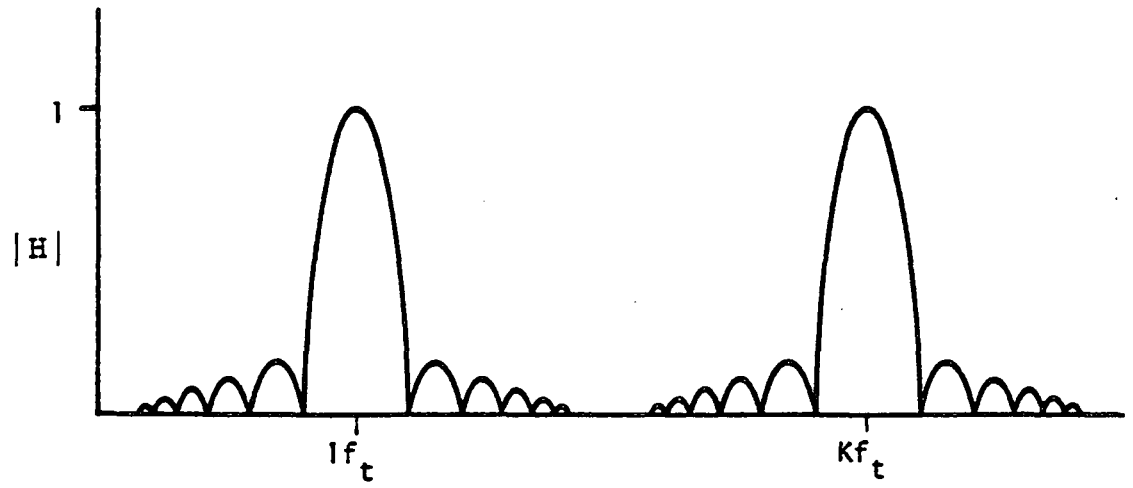

Figure 1. TDA Comb Filter

4.3 Order-Sampled Time Domain Averaging

Order-sampled time domain averaging is a simple but powerful extension of the theory presented for time domain averaging. Order-sampling implies that the analog-to-digital sampling of the raw data is keyed to some specific time parameter of interest, such as the rotational speed (synchronous frequency) of a particular rotating machine. The order-sampling of the raw data allows the effectiveness of the time domain averaging technique to be focused in a particular time frame. Since the data acquisition is totally in phase (coherent) with the events of interest, extraneous noise from other nonsynchronous sources can be reduced.

4.4 Random Decrement Analysis

The response of a system to a random input may be decomposed into a deterministic part (the homogeneous solution) and a random part, which we may assume to have zero means with no loss in generality. To isolate the deterministic part of the signal, we can average in such a way as to generate a so-called random decrement signature, or randomdec signature [5]. A randomdec signature may be generated in one of three ways. First, the samples to be averaged may be acquired by always starting with a constant amplitude. This method will yield a free decay step response. The second method involves acquiring samples when the amplitude [y(t)] equals zero and the slope is positive (or $dy/dt > 0$). This method gives a free decay positive impulse response. The third method involves acquiring samples when $y(t)=0$ and $dy/dt < 0$ and yields a free

decay negative impulse response. The free decay response can be described by the ensemble average

$$\delta(\tau) = 1/N \sum_{n=1}^{N} y(tn+\tau),$$

where y(t) is the random response.

The following conditions are also applied:

t_n = t when y = y_s for method 1,

t_n = t when y = 0 and dy/dt > 0 for method 2,

and t_n = t when y = 0 and dy/dt < 0 for method 3,

where y_s is the threshold amplitude for method 1. Figure 2 describes the process where a random signature is generated by method 1 [6].

Analysis of randomdec signatures is often used to detect changes in a random response curve when the input signal is not known. The response curve itself may be so complicated and variable that it cannot be used to detect changes in the system although the important information is contained within the time history. The randomdec signature computed by method 1 has several properties that make it useful as a failure detection mechanism. The first important property is that the signature has a constant amplitude, which respresents a calibrated level in the response curve. This property makes the signature level independent of changes in the intensity of the input. The fixed amplitude also serves to stabilize the form of the signature if damping nonlinearities with amplitude are present. A second important property lies in the randomdec signature units, which are the same as the original time history since only signal additions are performed (in contrast to correlation techniques, which involve multiplication).

As structural flaws or cracks begin to develop in, say, the bearing races of a pump, additional degrees of freedom, which will be excited by ball bearing impacts and other forces, will be introduced. The additional degrees of freedom will be manifest in altered structural modes that will modify the randomdec signature, providing an indication of possible incipient failure. Random decrement analysis allows the

detection of changes in the system characteristics by extracting the impulse response function from the system response function without specific knowledge of the system inputs. Another advantage of the technique is the ability to detect low level periodic data in the presence of high level random components.

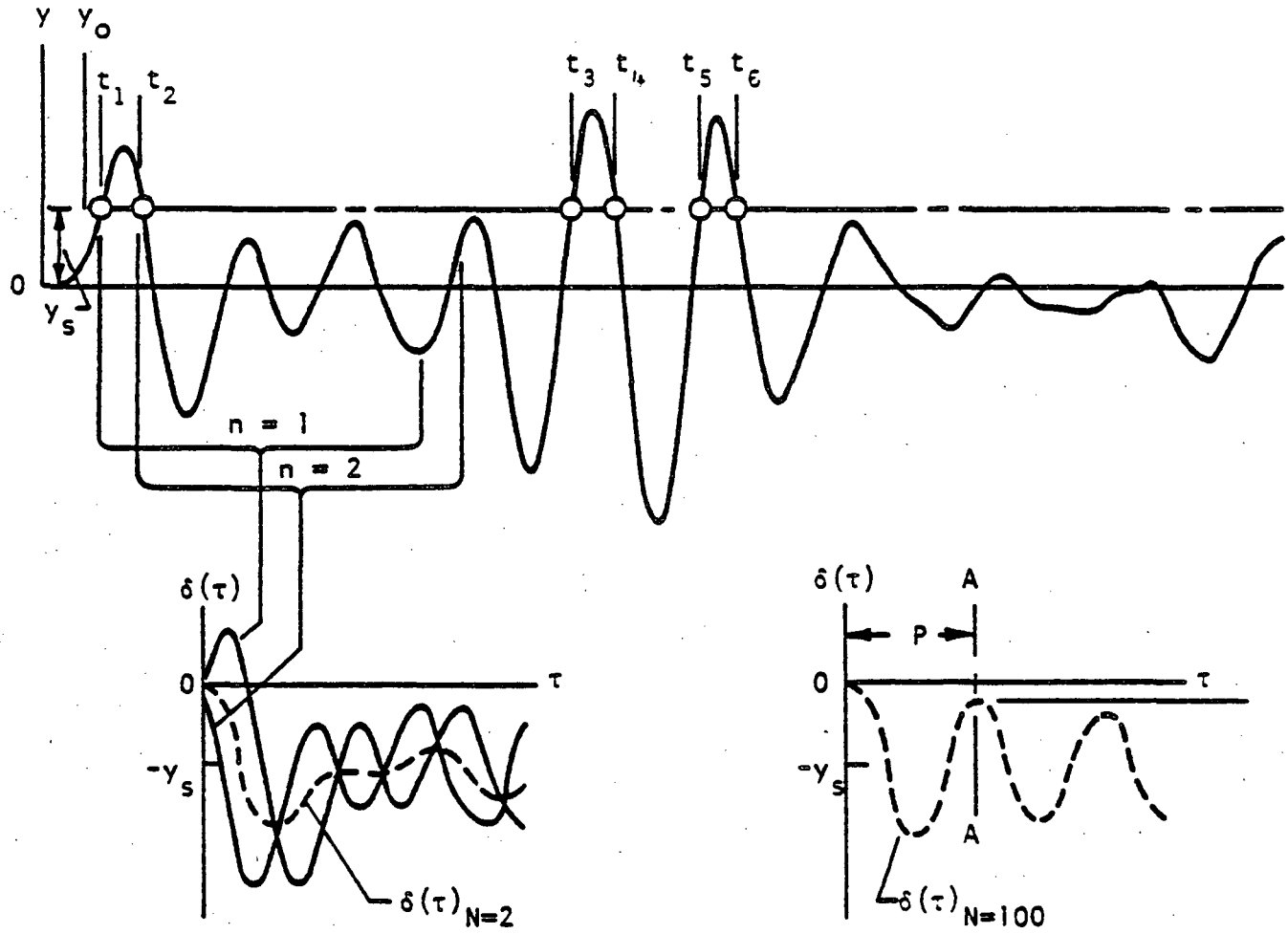

Figure 2. Evolution of a Random Decrement Signature

4.5 Cepstrum Analysis

The power cepstrum (originally called cepstrum) was first defined by Bogert, Healy and Tukey [7] as the power spectrum of the logarithm of the ordinary power spectrum. This may be written as [8]

$$C_x(\tau) = \left| \mathcal{F} \left\{ \log \left[S_{xx}(f) \right] \right\} \right|^2,$$

where

$$S_{xx}(f) = |F_x(f)|^2$$

and $$F_x(f) = \mathcal{F}\{f_x(t)\}.$$

The variable τ in the cepstrum is called the quefrency. Quefrency may be interpreted as the rate of fluctuation of related peaks in the power spectrum. For example, a high quefrency represents a rapid fluctuation in the spectrum and a low quefrency represents a slow fluctuation.

Cepstrum analysis may be applied to signal recognition by the response power spectrum for the single input case as follows:

$$S_{yy}(f) = |H(f)|^2 S_{xx}(f),$$

where

$S_{yy}(f)$ = power spectrum of the measured response,

$S_{xx}(f)$ = power spectrum of the internal source,

and $H(f)$ = transfer function from the internal source to the external measured response.

The logarithmic representation can be written as

$$\log\left[S_{yy}(f)\right] = \log\left[|H(f)|^2\right] + \log\left[S_{xx}(f)\right].$$

The cepstrum of the measured response is then

$$C_{yy}(\tau) = \left|\mathcal{F}\left\{\log\left[S_{yy}(f)\right]\right\}\right|^2$$

$$= \left|\mathcal{F}\left\{\log\left[|H(f)|^2\right]\right\}\right|^2 + \left|\mathcal{F}\left\{\log\left[S_{xx}(f)\right]\right\}\right|^2.$$

The product of the source spectrum and the transfer function has now become a sum. As a result, if the quefrency of the source spectrum is well separated from the quefrency of the transfer function, the two will be easily discernible in the response cepstrum.

4.6 Adaptive Noise Cancellation (Adaptive Filtering)

In general, the filtering process is used to reject the undesirable content and/or to extract desirable information from a contaminated source containing both. Historically, filters were designed with some a priori knowledge of the signal or noise characteristics to be extracted or rejected. Adaptive filters, however, have the ability to adjust their own parameters as an automonous system, therefore requiring little or no a priori knowledge of the signal or noise. As a result, the process of adaptive noise cancellation using adaptive filtering can be used with problems whose inputs are deterministic or stochastic, stationary or time variable. The concept of adaptive noise cancellation is a means by which signals corrupted by additive noise or interference can be estimated. The method uses a "primary" input containing both the desirable signal and noise along with a "reference" signal correlated in some unknown way with primary noise. The reference input is adaptively filtered and then subtracted from the primary input to yield an estimate of the desired signal [9].

The general concept of adaptive noise cancellation is discussed in detail in reference 9, and the use of the process as applied to machine monitoring is discussed in reference 10. An adaptive noise canceller as applied to a simplified model of a typical machine is shown in figure 3. The following theoretical discussion (taken from reference 10) presents a description of the methodology associated with the contamination of low level bearing signals as a result of signal path. The discussion utilizes z-transform theory and defines the relationship between the signal-to-noise ratios at the primary/reference inputs and the output of the adaptive noise cancellers.

The primary input consists of signal and noise components that are assumed to have propagated through channels with transfer functions L(z) and P(z) and with impulse responses l(j) and p(j) respectively. The primary input is then the sum of $s_j * l(j)$ and $n_j * p(j)$, where the * denotes the convolution integral. Likewise, the reference input consists of signal and noise components that are assumed to have propagated through channels with transfer functions G(z) and H(z) and with impulse responses g(j) and h(j) respectively. The reference input is the sum of $s_j * g(j)$ and $n_j * h(j)$. For the purpose of analysis, all propagation paths are assumed to be equivalent to linear time invariant filters. The error signal ϵ_j is the output of the noise canceller. The unconstrained Wiener filter theory can now be applied to the analyses of the adaptive noise cancelling problem of figure 3.

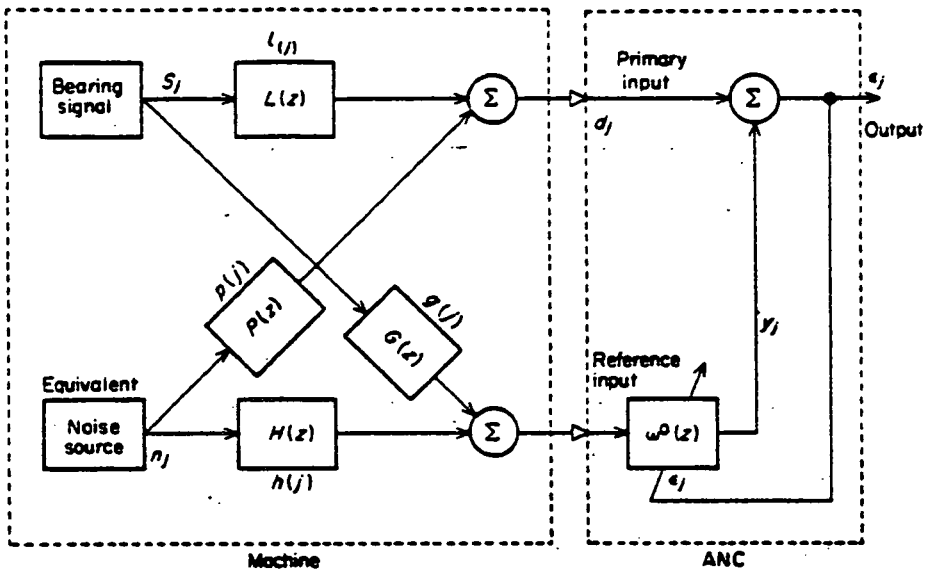

Figure 3. Adaptive Noise Cancelling Applied to a Simplified Model of a Machine (from ref. 10)

For stochastic stationary inputs, the steady state performance of adaptive filters closely approximates that of fixed Wiener filters, and Wiener filter theory thus provides a convenient tool for mathematically analyzing statistical noise cancelling problems. A classic Wiener filter with a single input and a single output is shown in figure 4. The assumptions here are that the input signal x_j, the output signal y_j, and the desired response d_j are discrete in time and also that the input signal and the desired response are statistically stationary. The error signal is then $\epsilon_j = d_j - y_j$. The filter is linear, discrete, and designed to be optimal in the least mean square (LMS) sense. It is composed of an infinitely long, two-sided tapped delay line. The optimal unconstrained Wiener transfer function is given by

$$\omega^0(z) = S_{xd}(z)/S_x(z),$$

where $S_{xd}(z)$ is defined as the cross power spectrum between the input signal and the desired response and $S_x(z)$ is the power spectrum of the input signal.

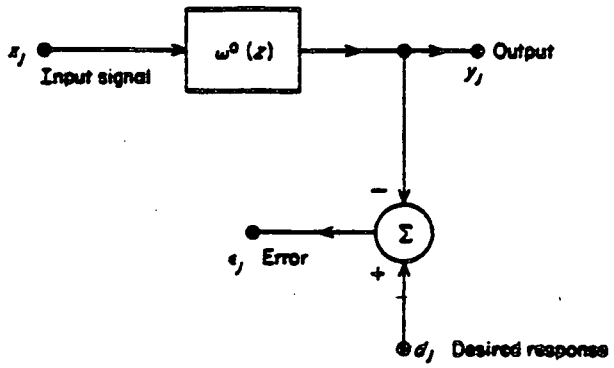

Figure 4. Single Channel Wiener Filter
(from ref. 10)

If the adaptive process in figure 3 has converged and the minimum mean square solution has been found then the adaptive filter is equivalent to a Wiener filter. The power spectrum of the signal, s_j (see figure 3) is $S_s(z)$ and that of the noise, n_j, is $S_n(z)$. The power spectrum of the reference input is then given by

$$S_x = S_s(z)\left|G(z)\right|^2 + S_n(z)\left|H(z)\right|^2,$$

and the cross spectrum between the reference and the primary input is

$$S_{xd} = G^*(z)L(z)S_s(z) + H^*(z)P(z)S_n(z).$$

Assuming that the adaptive process has converged,

$$\omega^0(z) = \frac{S_s(z)G^*(z)L(z) + S_n(z)H^*(z)P(z)}{S_s(z)\left|G(z)\right|^2 + S_n(z)\left|H(z)\right|^2}.$$

The output signal-to-noise density ratio is defined as

$$\zeta_{out}(z) \triangleq S_{s\ out}(z)/S_{n\ out}(z),$$

where $S_{s\ out}(z)$ is the power spectrum of the signal at the noise canceller output and $S_{n\ out}(z)$ is the power spectrum of the noise at the canceller output.

The transfer function of the propagation path from the signal input to the noise canceller output is $L(z) - G(z)\omega^0(z)$, thus the power spectrum of the signal at the canceller's output is

$$S_{s\ out}(z) = S_s(z)\left|L(z) - G(z)\omega^0(z)\right|^2,$$

Substituting in this the value of $\omega^0(z)$,

$$S_{s\,out}(z) = S_s(z) \left| \frac{S_n(z)L(z)\,|H(z)|^2 - G(z)H^*(z)P(z)S_n(z)}{S_s(z)\,|G(z)|^2 + S_n(z)\,|H(z)|^2} \right|^2$$

Similarly, the transfer function of the propagation path from the noise input to the canceller output is $P(z) - H(z)\omega^0(z)$, therefore the power spectrum of the noise at the canceller output is

$$S_{n\,out}(z) = S_n \frac{P(z)\,|G(z)|^2 S_s(z) - H(z)G^*(z)L(z)S_n(z)}{S_s(z)\,|G(z)|^2 + S_n(z)\,|H(z)|^2}^2,$$

and

$$\zeta_{out}(z) = \frac{S_s(z)}{S_n(z)} \frac{\left| S_n(z)L(z)\,|H(z)|^2 - G(z)H^*(z)P(z)S_n(z) \right|^2}{\left| S_s(z)P(z)\,|G(z)|^2 - H(z)G^*(z)L(z)S_s(z) \right|^2};$$

$$\zeta_{out}(z) = \frac{S_n(z)}{S_s(z)} \frac{|L(z)H(z)H^*(z) - G(z)H^*(z)P(z)|^2}{|P(z)G(z)G^*(z) - G^*(z)L(z)H(z)|^2}$$

$$= \frac{S_n(z)\,|H((z)|^2}{S_s(z)\,|G^*(z)|^2} \left| \frac{L(z)H(z) - G(z)P(z)}{P(z)G(z) - L(z)H(z)} \right|^2$$

$$= \frac{S_n(z)}{S_s(z)} \left| \frac{H^*(z)}{G^*(z)} \right|^2 |-1|^2.$$

Since $|H^*(z)/G^*(z)|^2 = |H(z)/G(z)|^2$,

$$\zeta_{out}(z) = \frac{S_n(z)}{S_s(z)} \left| \frac{H(z)}{G(z)} \right|^2.$$

The signal-to-noise density ratio at the reference input $\zeta_{ref}(z)$ can be expressed as

$$\zeta_{ref}(z) = S_{s\,ref}(z) / S_{n\,ref}(z),$$

where $S_{s\,ref}(z) = S_s(z)\,|G(z)|^2,$

$S_{n\,ref}(z) = S_n(z)\,|H(z)|^2.$

Substituting, one obtains

$$\zeta_{ref}(z) = S_s(z) \left|G(z)\right|^2 / S_n(z) \left|H(z)\right|^2$$

and

$$\zeta_{out}(z) = 1 / \zeta_{ref}(z).$$

Therefore, the signal-to-noise density ratio at the noise canceller output and at the reference input have a reciprocal relationship at all frequencies if the adaptive solution is unconstrained and the noises in the primary and the reference inputs are mutually uncorrelated.

The output of the adaptive noise canceller depends on the input signals in the following ways:

- If the signal-to-noise density ratio at the reference input is low, the output noise will be low; that is, the smaller the signal component in the reference input, the greater the noise cancellation.
- If the signal-to-noise density ratio in the primary input is low, the filter will more effectively cancel the noise rather than the signal.

In essence, this theoretically implies that the noise contaminating the signal at the primary input of the adaptive filter can be totally rejected or cancelled at the output if the reference signal contains none of the desired signal (zero signal-to-noise ratio) and the noise at the primary and reference inputs are correlated in some way. In practice, total cancellation is not realistic; however, the achievable noise cancellation at the output of the filter is on the order of the reciprocal of the signal-to-noise ratio at the reference input.

C-2

Section 5

DATA ANALYSIS AND RESULTS

Each of the six identified data enchancement or analysis techniques were applied to selected sets of SSME test data or laboratory prepared test signals. A summary of the types of data utilized for each technique is given in table 1. Table 2 provides a breakdown of the SSME tests utilized and general information associated with each test group.

It should be noted that the PSD was utilized more often as a comparative starting point from which the effectiveness of the other techniques could be evaluated rather than a data enhancement technique itself. The PSD was the logical choice for this role because it is a well-known, basic spectral analysis format for random data and has been routinely applied to SSME data. In all cases, the data reduction of the transducer output signals was performed using a digital signal analyzer operating under microcomputer control. As a result, software development to implement each technique in addition to providing control of instrument interaction was required, and for completeness that software has been included along with the resulting spectra.

5.1 Data Selection Criteria

The data to be used as test cases for the evaluation of any given technique were selected with the complexity of the technique and the availability of the various types of data in mind. For the most part, each technique was first applied to some type of laboratory signal to obtain a familiarity with the technique under controlled circumstances. Based upon the performance of the technique on the laboratory signals, a second type of data was selected. Normally, the data chosen was SSME test data. Early in the program, however, data from a laboratory test performed on a small turbopump similar to the HPOTP was available and was used as a test case for some of the techniques.

SSME test cases were selected such that the same HPOTP was used for a number of tests (typically 4 or 5 consecutive tests). It was believed that these test groups would

TABLE 1. Analysis Technique/Data Type Summary

Data Type	Analysis Technique					
	PSD	TDA	OSTDA	Randomdec	Cepstrum	ANC
Laboratory Test Signals	X	X		X	X	X
Saunders' Laboratory Bearing Test Signals	X	X	X			
SSME Static Test Firing Signals	X	X	X			X

TABLE 2. SSME Test Data Utilization Summary

HPOTP Serial Number	Engine Serial Number	Test Stand/ Test Number	Total Run Time Seconds	Comments
9008	2004	902/187-193	2400	Only test 193 analyzed. Bad #3 bearing discovered after test. Applied techniques: PSD, TDA, OSTDA, ANC.
0009	0009	901/290-294	2500	Only test 294 analyzed. Designated as test with good bearings. Applied techniques: PSD, TDA, OSTDA.
2206	0009	901/301	820	Single test run with known bearing flaw (spalled balls). Applied techniques: PSD, TDA, OSTDA, ANC.
0209 0209R1	0107 0107	901/339-343 901/351-352	2500	Test 339 was green run for pump. Adaptive filter test set 1. Inspection of pump performed after test 343; Boroscope indicated no apparent bearing damage. Slight spalling of bearing balls discovered after test 352. Applied techniques: PSD, ANC.
2113	2014	901/367-372	2000	Adaptive filter test set 2. Test 372 not reduced. Applied techniques: PSD, ANC.
2310	2010	902/271-276	2100	Adaptive filter test set 3. Test 276 not reduced. Applied techniques: PSD, ANC.

provide an abundance of data that would be representative of a specific pump's operation over a relatively long period of time. Generally, a group of SSME tests would be chosen when a completely refurbished pump was first installed on an engine, and all subsequent tests performed with the same pump were added to the group. If a particular bearing condition was known to exist, specific SSME tests were chosen to provide test cases that could be associated with the particular defects and/or operational configuration. In general, SSME tests are routinely performed with varying run times and power levels. As a result, some tests for a given pump did not provide a sufficient run time or maintain a particular power level for a period long enough to be properly analyzed. Therefore, data from some tests in a series were not reduced. For the most part, SSME test cases were chosen with operational power levels of 100-109 percent. Segments of the test run where a constant power level (either 100 percent or 109 percent) was maintained were isolated and analyzed using a particular data enhancement technique. Therefore, the entire test run was seldom reduced, and the total run time reflected in table 2 has no relationship to any given power level, only total pump operation.

5.2 HPOTP Spectral Characteristics

A typical PSD reduced from the signals provided through one of the accelerometers mounted on the flange at the turbine end of the HPOTP is shown in figure 5. This PSD was computed over the frequency range of 0-5 kHz with a resolution bandwidth (Δf) of 12.5 Hz. The spectrum is normalized to a 1-Hz basis and contains spectral information that is directly related to the dynamic operation and environment of the HPOTP. The most notable characteristics of this PSD are three prominent peaks in the spectrum. The lowest frequency peak is defined as the fundamental, or synchronous, frequency (1N) and is associated with the rotational speed of the main shaft. The second and third prominent peaks in the spectrum correspond to the fourth (4N) and eighth (8N) harmonics of the shaft rotational speed. These 4N and 8N peaks are quite pronounced and have been reinforced by the presence of a four-blade impeller attached to the shaft. Since these peaks are related to the rotational speed of the main shaft and this speed is relatively constant for a given power level, these peaks are quite narrow in width, corresponding to very narrow band energy concentrations. The lower level and more broadband random peaks constitute the background noise level of the spectrum. Contained within this background noise are the remaining harmonics (2N, 3N, 5N, 6N, etc.) of the rotational shaft speed. Since these harmonics are not readily identifiable,

SSME TEST 902-272 HPOT RAD 135 ACCEL. 109% PWL

TYPE OF ANALYSIS: PSD DATA TAPE:08 CH. NO.:09

DATA SLICE TIME INTERVAL=10:34:55-10:35:25

BANDWIDTH= 12.5 Hz

COMPOSITE= 1.501e 01 G's rms

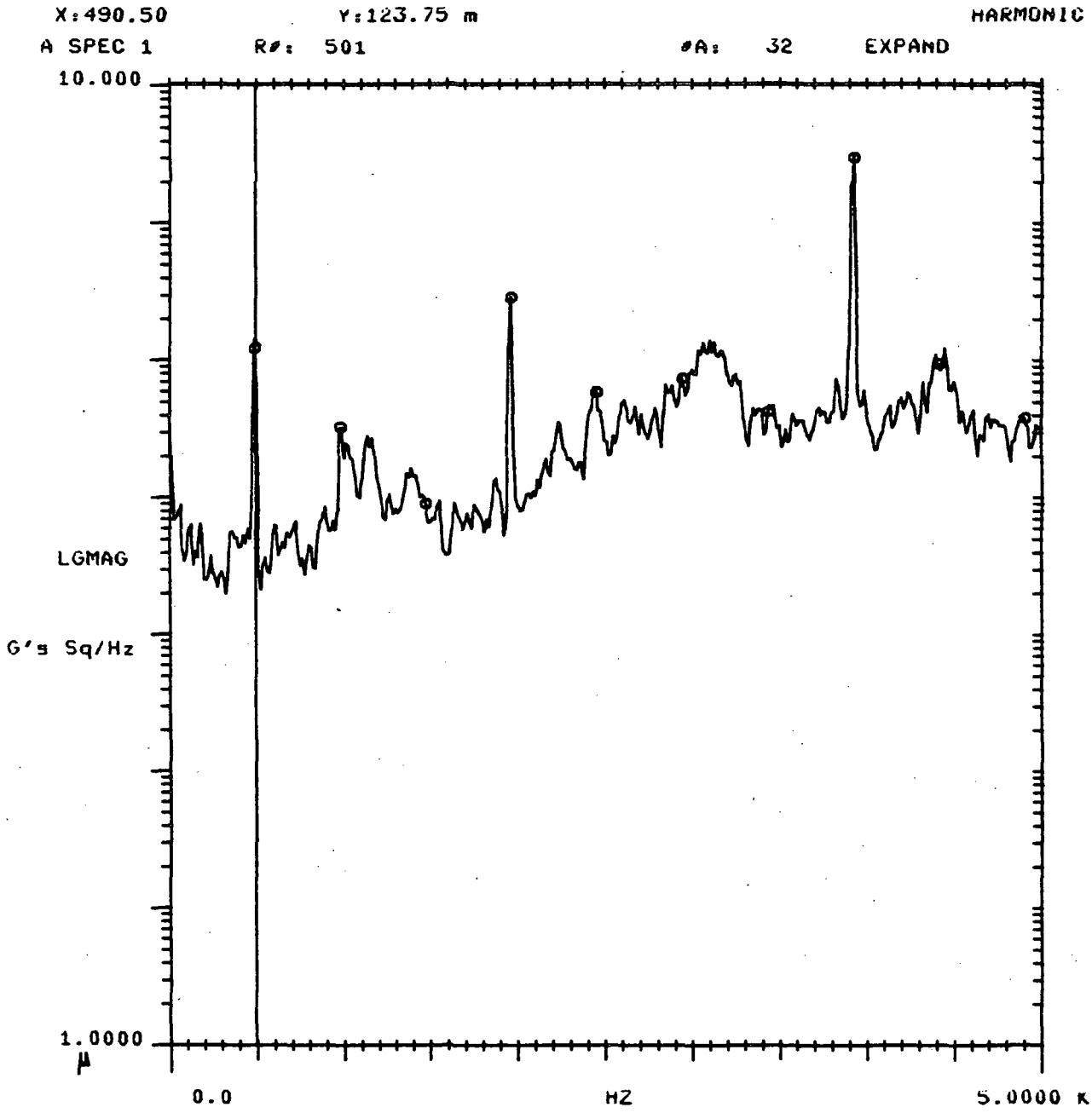

Figure 5. Typical HPOTP Acceleration PSD

they are said to be masked by the random noise content of the spectrum. In addition to the rotational speed/blade pass harmonics, other spectral components associated with dynamic operation of the HPOTP are also being masked by this background noise. Included among the masked spectral components are the inner/outer race ball-pass frequencies and ball-spin frequencies associated with the main bearings. It is interesting to note that an increase in the amplitude of the broadband random spectral data occurs in regions corresponding with these computed frequencies. These frequencies have been approximated through analytical computations and are contained in table 3.

TABLE 3. HPOTP Bearing Frequencies

Location	Frequency
Cage	0.427 x sync
Ball Pass:	
(a) Inner raceway	7.45 x sync
(b) Outer raceway	5.55 x sync
Ball Spin	3.13 x sync

5.3 Time Domain Averaging

Two separate but related approaches to the implementation of time domain averaging as a data enhancement/incipient failure detection technique were investigated. The first of these involved the development of computer software to perform the appropriate time shifting (nT) and averaging while the second approach used the more conventional technique of digitally acquiring blocks of analog data by using a predetermined trigger condition and averaging the entire data blocks in the time domain. The details associated with the implementation of each technique and the results achieved with each are discussed in the following sections. A flowchart depicting the basic operation of the software developed for implementation on an HP 5451C Fourier analyzer is shown in figure 6 and a listing is provided in table 4.

5.3.1 Shift-and-Add Time Average

Several generations of TDA software were developed with each following the same basic flow and each successive generation incorporating new refinements. In the first generation, the software initiated the acquisition of a single block of time data as

TABLE 4. TDA Software Listing

```
  1 L     1500
  5 Y     5838      15
 10 Y     5821       6
 15 Y     5865       6
 20 Y     5814
 24 BS    1024
 28 Y     5819       1        1
 34 Y R     2000
 39 Y     5819       2        1
 45 Y R     2001
 50 Y :     2000       1    2000D
 57 Y :        0    2000D    2001D
 64 Y :     2000       1    2000D
 71 Y A-       0      0D        2
 78 L     1510
 82 Y     5814
 86 CL       2
 90 Y *     2002      0D    2001D
 97 Y :     2002       1    2002D
104 L     1520                    MS33 16
108 CL
111 CL       1                     MS23
115 X<       5
119 X>       1
123 L     1521
127 -        1      0D
132 A+       1
136 #     1521      10        0
142 :        0      10
147 BS     512
151 F
154 *-
157 L     1530
161 TL

164 Y     5800
168 Y     5808     900      500
174 Y     5819      11
179 Y     5808     900      750
185 Y     1809    2000
190 Y     5808     850      750
196 Y     1809    2002
201 Y -          1        0
207 L     1531
211 Y A+         1
216 #     1531       0        0
222 Y     5820
226 L     1532
230 Y A+         1
235 #     1532      20        0
241 Y A+         0
246 BS    1024
250 #     1510       5        0
256 .
```

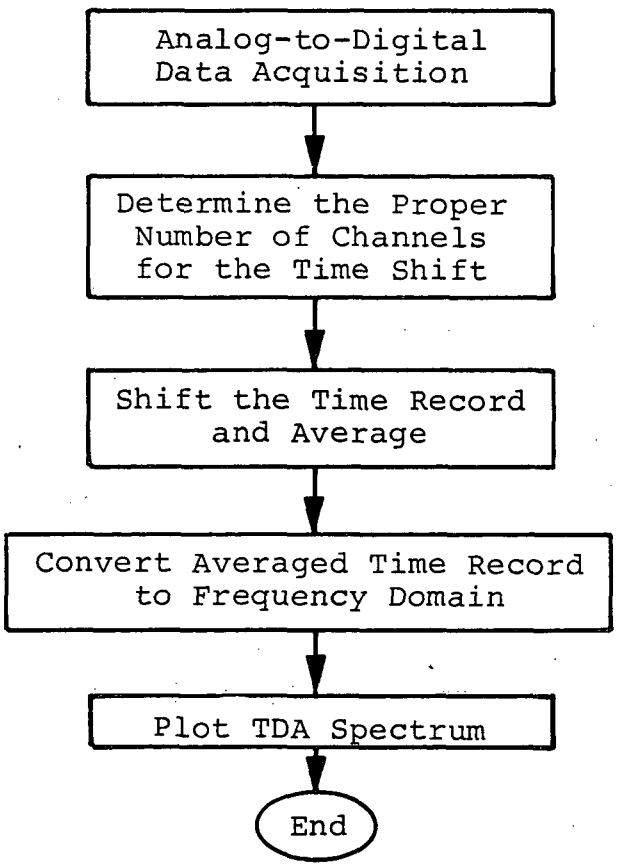

Figure 6. TDA Software Flowchart

specified by the HP 5451C front panel switches controlling the digital sample rate (Δt). The software then allowed the user to specify the desired TDA filter frequency (f_d). To perform the time averages, the original data block was shifted an integer number of Δt's and then averaged. This "shift-and-add" process was repeated until the user-specified number of averages was complete. In most cases, the desired TDA period ($T_d = 1/f_d$) did not coincide with an integer number of Δt's. Therefore, a TDA filter sweep was incorporated into the software to calculate the number of Δt's ($n\Delta t$) closest to T_d, and five separate time averages beginning with $T_a = (n-2)\Delta t$ and ending with $T_a = (n+2)\Delta t$ were then calculated for the original block of data.

To evaluate the TDA software, a complex periodic signal containing a variety of frequency components with two known levels was synthesized in the laboratory for use as a test case. A TDA filter sweep around 2441.4 Hz, 3418.0 Hz, and 12,500 Hz was performed, and some interesting results emerged. It was noted that the level of the test signal was reduced in some cases but not in others. As a result, an unanticipated problem associated with the block shift TDA technique became apparent. The difficulty arose from the fact that only under special circumstances did the center frequency of the TDA filter correspond with the center of a frequency resolution filter of the FFT. As an example, consider the case where data is acquired in a 2048-point data block with a sample rate (Δt) of 20 microseconds and a resulting frequency resolution (Δf) of 97.656 Hz. For this case, the center frequency of the TDA filter generated from a 20-Δt shift is $1/20\Delta t$ or 2500 Hz. This frequency does not correspond to an integral number of Δf's (2500 Hz = 25.6 Δf); however, if a TDA filter generated by a 16-Δt shift ($1/16\Delta t$ = 3125 Hz) is considered, an exact correspondence to the thirty-second narrow band filter (or 3125 = 32 Δf) is obtained. From this argument, it can be seen that the selection of the Δt shift can be quite critical and therefore restricts the usefulness of the shift-and-add time domain averaging technique.

5.3.2 Triggered Time Average

The second TDA technique studied involved acquiring analog data by using a trigger and averaging entire data blocks in the time domain. When a trigger condition (based on the periodic signal to be extracted) was met, the data acquisition for each data block began. Laboratory data was generated by combining a random signal with a 3125-Hz sinusoidal signal in an electronic summing network. The data acquisition trigger was generated by converting the sine wave to a pulse through a ratio frequency

synthesizer (VIC960B). The pulse as used as a trigger to initiate each analog-to-digital data acquisition process. A block diagram of this setup is shown in figure 7. It should be noted that this procedure produces the same in-phase relationship between the sinusoidal component of each successive time domain data block, as did the previously described shift-and-add TDA technique.

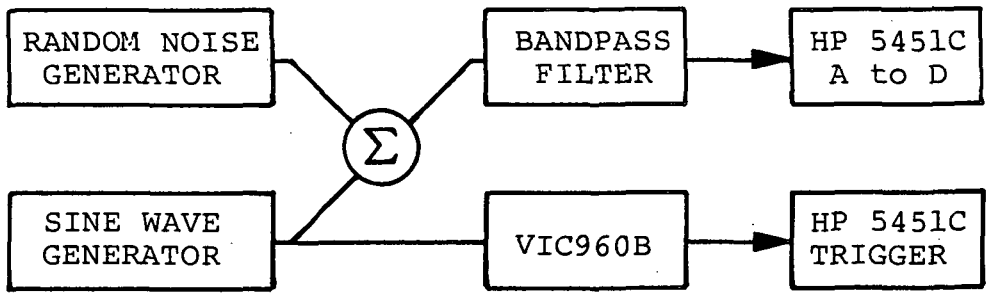

Figure 7. TDA Laboratory Data Block Diagram

The triggered time domain average technique was applied to three sets of laboratory synthesized test data. The test signals were composed of a sinusoidal component (3125 Hz) combined with white random noise. The first set of test data contained a sinusoidal component whose rms level was approximately 3 dB above the random signal. Figure 8 contains the PSDs for the sinusoid, sinusoid + random components, and various combinations of time/frequency domain averages or ensembles (TDA/FDA). One should note that the sinusoidal component can be readily identified in all the PSDs. It is also apparent from figure 8c and d, however, that the level of the random components has been reduced by approximately two decades. In addition, one should note the smoothing effect on the random components in the spectra. This should be expected since the process (FDA) is the same as the normal PSD ensemble computation.

Since the sinusoidal component of the test signal was pronounced in all the PSDs from the outset, a second set of data was synthesized by using the same random signal, but the rms value of the sinusoid was reduced to approximately 10 dB below that of the random signal. As can be seen in figure 9, the sinusoidal component cannot be identified in the PSD of the combined signal. After 50 TDA computations and 5 frequency domain averages (ensembles), however, the sinusoid can just be recognized.

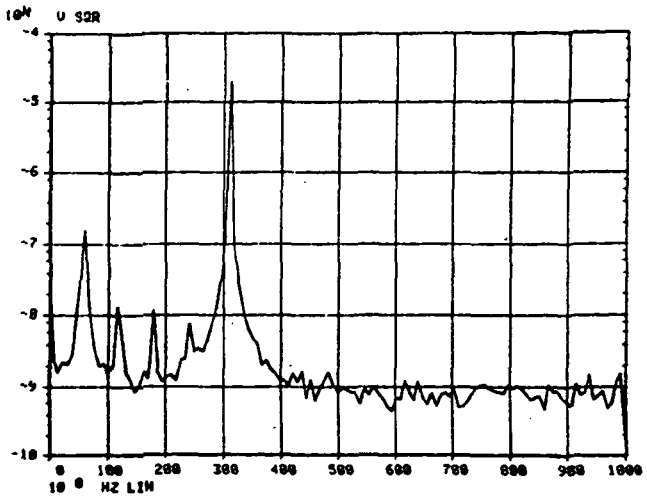

(a) Sinusoidal Component (3125 Hz)

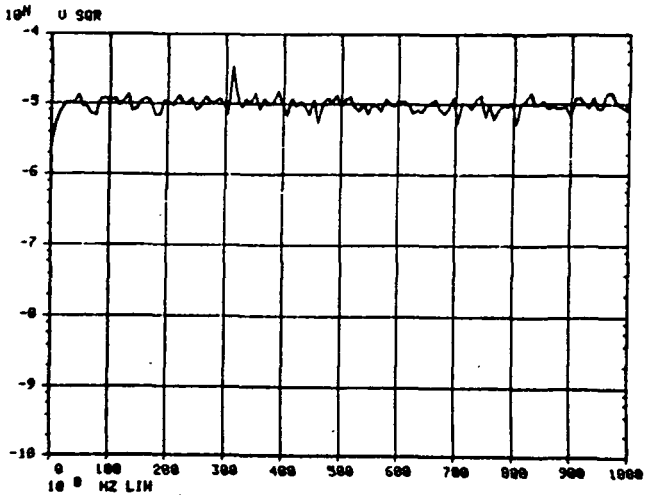

(b) Sinusoid + Random

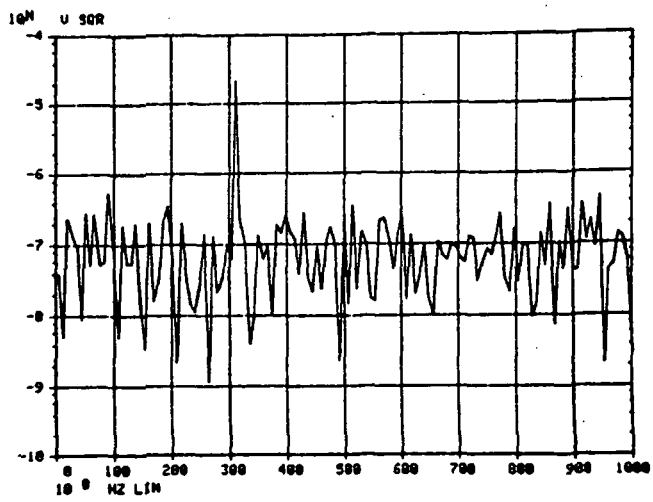

(c) 100 TDAs/1 FDA

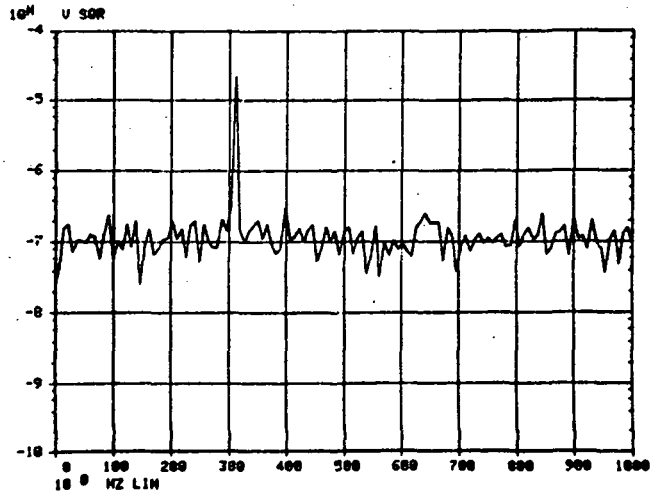

(d) 100 TDAs/5 FDAs

Figure 8. TDA Results With Sinusoid 3 dB Above Random Level

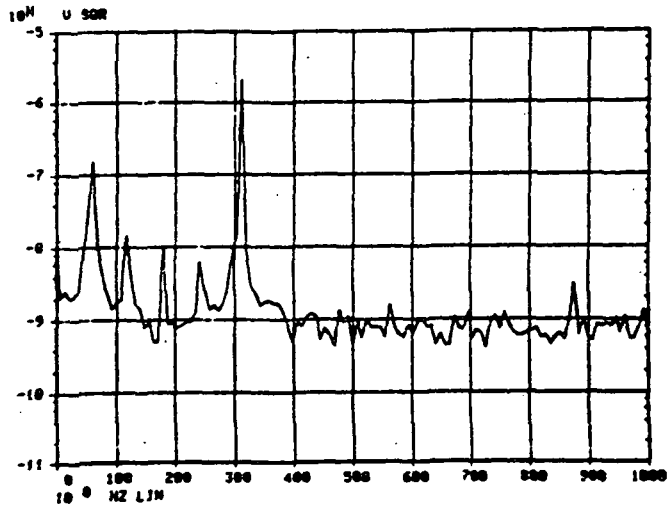

(a) Sinusoid

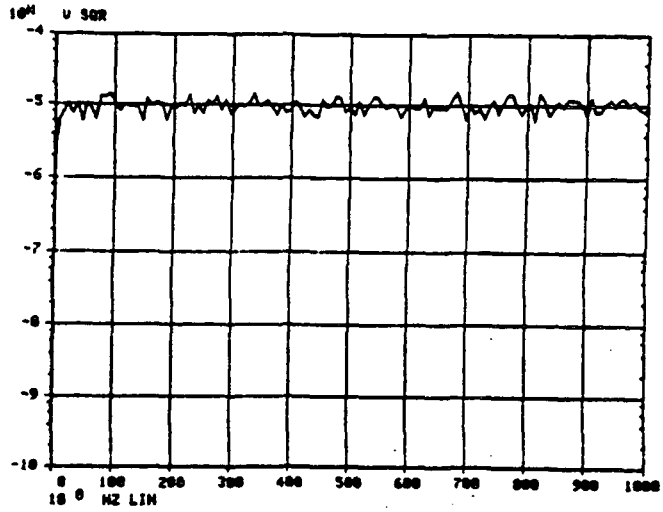

(b) Sinusoid + Random

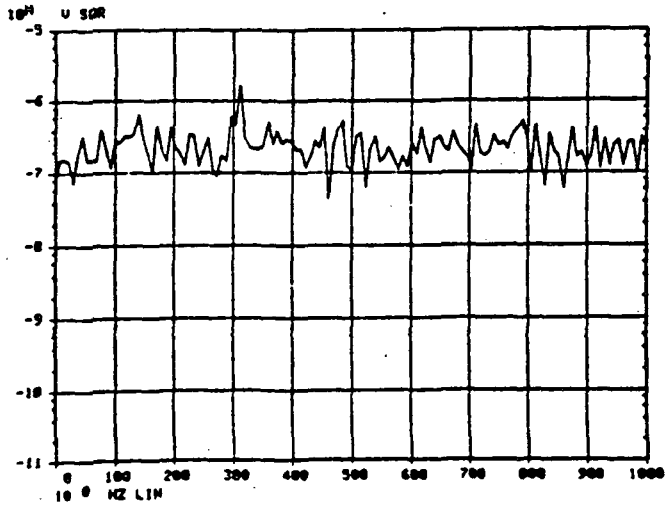

(c) 50 TDAs/5 FDSs

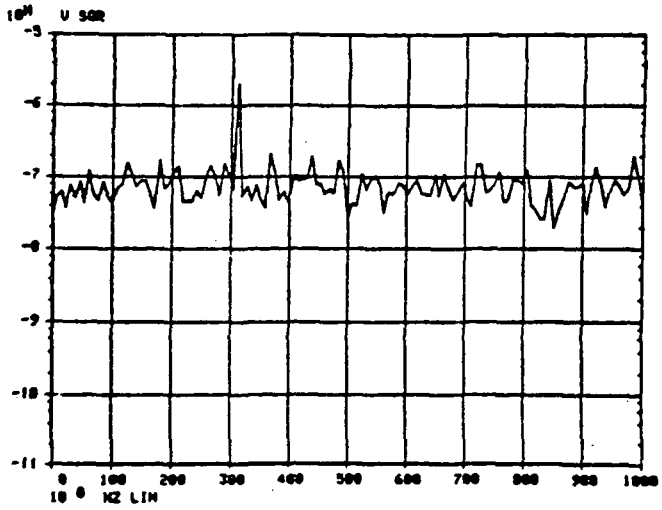

(d) 150 TDAs/5 FDAs

Figure 9. TDA Results With Sinusoid 10 dB Below Random Level

By the time 150 TDAs along with the 5 FDAs have been completed, the sinusoidal component is definitely identifiable. Again, a reduction of approximately two decades has been achieved through the application of the TDA/FDA technique.

Finally, a third test signal was used in which the rms level of the sinusoid was reduced by an additional 7 dB (-17 dB total) below that of the same random signal. Once again the sinusoid could be identified, but a substantial number of TDA were required (see figure 10). Figure 11 is a graphical depiction of the effectiveness of the TDA technique as a function of the number of time and frequency domain averages for both linear and autospectral density analyses.

From an examination of the three sets of data and the evaluation of the magnitude of the random noise with respect to the number of TDAs, a trend that closely follows the prediction of the TDA mathematics was noted. Namely, the magnitude of the noise was reduced by approximately the square root of the number of TDAs. At the same time, the magnitude of the sinusoid remained unaffected. The effect of ensemble autospectral averaging (FDA) serves only to "smooth" the random signal.

5.3.3 TDA Technique Evaluation

In evaluating the two time domain averaging techniques described, it was seen that TDA can be a useful tool for extracting low level periodic information from a high level random signal. To perform the number of time domain averages necessary to lower the random signal level to below that of the target information, however, the amount of continuous raw data (time) required becomes greater as the magnitude of the periodic information with respect to the random signal decreases. Also, as previously discussed, it is necessary to have some a priori knowledge of the signal to be extracted. This information may take the form of a user-defined TDA filter center frequency, as with the shift-and-add software, or a trigger related to the signal that is being extracted. For application to incipient failure detection of bearing degradation, the required a priori knowledge is not always available. For example, the accuracy of ball-pass frequency calculations is affected by how closely the ball slippage can be approximated. For this reason, even when using the triggered time average technique, the data must be reduced using several different trigger, or TDA filter, frequencies covering a range surrounding the calculated ball-pass frequencies.

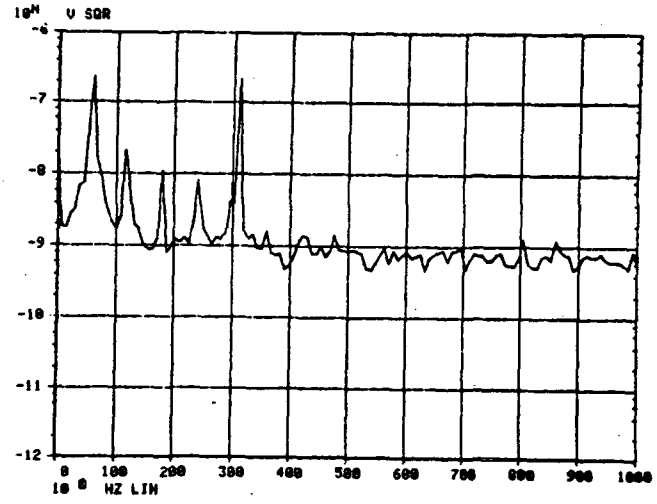

(a) Sinusoid Component (3125 Hz)

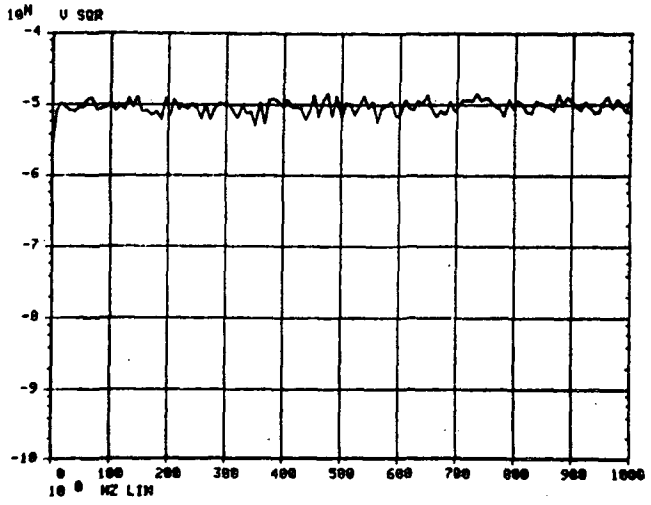

(b) Sinusoid + Random

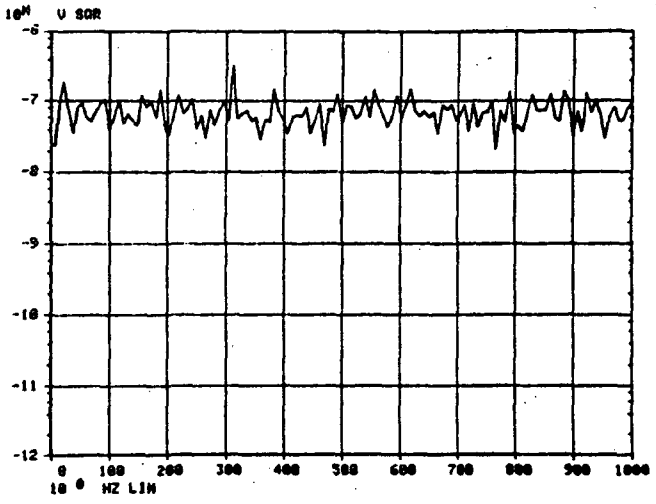

(c) 150 TDAs/5 FDAs

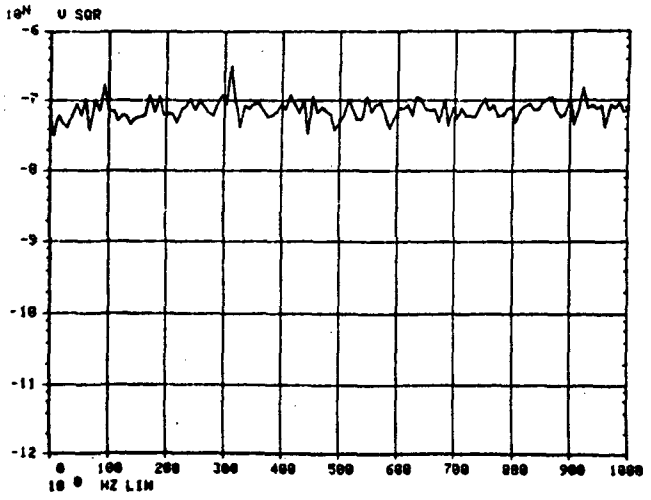

(d) 150 TDAs/10 FDAs

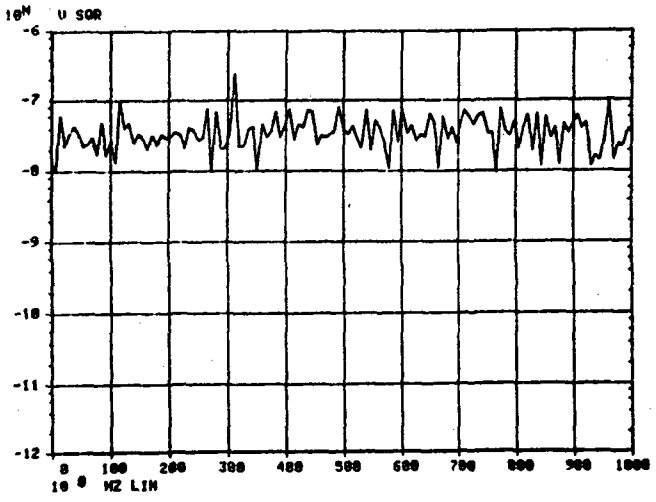

(e) 300 TDAs/5 FDAs

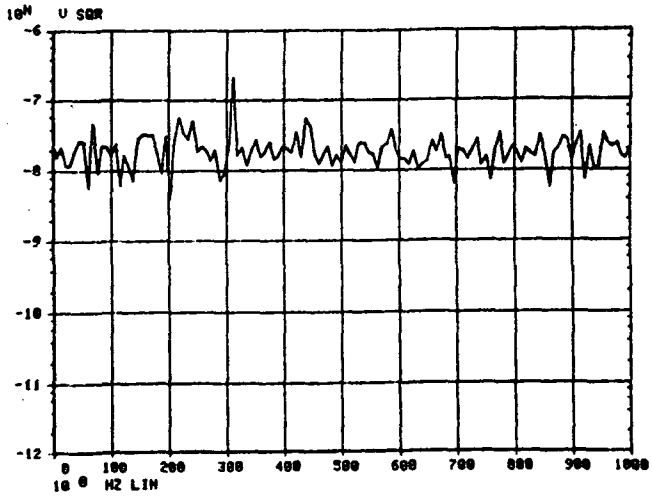

(f) 600 TDAs/5 FDAs

Figure 10. TDA Results With Sinusoid 17 dB Below Random Level

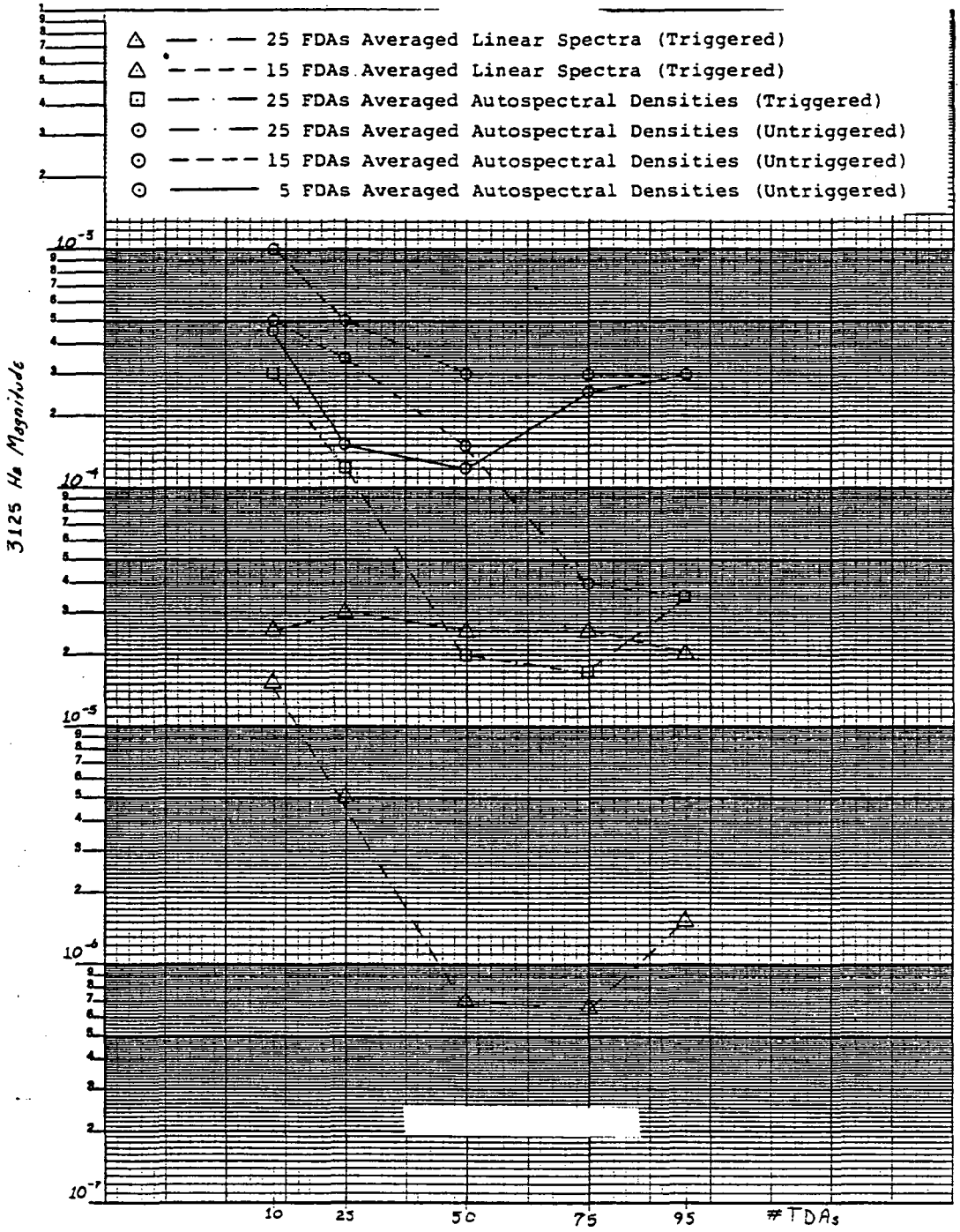

Figure 11. TDA Performance Summary as a Function of the Number of Frequency and Time Domain Averages

Of the two techniques discussed, the software shift-and-add technique shows promise but requires more development. This technique would be of most value when a trigger related to the periodic signal being extracted is not available. The triggered time averaged method, however, appears to be useful as long as a trigger signal is available. When a trigger signal is unavailable, further work needs to be conducted in an effort to isolate a suitable trigger from, possibly, a shaft or turbine blade passage harmonic.

5.4 Order-Sampled Time Domain Averaging

Based on the work and conclusions described in the previous section, the triggered time average technique was combined with order ratio sampling for futher evaluation and development. Order sampling simply means that the analog-to-digital (A-to-D) sample rate is keyed to the rotational speed of the machine whose signature is being analyzed. When this sampling is implemented by the HP 5451C, the number of orders of the revolution that can be resolved in the spectrum is one-half of the sampling rate. This is called the Nyquist frequency, as treated in Shannon's sampling theorem. In other words, if an analysis of ten orders of the revolution rate is desired, the A-to-D sampling must be triggered at 20 times the rotation frequency (20N). Obviously, like TDA, order sampling requires a speed probe, or tachometer. As with the TDA trigger, the sample rate trigger is generated by a ratio frequency synthesizer from a speed probe or a detectable machine harmonic (such as blade passage) in the data.

5.4.1 Laboratory Data Evaluation

The order-sampled time domain averaging (OSTDA) technique was used to reduce bearing test data generated by the MSFC Dynamics Lab. Briefly, this test involved a small turbopump with two main ball bearings. The pump was turned at approximately 850 rpm (14.2 Hz) by an electric drill motor. Several tests were run, each under different conditions. At least one test was run with a known flaw (a hole drilled in the outer race) in one of the bearings. The actual condition of each bearing during the tests was not revealed so that the data might be viewed objectively. During each test, acceleration data on the pump housing above each bearing as well as a tachometer signal were recorded on magnetic tape. Before the data were reduced, some calculations were made to approximate some of the bearing characteristics, such as inner and outer race ballpass frequencies, ball spin frequency, etc. These characteristic frequencies are listed in table 5. (These tests have been referred to as the

Saunders' bearing tests because they were conducted by Jerry Saunders of the MSFC Dynamics Lab.) The data reduction instrumentation used for these tests is shown in figure 12. The output of the VIC 960 is a square wave whose frequency is a ratio of the input periodic signal. The square wave output was bandpass filtered around the fundamental to produce a sine wave. These sine wave signals were used for the data acquisition and sample rate triggers.

TABLE 5. Characteristic Frequencies for Saunders' Bearing Test

	Frequency at 850 rpm (Hz)	f_i/f_{sync}
Synchronous	14.17	1.00
Ball Spin	38.96	2.75
Ball Pass:		
(a) Outer Raceway	59.50	4.20
(b) Inner Raceway	82.88	5.85

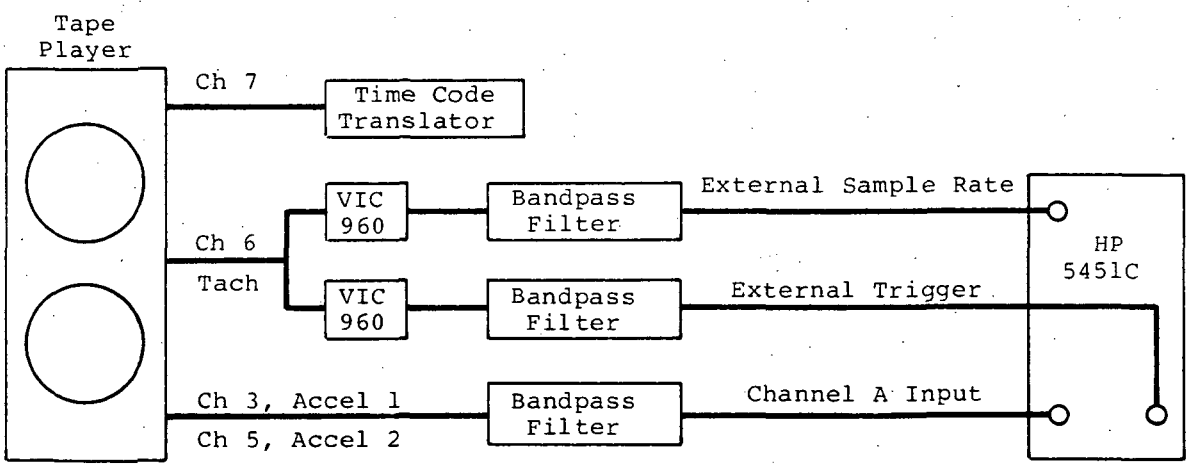

Figure 12. Block Diagram of the Data Reduction Instrumentation for Saunders' Bearing Tests

Figures 13 and 14 contain the reduced data from two of Saunders' bearing tests (test 2). The data set includes a baseline order-sampled autospectrum and OSTDA calculated spectra for each frequency in table 5. OSTDA calculations were included for the 1N case so that all harmonics of the shaft frequency could be viewed. (N

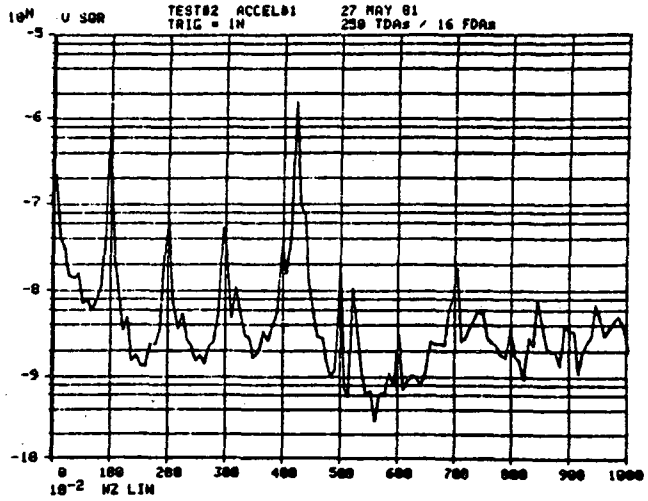

(a) 1N OSTDA

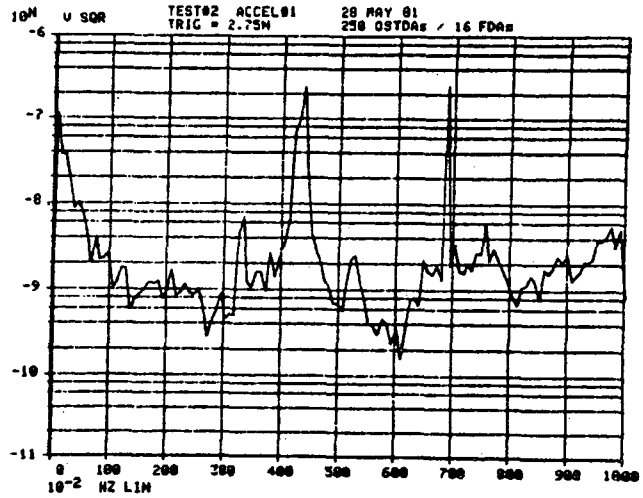

(b) 2.75N OSTDA

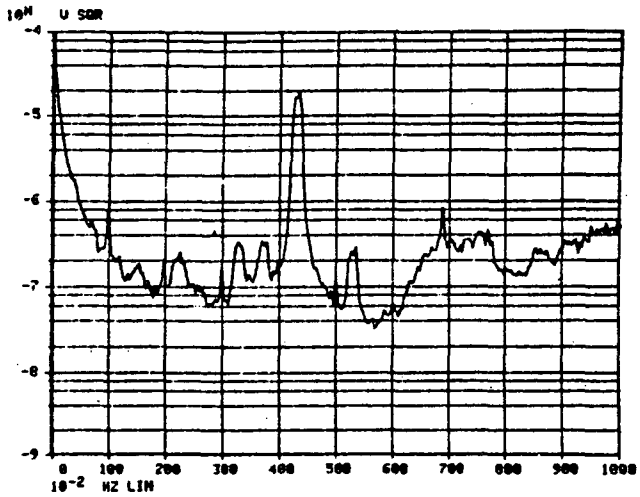

(c) Baseline Autospectrum

DATA NOT AVAILABLE

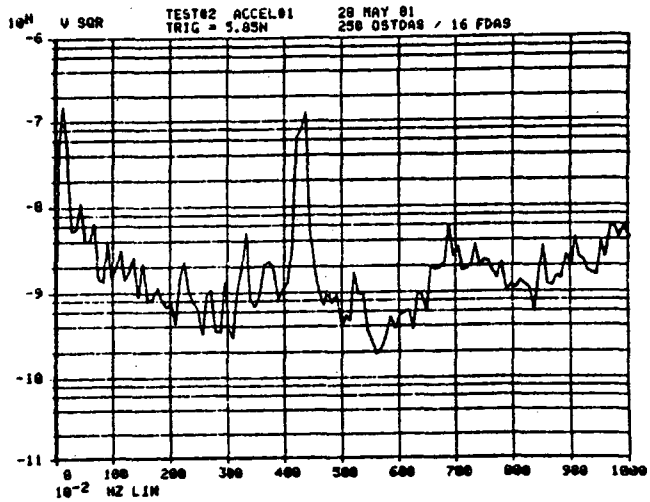

(d) 4.2N OSTDA

(e) 5.85N OSTDA

Figure 13. OSTDA Results for Saunders' Bearing Test 2, Accelerometer 1; 250 TDAs/16 FDAs

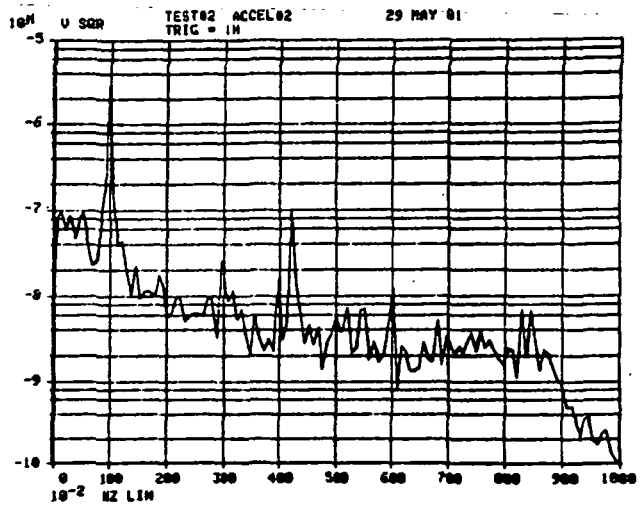

(a) 1N OSTDA

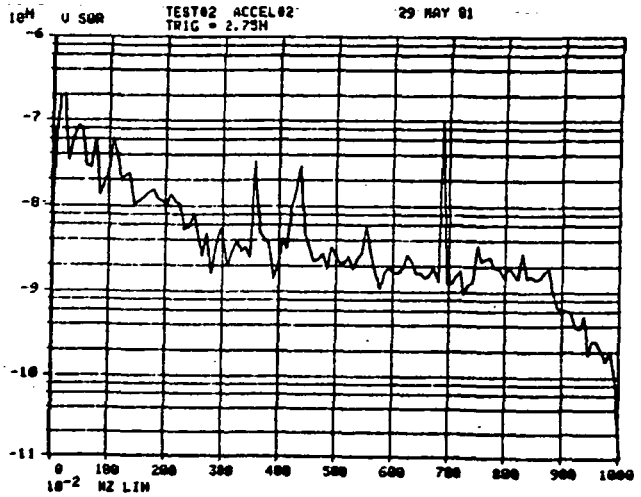

(b) 2.75N OSTDA

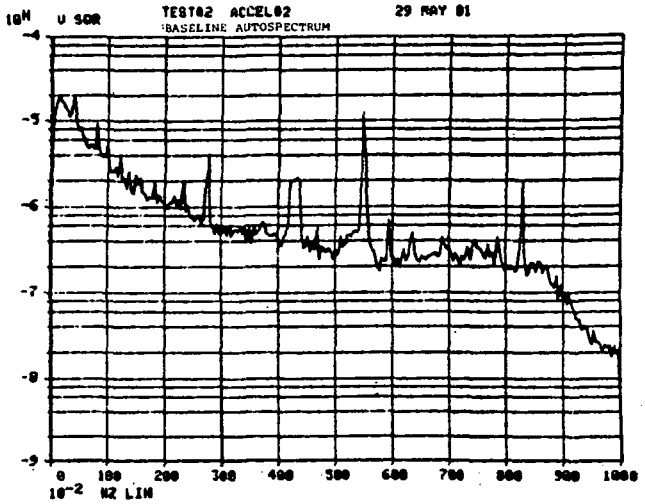

(c) Baseline Autospectrum

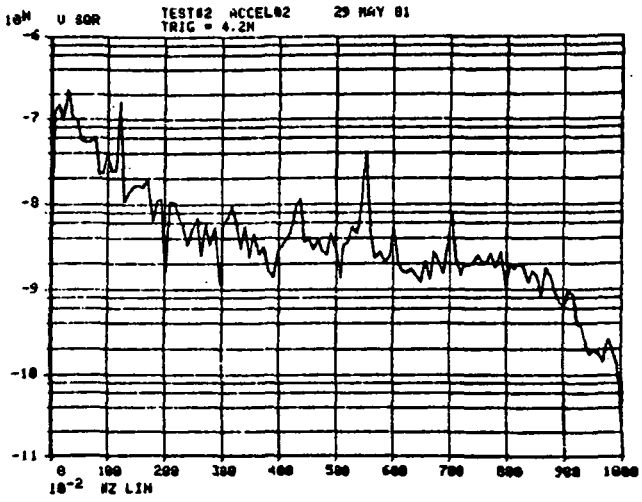

(d) 4.2N OSTDA

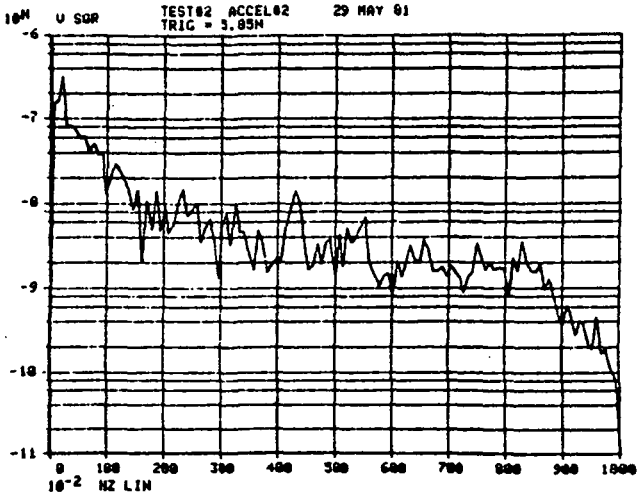

(e) 5.85N OSTDA

Figure 14. OSTDA Results for Saunders' Bearing Test 2, Accelerometer 2; 250 TDAs/16 FDAs

refers to the synchronous frequency, or running speed, of the machine.) No OSTDA calculations were performed at the 4.2N frequency because the 60-Hz line noise was dominant in all data from accelerometer 1. For all data sets reduced from Saunders' tests, 250 time averages were calculated. The time domain averaged data was converted to an autospectrum and averaged with 15 other similar ensembles. Table 6 lists the keyboard program used to calculate the baseline autospectra, and table 7 lists the keyboard program used to calculate the OSTDA spectra.

Figure 13 contains the baseline autospectrum for test 2, accelerometer 1. The first feature of this spectrum that should be noted is the presence of peaks associated with the first, second, third, and fifth orders of the synchronous frequency. In addition, extraordinarily wide peaks are present at 3.25N, 3.75N, 4.2N, and 5.25N. It is hypothesized that this phenomenon is caused by the presence of frequencies that are not constant with respect to the pump speed. The 4.2N peak is known to be a 60-Hz line noise whose frequency is constant; however, the pump speed is not constant. Therefore, the normally narrow frequency component appears widened due to the 1N order sampling. Also, a very sharp peak stands out at approximately 6.85N. This peak was also present in the OSTDA spectra calculated for the 2.75N, 3.75N, and 5.85N triggers, but it could not be seen in the OSTDA spectrum calculated with a 6.85N trigger. The OSTDA spectrum for a 1N trigger clearly shows all the harmonics of the synchronous through the seventh, and the noise floor has been reduced by approximately 20 dB. Although the remaining OSTDA spectra show a reduction of the noise floor, none of the corresponding peaks are pronounced.

The data reduced from Saunders' test 2, accelerometer 2 is presented in figure 14. In the baseline autospectrum for accelerometer 2 none of the synchronous harmonics are prominent; however, sharp peaks at 2.75N and 5.5N are noticed. The peak at 4.2N is again caused, at least in part, by 60-Hz line noise, though the magnitude is not as dominant as in the accelerometer 1 data. The 1N OSTDA spectrum shows the 1N, 3N, 4N, and 6N harmonics of the shaft speed clearly. As was the case with the data from accelerometer 1, no peaks at the other OSTDA trigger frequencies can be seen in the remaining OSTDA spectra.

Figures 15 and 16 contain the reduced data from Saunders' test 3 for accelerometers 1 and 2 respectively. The same trends are noted in this data; however, the noise floor is

TABLE 6. Order-Sampled Autospectrum Software Listing

```
                                                  27 MAY 81
 1 L        0
 5 BS     512                                     BASELINE AUTOSPECTRUM
 9 Y     5865        5                           ORDER SAMPLED @ 20*N
14 Y     5818        1                           FREE RUN TRIGGER
19 CL       1
23 L        1
27 CL
30 RB
33 *        0     735
38 :        0   10000
43 F
46 *-
49 A+       1
53 X>       1
57 #        1     100        0
63 :        1     100
68 *        1       2
73 X<       1
77 TL
80 Y K
84 .
```

TABLE 7. Order-Sampled Time Domain Averaging Software Listing

```
 1 L        0                                    28 MAY 81
 5 Y     3865        5
10 Y     5818        1                           TDA CALCULATIONS
15 BS     256                                    ORDER SAMPLED
19 CL       2
23 Y -          1       0
29 L        1
33 CL       1
37 L        2
41 CL
44 RB
47 A+       1
51 X>       1
55 #        2     250        0
61 :        0     250
66 F
69 *-
72 A+       2
76 X>       2
80 Y A+         1
85 Y IF         1       4       2      -2
93 D
96 Y -          1       0
182 #       1      16        0
108 :       0      16
113 *       0     735
118 *       0     735
123 :       0   10000
128 :       0   10000
133 *       0       2
138 X>      2
142 TL
145 Y K
149 .
```

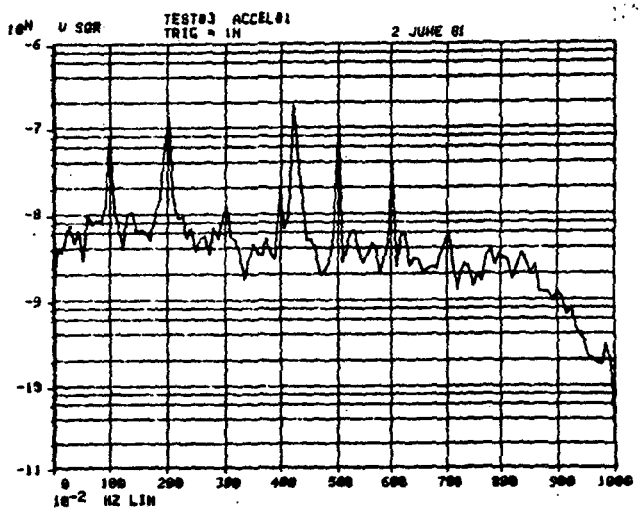

(a) 1N OSTDA

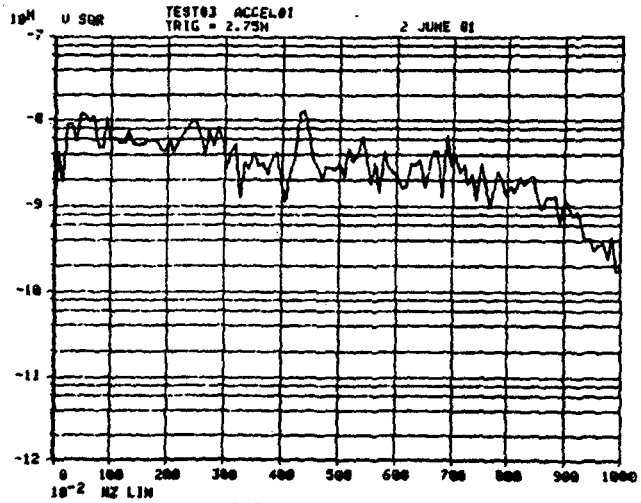

(b) 2.75N OSTDA

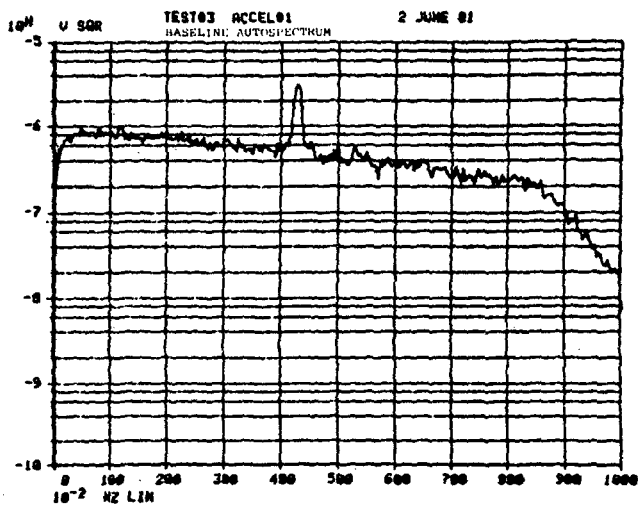

(c) Baseline Autospectrum

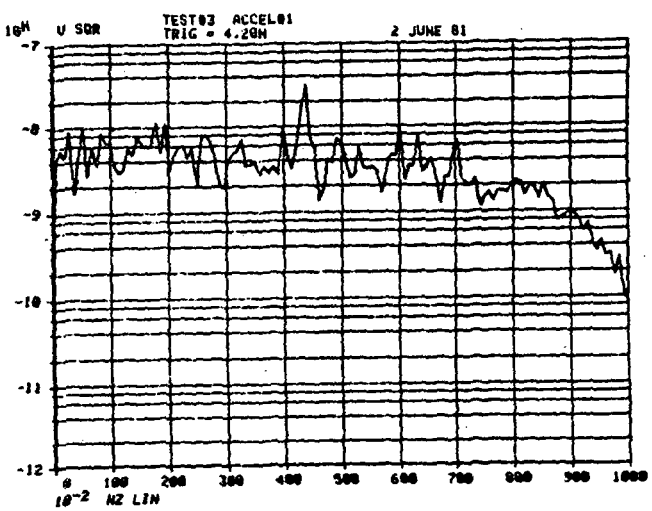

(d) 4.2N OSTDA

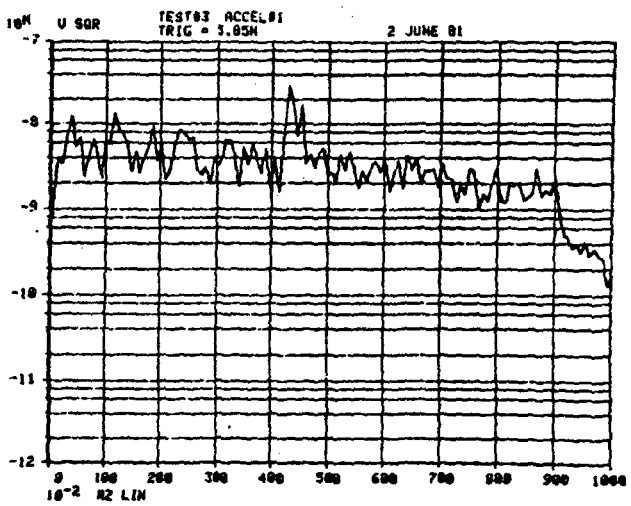

(e) 5.85N OSTDA

Figure 15. OSTDA Results for Saunders' Bearing Test 3, Accelerometer 1; 250 TDAs/16 FDAs

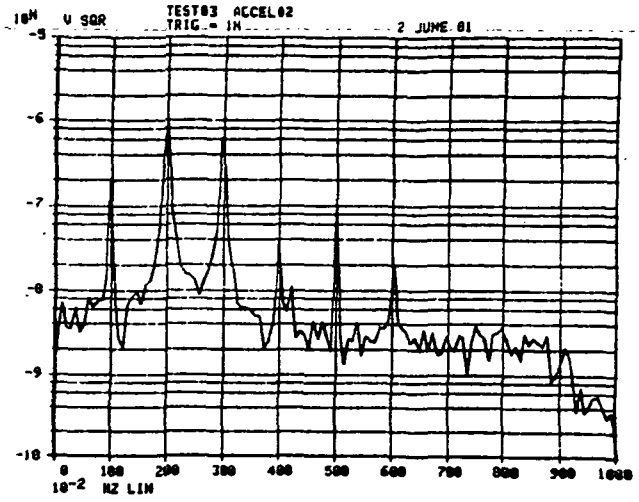

(a) 1N OSTDA

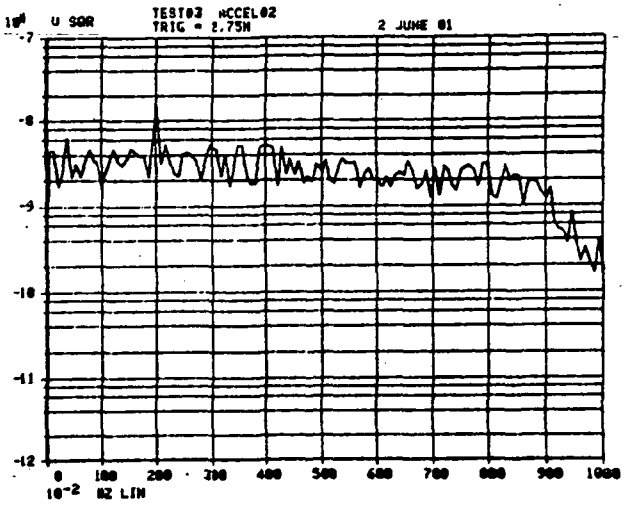

(b) 2.75N OSTDA

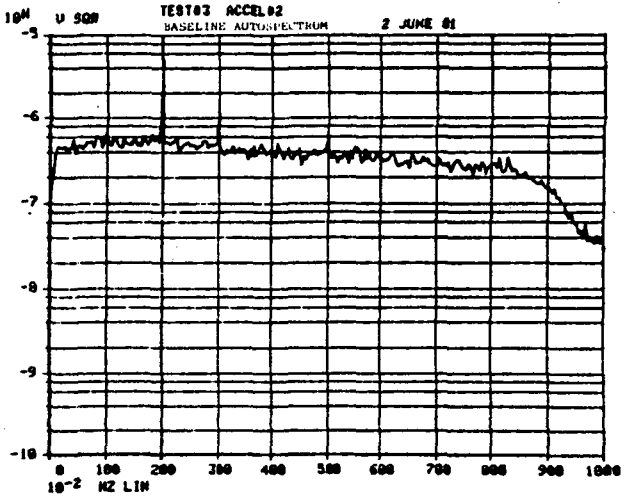

(c) Baseline Autospectrum

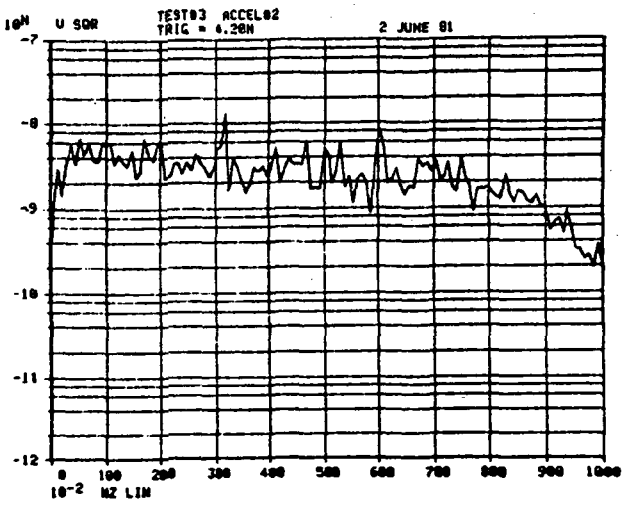

(d) 4.2N OSTDA

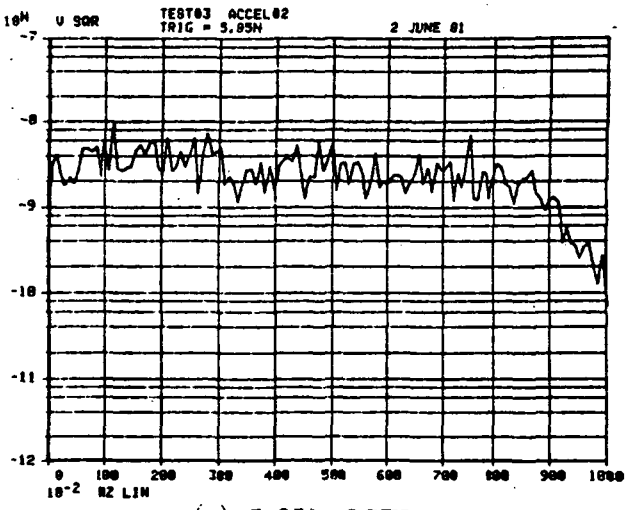

(e) 5.85N OSTDA

Figure 16. OSTDA Results for Saunders' Bearing Test 3, Accelerometer 2; 250 TDAs/16 FDAs

higher on both accelerometer 1 and accelerometer 2 during test 3. As with the test 2 data, the 60-Hz line noise is present in accelerometer 1; however, the 60-Hz noise is absent in the accelerometer 2 data.

The most important observations to be made from these test data sets are the remarkable performance of the 1N triggered OSTDA spectra and the absence of any of the expected peaks in the remaining OSTDA spectra. As indicated by the 1N OSTDA data, the technique appears to function well. The order sampling makes the spectra much easier to read and, more importantly, centers the synchronous harmonics in the same frequency band of the analyzer regardless of any speed variations of the machine. The absence of expected peaks in the other OSTDA spectra might possibly indicate that the calculations of the bearing characteristics are in error. Ball slippage, for example, is a key parameter in the calculations and is very difficult to approximate. These characteristic frequencies might be "found" by calculating several separate OSTDA spectra and sweeping the trigger frequency (changing the trigger frequency for each OSTDA spectrum) over a small range around the calculated characteristic frequency. This possibility was not pursued due to time restrictions. The poor performance of the OSTDA technique to extract those peaks which can already be clearly seen in the baseline autospectrum cannot be explained at this time, although it may be an indication of the narrowness of the main lobe of the TDA comb filter. Further work will be necessary to evaluate the OSTDA sweep concept and to determine why OSTDAs triggered at the 3.25N, 3.75N, 5.25N, and 6.85N could not produce the peaks seen in the baseline autospectra.

5.4.2 SSME Dynamic Data Evaluation

The performance of the OSTDA technique when applied to Saunders' bearing test data had not been extremely successful. The 1N-triggered OSTDA had reduced the random background noise by approximately 20 dB, however, and the harmonics related to the synchronous (1N) had been enhanced. With these points in mind, the determination of how effective the 1N-triggered OSTDA techniques would be on actual HPOTP vibration data remained to be made. Therefore, the OSTDA technique was applied to vibration data from SSME hot firing tests 193, 294, and 301. Each test had three accelerometers oriented radially on the pump end of the high pressure oxidizer turbopump (HPOTP). Due to the absence of a speed probe on any of the tests, a substitute tachometer signal had to be found. To synthesize this tach signal, the

vibration signal was enhanced in the time domain by using Digital Audio Corporation's adaptive filter (DAC 1024I). The output of the DAC 1024I was bandpass filtered around either the 4N or 8N peak in the signature. This signal was the input to the VIC 960 frequency ratio synthesizers which outputted, after filtering, the signals required for the order sampling and data acquisition triggers. (See figure 17 for a block diagram of the data reduction instrumentation.) This technique for synthesizing a tachometer signal worked well as long as a pump shaft harmonic of adequate strength was available. The same software used for the Saunders' data, shown in tables 6 and 7, was used to reduce the SSME vibration data.

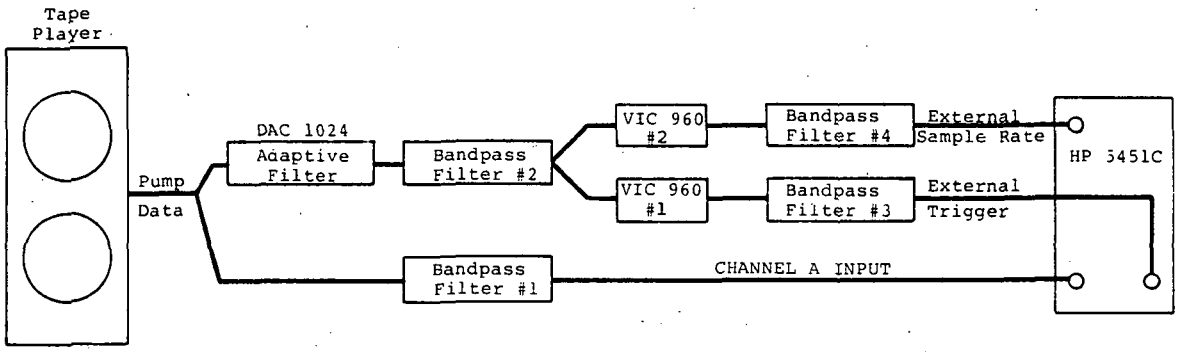

Figure 17. Block Diagram of Data Reduction Instrumentation for SSME Pump Vibration Data

SSME test 193 was conducted with a 368-second burn at 109 percent of the engine's rated power. Channel 6 of the data tape contains vibration data from an accelerometer mounted radially, 45 degrees from the reference axis. Channel 8 is data from a radial accelerometer mounted at 90 degrees, and channel 9 is radial acceleration data at 135 degrees. For all three data channels, the sampling and data acquisition triggers were synthesized from the 8N component of the vibration signature. OSTDA data was reduced with a 1N time average trigger. The OSTDA calculations were made for five overlapping 75-second segments of the 109% power run. Data from each accelerometer was reduced using the OSTDA; however, since the resulting data was quite consistent from accelerometer to accelerometer, only selected data from the 135^{o} accelerometer (channel 9) for each test has been included in this report. Figures 18 through 20 contain a baseline order-sampled autospectrum along with selected 1N-triggered OSTDA spectra for tests 193, 294, and 310 respectively. The sampling and

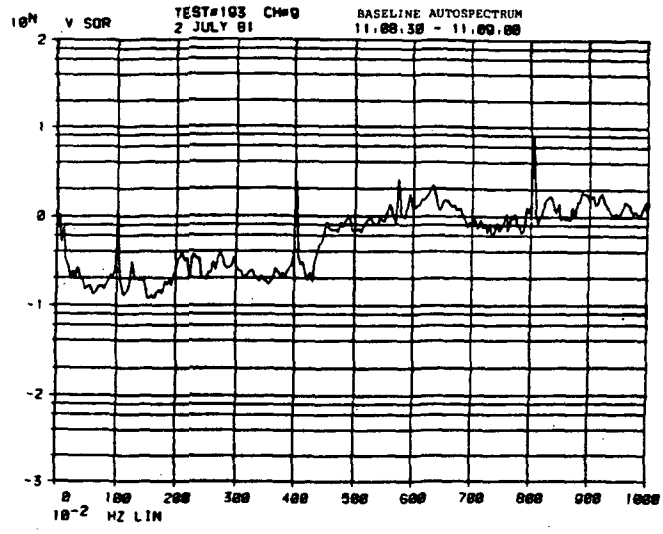

(a) 11:08:30 - 11:09:00

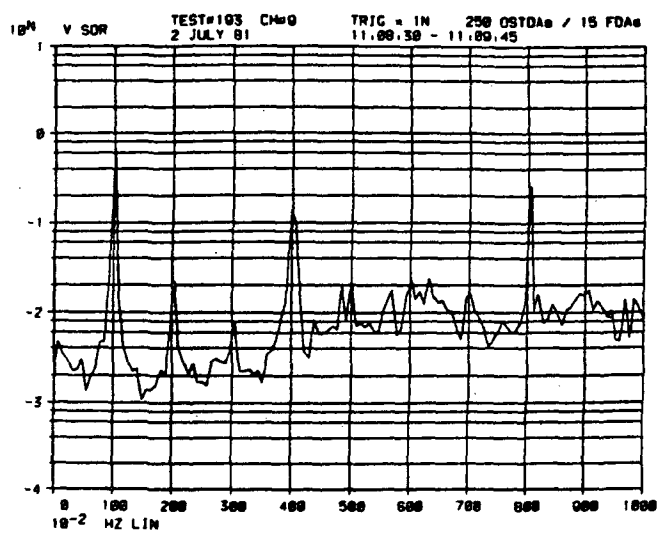

(b) 11:08:30 - 11:09:45

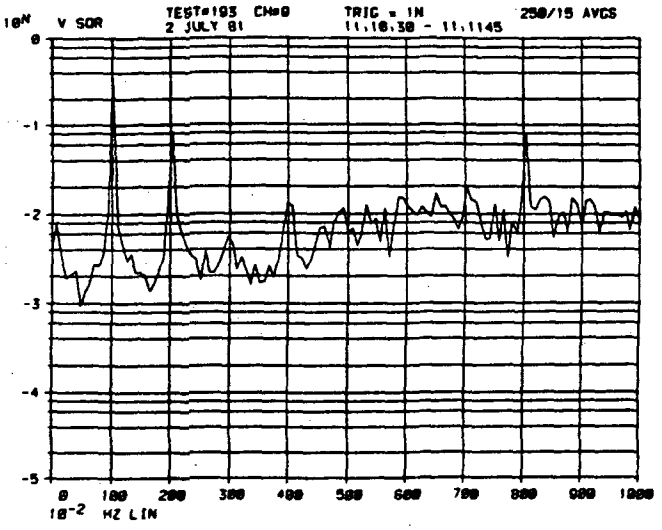

(c) 11:10:30 - 11:11:45

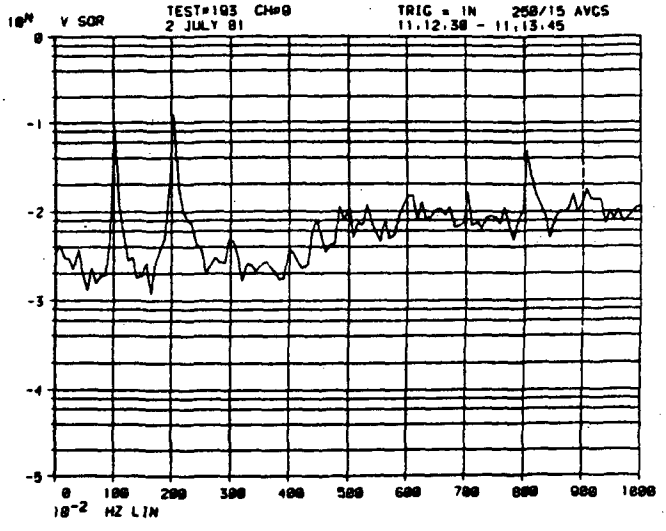

(d) 11:12:30 - 11:13:45

Figure 18. 1N-OSTDA Results for Test 193, Channel 9; 250 OSTDAs/15 FDAs for Selected Time Slices

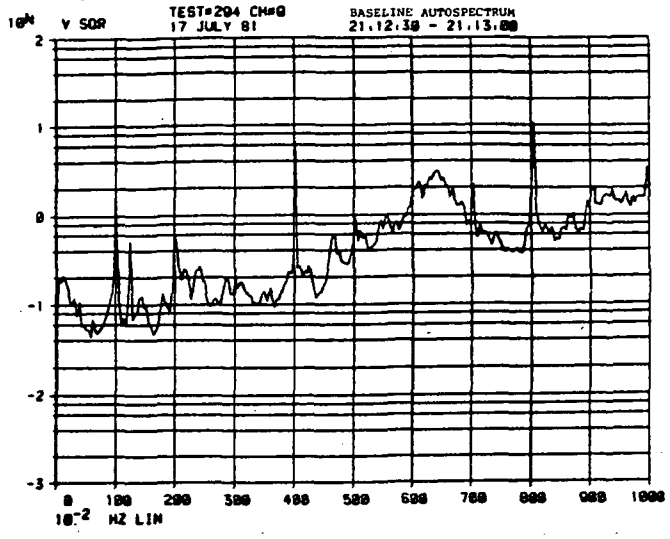

(a) 21:12:30 - 21:13:00

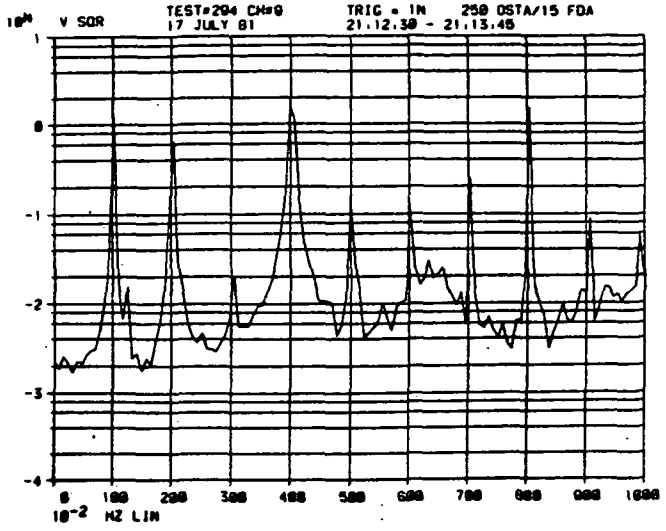

(b) 21:12:30 - 21:13:45

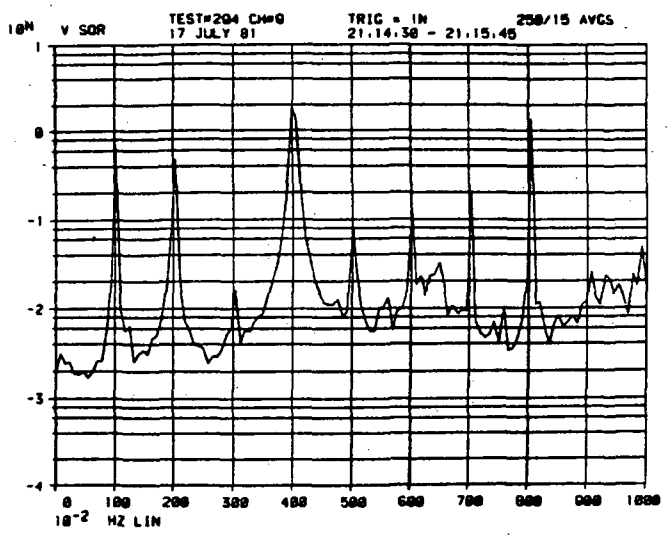

(c) 21:14:30 - 21:15:45

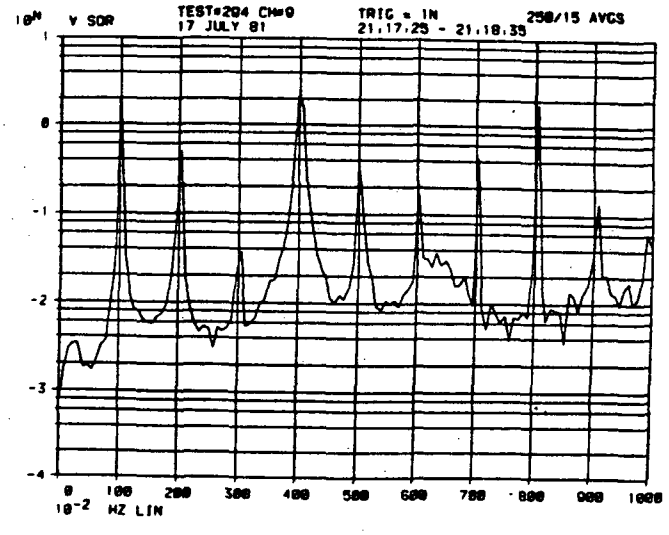

(d) 21:17:25 - 21:18:35

Figure 19. 1N-OSTDA Results for Test 294, Channel 9; 250 OSTDAs/15 FDAs for Selected Time Slices

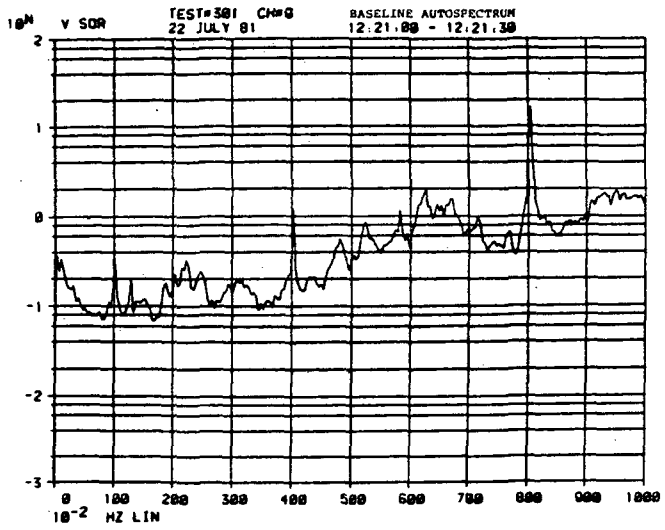

(a) 12:21:00 - 12:21:30

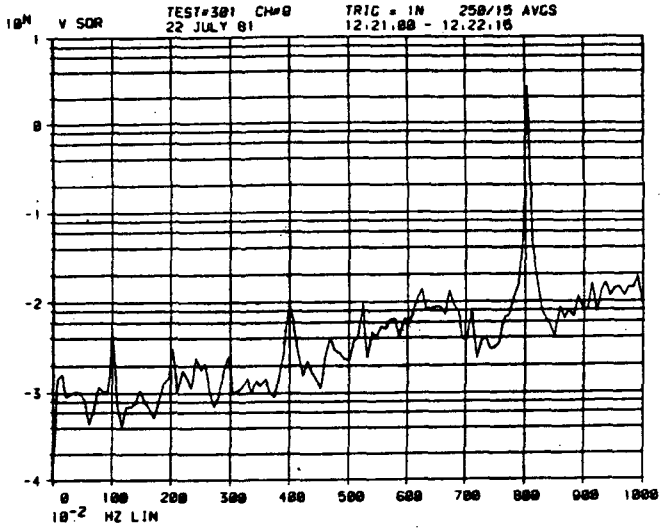

(b) 12:21:00 - 12:22:15

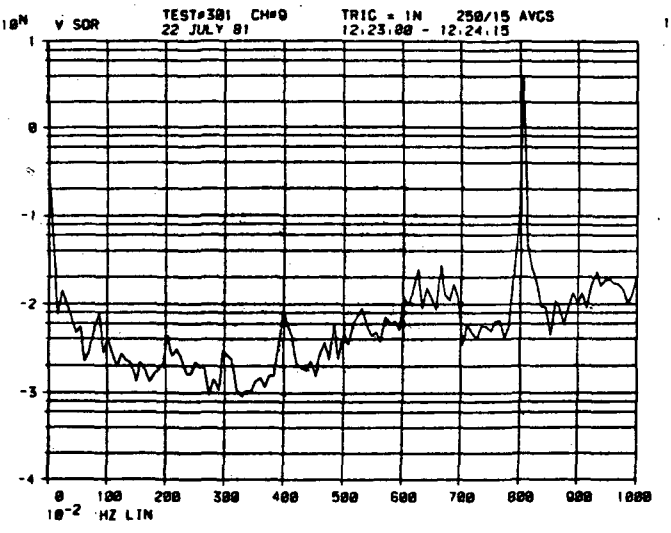

(c) 12:23:30 - 12:45:15

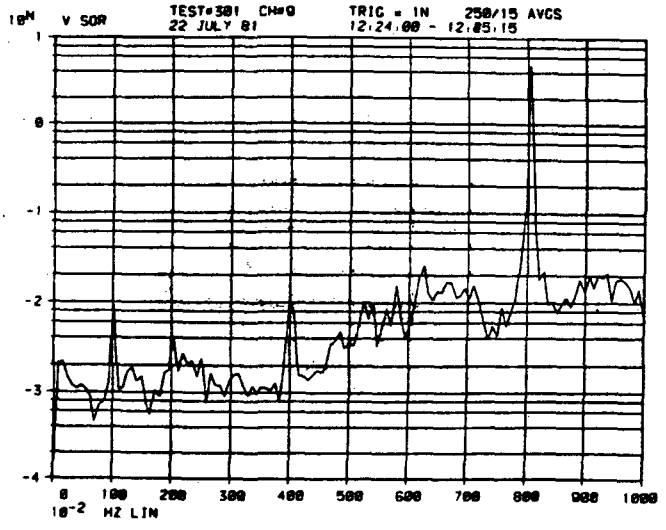

(d) 12:24:00 - 12:25:15

Figure 20. 1N-OSTDA Results for Test 301, Channel 9; 250 OSTDAs/15 FDAs for Selected Time Slices

data acquisition triggers were synthesized from channel 6 since the 8N component was well pronounced in the signature. The sampling rate for all sets of data was 20N, and the data was filtered from 1 to 5000 Hz.

As with the Saunders data, the 1N OSTDA performed well, and several shaft harmonics were exposed by reducing the amplitude of the noise floor. Reducing this data over a period of time allowed for a course trend analysis. For example, the magnitude of the 2N peak for test 193 showed a sharp increase in amplitude as time passed. This change might be an indicator of bearing degradation or an elliptical shaft orbit. The same trend in the magnitude of the 2N peak was noticed in all the data channels from test 193. Following test 193, the HPOTP was disassembled, and the pump's No. 3 bearing was found to be damaged.

SSME test 294 consisted of a 576-second run with the engine running at 102 percent of its rated power. The pump was known to contain good bearings at the beginning of this test. The 4N component was filtered and used for the sampling triggers. In studying the trends from this data, the magnitudes of the synchronous harmonics held relatively steady over the entire period of the 102% power run. The only significant change was a slight decrease in the magnitude of the 8N peak.

The HPOTP used for test 301 contained a bearing with a known flaw (spalled balls). Ten seconds after engine startup, a 510-second run was conducted with the engine operating at 100% power. During the early part of this run, none of the synchronous harmonics appeared with a magnitude significant enough to be used as a tachometer signal. For this reason, the OSTDA data reduction was not begun until four minutes into the 100% power run. At that time, the 8N component became strong enough and was used as the pump speed indicator or tachometer signal. The channel 6 data showed no synchronous harmonics other than 1N and 8N, and these peaks remained at approximately the same magnitude throughout the remainder of the 100% power run. Channel 8 also showed only 1N and 8N components, each increasing slightly in magnitude throughout the run. Channel 9 (see figure 20c) showed a 1N component which dropped out but reappeared as the test progressed. Channel 9 also showed a 4N component that was not present in the data for the other two channels. The magnitudes of 4N and 8N components remained fairly steady.

These three tests (193, 294, and 301) represent three different conditions of the HPOTP bearings. Following test 193, the bearings were known to be bad and were believed to have gone bad during the test. The 2N harmonic, as noted, could be an indicator of this bearing's degradation. Test 294 had good bearings installed before the test. The synchronous harmonics are present and high in magnitude but relatively constant. Test 301 was known to have had bad bearings installed before the test. Most of the synchronous harmonics are absent, and those that do appear remain constant. However, the noise floor in test 301 is much higher relative to the synchronous and blade passage peaks than in the other tests. No positive indicators of bearing degradation could be deduced from these data sets.

5.5 Random Decrement Averaging

To develop and evaluate the randomdec technique, software was developed for use with the HP 5451C Fourier analyzer. Basically the software controlled the acquisition of a time domain data block and searched through the data until the threshold condition was met. This point was then shifted to the beginning of the data block, and this "new" time function was added to the original data block. The shifted data block was then searched until the next point to meet the threshold requirement was located. Once again the block was shifted and averaged with the previous two data blocks. The process was repeated until all the usable data in the original time signal had been utilized. Figure 21 is a general flowchart of the basic randomdec software, and a program listing is provided in table 8.

Five sets of laboratory-generated data were used to evaluate the random decrement averaging technique. Each data set consisted of a time domain waveform that was formed by the superposition of a 3125-Hz sinusoid and varying levels of random noise. Set 1 contained a relatively low level of random noise and was randomdec averaged using a threshold of 0.1 volt (y_s = 0.1). Figure 22 shows the test signal and the resulting randomdec-averaged signal. Clearly, the randomdec technique was effective in reducing the random noise contamination and produced a relatively "clean" sinusoid.

For set 2, a random signal of the same magnitude as set 1 was combined with a 3125-Hz sinusoid whose magnitude was 10 dB lower than in set 1. As can be seen from figure 22, the superposition of these two waveforms still maintains some indications of periodicity. The randomdec software operated on this signal with a threshold of 0.05

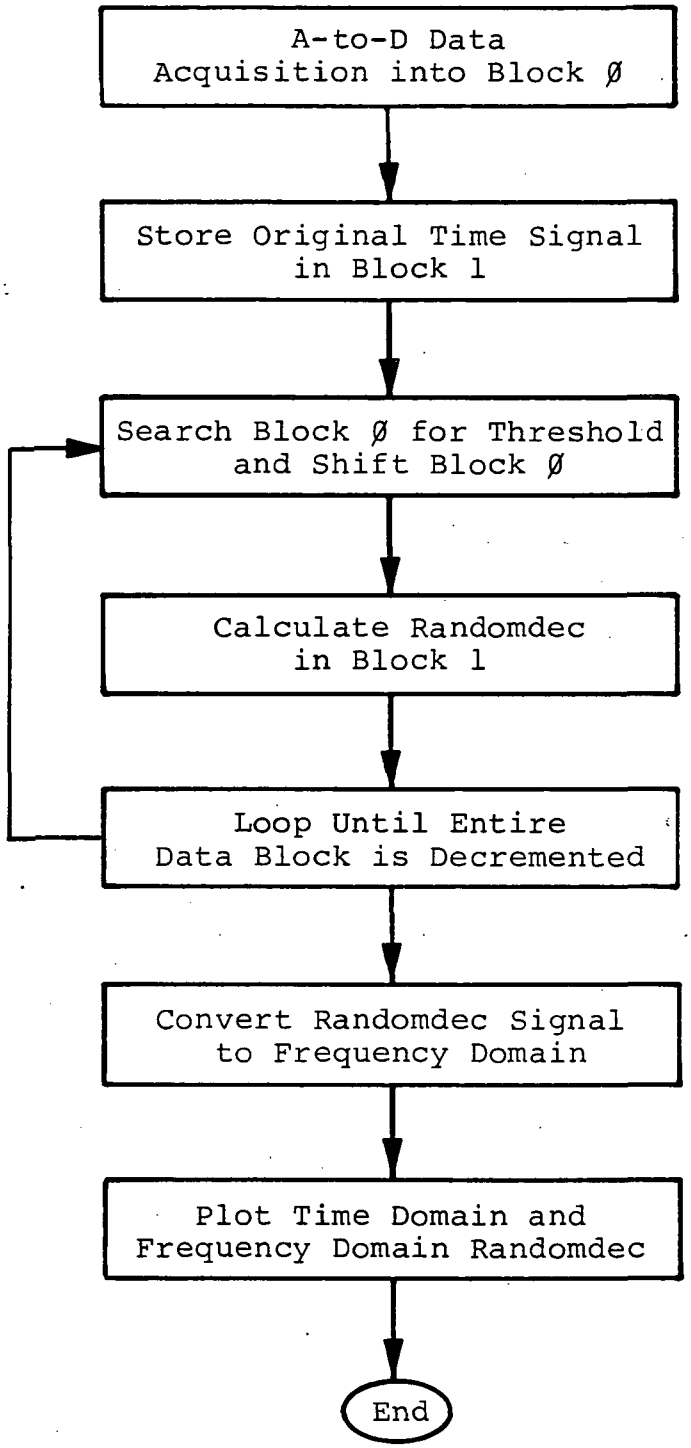

Figure 21. Flowchart of Basic Randomdec Software

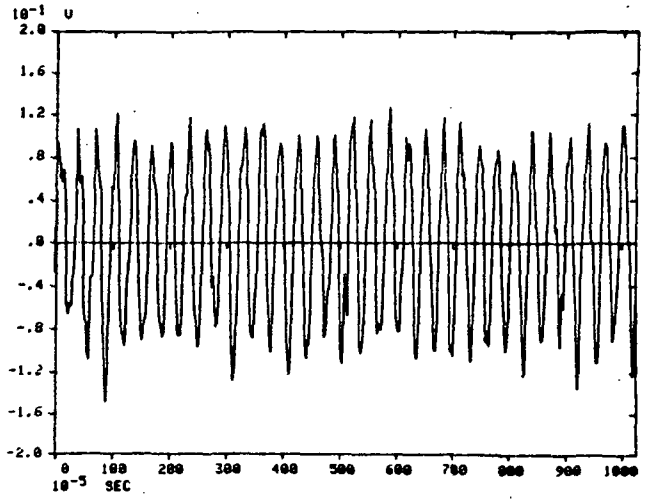

Test Set 1 Input

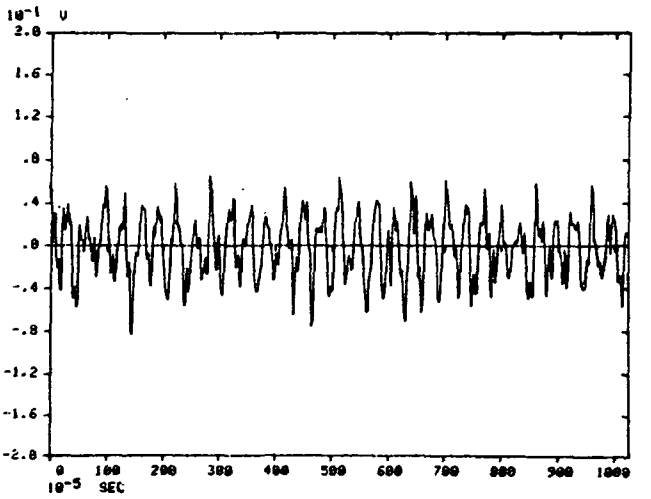

Test Set 2 Input

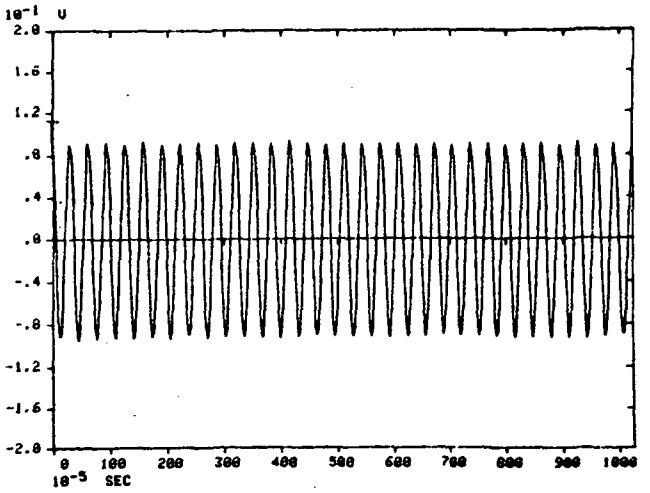

Randomdec Output, y_s = 0.1 volt

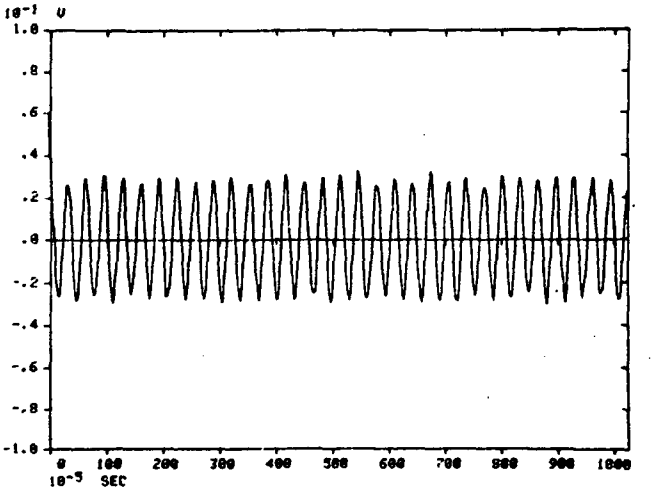

Randomdec Output, y_s = 0.05 volt

Figure 22. Randomdec Results for Test Cases 1 and 2

volts. The resulting randomdec average is also shown in figure 22. Once again, a relatively uncontaminated sinusoid is produced with only small variations in amplitude apparent.

TABLE 8. Randomdec Software Listing

```
  1 L    3600
  5 BS   4096
  9 CL
 12 CL      1
 16 CL      2
 20 CL      3
 24 CL      4
 28 CL      5
 32 CL      6
 36 Y    5821      6
 41 Y    5838     36
 46 Y    5814
 50 Y    5819      1       1
 56 Y R        0       1
 62 Y    5819      2       1
 68 Y R        2       3
 74 Y A-       4      8D      1D
 81 Y IF       2       0       1       2
 89 Y _        2      4D
 95 Y :        5      8D      1D
102 Y *        5      5D       3
109 L    3601
113 Y    5814
117 Y    5819      3       1
123 Y R    2000
128 MS       31      1
133 Y _       6       1
139 L    3610
143 BS       0D
147 CL
150 CL      1
154 CL      2
158 Y _       7       0
164 Y _       8       1
170 RA
173 X>       1
```

```
177 L    3611
181 Y _        9       0
187 L    3612
191 Y A+       9
196 Y X<    2001       1      9D
203 Y IF    2001    2000D      1       1
211 J    3612
215 _          1      9D
220 X<         1
224 A-         2
228 :          0      8D
233 A+         2
237 X>         2
241 Y A+       8
246 Y A+       7      7D      9D
253 Y IF       8      2D       2       2
261 Y IF       7      4D       1       2
269 J    3611
273 L    3620
277 X<         2
281 BS        1D
285 F
288 *-
291 A-        5D
295 :          0      6D
300 A+        5D
304 X>        5D
308 Y A+       6
313 @    3610        3D       0
319 L    3690
323 X<        5D
327 TL
330 Y    5800        6       0       0     100
338 Y    5808      400       0
344 Y /L       0      10
350 Y    5820
354 .
```

Data set 3 showed an interesting development in the operation of the randomdec technique. In this case the magnitude of the sinusoid has been reduced an additional 10 dB, removing any semblance of periodicity in the test signal. After randomdec averaging the input signal using a threshold of $y_s = 0.03$ volts, the resulting waveform resembled, to some degree, the input signal used for data set 2. Based on this observation, a second randomdec average was performed using a threshold of $y_s = 0.006$. The resulting second randomdec averaged waveform appears to be very periodic, as can be seen in figure 23.

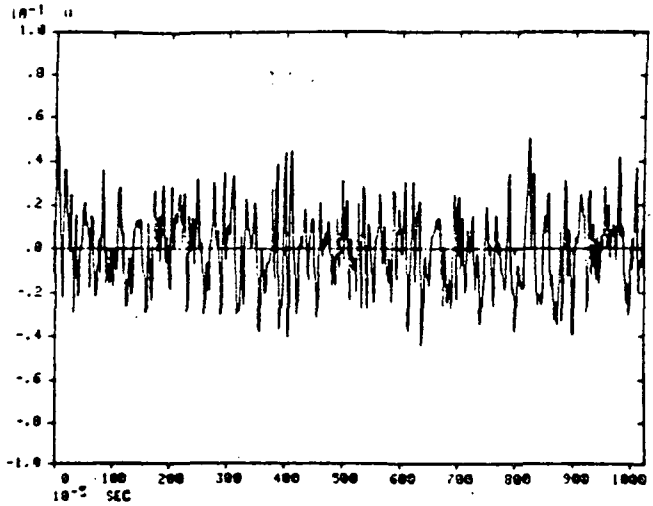

Test Set 3 Input

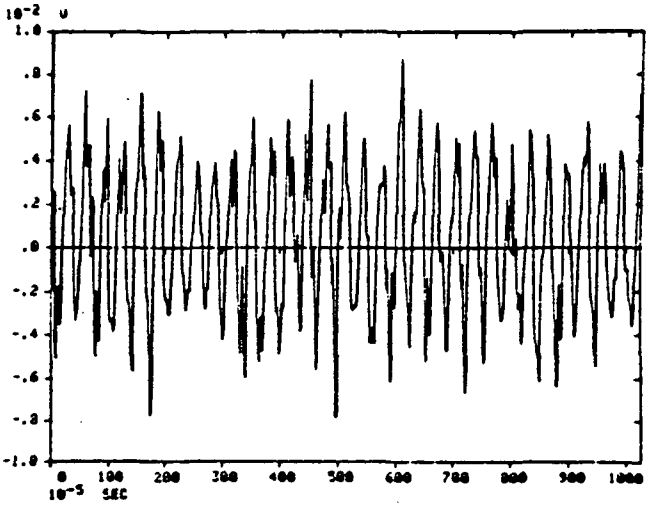

First Randomdec, y_s = 0.03 volt

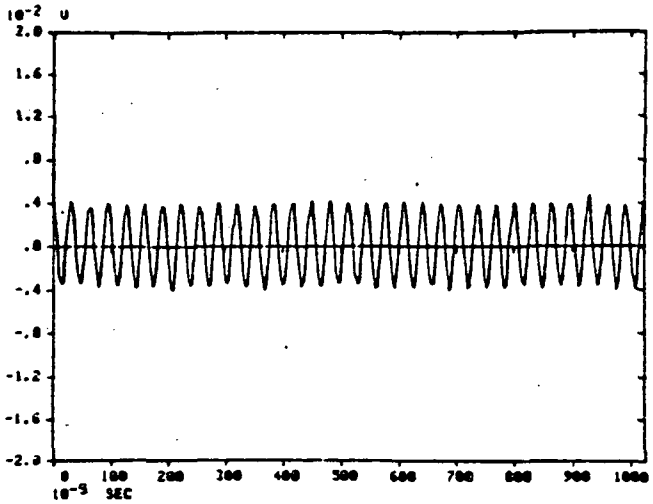

Second Randomdec, y_s = 0.006 volt

Figure 23. Randomdec Results for Test Case 3

The evaluation of data set 4 was similar to set 3 in that multiple randomdec averages were performed on the original time waveform. For each successive randomdec, the input was the previous randomdec output. The magnitude of the sinusoid was reduced by an additional 10 dB from that in set 3, and the threshold for the first randomdec was y_s = 0.05 volts, with this threshold level being decreased for each successive randomdec operation. The second threshold was y_s = 0.01; the third, y_s = 0.001; the fourth, y_s = 0.0003; and the first randomdec threshold was y_s = 0.0002. From figure 24, one can see that the output of each successive randomdec operation is more periodic, or "cleaner," than the previous.

The results for the final set of data (set 5) is shown in figure 25. For this test set the input was basically the same as for set 4; however, the randomdec operation was performed only once using a threshold of y_s = 0.0002 volts. This was the same threshold level used for the last randomdec operation of set 4. Note that the resulting waveform is quite different from the output of the fifth randomdec in set 4 (figure 25) and exhibits very little periodicity. In addition, a negative dc shift has appeared and cannot be explained at this time.

From the five test cases, it is apparent that the randomdec averaging technique shows promise in reducing the random contamination present in a given waveform. As noted from the comparison of sets 4 and 5, however, the threshold appears to hold the key to the randomdec operation. The questions of what threshold should be used, how many randomdec operations need to be performed, and in what steps should they be performed have yet to be investigated and could be difficult to determine and/or estimate with respect to actual HPOTP data.

5.6 Cepstrum Analysis

To understand and evaluate the cepstrum analysis technique, it was used as a tool in reducing laboratory-generated data. This data consisted of an electronically summed complex periodic signal, such as a square wave and/or a square wave combined with a sine wave.

A short keyboard program was written for the HP 5451C to generate the cepstrum. The software calculated an averaged log power spectrum, following which several individual keystroke commands were performed in order to calculate the cepstrum.

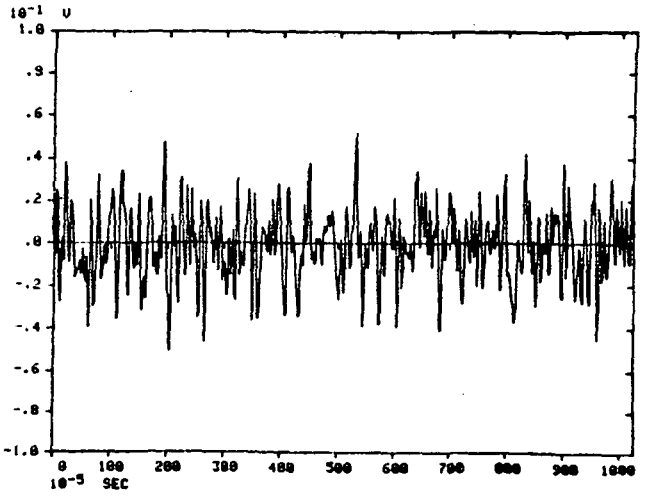

Input

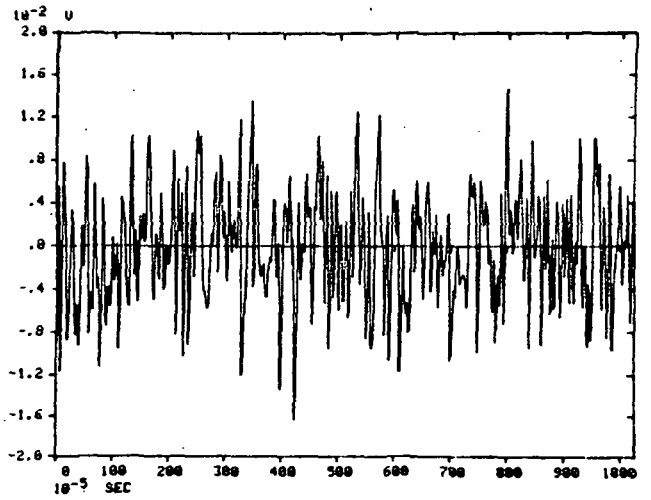

First Randomdec, y_s = 0.05 volt

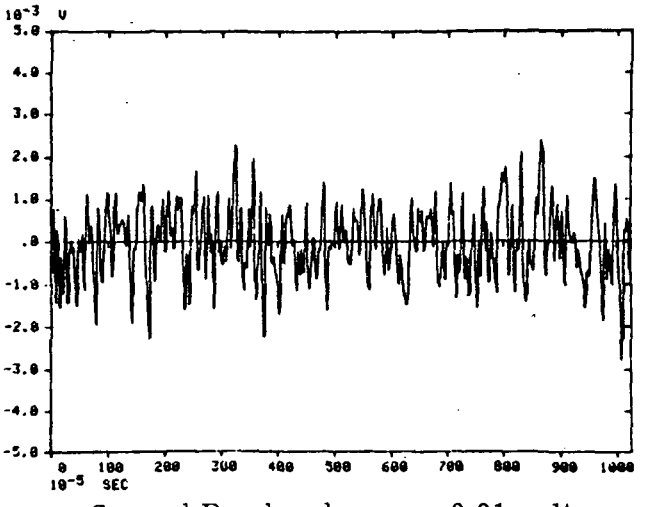

Second Randomdec, y_s = 0.01 volt

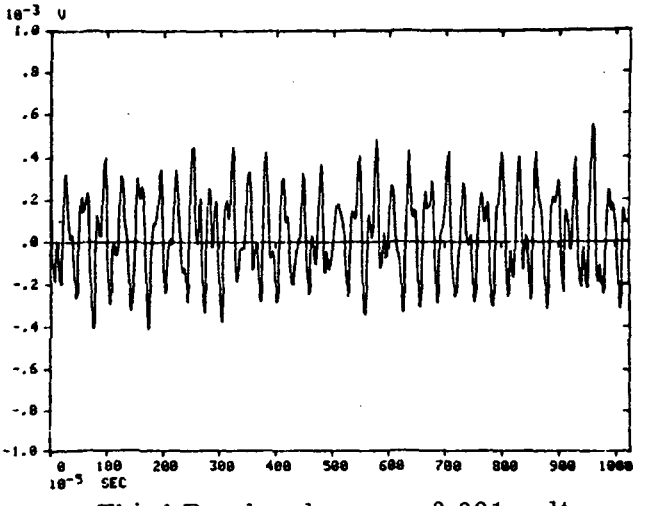

Third Randomdec, y_s = 0.001 volt

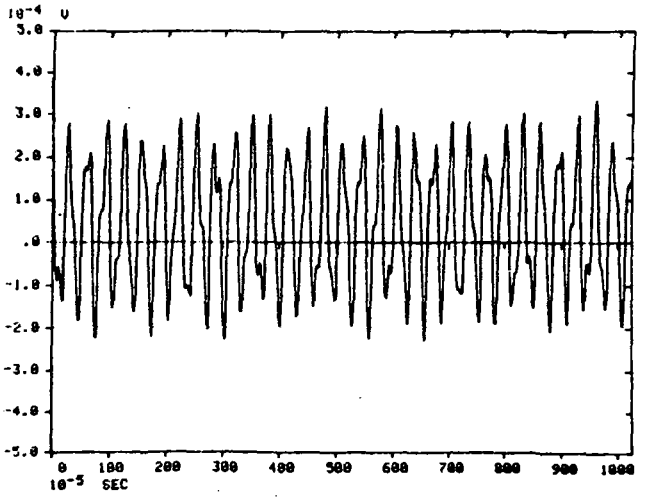

Fourth Randomdec, y_s = 0.0003 volt

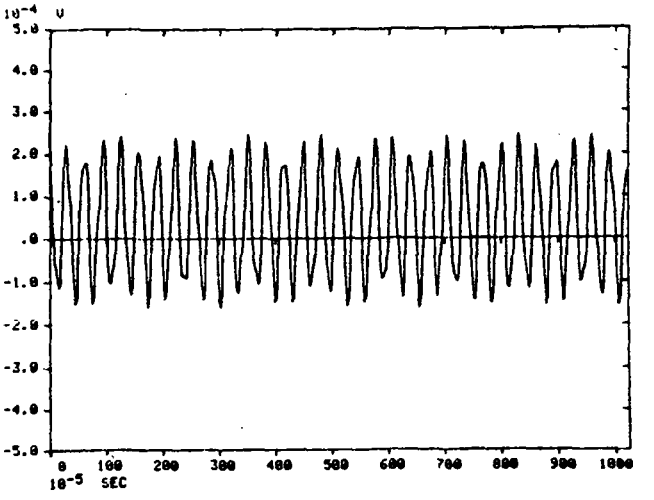

Fifth Randomdec, y_s = 0.0002 volt

Figure 24. Randomdec Results for Test Case 4

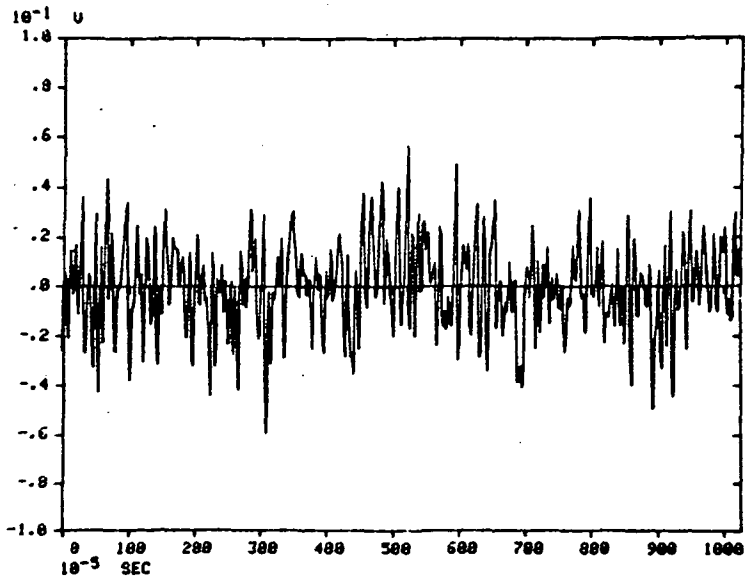

Input

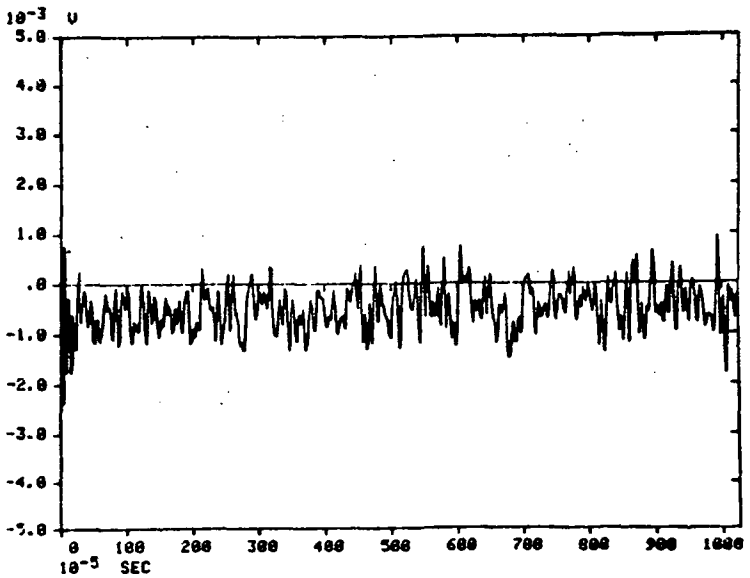

Randomdec, y_s = 0.0002 volt

Figure 25. Randomdec Results for Test Case 5

These additional keystrokes included an inverse Fourier transform and self-multiplication (or squaring). In some cases, the first and last channels of the Fourier-transformed log power spectrum were cleared (set to zero) before the cepstrum calculation was completed. This clearing of the first and last channels was solely for the purpose of enhancing the scale of the displayed cepstrum. A listing of the cepstrum software is presented in table 9.

TABLE 9. Cepstrum Software Listing

(a) Program 1

```
 1 L       0                    20 FEB 81
 5 CL                           CEPSTRUM PROGRAM
 8 CL      1
12 CL      2                    ADDITIONAL PROCESSES
16 L       1                    F
20 RA                           *
23 F                            TL
26 *-
29 A+      1                    FOR DC CLEARED CEPSTRUMS
33 X>      1                    F
37 #       1     25       0     CL0 0 1
43 :       0     25             CL0 (N1) (N2)
48 *       0      2             [ N1 = BS/2; N2 = BS ]
53 X>      1                    X
57 X>      2                    TL
61 TL
64 Y K
68 .
```

(b) Program 2

```
 1 L          0
 5 Y -          0      10
11 Y -          1       1
17 L         1
21 Y X>         1       0      0D
28 Y A+         0      0D      10
35 #         1      50      0
41 L         2
45 X>        1
49 TL
52 F
55 CL        0      0
60 *
63 Y K
67 Y      5920
71 D
74 L         3
78 X<        1
82 Y K
86 Y      5820
90 .


26 FEB 81
CEPSTRUM ANALYSIS
SAMPLE CASE SET#2
```

Figure 26 show typical results of the cepstrum technique performed on a complex periodic signal composed of a 200-Hz square wave and a 700-Hz sinusoid. Since the square wave generator output is a distorted signal, low amplitude even harmonics are seen in figure 26 in addition to the expected odd harmonic components. The spacing of the various peaks are also noted on the figure. The cepstrum was generated by performing the following individual operations:

```
F          (Inverse Fourier Transform).
CL 0  0    (Clear channel 0 (dc)).
CL 0 4095  (Clear the last channel of the data block).
*          (Square the function's magnitude).
D  0 255   (Display the first 256 channels of the function).
```

Only the first 256 channels have been displayed for the purpose of clarity. Noted on figure 26b are the locations of the quefrency associated with various frequency spacings in the original power spectrum. It is obvious from figure 26 that interpretation of the cepstrum requires experience. Because of the complexity of this cepstrum, a simplified set of test data was generated to evaluate the cepstrum technique.

Figure 27 presents a set hand-generated power spectrum. The keyboard program listed in table 9b was written to perform the following functions on the hand-generated power spectra.

```
TL         (Convert the power spectrum to log amplitude).
F          (Inverse Fourier Transform).
CL 0 0     (Clear the dc channel).
*          (Square the time function).
Y  K       (Plot the cepstrum).
```

Figure 27a shows the power spectrum and the linear cepstrum of a complex periodic signal composed of a 200-Hz and a 400-Hz sine wave of equal amplitudes. Note the repetitive character of the main lobes and the two smaller side lobes in the cepstrum. The quefrency of the first main lobe corresponds to a spacing of 200 Hz in the original power spectrum. The overall character of the cepstrum is the same as that expected for the square of a complex periodic signal. A number of test cases were analyzed, and the quefrequency of the first main lobe continued to correspond to a spacing of 200 Hz in the power spectrum.

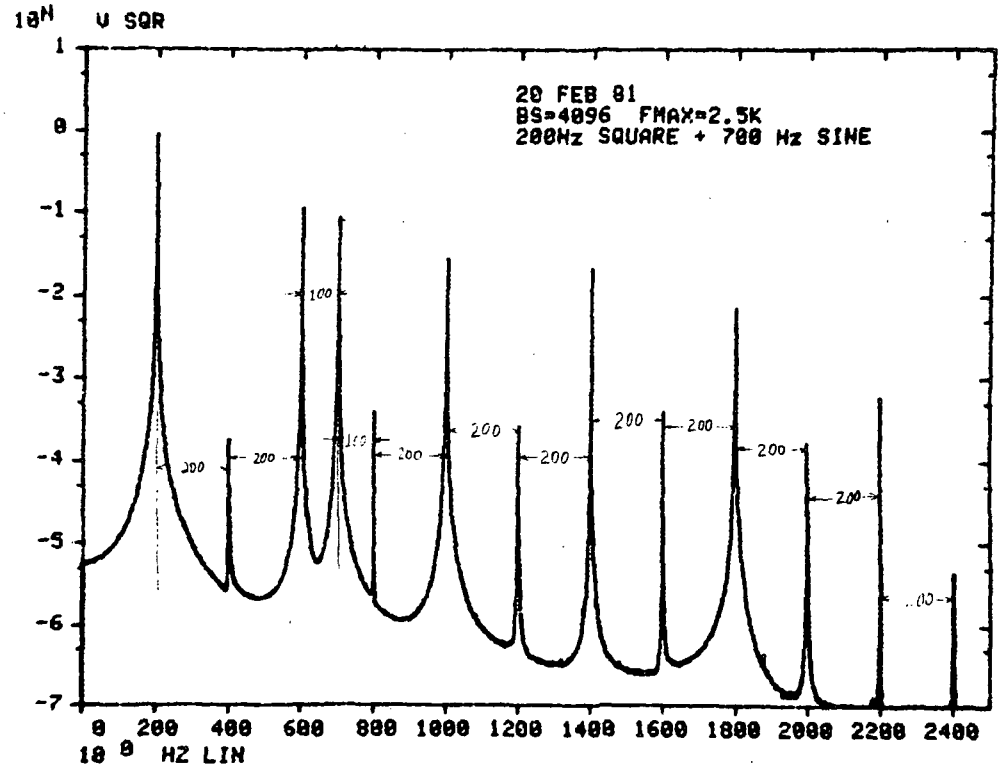

(a) 200-Hz Square Wave + 700-Hz Sinusoid PSD

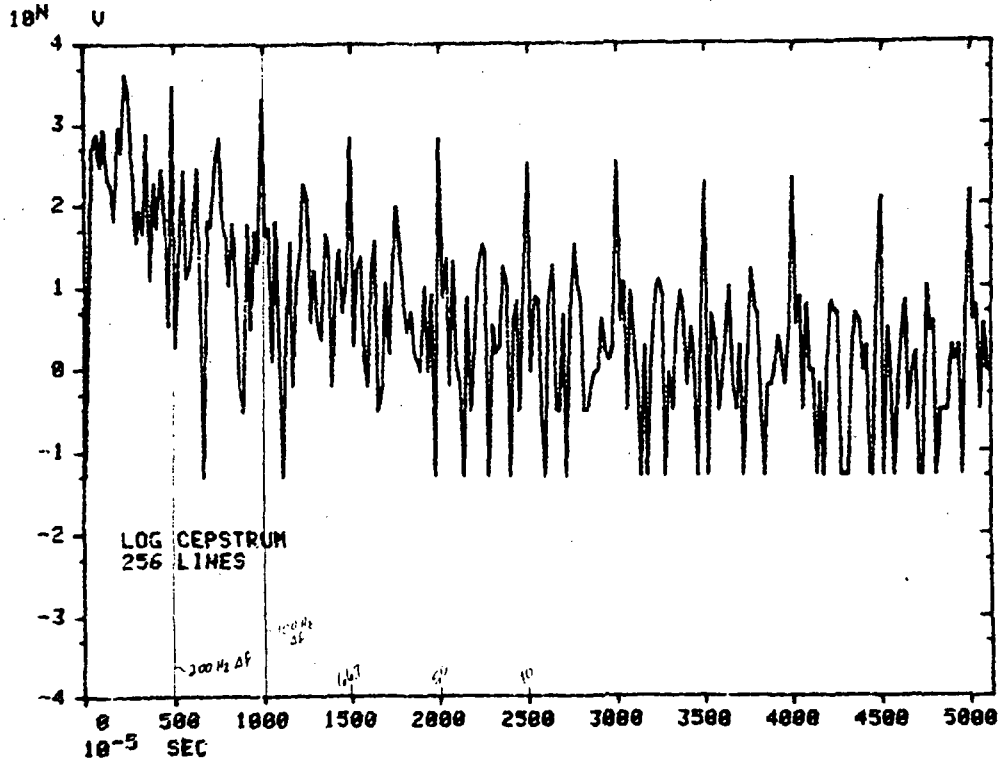

(b) Cepstrum

Figure 26. Autospectrum (PSD) and Cepstrum of 200-Hz Square Wave + 700-Hz Sinusoid

2-Component Spectrum,
200-Hz Separation

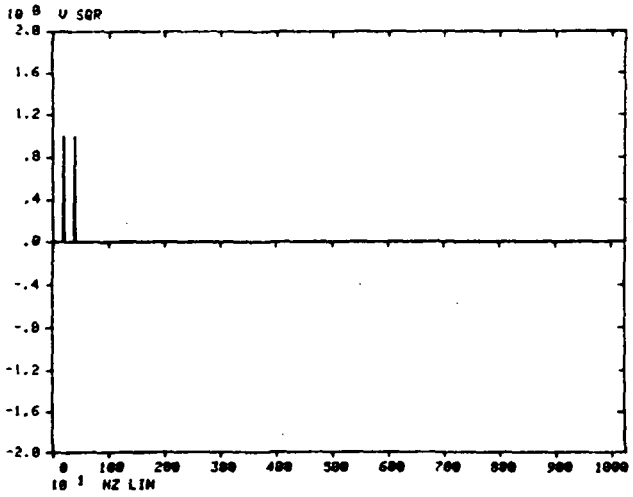

(a) Spectrum

4-Component Spectrum,
200-Hz Separation

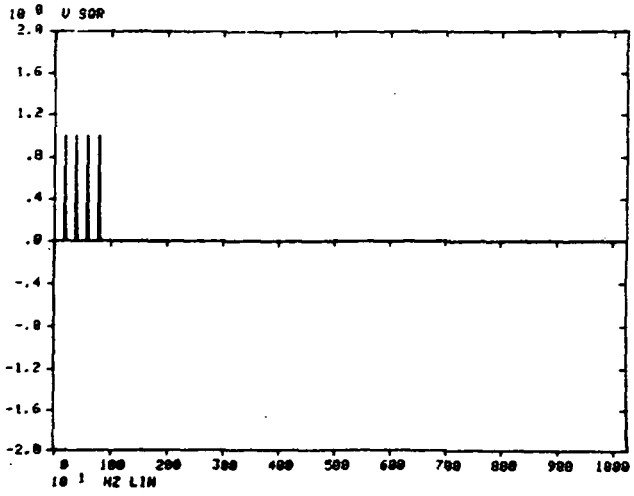

(b) Spectrum

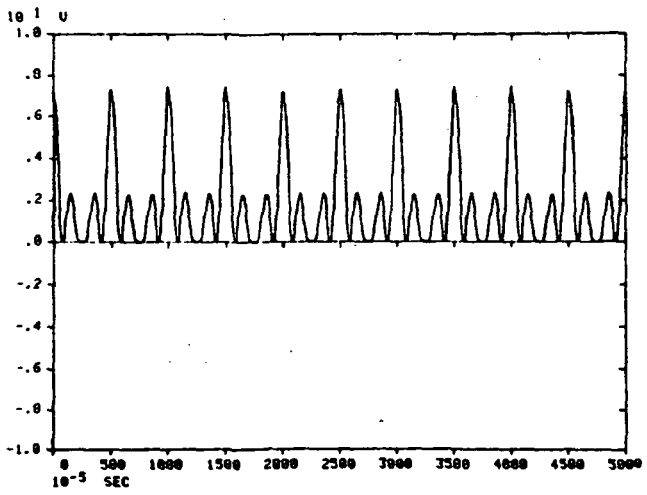

(a) Cepstrum

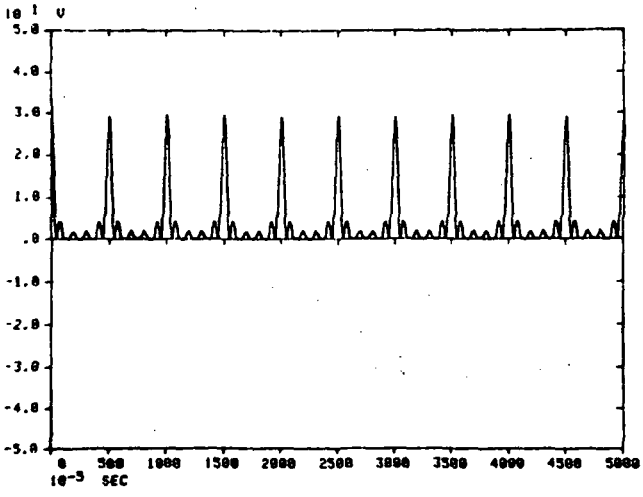

(b) Cepstrum

Figure 27. Hand-Generated Spectrum and Computed Cepstrum

A second case, shown in figure 27b, indicates the generation of more side lobes as the number of harmonics increased from two to four. Typically, rotating machinery spectrum signatures contain many harmonic peaks whose varied amplitudes indicate a variety of conditions. The cepstrum of this type of signature would certainly be more complex than that in our first example, and its interpretation would require a great deal of insight into the operation of the system and experience in cepstrum analysis.

As a final experiment, a third set of data was reduced by using the cepstrum technique to investigate its noise reduction capabilities. For this evaluation test, a 200-Hz square wave was combined with white random noise. Figure 28 displays the power spectra for the random signal, square wave, and their sum along with the resulting cepstrum. Some peaks are present in the cepstrum, but the effect of the random noise contamination is more prominent. The cepstrum has a distinctly random appearance, and as a result, the quefrency associated with the harmonic separation in the summed spectrum cannot be identified.

In application to rotating machinery analysis, little new information is gained over the power spectrum by performing cepstrum analysis; however, certain types of information may become more predominant, depending on the application. Furthermore, the mathematics defining the cepstrum suggests no increase in the signal-to-noise ratio by performing the cepstrum calculations. For the case at hand, an increase in signal-to-noise ratio is required if a reliable incipient failure technique is to be developed for the prevention of SSME bearing failure.

5.7 Adaptive Noise Cancellation (ANC)

The ANC data enhancement technique centers around the utilization of a real-time high-speed special-purpose digital signal processing computer commonly referred to as an "adaptive filter." Basically, the instrument consist of a processor and digital filter specifically designed for the cancellation of degrading noise from desired signals. The unit provides the unique ability to quantitize the signature of a given signal (defined as a reference) and remove (subtract) that signature from another signal containing both the desired signal and noise (defined as the primary signal). The processer's parallel-pipeline computer architecture permits the filtering process to occcur simultaneously with the filter's adaption coefficient generation. This continuous processing capability and a 1024th order filter size allows for the continuous estimation and removal of the

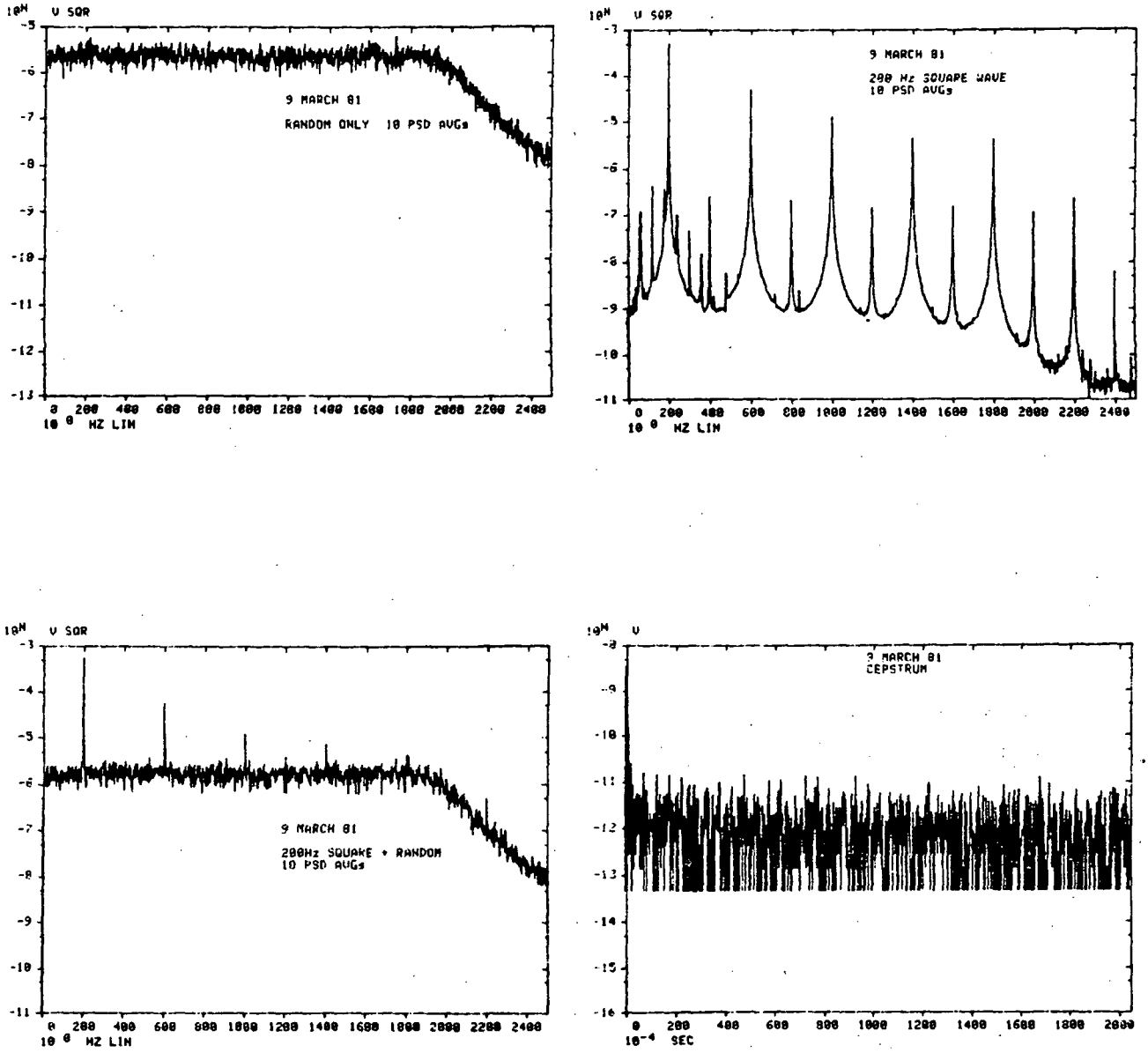

Figure 28. Spectra and Cepstrum of 200-Hz Square Wave + White Noise

reference signal from the primary, even when the character of the reference signal varies with time.

Figure 29 is a block diagram of the overall two-channel noise estimation/cancellation process. The particular adaptive filter used during this investigation was the Digital Audio Corporation's DAC 1024I, and a block diagram of the DAC 1024 hardware architecture is presented in figure 30.

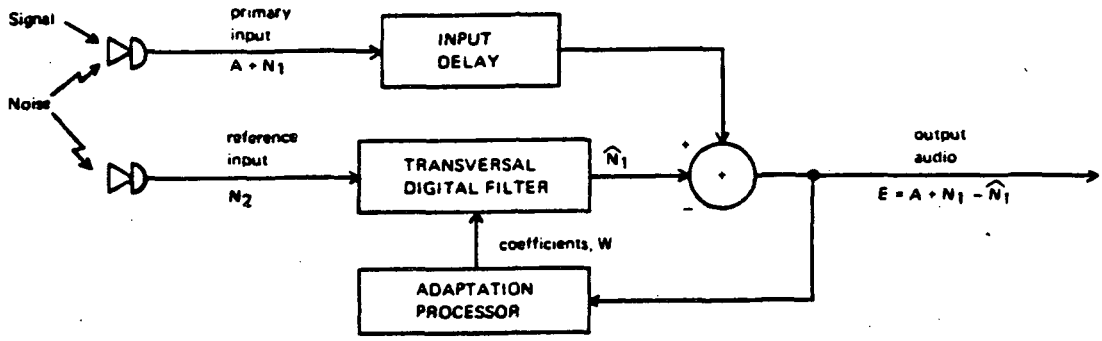

Figure 29. Adaptive Noise Cancellation Process

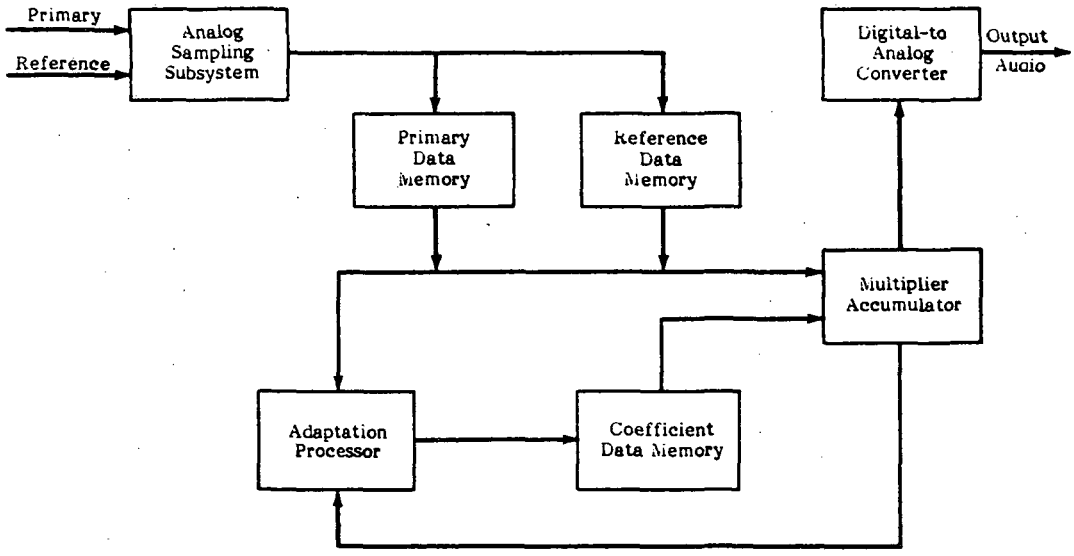

Figure 30. DAC 1024 Hardware Architecture

To evaluate the effectiveness of the adaptive filter/ANC data enhancement technique for application as an incipient failure detection technique, the adaptive filter (DAC 1024I) was incorporated into a microcomputer-controlled data reduction/analysis system shown in figure 31. Adaptive filtering was applied to test data from several SSME hot firings. The SSME tests used as test cases were performed with the same HPOTP and are identified in table 2. As before, the data reduction efforts concentrated on the accelerometer signals from the externally mounted accelerometers located radially around the turbine end flange of the pump housing. The work performed during this investigation was divided into three basic areas: software development, data reduction/analysis, and ANC technique evaluation.

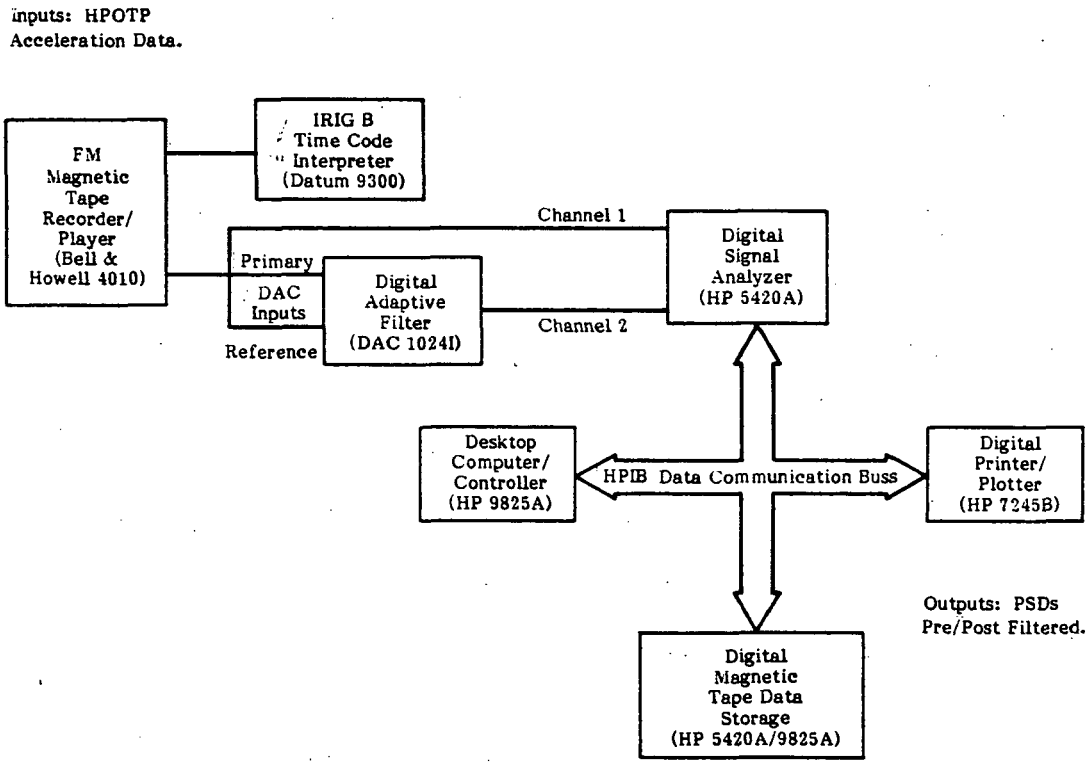

Figure 31. Data Reduction/Analysis System Block Diagram for Adaptive Noise Cancellation

5.7.1 **Software Development**

With the establishment of a data base containing representative HPOTP acceleration signatures as a principal objective, software was developed and implemented on an HP 9825A desktop computer/controller to provide the necessary instrument interaction for acquiring and storing pre/post-adaptive filtered power spectral densities. A flowchart depicting the overall operation of the software is presented in figure 32. The interactive software consisted of a driver program and five interrelated programs written to perform specific tasks. The five principal functions or tasks performed through the software were (1) data acquisition and storage, (2) data display, (3) data editing, (4) data search and sorting, and (5) data plotting. A flowchart depicting the operational sequence corresponding to each of the programs is presented in figure 33. The driver program was written such that any of the program options could be utilized and/or accessed by simply pressing a predefined special function key on the computer.

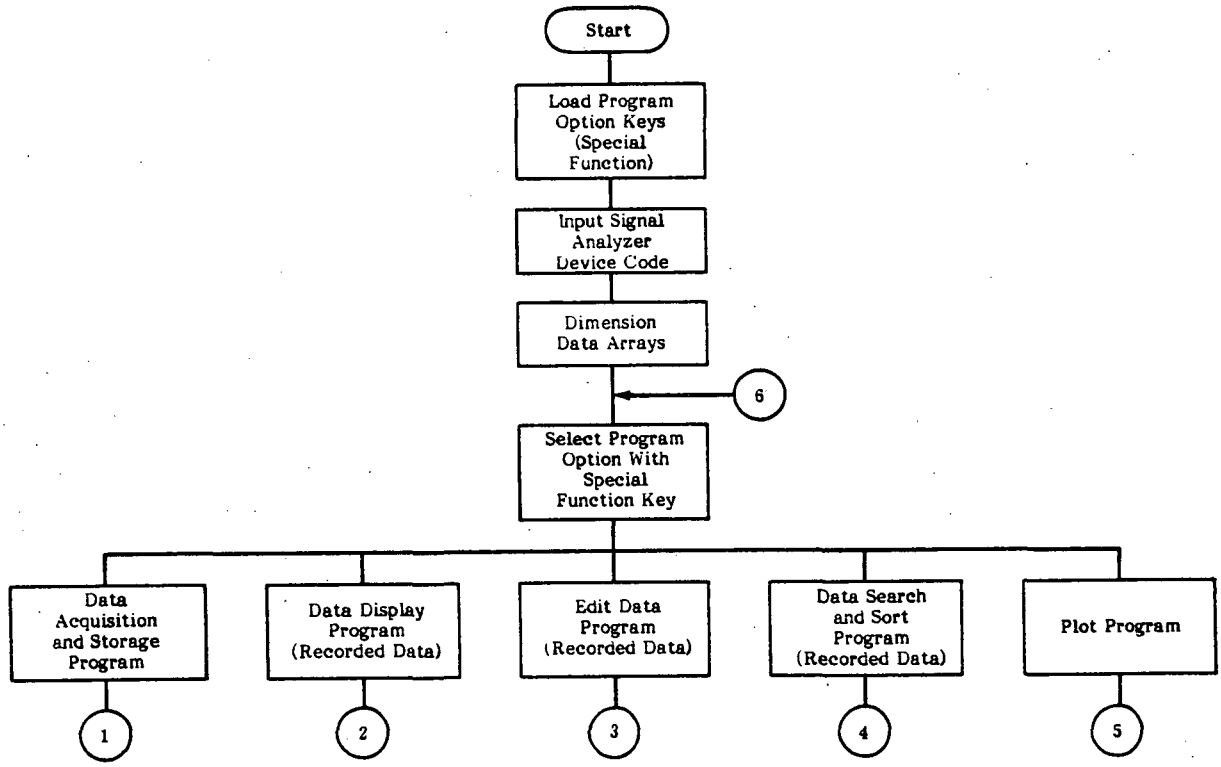

Figure 32. Overall Data Reduction/Analysis Software Flowchart

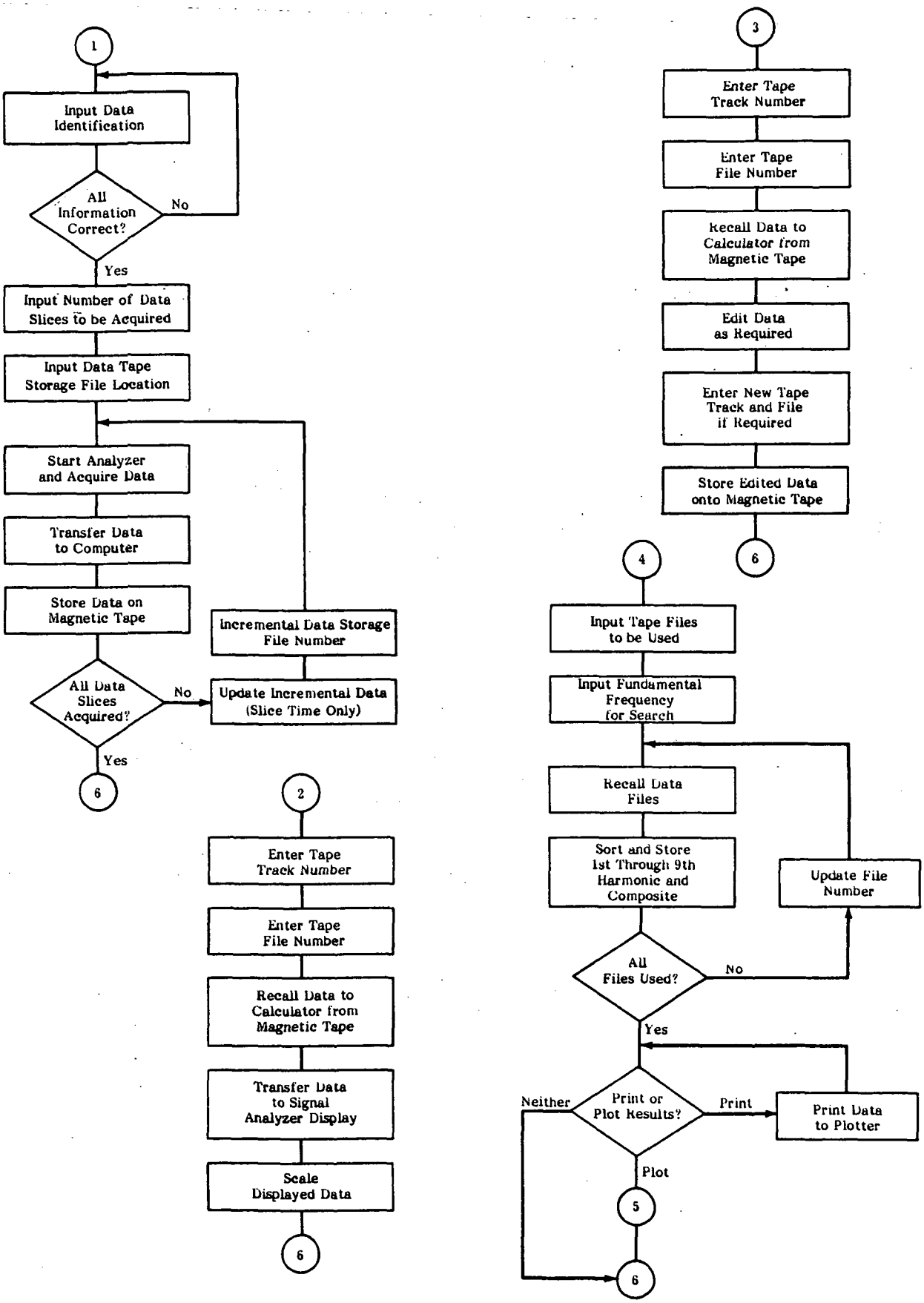

Figure 33. Individual Flowcharts for Data Reduction Analysis Software

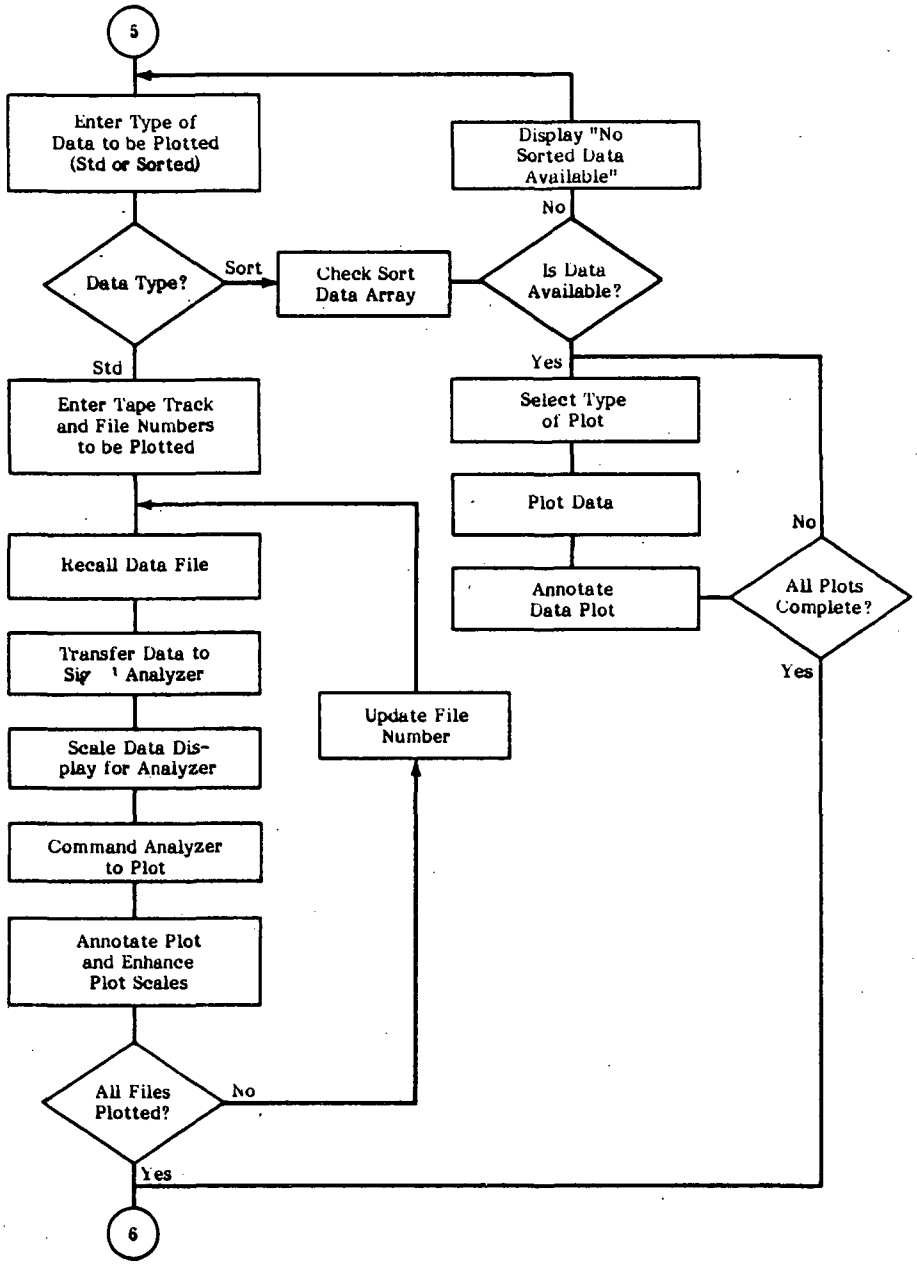

Figure 33. Individual Flowcharts for Data Reduction Analysis Software - Concluded

In practice, all the programs could not be maintained in the computer's memory simultaneously with a large data base. For this reason, programs 1 and 4 were sectionalized to provide the functions of either data acquisition or data base manipulation, respectively. A listing of the software developed to perform data acquisition and storage is presented in table 10. Since computer memory was limited, the establishment of a very large data base containing all the PSDs from all the test cases was not considered practical. With the individual PSDs and appropriate identifiers (test number, analysis type, time slice, data channel, analysis bandwidth, and composite level) stored on magnetic tape, the development of a small data base associated with specific parameters of interest was adopted as a more practical solution. As a result, data bases associated with each pump were developed. To construct these data bases, the search-and-sort program was developed. With the data base file numbers corresponding to the PSDs of interest and the fundamental (synchronous) frequency as inputs, each data file was loaded and a computer search and sort on the first 10 harmonically related components was performed. Each data base contained the amplitude and frequency of the sync-related harmonics along with the composite levels associated with all data slices from all tests using the same HPOTP at a given power level. From these data bases, the variation of the sync-related harmonics and composite levels could be ascertained as a function of data slice/time. A listing of the software developed to search and sort these parameters is presented in table 11.

5.7.2 Data Reduction and Analysis

Three test cases and two single test runs were reduced using the adaptive noise cancellation data enhancement technique. Each test case was comprised of a number of individual test runs that were performed with the same HPOTP or single test runs where specific bearing conditions were known. Adaptive filtered and nonadaptive filtered PSDs were computed from the data on a periodic basis. The data reduction time period was based on a 30-second data time slice interval. The 30-second time duration was chosen because it allowed approximately 10 seconds for adaptation time, 10 seconds for data acquisition/PSD computation (32 averages), and 10 seconds for data storage. As a result of this timing, the computed PSDs were representative of data intervals occurring approximately 20 seconds apart. A pictorial representation of this data reduction time slice scheme is presented in figure 34.

TABLE 10. Data Acquisition Program Listing

```
0: "NASA/MSFC SSME DATA ANALYSIS PROGRAM":
1: ent "ANALYZER HPIB DEVICE CODE",D
2: dev "SA",D
3: oni 7,"INT SRQ";eir 7;0}G
4: gto "SELECTIONS"
5: "INT SRQ":dtords("SA")}Q;dsp "SRQ RECIEVED Q=",Q
6: if Q=150;cmd 7,"?D%";gto "RTN"
7: if Q=170;cmd 7,"?E$";gto "RTN"
8: if Q=142;0}G;dsp "5420 PLOT ACTION";gto "RTN"
9: if Q=137;0}G;dsp "Device clear ack";gto "RTN"
10: if Q=140;0}G;gto "ASCII SAVE TO CONTROLLER"
11: if Q=160;0}G;gto "ASCII RECALL FROM CONTROLLER"
12: if Q=144;gto "ASCII DATA ONLY PRINT TO CONTROLLER"
13: if Q=145;0}G;gto "ASCII DATA/HEADER PRINT TO CONTROLLER"
14: if Q=101;gto "ADC OVERFLOW"
15: if Q=102;0}G;gto "PAUSE ON IMPACT"
16: if Q=104;0}G;gto "END OF MEASUREMENT"
17: if Q=105;0}G;gto "END OF CARTRIDGE ACTION"
18: if Q=106;0}G;gto "COMMAND ERROR"
19: if Q=107;0}G;gto "GENERAL ERROR"
20: if Q=110;0}G;gto "FATAL ERROR"
21: "ASCII SAVE TO CONTROLLER":
22: fmt 2,z,e14.6,/
23: for I=1 to 16;dsp "Transfering data header";red "SA.2",H[I];next I
24: for I=1 to H[3]/2;dsp "Transfering data";red "SA.2",D[I];next I
25: dsp "DATA TRANSFER COMPLETE"
26: gto "RTN"
27: "ASCII RECALL FROM CONTROLLER":
28: fmt 2,z,e14.6,/
29: for I=1 to 16;wrt "SA.2",H[I];next I
30: for I=1 to H[3]/2;wrt "SA.2",D[I];next I
31: gto "RTN"
32: "ASCII DATA ONLY PRINT TO CONTROLLER":
33: red "SA",Z;red "SA",P;0}G
34: gto "RTN"
35: "ASCII DATA/HEADER PRINT TO CONTROLLER":
36: gto "RTN"
37: "ADC OVERFLOW":
38: prt "ADC OVERFLOW"
39: gto "RTN"
40: "PAUSE ON IMPACT":
41: dsp "Not programed as yet"
42: gto "RTN"
43: "END OF MEASUREMENT":
44: dsp "Measurement Complete"
45: gto "RTN"
46: "END OF CARTRIDGE ACTION":
47: dsp "Recall/Save In-progress"
48: gto "RTN"
49: "COMMAND ERROR":
50: dsp "COMMAND ERROR ENCOUNTERED";stp
51: gto "RTN"
52: "GENERAL ERROR":
53: dsp "GENERAL ERROR ENCOUNTERED";stp
54: gto "RTN"
55: "FATAL ERROR":
56: dsp "FATAL ERROR ENCOUNTERED";beep;beep;stp
57: gto "RTN"
58: "RTN":eir 7;iret
59: "SELECTIONS":
60: fmt 0
61: "DIMENSIONS":
62: dim H[16],D[512],I$[64],A$[64],S$[48],C$[32],B$[24],C[1],S[20,10],P[20
63: dim F[20,10]
64: "DATA PLOT LABLES":
65: "SSME TEST          HPOT RAD      ACCEL.        % PWL"}I$
66: "TYPE OF ANALYSIS:                DATA TAPE:    CH. NO.:   "}A$
67: "DATA SLICE TIME INTERVAL=                                 "}S$
68: "BANDWIDTH=        Hz"}B$
69: "COMPOSITE=            G's rms"}C$
```

TABLE 10. Data Acquisition Program Listing - Continued

```
70: dsp "SELECT PROG OPTIONS---S/F KEYS";stp
71: "START":
72: oni 7,"INT SRQ";eir 7;0}G
73: cll 'TEST ID'
74: "MEASURE":
75: oni 7,"INT SRQ";eir 7;0}G
76: if cap(A$[19,21])="TFE";ent "DAC CAL FACTOR=",C[1]
77: if cap(A$[19,21])#"TFE";1}C[1]
78: ent "9825 TAPE TRK:",T,"9825 TAPE STORAGE FILE NUMBER?",F
79: if F>32;beep;dsp "FILE NO TOO LARGE";wait 2000;jmp -1
80: if T<0;dsp "Tape track can only be 0 or 1";wait 1000;jmp -2
81: if T>1;dsp "Tape track can only be 0 or 1";wait 1000;jmp -2
82: trk T;1}J;prt "TAPE TRK=",T
83: ent "NUMBER OF SLICES TO BE TAKEN?",O
84: "RE-MEASURE":
85: cll 'MEASURE DATA'
86: cll 'DATA TRANSFER TO CALCULATOR'
87: cll 'RECORD DATA ON 9825 TAPE'
88: prt S$[27]
89: cll 'INTERVAL UP-DATE'
90: if J<0;J+1}J;gto "RE-MEASURE"
91: dsp "MEASUREMENT OF DATA COMPLETE";stp
92: "MANIPULATE":
93: oni 7,"INT SRQ";eir 7;0}G
94: ent "TAPE TRACK?",T
95: if T>1;jmp -1
96: if T<0;jmp -2
97: trk T
98: ent "FIRST FILE NUMBER?",F
99: ent "LAST FILE NUMBER?",L
100: "LOOP":
101: cll '9825 TAPE RECALL'
102: cll 'DATA MANIPULATION'
103: if r1<0;dsp "DISPLAY RECALL COMPLETE";0}r1;stp
104: wrt "SA","0,5000XCEXXC.00000099,10.09YCEXYC"
105: wrt 705,"PG"
106: fmt 5,5/
107: wrt 706.5
108: wrt 706,I$;wrt 706,"";wrt 706,cap(A$);wrt 706,"";wrt 706,S$;wrt 706,""
109: wrt 706,B$;wrt 706,"";wrt 706,C$;wrt 706,""
110: fmt 4,33/,"G's Sq/Hz"
111: wrt 706.4
112: cll 'PLOT'
113: cll 'PLOT TICS'
114: if F<L;F+1}F;gto "LOOP"
115: dsp "SPECIFIED DATA PLOTTED";stp
116: "INTERVAL UP-DATE":
117: fxd 0
118: S$[35,42]}S$[26,33];val(S$[32,33])}S;S+U}S
119: if S<10;str(S)}S$[41,42];"0"}S$[41,41];jmp 12
120: if S<60;str(S)}S$[40,42];jmp 11
121: if S=60;"00"}S$[41,42];val(S$[38,39])+1}V;gto "LOADV"
122: if S>60;S-60}S
123: if S<10;str(S)}S$[41,42];"0"}S$[41,41];val(S$[38,39])+1}V;gto "LOADV"
124: if S>=10;str(S)}S$[40,42];val(S$[38,39])+1}V
125: "LOADV":
126: if V<10;str(V)}S$[38,39];"0"}S$[38,38];jmp 5
127: if V<60;str(V)}S$[37,39];jmp 4
128: if V=60;"00"}S$[38,39];val(S$[35,36])+1}V
129: if V<10;str(V)}S$[35,36];"0"}S$[35,35];jmp 2
130: if V<60;str(V)}S$[34,36]
131: ":"}S$[28,28]}S$[31,31]}S$[37,37]}S$[40,40];"-"}S$[34,34]
132: fxd 2
133: ret
134: "TEST ID":
135: dsp "Ready to enter data ID.--CONT";stp
136: ent "Test Number?--XXX-XXX--CONT",I$[11,17];ent "PWL-XXX--CONT",I$[42,44]
137: ent "Accel Location?--XXX--CONT",I$[28,30]
```

TABLE 10. Data Acquisition Program Listing - Continued

```
138: ent "Type of analysis performed?",A$[19,30]
139: ent "TAPE NO.?-XX",A$[43,44]
140: ent "DATA CHANNEL NO.?--XX",A$[54,55]
141: ent "Data Slice Time=XX:XX:XX-XX:XX:XX-CONT",S$[26],"SLICE DURATION",U
 42: ":"}S$[28,28]}S$[31,31]}S$[37,37]}S$[40,40];"-"}S$[34,34]
 43: if flg1;cfg 1;dsp "TEST ID UP-DATED";stp
 44: ret
 45: "MEASURE DATA":
146: oni 7,"INT SRQ";eir 7;0}G
147: wrt "SA","1TC1FM1LM"
148: "MEASUREMENT START":
149: dsp "CHECK SET-UP!--CONT TO START";stp
150: 1}G
151: wrt "SA","MRST"
152: if G#0;dsp "MEASUREMENT IN PROGRESS";jmp 0
153: beep;wrt "SA","MR"
154: if flg1;cfg 1;dsp "MEASUREMENT COMPLETE";stp
155: ret
156: "5420 DATA TAPE RECALL":
157: oni 7,"INT SRQ";eir 7;0}G
158: if flg1;ent "DATA RECORD TO BE RECALLED?",R
159: 1}G
160: fxd 0
161: wrt "SA",R,"RA"
162: if G#0;dsp "5420 TAPE RECALL",R;jmp 0
163: fxd 2
164: if flg1;cfg 1;dsp "RECALL COMPLETE";stp
165: ret
166: "5420 DATA TAPE SAVE":
167: oni 7,"INT SRQ";eir 7;0}G
168: if flg1;ent "RECORD NO FOR DATA SAVE?",R
169: 1}G;fxd 0
170: wrt "SA",R,"SA"
171: if G#0;dsp "5420 TAPE SAVE",R;jmp 0
172: fxd 2
173: if flg1;cfg 1;dsp "DATA SAVE COMPLETE";stp
174: ret
175: "DATA TRANSFER TO CALCULATOR":
176: oni 7,"INT SRQ";eir 7;0}G
177: 1}G
178: wrt "SA","0,5000XCPW"
179: wrt "SA",",0,1PR"
180: 1}G;wrt "SA","PR"
181: if G#0;jmp 0
182: wrt "SA","XC"
183: 1}G
184: wrt "SA","501SA"
185: if G#0;jmp 0
186: if A$[19,21]#"TFE";1}C[1]
187: P/C[1]^2}P;\P}P
188: flt 3;str(P)}C$[11,21];fxd 2
189: str(H[13])}B$[11,15]
190: if flg1;cfg 1;dsp "TRANSFER COMPLETE";stp
191: ret
192: "DATA MANIPULATION":
193: 1}G
194: if cap(A$[19,21])="PSD";jmp 4
195: dsp "TFE-PSD"
196: for I=1 to H[3]/2;(D[I]/C[1]^2)^2}D[I];next I
197: jmp 3
198: dsp "ORIG PSD"
199: for I=1 to H[3]/2;D[I]^2}D[I];next I
200: 1}G;wrt "SA","501RA"
201: if G#0;jmp 0
202: ret
203: "RECORD DATA ON 9825 TAPE":
204: if flg1;ent "9825 TAPE TRK?",T,"9825 TAPE FILE NO.?",F
205: trk T;dsp "SAVING F#",F,"TRK#",T
```

TABLE 10. Data Acquisition Program Listing - Concluded

```
206: rcf F,H[*],D[*],I$,A$,S$,C$,B$,C[*]
207: fxd 0
208: prt "Tape file used?",F
209: fxd 2
210: F+1}F
211: if flg1;cfg 1;dsp "9825 TAPE SAVE COMPLETE";stp
212: ret
213: "9825 TAPE RECALL":
214: if flg1;ent "9825 TAPE TRK?",T,"9825 TAPE FILE NO?",F
215: trk T;dsp "RECALLING  F#",F,"TRK#",T
216: ldf F,H[*],D[*],I$,A$,S$,C$,B$,C[*]
217: if flg1;cfg 1;dsp "9825 TAPE RECALL COMPLETE";stp
218: ret
219: "PLOT":
220: oni 7,"INT SRQ";eir 7;0}G
221: 1}G
222: wrt "SA",",,1PL,1PL0,200,1600PL1,7000,9000PLPL"
223: if G#0;jmp 0
224: if flg1;cfg 1;dsp "5420 PLOT COMPLETE";stp
225: ret
226: "PLOT TICS":sfg 2
227: scl 0,5000,-7.00043,.017
228: xax -7,100,0,5000,0;xax .017,100,0,5000,0
229: "SET":
230: 1e-7}Y
231: "RETURN":
232: plt 0,log(Y),1
233: plt -50,log(Y),2
234: plt 0,log(Y),1
235: if Y<1e-7;Y+1e-8}Y;gto "RETURN"
236: if Y<1e-6;Y+1e-7}Y;gto "RETURN"
237: if Y<1e-5;Y+1e-6}Y;gto "RETURN"
238: if Y<1e-4;Y+1e-5}Y;gto "RETURN"
239: if Y<1e-3;Y+1e-4}Y;gto "RETURN"
240: if Y<1e-2;Y+1e-3}Y;gto "RETURN"
241: if Y<1e-1;Y+1e-2}Y;gto "RETURN"
242: if Y<1e0;Y+1e-1}Y;gto "RETURN"
243: if flg2;scl -5000,0,-7.00043,.017;cfg 2;gto "SET"
244: ret
245: end
*7691
```

TABLE 11. Search and Sort Program Listing

```
0: "NASA/MSFC SSME HARMONIC SEARCH/PLOT DATA ANALYSIS PROGRAM(AMP)":
1: ent "ANALYZER HPIB DEVICE CODE",D
2: dev "SA",D
3: oni 7,"INT SRQ";eir 7;0}G
4: gto "DIMENSIONS"
5: "INT SRQ":dtords("SA")}Q;dsp "SRQ RECIEVED Q=",Q
6: if Q=150;cmd 7,"?D%";gto "RTN"
7: if Q=170;cmd 7,"?E$";gto "RTN"
8: if Q=142;0}G;dsp "5420 PLOT ACTION";gto "RTN"
9: "RTN":eir 7;iret
10: "DIMENSIONS":
11: fmt 0
12: ent "Total No. of data slices(120max)",S
13: dim H[16],D[512],I$[64],A$[64],S$[48],C$[32],B$[24],C[1]
14: dim S[S,11]
15: "SELECTIONS":
16: dsp "SELECT PROG OPTIONS---S/F KEYS";stp
17: "SEARCH AND SORT":
18: oni 7,"INT SRQ";eir 7;0}G
19: fxd 2;ina S;1}M;0}X
20: ent "NUMBER OF TESTS TO BE USED?",E
21: "LOOP SEARCH":X+1}X;dsp "",S-M+1,"DATA SLICES MAY BE STORED";wait 1000
22: ent "TAPE TRACK?",T
23: if T<0;jmp -1
24: if T>1;jmp -2
25: trk T
26: ent "STARTING 9825 TAPE FILE NUMBER?",F
27: ent "LAST 9825 TAPE FILE NUMBER?",L
28: ent "FUNDAMENTAL FREQUENCY FOR SEARCH?",C
29: for I=M to M+(L-F)
30: cll '9825 TAPE RECALL'
31: 1}K
32: I+X/10}S[I,1];val(C$[11,20])}S[I,11]
33: for J=1 to 9
34: JC/H[13]}A;prnd(A,0)}A;A+1}A
35: D[A-5]}W;W/C[1]^2}W;W}S[I,K+1]
36: D[A-4]}W;W/C[1]^2}W;if W>S[I,K+1];W}S[I,K+1]
37: D[A-3]}W;W/C[1]^2}W;if W>S[I,K+1];W}S[I,K+1]
38: D[A-2]}W;W/C[1]^2}W;if W>S[I,K+1];W}S[I,K+1]
39: D[A-1]}W;W/C[1]^2}W;if W>S[I,K+1];W}S[I,K+1]
40: D[A]}W;W/C[1]^2}W;if W>S[I,K+1];W}S[I,K+1]
41: D[A+1]}W;W/C[1]^2}W;if W>S[I,K+1];W}S[I,K+1]
42: D[A+2]}W;W/C[1]^2}W;if W>S[I,K+1];W}S[I,K+1]
43: D[A+3]}W;W/C[1]^2}W;if W>S[I,K+1];W}S[I,K+1]
44: D[A+4]}W;W/C[1]^2}W;if W>S[I,K+1];W}S[I,K+1]
45: D[A+5]}W;W/C[1]^2}W;if W>S[I,K+1];W}S[I,K+1]
46: K+1}K
47: next J
48: F+1}F
49: next I
50: if E>X;dsp "INSERT NEXT TEST TAPE-CONT";stp ;I}M;gto "LOOP SEARCH"
51: fxd 2
52: prt "Data slices=",I-1;prt "Tests=",X
53: dsp "TAPE SEARCH COMPLETE";stp
54: "PLOT SEARCH":0}H}N}r1}r2;1}B
55: oni 7,"INT SRQ";eir 7;0}G
56: ent "PLOT DESIRED?--(1)Yes,(0)No",P
57: if P≠1;gto "SELECTIONS"
58: ent "HAR vs DATA SLICE?-(1)Yes,(0)No",H
59: if H=0;jmp 8
60: if H≠1;jmp -3
61: 1}H;ent "HARMONIC TO BE PLOTTED?",N;N+1}N
62: ent "FIRST DATA SLICE?",r1,"LAST DATA SLICE?",r2
63: ent "PLT ABS VAL OF HAR?-(1)Yes (0)No",r3;if r3=1;jmp 3
64: ent "PLT NOR VAL OF HAR?-(1)Yes (0)No",r3;if r3=1;0}r3;cll 'REF'
65: if r3≠0;jmp -2
66: gto "TITLE"
67: ent "HAR PSD vs HAR?-(1)Yes,(0)No",H
68: if H=0;jmp 8
69: if H≠1;jmp -2
```

TABLE 11. Search and Sort Program Listing - Continued

```
70: 2}H;ent "DATA SLICE TO BE PLOTTED?",N
71: ent "FIRST HAR TO BE USED?",r1,"LAST HAR TO BE USED?",r2
72: ent "PLT ABS VAL OF HAR?-(1)Yes (0)No",r3;if r3=1;jmp 3
73: ent "PLT NOR VAL OF HAR?-(1)Yes (0)No",r3;if r3#1;jmp -1
74: 0}r3;cll 'REF'
75: gto "TITLE"
76: ent "Composite vs Data Slice?-(1)Yes,(0)No",H
77: if H=0;gto "END PLOT"
78: if H#1;jmp -2
79: 3}H;11}N
80: ent "FIRST DATA SLICE?",r1,"LAST DATA SLICE?",r2
81: ent "PLT ABS VAL OF COMP?-(1)Yes (0)No",r3;if r3=1;jmp 3
82: ent "PLT NOR VAL OF COMP?-(1)Yes (0)No",r3;if r3=1;0}r3;cll 'REF'
83: "TITLE":
84: fmt 5,5/
85: wrt 706.5
86: ent "Plot ID?(48 char max)",S$;wrt 706,S$;wrt 706,I$[19,64];wrt 706,A$
87: fxd 0
88: if r3=0;jmp 7
89: if H=1;wrt 706,"ABS VAL OF HAR NO. ",N-1
90: if H=1;wrt 706,"DATA SLICE NUMBER",r1,"       THROUGH  ",r2
91: if H=2;wrt 706,"ABS VAL OF HAR",r1,"   THROUGH ",r2
92: if H=2;wrt 706,"FOR DATA SLICE NUMBER",N
93: if H=3;wrt 706,"ABS VAL OF COMPOSITE VALUES"
94: if H=3;wrt 706,"DATA SLICE NUMBER",r1,"       THROUGH  ",r2
95: if r3=1;jmp 7
96: if H=1;wrt 706,"VAL OF HAR NO. ",N-1,"   WRT",K,"  OF SLICE",J
97: if H=1;wrt 706,"FOR DATA SLICE ",r1,"  THROUGH    ",r2
98: if H=2;wrt 706,"VAL OF HARMONIC",r1,"   THROUGH  ",r2,"  WRT",K
99: if H=2;wrt 706,"FOR DATA SLICE",N
100: if H=3;wrt 706,"VAL OF COMPOSITE VALUES WRT COMPOSITE OF SLICE",J
101: if H=3;wrt 706,"FOR DATA SLICE ",r1,"  THROUGH    ",r2
102: fxd 2
103: cll '9825 SEARCH PLOT'
104: "END PLOT":
105: dsp "SEARCH PLOT COMPLETE";stp
106: "REF":
107: ent "HAR# FOR REF?",K,"SLICE # FOR REF?",J;S[J,K+1]}B
108: ret
109: "RECORD DATA ON 9825 TAPE":
110: if flg1;ent "9825 TAPE TRK?",T,"9825 TAPE FILE NO.?",F
111: trk T;dsp "SAVING F#",F,"TRK#",T
112: rcf F,H[*],D[*],I$,A$,S$,C$,B$,C[*]
113: fxd 0
114: prt "Tape file used?",F
115: fxd 2
116: F+1}F
117: if flg1;cfg 1;dsp "9825 TAPE SAVE COMPLETE";stp
118: ret
119: "9825 TAPE RECALL":
120: if flg1;ent "9825 TAPE TRK?",T,"9825 TAPE FILE NO?",F
121: trk T;dsp "RECALLING  F#",F,"TRK#",T
122: ldf F,H[*],D[*],I$,A$,S$,C$,B$,C[*]
123: if flg1;cfg 1;dsp "9825 TAPE RECALL COMPLETE";stp
124: ret
125: "PLOT":
126: oni 7,"INT SRQ";eir 7;0}G
127: 1}G
128: wrt "SA",",,1PL,1PL0,200,1600PL1,7000,9000PLPL"
129: if G#0;jmp 0
130: if flg1;cfg 1;dsp "5420 PLOT COMPLETE";stp
131: ret
132: "9825 SEARCH PLOT":
133: fxd 9
134: wrt 705,"IP1500,2500,6000,8500"
135: ent "PLOT TYPE--(1)LIN, (2)LOG",r6
136: if r6=1;gto "LIN PLOT"
137: if r6=2;gto "LOG PLOT"
138: if r6#2;jmp -3
139: "LOG PLOT":-6}r3;1}r4
```

TABLE 11. Search and Sort Program Listing - Continued

```
140: scl r1,r2,r3,r4
141: if H=1 or H=3;cll 'LOG PLOT 1'
142: if H=2;cll 'LOG PLOT 2'
143: gto "AXIS"
144: "LIN PLOT":
145: if H=1;0}r3;2}r4;scl r1,r2,r3,r4;cll 'LIN PLOT 1'
146: if H=2;0}r3;2}r4;scl r1,r2,r3,r4;cll 'LIN PLOT 2'
147: if H=3;0}r3;9}r4;scl r1,r2,r3,r4;cll 'LIN PLOT 1'
148: "AXIS":
149: line ;fxd 0;xax r3,1,r1,r2,4;xax r4,1,r1,r2;fxd 1
150: if r6=2;yax r1,1,r3,r4,1;yax r2,1,r3,r4;gto "LOG TICS"
151: if r6=1;yax r1,.1,r3,r4,5;yax r2,.1,r3,r4;gto "LABLE AXIS"
152: "LOG TICS";sfg 2
153: scl 0,10,r3,r4
154: "SET":
155: 10^r3}Y
156: "RETURN":
157: plt 0,log(Y),1
158: plt -.1,log(Y),2
159: plt 0,log(Y),1
160: if Y<1e-6;Y+1e-7}Y;gto "RETURN"
161: if Y<1e-5;Y+1e-6}Y;gto "RETURN"
162: if Y<1e-4;Y+1e-5}Y;gto "RETURN"
163: if Y<1e-3;Y+1e-4}Y;gto "RETURN"
164: if Y<1e-2;Y+1e-3}Y;gto "RETURN"
165: if Y<1e-1;Y+1e-2}Y;gto "RETURN"
166: if Y<1e0;Y+1e-1}Y;gto "RETURN"
167: if Y<1e1;Y+1e0}Y;gto "RETURN"
168: if flg2;scl -10,0,r3,r4;cfg 2;gto "SET"
169: "LABLE AXIS":
170: scl 0,10,0,10
171: if H=2;plt 4,-.9,1;lbl "HARMONIC"
172: if H=1 or H=3;plt 4,-.9,1;lbl "DATA SLICE"
173: if H=3;csiz 1.5,2,1,90;plt -1.5,4,1;lbl "AMPLITUDE (g's rms)";jmp 2
174: csiz 1.5,2,1,90;plt -1.5,4,1;lbl "AMPLITUDE (g sq/hz)"
175: csiz 1.5,2,1,0
176: if r6=2;plt -1,9.75,1;lbl "10"
177: 0}H;pen# 0
178: ret
179: "LOG PLOT 1":
180: pen# 1;plt r1,r3,1
181: frc(S[r1,1])}X
182: for I=r1 to r2
183: plt I,log(S[I,N]/B);if frc(S[I,1])=X;lbl "X";X+.1}X;plt I,log(S[I,N]/B)
184: next I
185: ret
186: "LOG PLOT 2":
187: pen# 1;plt r1,r3,1
188: for I=r1 to r2
189: plt I,log(S[N,I+1]/B)
190: next I
191: ret
192: "LIN PLOT 1":
193: pen# 1;plt r1,r3,1
194: frc(S[r1,1])}X
195: for I=r1 to r2
196: plt I,S[I,N]/B;if frc(S[I,1])=X;lbl "X";X+.1}X;plt I,S[I,N]/B
197: next I
198: ret
199: "LIN PLOT 2":
200: pen# 1;plt r1,r3,1
201: for I=r1 to r2
202: plt I,S[N,I+1]/B
203: next I
204: ret
205: "PRINTS":
206: fmt 4,5/,2x,"ID",30x,"HARMONICS--g's sq/hz",/
207: fmt 5,z,2x,"no.",3x,"1st",5x,"2nd",5x,"3rd",5x,"4th",5x,"5th",5x,"6th"
208: fmt 6,z,5x,"7th",5x,"8th",5x,"9th",3x,"Pw. g-rms"
```

TABLE 11. Search and Sort Program Listing - Concluded

```
209: fmt 7,z,e10.2
210: fmt 8,z,f5.2
211: fmt 9,z,9f8.5
212: wrt 706.4;wrt 706.5;wrt 706.6;wrt 706
213: for I=1 to S
214: wrt 706.8,S[I,1]
215: for J=1 to 9
216: wrt 706.9,S[I,J+1]
217: next J
218: wrt 706.7,S[I,11]
219: wrt 706
220: next I
221: end
*1974
```

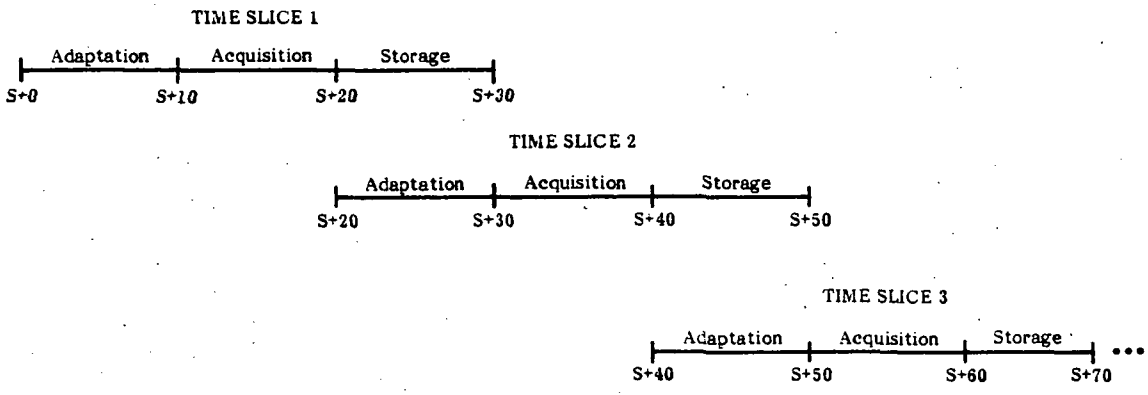

Figure 34. Data Reduction Time Slice Basis

In the case where nonadaptive filtered PSDs were computed, the first 10 seconds allocated for adaptation were skipped and the data acquisition cycle began as scheuled to ensure consistent data intervals for comparison. Using this scheme, hundreds of PSDs were computed from the test data. Since practicality does not allow all this data to be included in this report, the data has been screened to provide the most representative data for each test case.

To illustrate the noise reduction capabilities of the adaptive filtering, a typical pre- and post-filtered PSD is presented in figure 35. The post-filtered PSD is designated as the "TFE-PSD." In both spectra, the presence of the synchronous (1N), 2N, 4N, and 8N harmonics can be easily seen. In addition, a 2 to 3 decade (20 to 30 dB) reduction in

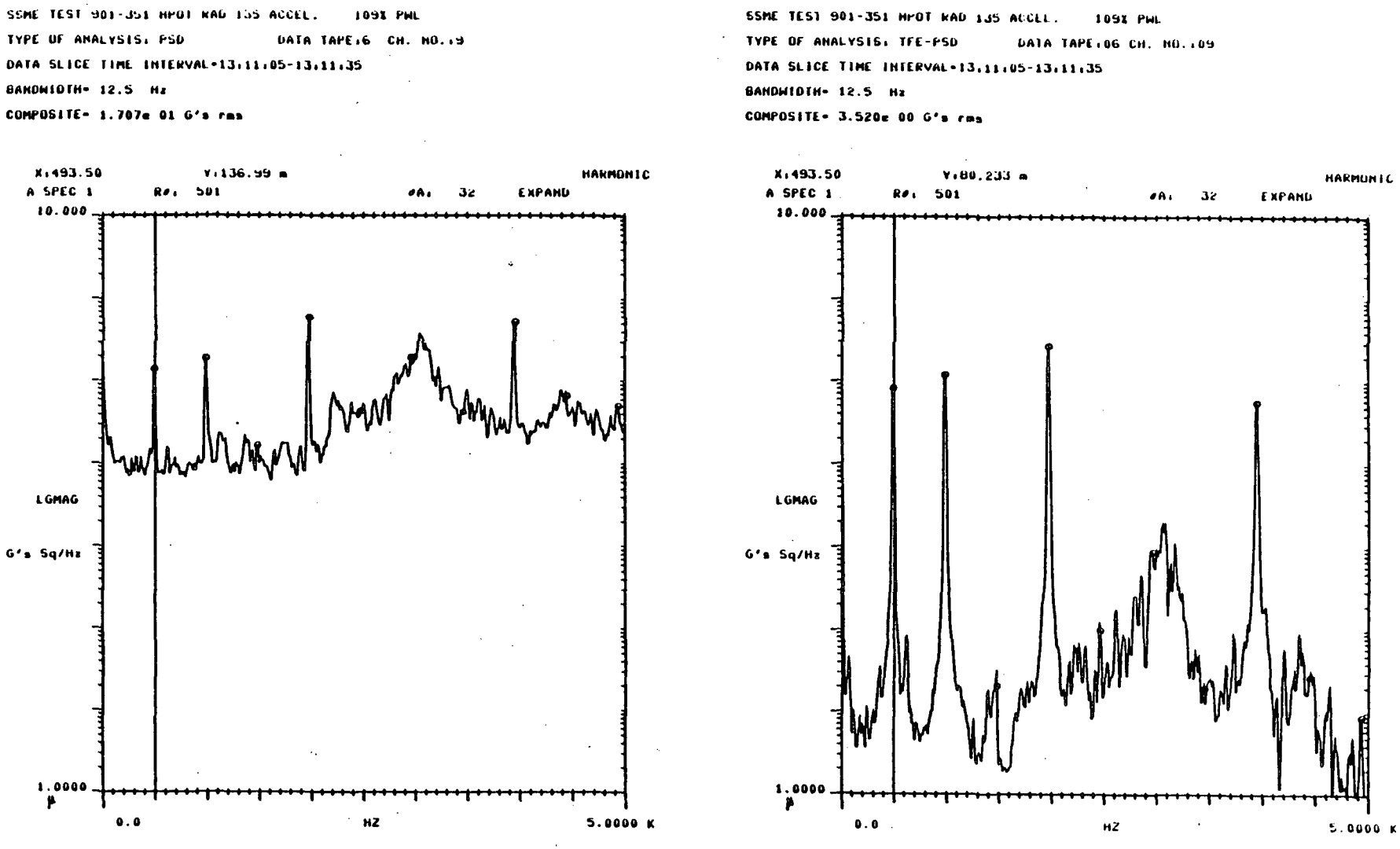

Figure 35. Typical Pre- and Post-Adaptive Filtered PSDs

the overall background noise level can be noted. It should be pointed out that the noise reduction process also tended to attenuate the amplitude of the various harmonics as well as the random noise components. Additionally, the higher order harmonics and/or frequency components appeared to have been attenuated more than the lower frequency information. Experiments were conducted and their results indicate that the attenuation did not appear to be due to a simple high frequency roll-off effect common to low-pass filtering. However, the attenuation effects did appear to remain constant for a given filter condition (setup). For this reason, a constant filter setup was maintained for all data reduced, and the assumption was made that this attenuation effect is constant for a given filter configuration. The adaptive filter setup configuration used for all data reduction is presented in table 12.

TABLE 12. DAC 1024I Adaptive Filter Configuration

Primary: 0.31 volts,	CC coupling,	-6dB Level
Reference: 0.31 volts,	CC coupling,	-6dB Level
Output: 1.2 volts,	CC coupling,	
Sample Frequency: 5 kHz		
Delay: 960 (maximum)		
Bandwidth: Wide		
Order: 448		
Filter Mode: TFE		
Algorithm: LMS		
Adaptation Time: 8 seconds		
Adaptation Mode: 8 sec adaptation; switch "off" and acquire data		
Threshold: ϕ		

Test case 1 was comprised of seven tests that were performed with HPOTP S/N 0209. The total run time accumulated on the pump was in excess of 2000 seconds. A total of 13 data slices were taken from tests 339, 341, and 351 at the 100% power level, and 61 data slices were reduced from tests 340, 341, 342, 343, 351, and 352 at the 109% power level. Test 339 had been designated at a "green" run for pump 0209, and a routine inspection and boroscope of bearing 3 was performed after test 343 with no indications of bearing degradation. After test 352, slightly spalled ball bearings were found during the pump overhaul. Since a rather limited number of 100% data slices were available for this first test case, the 109% power level data was chosen for analysis.

With the lengthy run time associated with pump 0209 and the progression from a newly refurbished pump to one containing a specific bearing defect, test case 1 possessed the best overall characteristics of the three test cases. Each of the three accelerometer

signals were reduced and used to develop a data base for pump 0209. Using the search and sort data base manipulation software, the amplitudes of the fundamental through the tenth harmonic were plotted as a function of data slice.

The behavior of the 1N, 2N, 4N, and 8N component of the spectra are shown in figures 36, 37, and 38 for the 135°, 90°, and 45° radial accelerometers, respectively. The remaining harmonics failed to show any consistent trend and have not been included. Each graph shows the amplitude variation ($g's^2/Hz$) of a given harmonic for each data slice for all tests contained in the data base. The beginning of each test is designated by an "X" on each plot. A gradual decline with some abrupt variations in the amplitude of the fundamental was noted in the 135° and 90° data, whereas the amplitude of the fundamental in the 45° data was extremely low at the beginning of test 340 and continued to decrease until the beginning of test 351 where the amplitude began and continued to increase until the end of test 352. At the end of test 352, the amplitude of the fundamental had reached within a decade of that for the 135° and 90° data in comparison to a 2- to 4-decade difference during tests 340 through 343. This behavior appears to be unusual but is supported by the similar behavior of the fundamental for the other test cases. Although the other test cases do not show such a marked difference, a gradual increase in the amplitude of the fundamental is apparent. The 2N and 4N components displayed a more consistent behavior for all accelerometer data although some distinctively abrupt changes in the amplitudes were noted. The 8N component displayed a much more erratic behavior with many abrupt increases and decreases in amplitude.

Test case 2 consisted of five tests (901-367 through 901-371) performed at 109% power level using HPOTP S/N 2113. A total of 50 data slices were reduced and used for analysis. Figures 39, 40, and 41 depict the amplitude behavior of the 1N, 2N, 4N, and 8N spectral components for the 135°, 90°, and 45° accelerometer data, respectively. As with test case 1, the fundamental component showed a gradual decline in amplitude for the 135° and 90° data; however, the 45° data was again inconsistent with the 135° and 90° data. In this case, the amplitude of the fundamental was somewhat low at the beginning of test 367, but its amplitude continued to decrease. This behavior is totally opposite that in test case 1 and does not agree with the general behavior for the remainder of the test cases. The 2N component shows an abrupt decrease at the beginning of test 367 but quickly increases to a relatively constant level for the 135°

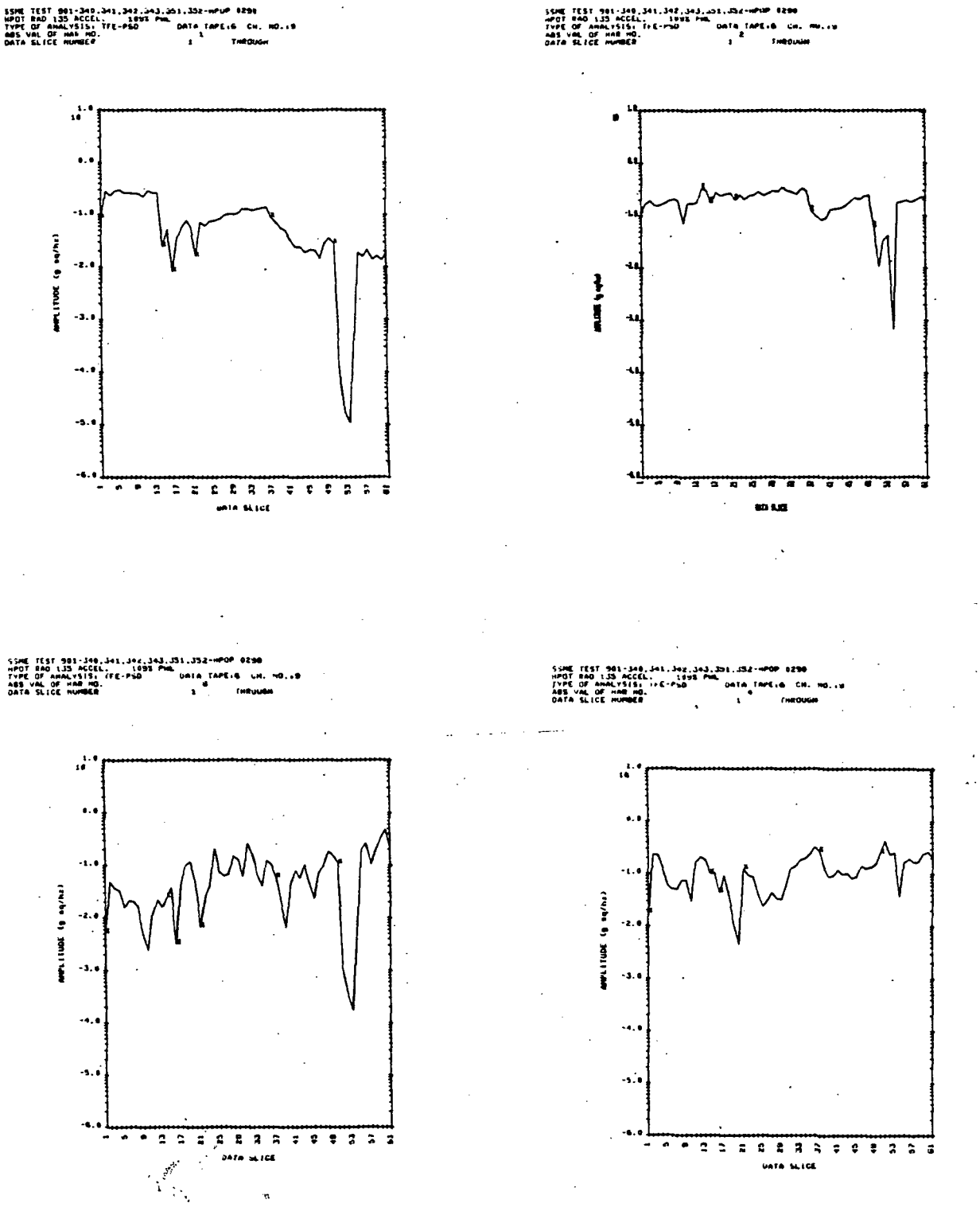

Figure 36. Test Case 1, 135° Accelerometer Harmonic Amplitude Variations as a Function of Data Slice

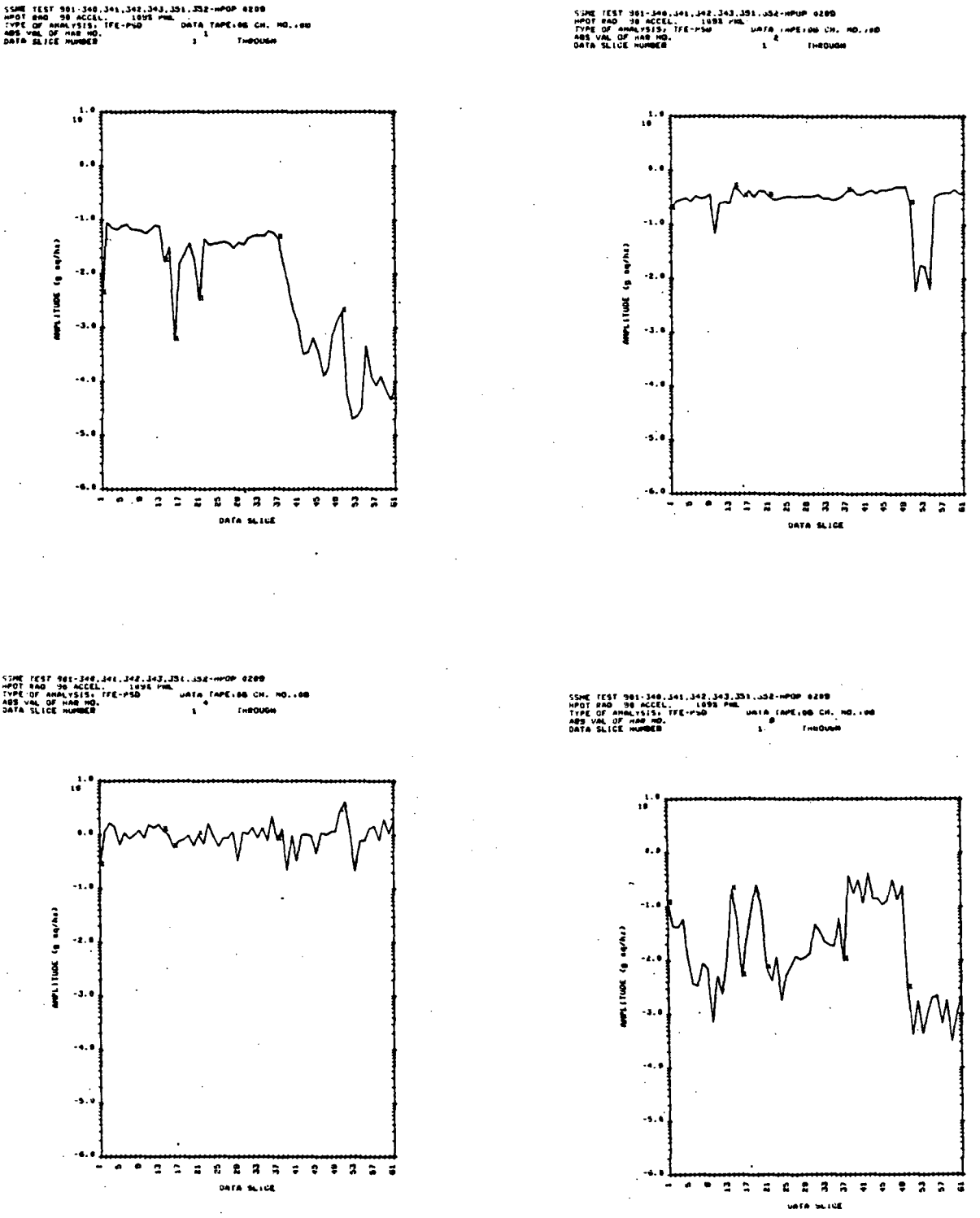

Figure 37. Test Case 1, 90° Accelerometer Harmonic Amplitude Variations as a Function of Data Slice

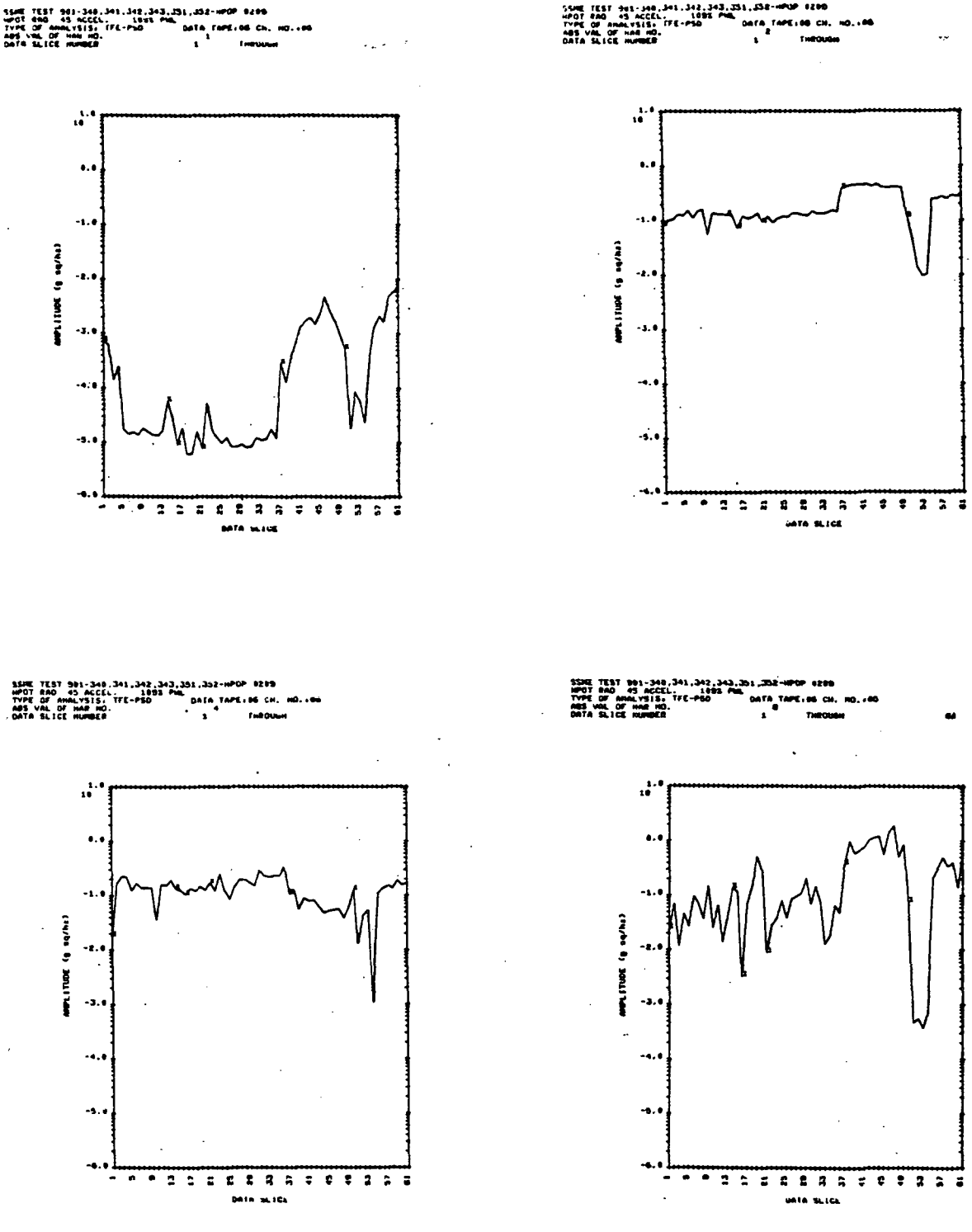

Figure 38. Test Case 1, 45° Accelerometer Harmonic Amplitude Variations as a Function of Data Slice

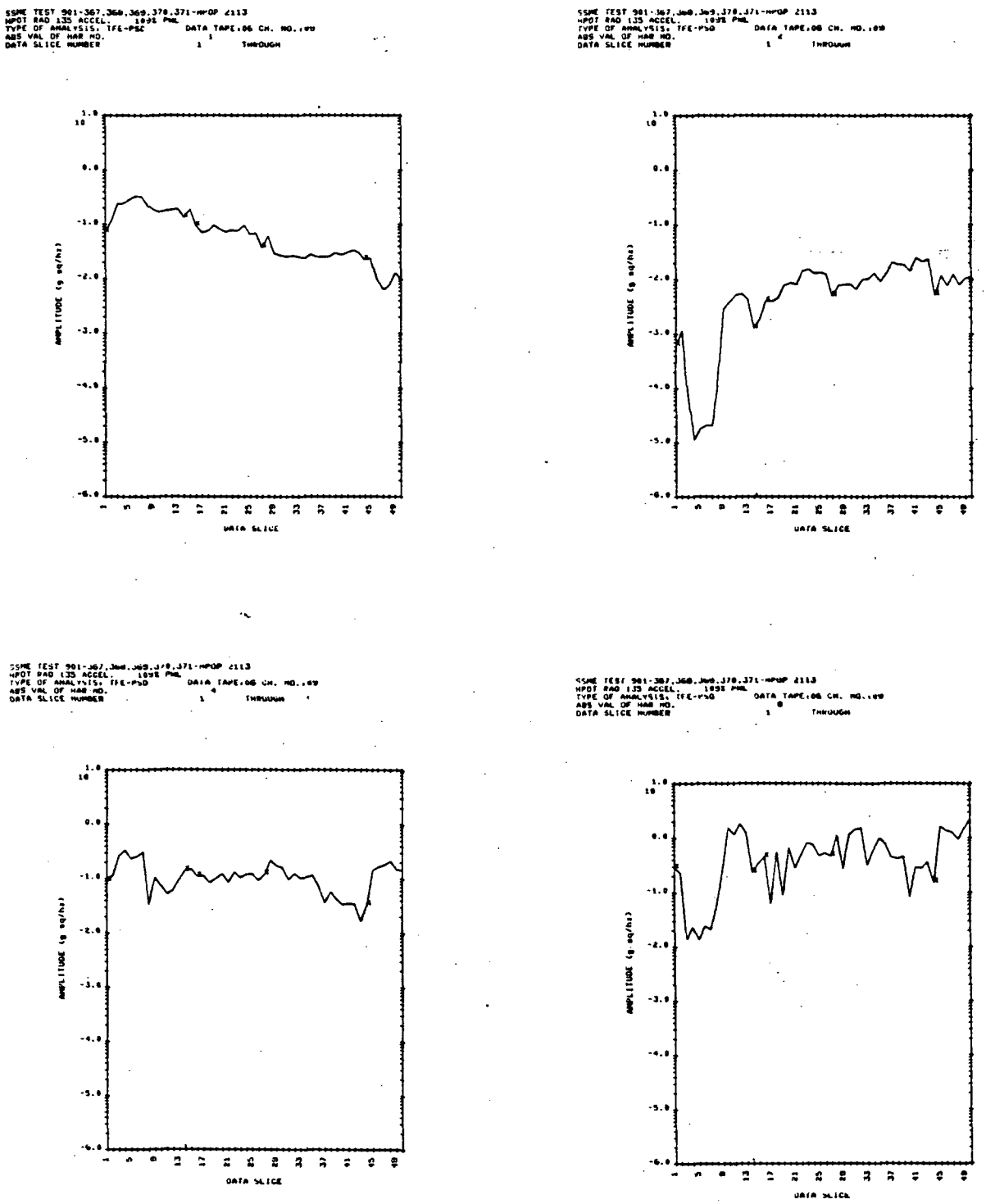

Figure 39. Test Case 2, 135° Accelerometer Harmonic Amplitude Variations as a Function of Data Slice

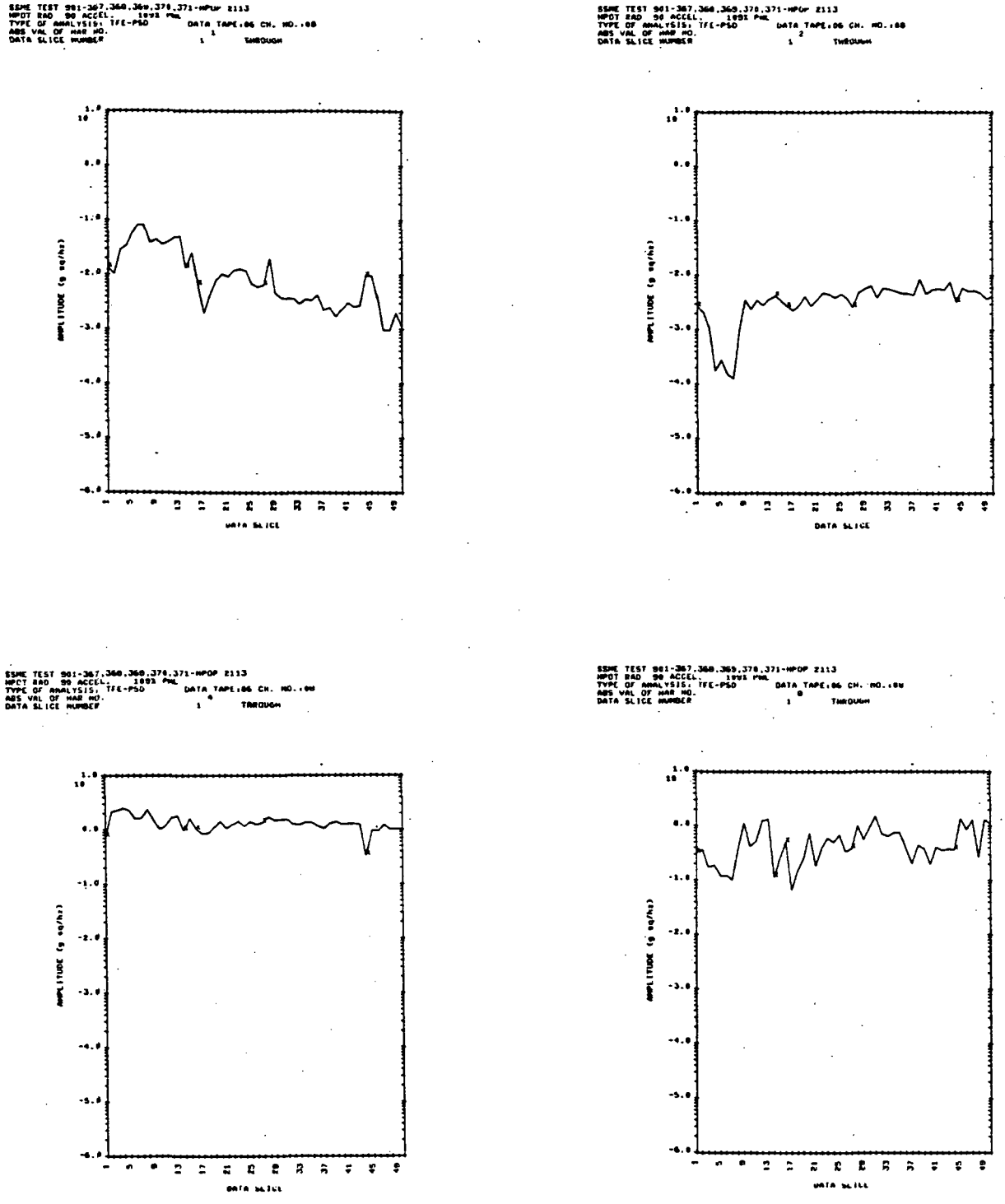

Figure 40. Test Case 2, 90° Accelerometer Harmonic Amplitude Variations as a Function of Data Slice

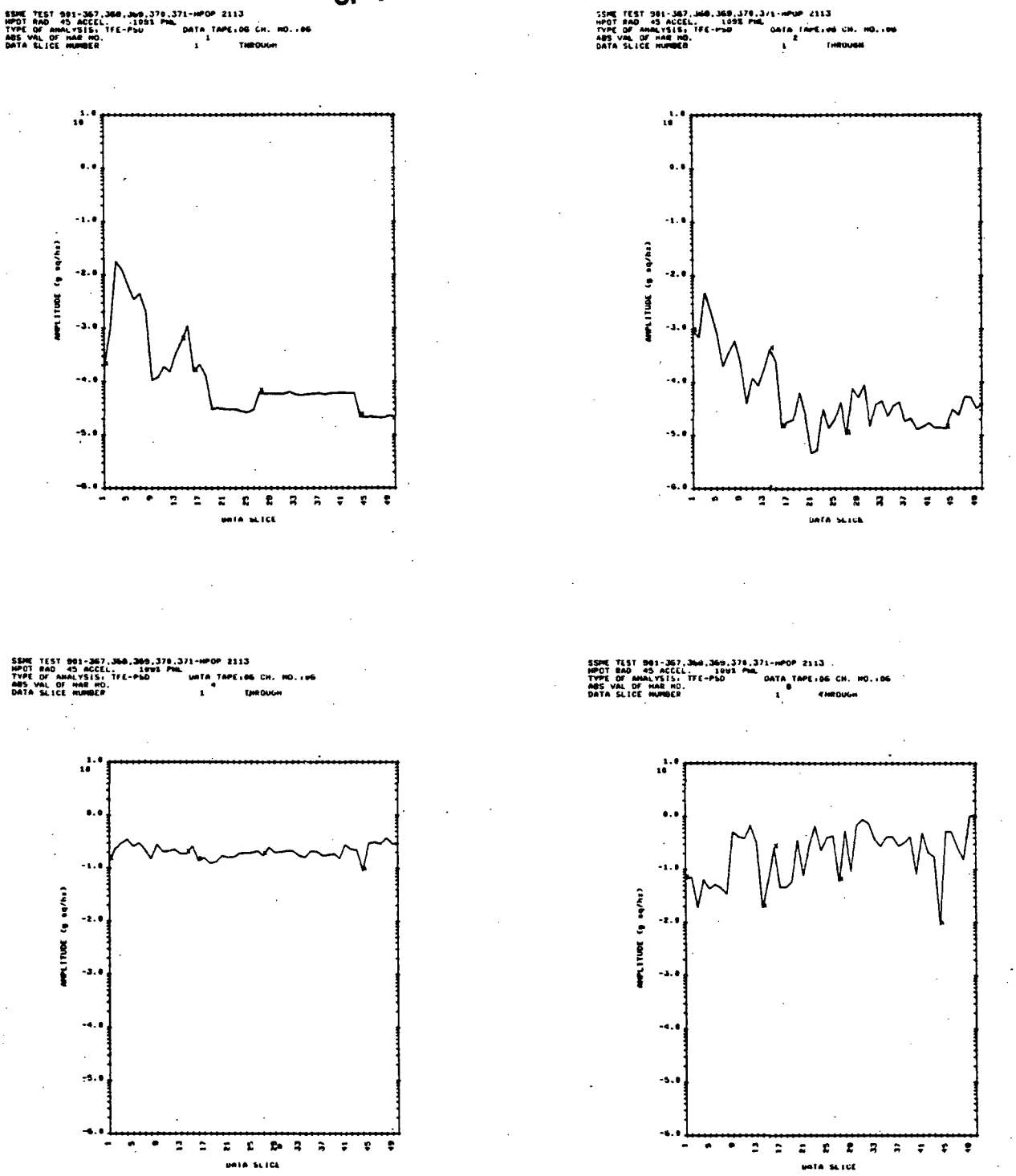

Figure 41. Test Case 2, 45° Accelerometer Harmonic Amplitude Variations as a Function of Data Slice

and 90° acceleration data. For the 45° data, the 2N component shows the same initial decrease in amplitude at the beginning of test 367 and continues to decrease to a relatively constant level. The amplitude of the 4N component shows an even more consistent behavior in test case 2 than in test case 1 with approximately the same amplitude. The 8N component was again erratic but was much more consistent than in test case 1 with amplitudes approximately a decade greater.

Test case 3 provided the most interesting behavior of the three test cases. This test case was comprised of four SSME tests (902-272 through -275) performed at a 109% power level with HPOTP S/N 2310. Forty data slices were reduced from these tests, and the behavior of the 1N, 2N, 4N, 6N, and 8N components of the spectra are shown in figures 42, 43, and 44 for the 135°, 90°, and 45° radial accelerometers, respectively. Once again the behavior of other harmonics have not been included. The most interesting characteristic associated with this group of data is related to the sudden decrease in the amplitude of the 1N, 4N, and 8N component while a correspondingly large increase in the 2N and 6N components. This behavior is consistently present at the beginning of test 273 in all accelerometer data and is prominent for approximately six data slices. Approximately halfway through test 273, the level of the 2N and 6N abruptly decreased while the amplitude of the 1N, 4N, and 8N increased to approximately the same levels as they were before this phenomenon occurred. With the exception of those characteristics just noted, the behavior of the 1N, 2N, 4N, and 8N components were essentially the same as in test case 1.

Two single-run tests were reduced using the adaptive filter; these tests were 902-193 and 901-301. Test 193 was a test that was conducted with know bad bearings in pump S/N 9008. Test 301 was included as an example of a test in which spalled ball bearings were found during a post-test inspection. Pump S/N 2206 was used during test 301. Test 193 provided 11 data slices and test 301 provided 16 data slices at the 109% power level. In comparison to test cases 1 through 3, these tests provided a relatively low number of data slices due to the short run duration. Any variations that might be noted in this data would most probably appear as random variations in test cases 1 through 3. For this reason, no attempt will be made to correlate any corresponding data although the same type of analysis was performed on both sets of data. Figures 45 through 49 are plots depicting the amplitude behavior of the 1N, 2N, 4N, and 8N components for the 135°, 90°, and 45° accelerometers, respectively. (No data was

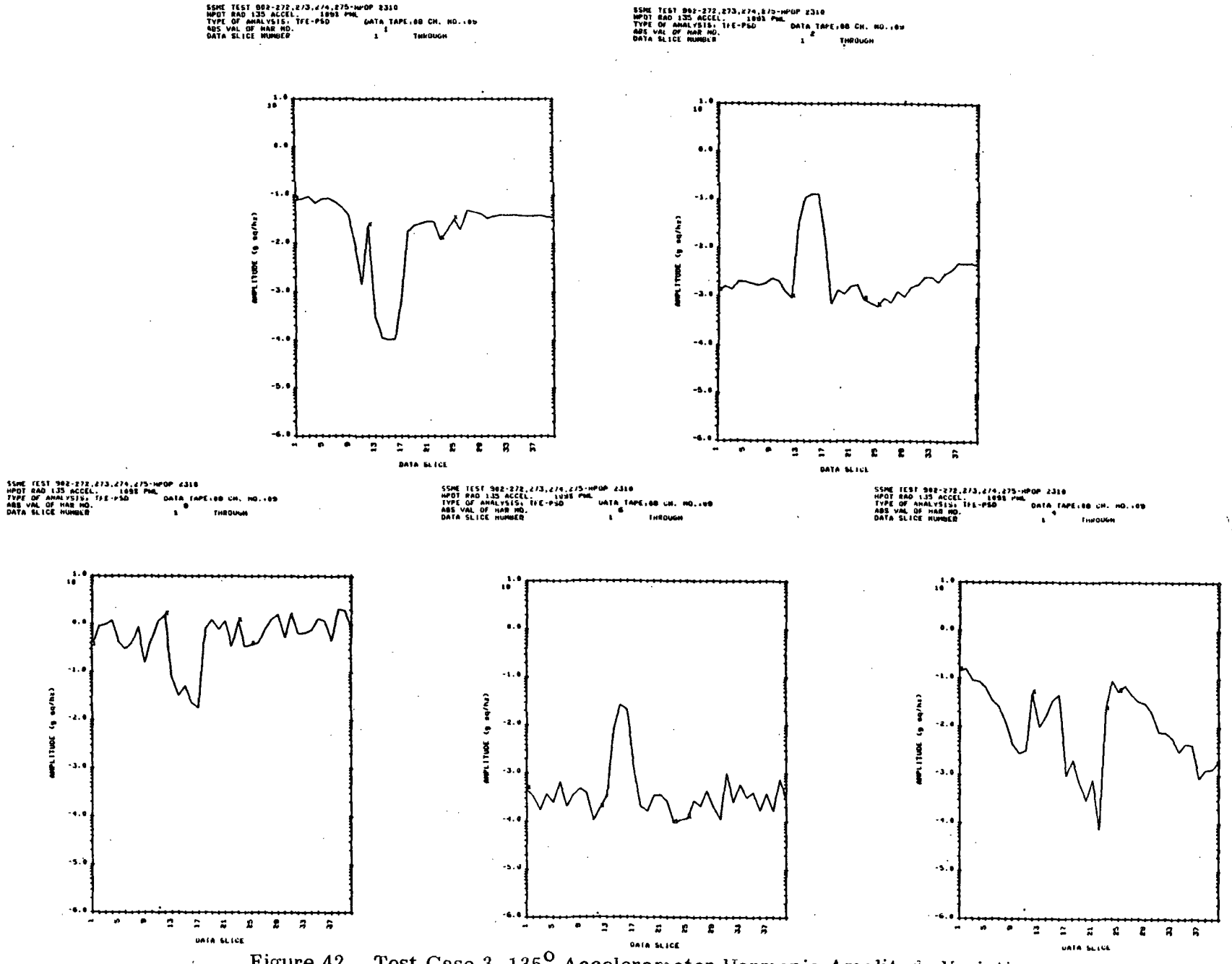

Figure 42. Test Case 3, 135° Accelerometer Harmonic Amplitude Variations as a Function of Data Slice

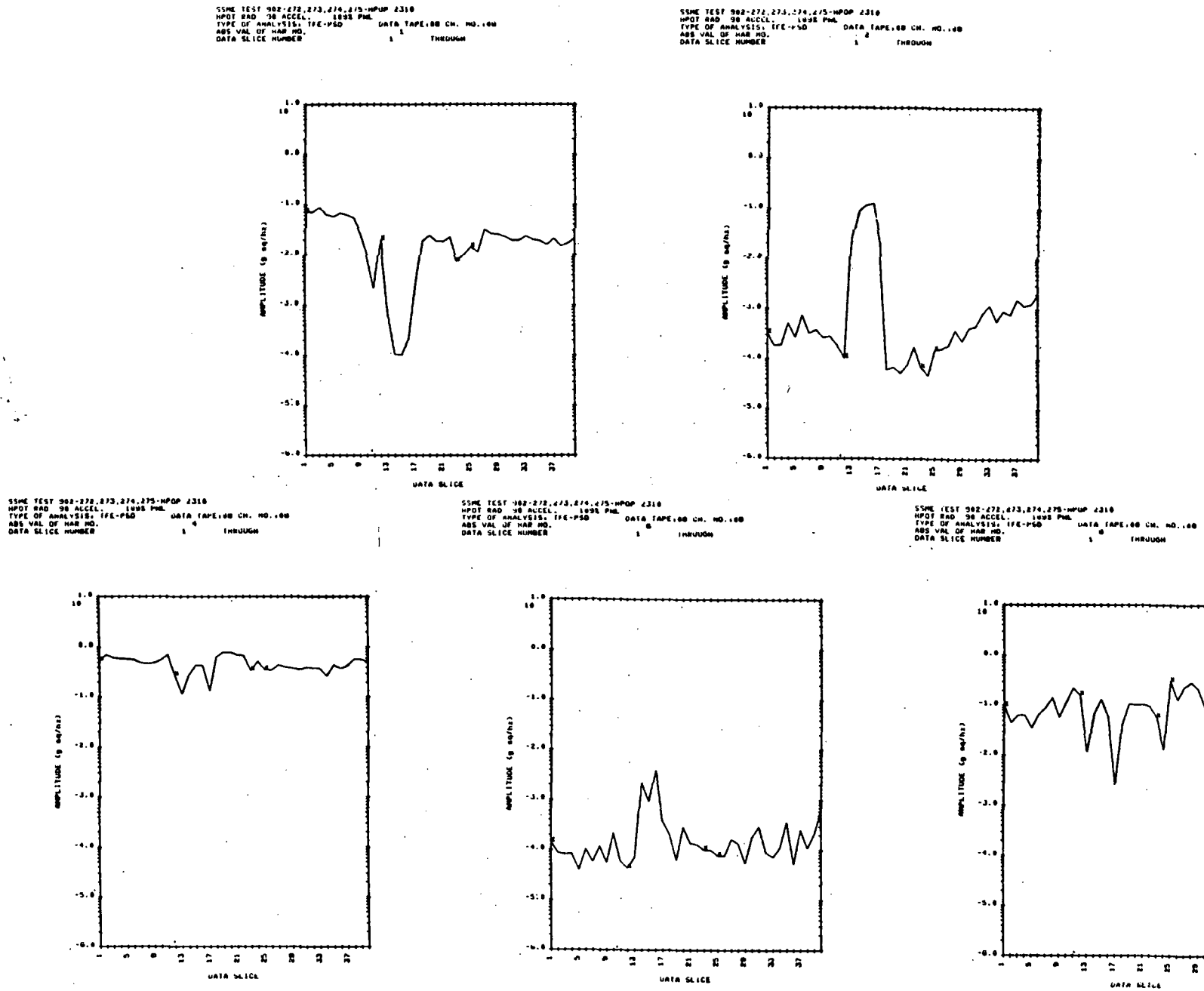

Figure 43. Test Case 3, 90° Accelerometer Harmonic Amplitude Variations as a Function of Data Slice

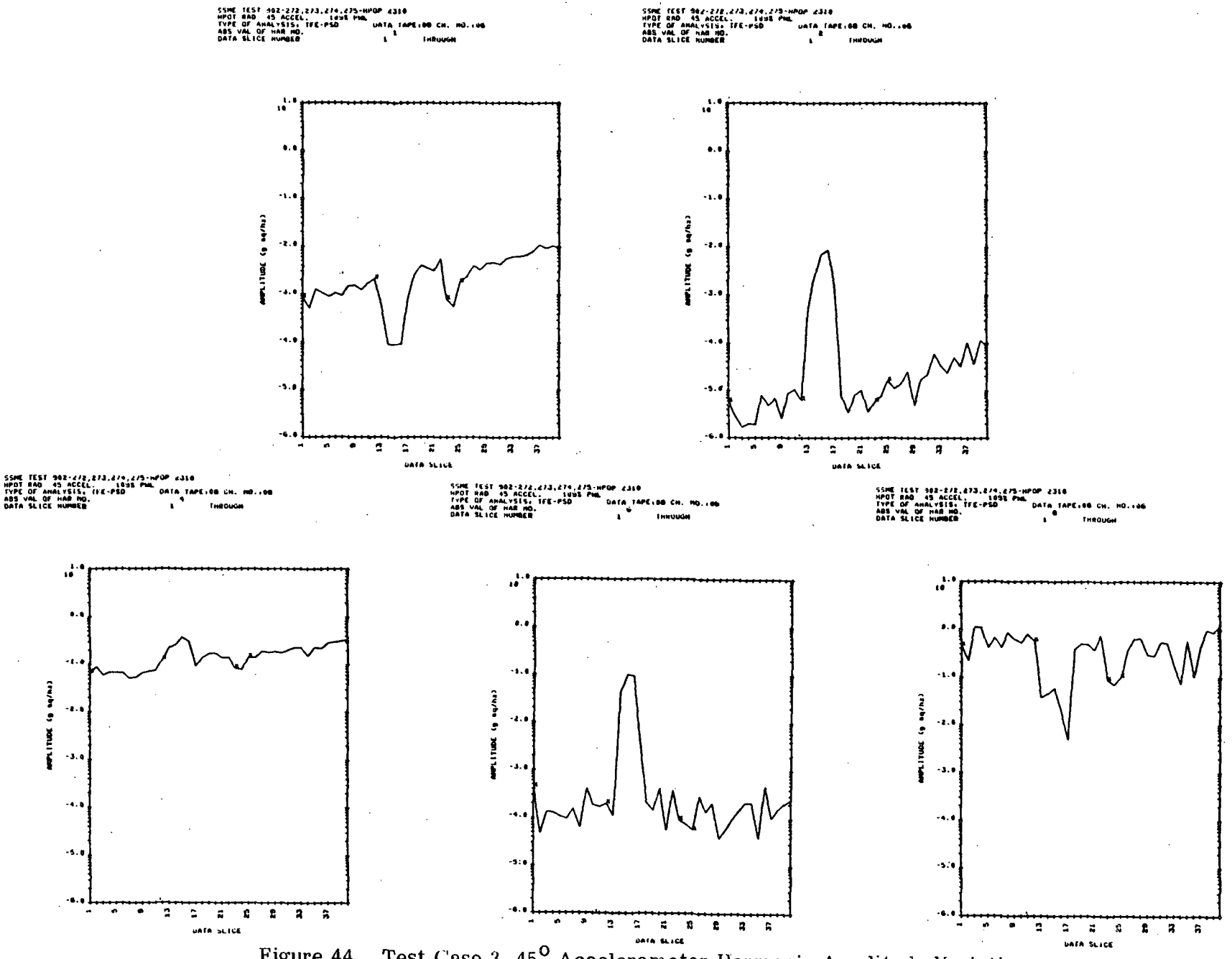

Figure 44. Test Case 3, 45° Accelerometer Harmonic Amplitude Variations as a Function of Data Slice

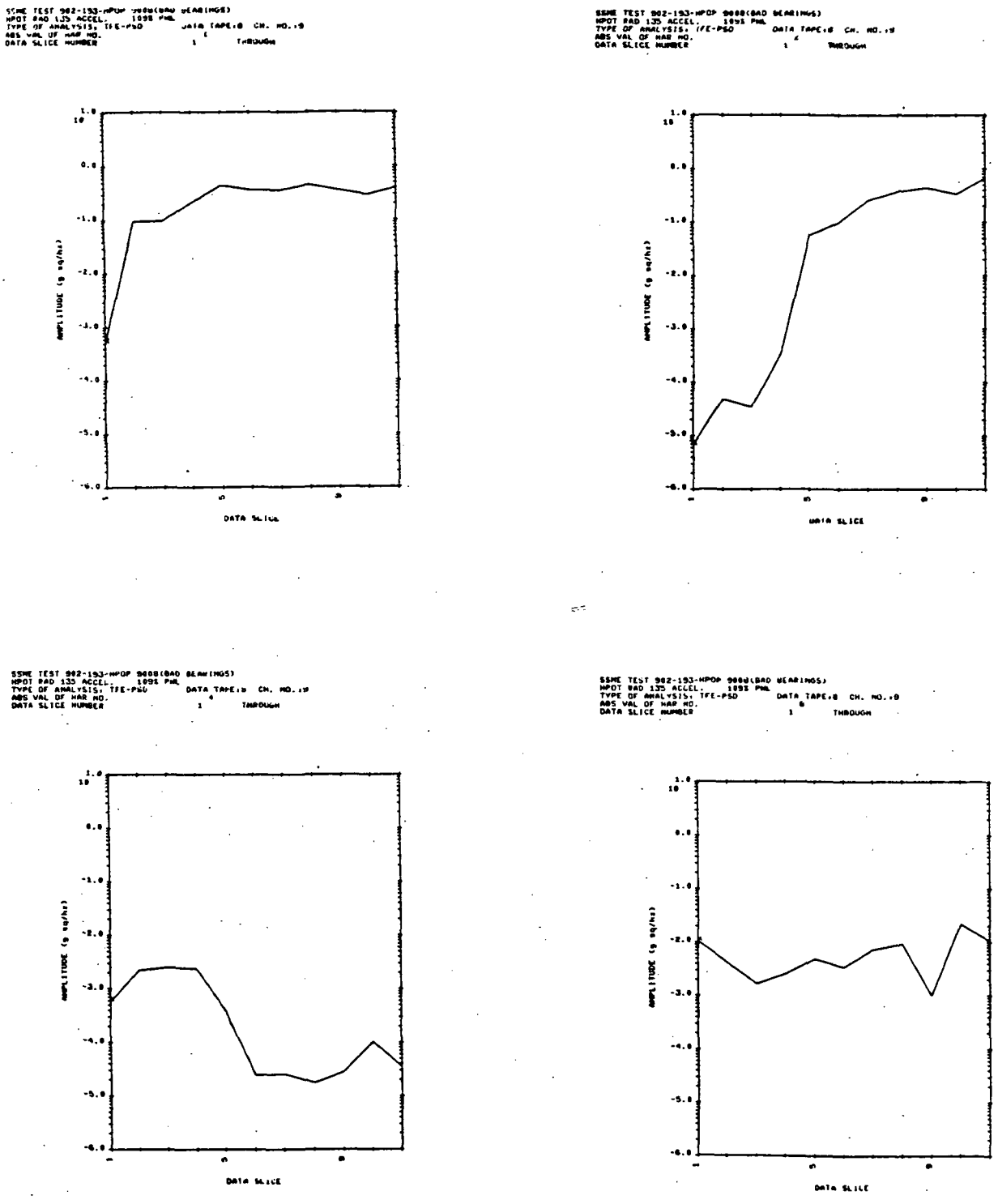

Figure 45. Test 902-193, 135° Accelerometer Harmonic Amplitude Variations as a Function of Data Slice

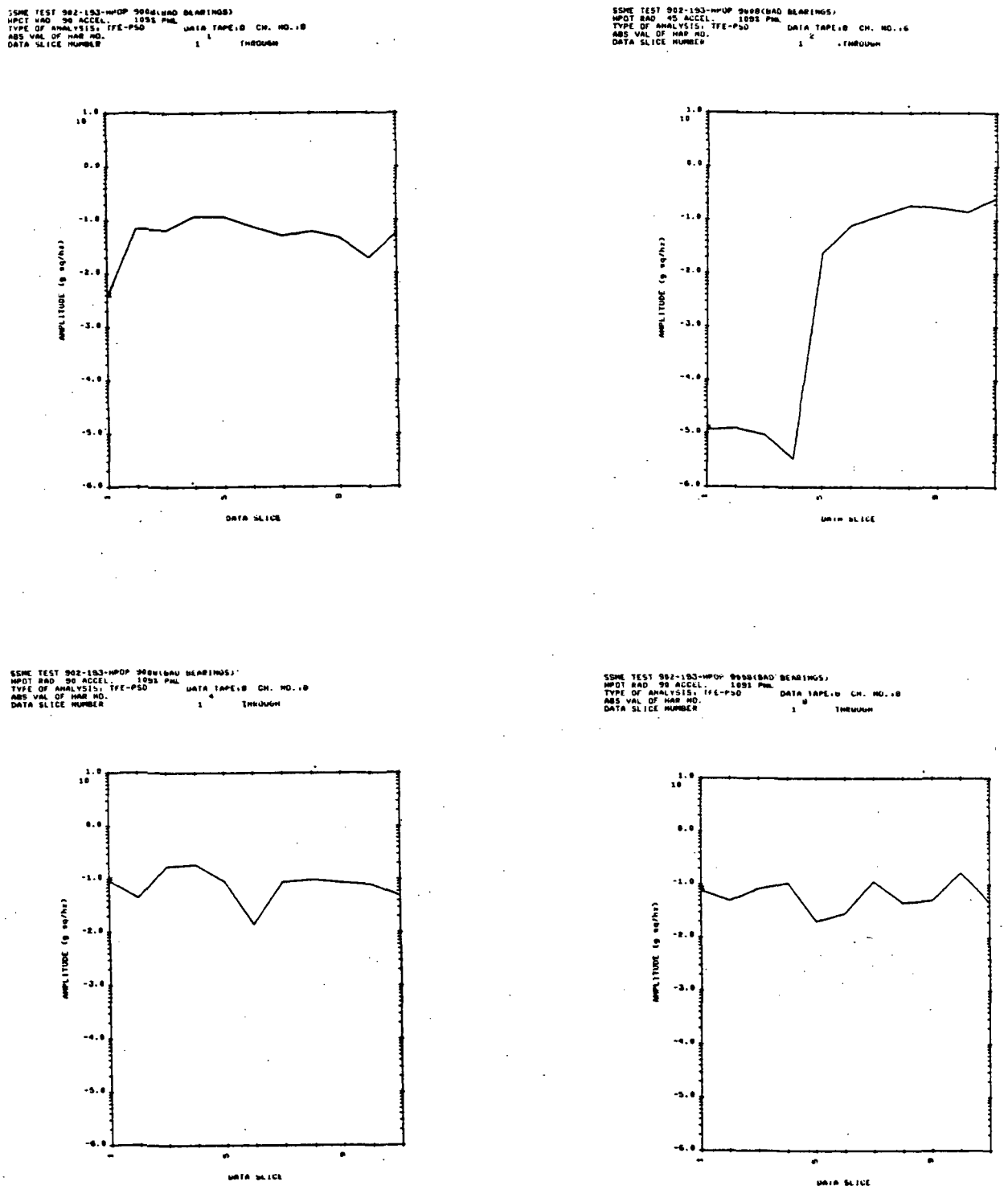

Figure 46. Test 902-193, 90° Accelerometer Harmonic Amplitude Variations as a Function of Data Slice

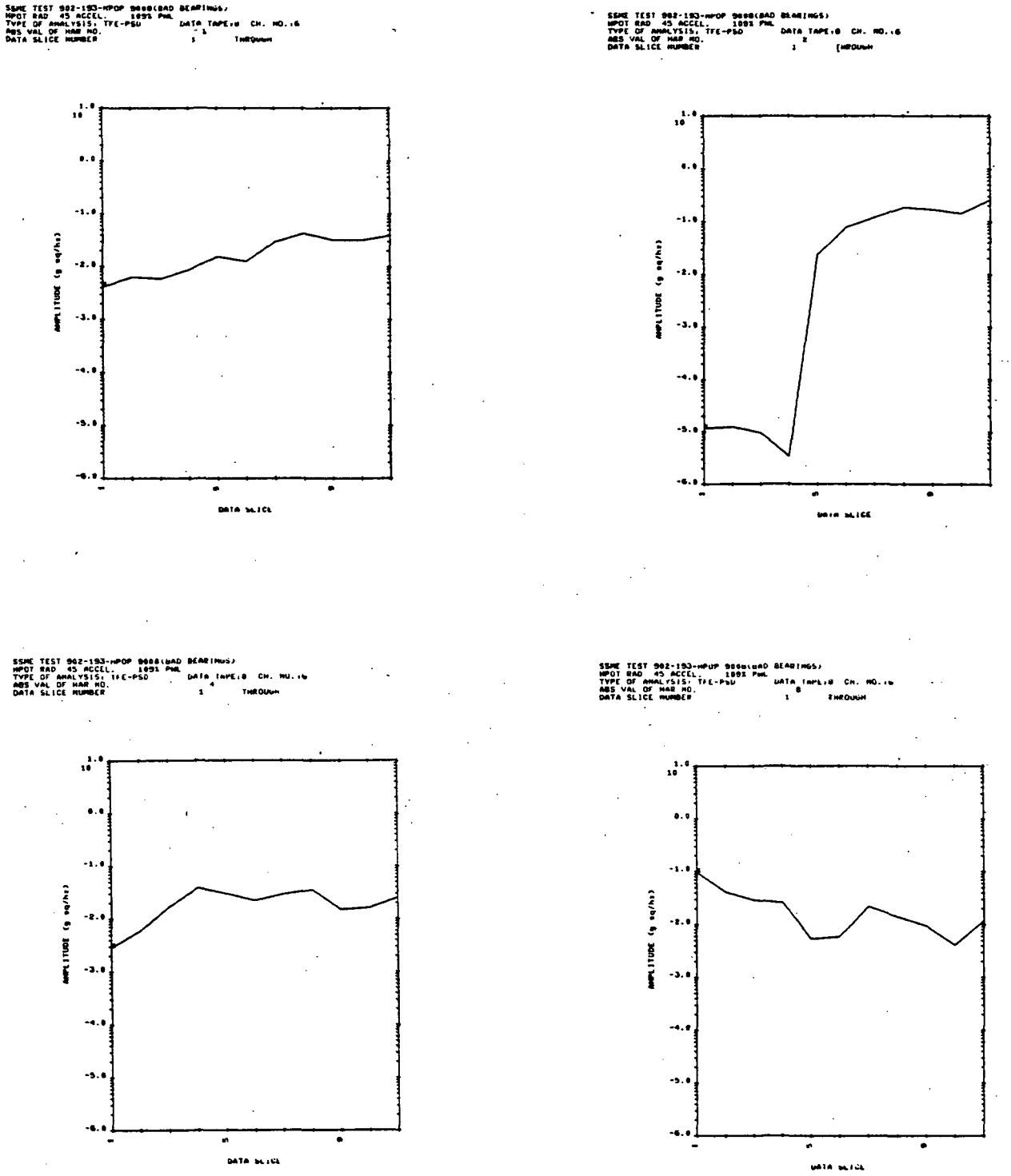

Figure 47. Test 902-193, 45° Accelerometer Harmonic Amplitude Variations as a Function of Data Slice

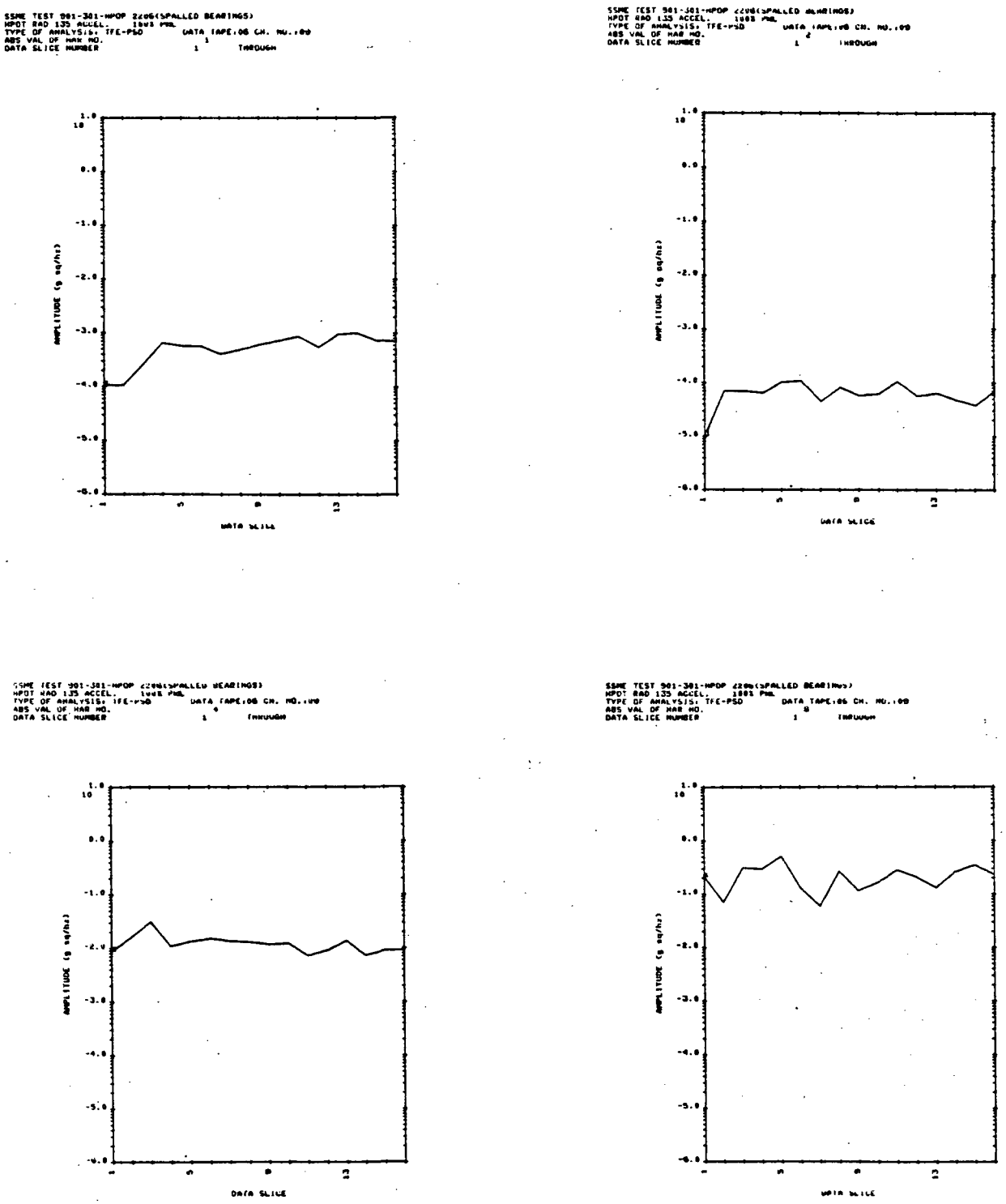

Figure 48. Test 901-301, 135° Accelerometer Harmonic Amplitude Variations as a Function of Data Slice

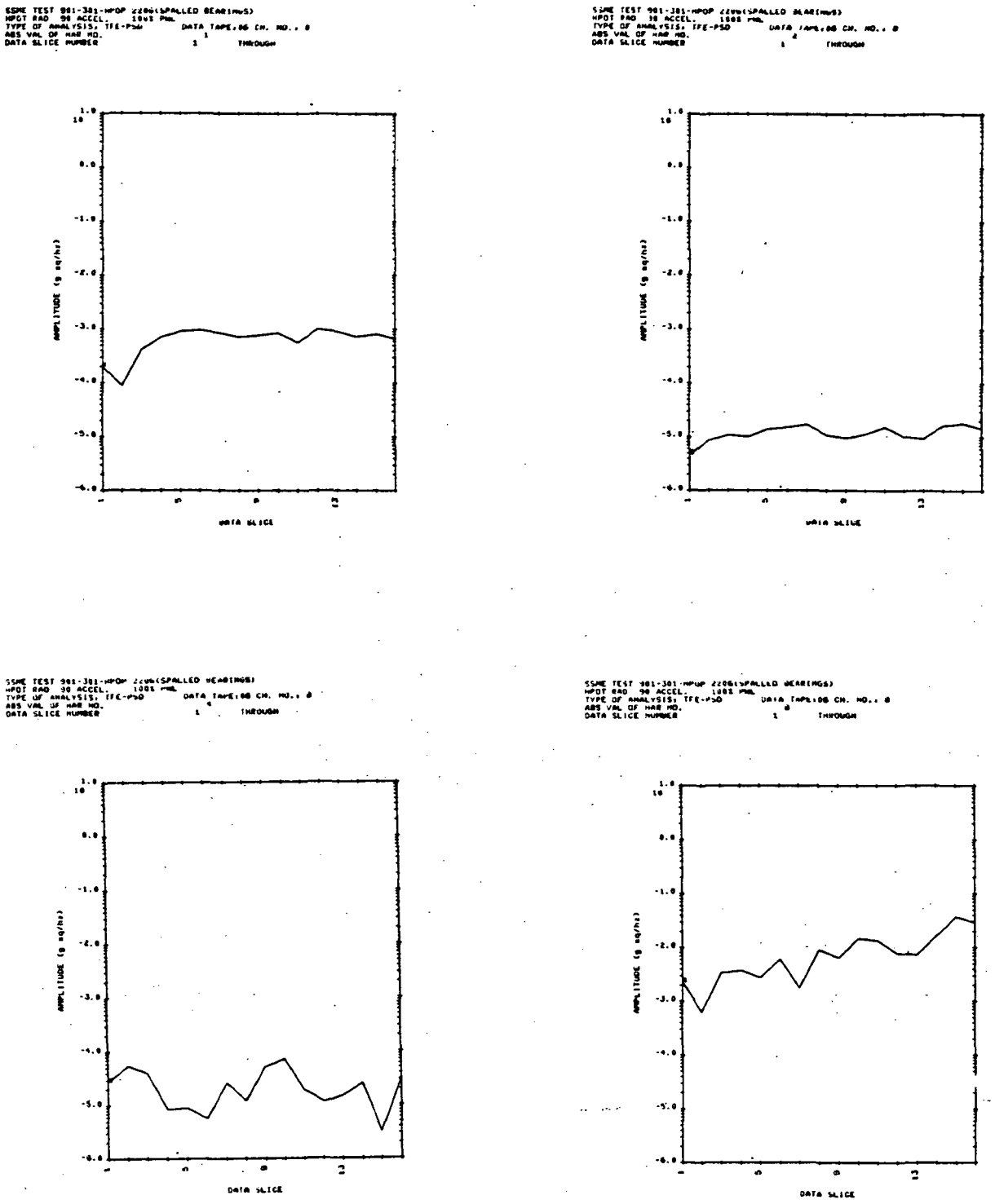

Figure 49. Test 901-301, 90° Accelerometer Harmonic Amplitude Variations as a Function of Data Slice

available from test 301 at the 45° accelerometer position.) The most notable characteristics from test 193 (bad bearings) is an increase in the amplitude of the 2N component and a slight decrease in the amplitudes of the 4N component. The 1N and 8N components show relatively slight variations. The behavior of all components for test 301 (spalled ball bearings) appeared to be relatively consistent without any large-scale variations being noted.

5.7.3 Technique Evaluation

From the data presented, it was apparent that the adaptive filter/adaptive noise cancellation technique was effective in reducing the random background noise contamination in a given spectra. However, the inconsistent attenuation characteristics of the adaptive filter could pose a severe problem if the assumption that the characteristics remains constant for a given setup is proven false. An in-depth investigation to determine attenuation characteristics of the adaptive filter as a function of frequency, signal-to-noise ratio, and other pertinent parameters is absolutely necessary. Once the attenuation question has been answered, the technique alone would be extremely powerful and could be used as a first-stage processor for any of the remaining techniques. The characteristics of the synchronous related components have not been extremely useful to this point. However, the capability to construct and manipulate these data base could prove to be the key to tracking bearing characteristics and determining incipient failure criteria.

Section 6

SUMMARY AND CONCLUSIONS

Six data analysis/data enhancement techniques have been addressed in this report. These were power spectral densities (PSDs), time domain averaging (TDA), order-sampled time domain averaging (OSTDA), random decrement averaging (randomdec), cepstrum analysis, and adaptive noise cancellation (ANC).

The transformation of time domain data into the frequency domain and the presentation of the frequency domain information in a PSD format provides an undeniably powerful data analysis technique. However, the computation of the PSD does not allow for any discrimination between signal and noise. Therefore, its usefulness as an incipient failure detection technique is very limited as a stand-alone tool for application to HPOTP data. On the other hand, use of the PSD in conjunction with some other data enhancement technique should prove to be extremely useful for incipient failure detection.

The TDA technique was proven to closely follow theory that predicts a signal-to-noise enhancement by a factor equal to the square root of the number of time averages. However, "leakage" associated with the digital sampling techniques and varying engine rpm proved to have significant negative impacts on the technique's performance. For these reason's, the technique was combined with order ratio sampling and was developed as OSTDA. As a data enhancement technique, the OSTDA combined the best features of the TDA with order sampling to reduced leakage and enhanced data plot readability. As a result, the OSTDA yielded a very suitable technique for detecting low-level periodic information in the presence of high-level random noise. Several restrictions associated with the time averaging techniques were uncovered, however, and tend to limit the usefulness of OSTDA as an incipient failure detection technique. The most important of these restrictions is the need for a speed probe or an rpm-related trigger signal. A trigger signal is required as both a time-averaging trigger and an order-sampling trigger. If the speed-related trigger is not available, the technique cannot be utilized unless some component of the signature can be filtered and used as a trigger signal. For the application at hand, the availability of such a well-defined component

cannot be anticipated, limiting the generality of the OSTDA technique. A second restriction associated with the time domain averaging technique is the necessity of a priori knowledge of the periodic signal to be extracted from the noise. To provide this knowledge, a better understanding of the phenomenon of bearing degradation would be necessary.

The random decrement averaging technique can be utilized without a speed-related trigger or any a priori knowledge of the periodic content of an input signal. In some cases, the randomdec technique provided a signal-to-noise enhancement of approximately 30 dB. Unfortunately, the 30-dB signal-to-noise increase was only observed during evaluation tests where the original signal-to-noise radio approached 0 dB. In addition, the magnitude of the periodic components of interest could not be accurately determined.

Cepstrum is a data analysis technique that has been used primarily in gear-box fault diagnostic applications. The interpretation of the reduced data using this technique is difficult for an inexperienced user. In addition, the mathematical basis defining the cepstrum does not provide an increase in signal-to-noise ratio. Therefore, the cepstrum, in much the same manner as the PSD, cannot provide data enhancement in cases where a signal is heavily masked by noise in the same spectral region. However, the cepstrum may show promise when used in conjunction with a technique that does improve the signal-to-noise ratio.

The adaptive noise cancellation technique is probabily the most straightforward data enhancement technique investigated to date. A remarkable increase in signal-to-noise has been seen in all cases. Problems associated with the nonuniform attenuation of low- and high-frequency components are of serious concern, and this behavior must be better understood before the adaptive filtering technique can be considered totally effective.

Each technique has been effective to some extent; however, none of the presently identified techniques by themselves have been developed to a point where consistent and comprehend able results relative to incipient failure detection have been obtained. In essence, the problems associated with incipiently detecting bearing failures ultimately depend upon an understanding of the phenomenon associated with bearing degradation and the spectral characteristics indicative of bearing failure.

Section 7

RECOMMENDATIONS

Based on collected information, investigative results, and the experience gained thus far concerning data enhancement techniques and incipient failure detection, the following recommendations are offered.

- With the major effort thus far being directed toward software development, implementation, and experimentation with a variety of data enhancement techniques, more research is required to determine and understand the phenomenon associated with bearing degradation through the classification of failure mechanisms and the identification of waveform and/or spectral characteristics indicative of bearing failure.

- The OSTDA, randomdec, and cepstrum software should be implemented on the HP 9825A computer-controlled analysis system to provide efficient comparison with ANC results.

- Independent laboratory investigations into the frequency-dependent attenuation effects of the adaptive filter must be performed.

- Further data reduction/analysis of common test cases consisting of SSME hot firing test data and/or independent bearing test data using the OSTDA, randomdec, cepstrum, and adaptive noise cancellation techniques (individually or in conjunction) is necessary to develop data bases more representative of component behavior under known operational conditions.

- Continuing review of the literature to identify new methods or variations in previously identified techniques should be maintained.

Section 8

REFERENCES

1. Gardner, Tony G. Incipient SSME Bearing Failure Detection--Data Enhancement Techniques. Wyle Laboratories Rept. TM 81-6, May 1981, 79 pp.

2. Gardner, Tony G. Incipient SSME Bearing Failure Detection--Evaluation of Four Data Enhancement Techniques. Wyle Laboratories Rept. TM 81-10, Aug. 1981, 271 pp.

3. Braun, S. The extraction of periodic waveform by time domain averaging. Acoustica, v. 32, No. 2, 1975, pp. 69-77.

4. _____. Signature analysis methods and applications for rotating machines. ASME paper 77WA/AUT5, American Society of Mechanical Engineers, 1977.

5. Ibrahim, S. R. Random decrement technique for modal identification of structures. Journal of Spacecraft, v. 14, No. 11, 1977, pp. 696-700.

6. Cole, H. A., Jr. On-line failure detection and damping measurement of aerospace structures by random decrement signatures. NASA CR 2205, Mar. 1973.

7. Bogert, B. P., M. J. R. Healy and J. W. Tukey. The quefrency analysis of time series for echoes: Cepstrum, pseudo-autocovariance, cross-cepstrum and Saphe cracking. Proc. Symp. Time Series Analysis. (M. Rosenblatt, ed.), 1963, pp. 209-243.

8. Randall, R. B. Application of B&K Equipment to Frequency Analysis, Bruel and Kjaer, Naerum, Denmark, 1977.

9. Widrow, B., et al. Adaptive noise cancelling: Principles and applications. IEEE Proc., v. 63, No. 12, Dec. 1975.

10. Chaturvedi, C. K., and D. W. Thomas. Adaptive noise cancelling and condition monitoring. J. Sound and Vibration, v. 76, No. 3, 1981, pp. 391-405.

Section 9

BIBLIOGRAPHY

1. Balderston, H. L. The broad range detection of incipient failure using the acoustic emission phenomena. Acoustic Emission, ASTM STP 505, American Society of Testing and Materials, 1972, pp. 297-317.

2. _____. The Detection of Incipient Failures in Bearings, Materials Evaluation, 1969, pp. 121-128.

3. Board, D. B. Incipient Failure Detection in High-Speed Rotating Machinery. 10th Symposium on Nondestructive Evaluation, San Antonio, Tex., 1975.

4. Bogert, B. P., M. J. R. Healy and J. W. Tukey. The quefrency analysis of time series for echoes: Cepstrum, pseudo-autocovariance, cross-cepstrum and Saphe cracking. Proc. Symp. Time Series Analysis. (M. Rosenblatt, ed.), 1963, pp. 209-243.

5. Braun, S. The extraction of periodic waveform by time domain averaging. Acoustica, v. 32, No. 2, 1975, pp. 69-77.

6. _____. Signature analysis methods and applications for rotating machines. ASME paper 77WA/AUT5, American Society of Mechanical Engineers, 1977.

7. Braun, S. G., and B. B. Seth. Signature Analysis Methods and Application for Rotating Machines. Proc. ASME Annual Winter Meeting, Atlanta, Ga., Aug. 1977.

8. Chaturvedi, C. K., and D. W. Thomas. Adaptive noise cancelling and condition monitoring. J. Sound and Vibration, v. 76, No. 3, 1981, pp. 391-405.

9. Cole, H. A., Jr. On-line failure detection and damping measurement of aerospace structures by random decrement signatures. NASA CR 2205, Mar. 1973.

10. Gardner, Tony G. Incipient SSME Bearing Failure Detection--Data Enhancement Techniques. Wyle Laboratories Rept. TM 81-6, May 1981, 79 pp.

11. _____. Incipient SSME Bearing Failure Detection--Evaluation of Four Data Enhancement Techniques. Wyle Laboratories Rept. TM 81-10, Aug. 1981, 271 pp.

12. Gupta, P. K., L. W. Winn, and D. F. Wilcock. Vibration Characteristics of Ball Bearings. Mechanical Technology, Inc. (Latham, N. Y.), paper.

13. Harting, D. R. Incipient Failure Detection by Demodulated Resonance Analysis. Instrumentation Technology, Sept. 1977, pp. 59-63.

14. Ibrahim, S. R. Random decrement technique for modal identification of structures. Journal of Spacecraft, v. 14, No. 11, 1977, pp. 696-700.

15. Kaiser, J. Untersuchungen uber das auftreten Gerauschen beim Zugversuch. Ph.D. thesis, Technisch Hochuchule, Munich, 1950; also Arkiv fur das Eisenhuttenwesen, AREIA, v. 24, No. 1/2, Jan/Feb. 1953, pp. 43-45.

16. Licht, Torben. Acoustic Emission. Bruel & Kjaer Tech. Review, No. 2, 1981.

17. Philips, G. J., and F. Hirschfeld. Rotating Machinery Bearing Analysis. Mechanical Engineering, July 1980, pp. 28-33.

18. Randall, R. B., and Jens Hee. Cepstrum Analysis. Bruel & Kjaer Tech. Review, No. 3, 1981.

19. Randall, R. B. Application of Bruel & Kjaer Equipment to Frequency Analysis, Bruel and Kjaer, Naerum, Denmark, 1977.

20. _____. Cepstrum Analysis and Gear Box Fault Diagnosis. Bruel & Kjaer Application Note No. 233, 1980.

21. Rindorf, H. J. Acoustic Emission Source Location in Theory and Practice. Bruel & Kjaer Tech. Review, No. 2, 1981.

22 Szenasi, F. R., and J. C. Wachel. Vibration and Noise in Pumps. Pump Handbook. McGraw-Hill Book Co., New York, 1976, pp. 9-87 - 9-97.

23. Taylor, James I. Evaluation of Machinery Condition by Spectral Analysis. Vibration Institute, 1979.

24. _____. Identification of Gear Defects by Vibration Analysis. Vibration Institute, 1979.

25. _____. Determination of Antifriction Bearing Conditions by Spectral Analysis. Vibration Institute (Clarendon Hills, Ill.), Rept. No. B256, 1978, 26 pp.

26. Widrow, B., et al. Adaptive noise cancelling: Principles and applications. IEEE Proc., v. 63, No. 12, Dec. 1975.